NOVEL BINDING PARTNERS OF PBF

IN THYROID TUMOURIGENESIS

By

Neil Sharma

A thesis presented to the College of Medical and Dental Sciences at the University of Birmingham for the Degree of Doctor of Philosophy

Centre for Endocrinology, Diabetes and Metabolism, School of Clinical and Experimental Medicine

August 2013

SUMMARY

Thyroid cancer is the most common endocrine cancer, with a rising incidence. The proto-oncogene *PBF* is over-expressed in thyroid tumours, and the degree of over-expression is directly linked to patient survival. PBF causes transformation *in vitro* and tumourigenesis *in vivo*, with PBF-transgenic mice developing large, macro-follicular goitres, effects partly mediated by the internalisation and repression of the membrane-bound transporters NIS and MCT8. NIS repression leads to a reduction in iodide uptake, which may negatively affect the efficacy of radioiodine treatment, and therefore prognosis.

Work within this thesis describes the use of tandem mass spectrometry to produce a list of potential binding partners of PBF. This will aid further research into the pathophysiology of PBF, not just in relation to thyroid cancer but also other malignancies. From this list, the interaction with three proteins was further investigated and validated by GST pull-down assays and/or co-immunoprecipitation. Thyroglobulin is an essential component of thyroid hormone synthesis. Preliminary studies suggested co-localisation with PBF within intra-cellular vesicles, although further research is needed to explore this functionally. Cortactin has a role in the cellular transport of proteins, and also promotes invadopodia formation and metastases in cancer. Co-localisation was observed in vesicles and at the membrane, with PBF additionally demonstrated in cell membrane projections – indicating a potential mechanism for the shuttling of PBF to and from the cell membrane, and its secretion. SRC is a tyrosine kinase intimately linked to cancer. SRC phosphorylated PBF, an effect abrogated by treatment with specific inhibitors, including PP1. Importantly, PP1 treatment was then found to increase iodide uptake in human primary thyroid cultures over-expressing PBF.

Overall, these data describe a list of possible binding partners for PBF, and specifically identify a novel potential therapeutic strategy for iodide-refractory thyroid cancer.

DEDICATION

For Hannah and Jake.

ACKNOWLEDGEMENTS

I would like to thank Professor Chris McCabe, Dr Martin Read and Professor Jayne Franklyn for their excellent supervision of this research project, and for their continued support of my academic aspirations. Thanks also to Dr Vicki Smith and Dr Kristien Boelaert for their patience, time and teaching, Dr Craig Doig for both his advice and constant questioning, and Dr Andrew Turnell and Dr Ashley Martin for their guidance and coaching through the world of proteomics. I am grateful to Rob, Greg, Craig, Gavin and Perkin for helping to keep me sane and slightly fit during my three years in the lab, as well as everyone on the 2nd floor IBR for providing a great working environment. Finally, thanks to Mr John Watkinson for his support in all aspects of my career and for giving me the opportunity to get started in research, and to Chris for helping to keep me here.

This work was funded by the Get Ahead Charitable Trust, the Royal College of Surgeons of England and the Medical Research Council, to whom I am grateful for their support and confidence.

ABBREVIATIONS

°C	Degrees centigrade
^{125}I	Iodine-125
^{131}I	Iodine-131
ATA	American Thyroid Association
ATC	Anaplastic thyroid cancer
BCA	Bicinchoninic acid
BSA	Bovine serum albumin
BTA	British Thyroid Association
cDNA	Complementary deoxyribonucleic acid
CI	Confidence interval
cpm	Counts per minute
Da	Dalton
DIT	Di-iodo-tyrosine
DMEM	Dulbecco Modified Eagle's Media
DMSO	Dimethyl sulfoxide
DNA	Deoxyribonucleic acid
DTC	Differentiated thyroid cancer
DTT	Dithiothreitol
EDTA	Ethylenediaminetetraacetic acid
EGFR	Epidermal growth factor receptor
ELISA	Enzyme Linked Immunosorbent Assay
ERE	Oestrogen response elements
ESI	Electrospray ionisation
FACS	Fluorescence activated cell sorting
FAK	Focal adhesion kinase
FAP	Familial Adenomatous Polyposis
FBS	Fetal bovine serum
FGF2	Fibroblast growth factor 2
FGFR	Fibroblast growth factor receptor
FNAC	Fine needle aspiration cytology
FTC	Follicular thyroid cancer
GST	Glutathione-S-Transferase
HA	Haemagglutinin
HBSS	Hanks Balanced Salt Solution
HPLC	High performance liquid chromatography
HRP	Horseradish peroxidase
HSP90	Heat shock protein 90
IP	Immunoprecipitation
kDa	Kilodalton
LB	Lysogeny broth
LC	Liquid chromatography
LRRK	Leucine-rich repeat kinase
m/z	Mass to charge ratio
MALDI	Matrix assisted laser desorption/ionisation

MAPK	Mitogen activated protein kinase
MCT8	Monocarboxylate transporter 8
MEN	Multiple endocrine neoplasia
MET	Hepatocyte growth factor
MIFC	Minimally invasive follicular carcinoma
MIT	Mono-iodo-tryosine
MNG	Multinodular goitre
mRNA	Messenger ribonucleic acid
MS/MS	Tandem mass spectrometry
MTC	Medullary thyroid cancer
NaI	Sodium Iodide
NCS	Newborn Calf Serum
NIS	Sodium-Iodide Symporter
NTRK1	Neurotrophic tyrosine receptor kinase type 1
PAX8	Paired box gene 8
PBF	PTTG Binding Factor (also PTTG1IP)
PBF-HA	Haemagglutinin-tagged PBF
PBF-Tg	PBF transgenic
PBS	Phosphate buffered saline
PCR	Polymerase chain reaction
PDGF-R	Platelet derived growth factor receptor
PEI	Polyethylenimine
PI	Protease inhibitor
PP1	Src-selective kinase inhibitor
PPARγ1	Peroxisome proliferator-activator receptor gamma 1
PTC	Papillary thyroid cancer
PTEN	Phosphatase and tensin homologue
PTTG	Pituitary tumor transforming gene
PTM	Post translational modification
PVDF	Polyvinylidene difluoride
pY174	PBF phosphorylated at Y174
RAF	Serine/threonine-protein kinase
RAS	Rat sarcoma viral oncogene
RET/PTC	Rearranged during transfection/Papillary thyroid cancer
RIPA	Radioimmunoprecipitation assay
RLN	Recurrent laryngeal nerve
RNA	Ribonucleic acid
RR	Relative Risk
RTK	Receptor tyrosine kinase
SDS	Sodium dodecyl sulphate
SDS-PAGE	SDS-polyacrylamide gel electrophoresis
SFK	SRC family kinase
SH2/3	Src homology domain 2/3
SILAC	Stable isotope labelling by amino acid in culture
SIR	Standardised incidence ratio
siRNA	Short interfering RNA
STN	Solitary thyroid nodule

SUMO	Small ubiquitin-like modifier
T/F	Transfection
T3	Tri-iodothyronine
T4	Tetraiodothyronine
TBS-T	Tris buffered saline with tween
TE	Transfection efficiency
TEMED	Tetramethylethylenediamine
Tg	Thyroglobulin
TKI	Tyrosine kinase inhibitor
TNM	Tumour, Node, Metastases
ToF	Time of flight
TRH	Thyrotropin releasing hormone
TSH	Thyroid stimulating hormone
UACA	Uveal autoantigen with coiled-coil domains and ankyrin repeats
USF1	Upstream transcription factor 1
UT	Untransfected
v/v	Volume to volume ratio
VEGFR	Vascular endothelial growth factor receptor
VO	Vector Only
w/v	Weight to volume ratio
WB	Western blot
WHO	World Health Organisation
WIFC	Widely invasive follicular carcinoma

PUBLICATIONS RELATING TO THIS THESIS

Smith VE*, Sharma N*, Watkins RJ, Read ML, Ryan GA, Kwan PP, Martin A, Watkinson JC, Boelaert K, Franklyn JA, McCabe CJ. Manipulation of PBF/PTTG1IP Phosphorylation Status; a Potential New Therapeutic Strategy for Improving Radioiodine Uptake in Thyroid and Other Tumors. *J Clin Endocrinol Metab*. 2013 Jul;98(7):2876-86. * = joint first author

Sharma N, Martin A, McCabe CJ. Mining the proteome: the application of tandem mass spectrometry to endocrine cancer research. *Endocr Relat Cancer*. 2012 Jul 22;19(4):R149-61.

Smith VE, Read ML, Turnell AS, Sharma N, Lewy GD, Fong JC, Seed RI, Kwan P, Ryan G, Mehanna H, Chan SY, Darras VM, Boelaert K, Franklyn JA, McCabe CJ. PTTG-binding factor (PBF) is a novel regulator of the thyroid hormone transporter MCT8. Endocrinology. 2012 Jul;153(7):3526-36.

Lewy GD, Sharma N, Seed RI, Smith VE, Boelaert K, McCabe CJ. The pituitary tumor transforming gene in thyroid cancer. *J Endocrinol Invest*. 2012 Apr;35(4):425-33.

Read ML, Lewy GD, Fong JC, Sharma N, *et al*. Proto-oncogene PBF/PTTG1IP regulates thyroid cell growth and represses radioiodide treatment. *Cancer Res*. 2011 Oct 1;71(19):6153-64.

Watkins RJ, Read ML, Smith VE, Sharma N, Reynolds GM, Buckley L, Doig C, Campbell MJ, Lewy G, Eggo MC, Loubiere LS, Franklyn JA, Boelaert K, McCabe CJ. Pituitary tumor transforming gene binding factor: a new gene in breast cancer. *Cancer Res*. 2010 May 1;70(9):3739-49.

TABLE OF CONTENTS

LIST OF FIGURES

LIST OF TABLES

Chapter 1 General Introduction

1.1 The Physiological Role of the Thyroid Gland

1.1.1 Thyroid structure and development

The thyroid is an important endocrine organ located in the anterior neck and is found in all vertebrates. In humans, it originates from the base of the tongue in the 3rd to 4th week gestation and migrates into the neck over the next few weeks. Macroscopically, it is composed of two lobes lying on either side of the trachea and connected by an isthmus (McGlashan 2008). Microscopically, the thyroid consists of many follicles - spheres of cuboidal follicular epithelial cells (Figure 1.1).

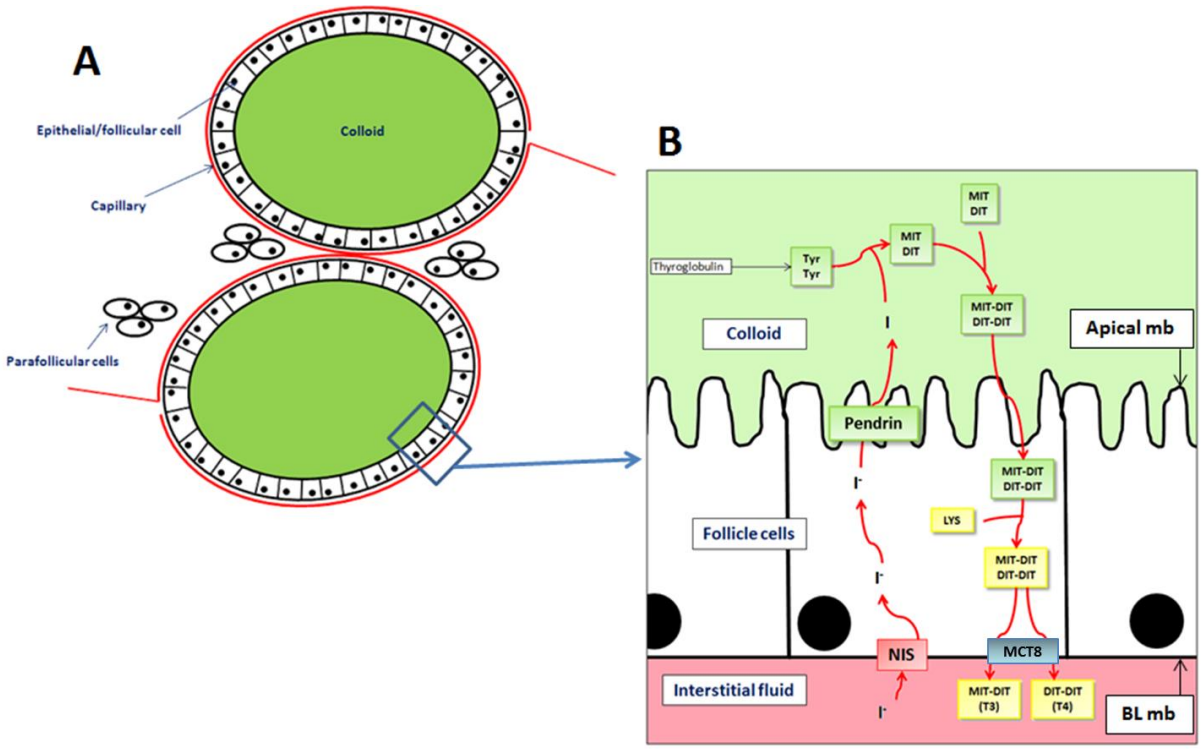

Figure 1.1 A - Cross-sectional structure of a thyroid follicle. B - Detail of a thyroid follicular cell, showing the process by which the follicle produces thyroid hormones. I = Iodine, Tyr = Tyrosine, MIT/DIT = Mono/Di-iodotyrosine, T3 = Triiodothyronine, T4 = Thyroxine, MCT8 = Monocarboxylate transporter 8, NIS = Sodium iodide symporter, Lys = Lysosome, BL = baso-lateral, mb = membrane.

There are around 3 million follicles in a healthy adult thyroid, each surrounding an area of protein-rich colloid which forms the bulk of the mass of the thyroid. The most abundant protein within the colloid is thyroglobulin, a 660 kDa dimeric protein synthesised in the endoplasmic reticulum. Each follicle is surrounded by a network of capillaries and clusters of parafollicular cells.

1.1.2 Thyroid hormone synthesis

The predominant role of the thyroid is to produce the thyroid hormones triiodothyronine (T3) and tetraiodothyronine ("thyroxine" or T4). The synthetic pathway is complex (Figure 1.1B) and dependent on the influx of iodide into the thyroid via the sodium-iodide symporter (NIS), a transmembrane glycoprotein located at the basolateral membrane of the thyroid follicular cell. NIS actively transports 2 sodium ions with 1 iodide ion, resulting in an intracellular iodide concentration up to 50 times higher than the plasma. Iodide diffuses across the cell, and is then transported across the apical membrane into the colloid by pendrin, where it is oxidated to iodine by thyroid peroxidase at the outer surface of the membrane. The reactive species liberated from this reaction iodinates thyroglobulin at its tyrosyl residues. The products of this iodination are monoiodotyrosine and diiodotyrosine, which in turn can combine to form the thyroid hormone triiodothyronine (T3) and thyroxine (T4), still bound to thyroglobulin. Thyroid-stimulating hormone (TSH), released from the anterior pituitary gland, binds to the TSH receptor on the basolateral membrane, stimulating endocytosis of thyroid hormones. T3 and T4 are liberated from thyroglobulin following the fusion of the endosomes with lysosomes, and subsequently transported across the basolateral membrane into the bloodstream via monocarboxylate transporter 8 (MCT8) (Di Cosmo et al. 2010; Trajkovic-Arsic et al. 2010).

The control of thyroid hormone production and secretion is via the hypothalamic-pituitary-thyroid axis, an endocrine negative feedback loop where low circulating levels of T3/T4 stimulate the hypothalamus to release thyrotropin releasing hormone (TRH). This stimulates the anterior pituitary to release thyroid stimulating hormone (TSH). As well as the effects on the secretion of T3 and T4, TSH also stimulates expression of NIS, thus acting throughout the pathway of thyroid hormone synthesis (Dohan et al. 2003).

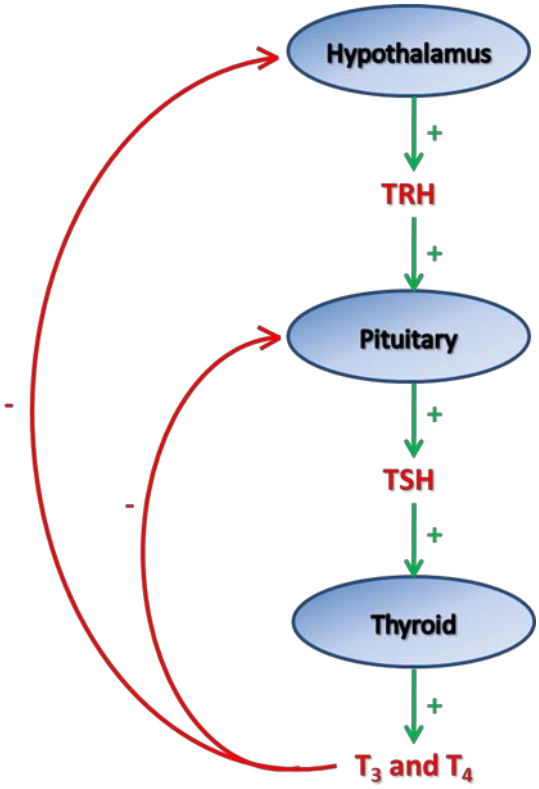

Figure 1.2 Hypothalamic-Pituitary-Thyroid axis. The release of TRH and TSH is under the control of a negative feedback loop by T3 and T4. TRH - Thyrotropin Releasing Hormone, TSH - Thyroid Stimulating Hormone.

1.1.3 The role of the thyroid gland in health

Both T3 and T4 are transported in the bloodstream bound primarily to thyroxine-binding globulin, with a smaller amount bound to either thyroxine-binding albumin or para-albumin. In the bound state, the hormones are inactive and it is therefore the free T3 and T4 (< 0.5 % of

total) that exert a cellular effect. T4 has a long half-life and acts as a pro-hormone for the biologically active T3. T4 is converted in the periphery to T3 by iodothyronine deiodinases, and then actively transported across the cell membrane by a small number of identified transporters, namely OATP1C1, monocarboxylate transporter (MCT) 8 and MCT10 (Visser et al. 2011). Thyroid hormone has a wide range of effects across the body, in general increasing metabolic rate and development, as summarised in Table 1.1.

Effect	Organ/tissue	Mechanism
Chronotropic/ Inotropic	Cardiovascular	Increase number/affinity of β-adrenergic receptors. Enhance response to circulating catecholamines.
Catabolic	Muscle	Increase protein breakdown.
	Adipose	Stimulate lipolysis.
Developmental	Central nervous system	Promote brain development.
	Bone	Promote skeletal growth.
Metabolic	Gastrointestinal tract	Increase carbohydrate absorption.
	General	Increase oxygen consumption by active tissues.
		Increase metabolic rate.

Table 1.1 Table detailing the systemic effects of thyroid hormone (Ganong 1997).

1.2 Thyroid Cancer

1.2.1 Incidence of Thyroid Cancer

Thyroid cancer is the commonest endocrine cancer, with an incidence of 3.6 cases per 100,000 per year in the UK. Women have a 2.5 times greater risk of developing thyroid cancer than men (5.6 vs 2.2 per 100,000), with a peak incidence during the 4th decade (Figure 1.3A) (Cancer Research UK 2013). The incidence of differentiated thyroid cancer (DTC) has almost tripled in the United States between 1975 and 2009, and the disease has the fastest rising incidence of any cancer in the USA (Figure 1.3B and C) (Howlader N 2012). The exact cause for this rise in incidence is unknown, but has been attributed to the increase in the detection of small, early tumours ("incidentalomas") during investigations for other conditions (Leenhardt et al. 2004; Cooper et al. 2009), and interestingly the rise is not associated with a corresponding rise in mortality (Figure 1.3D) (Howlader N 2012). However, the fact that the incidence of later stage cancers is also increasing implies that more sophisticated detection methods cannot account for the increase alone (Chen et al. 2009; Sipos and Mazzaferri 2010).

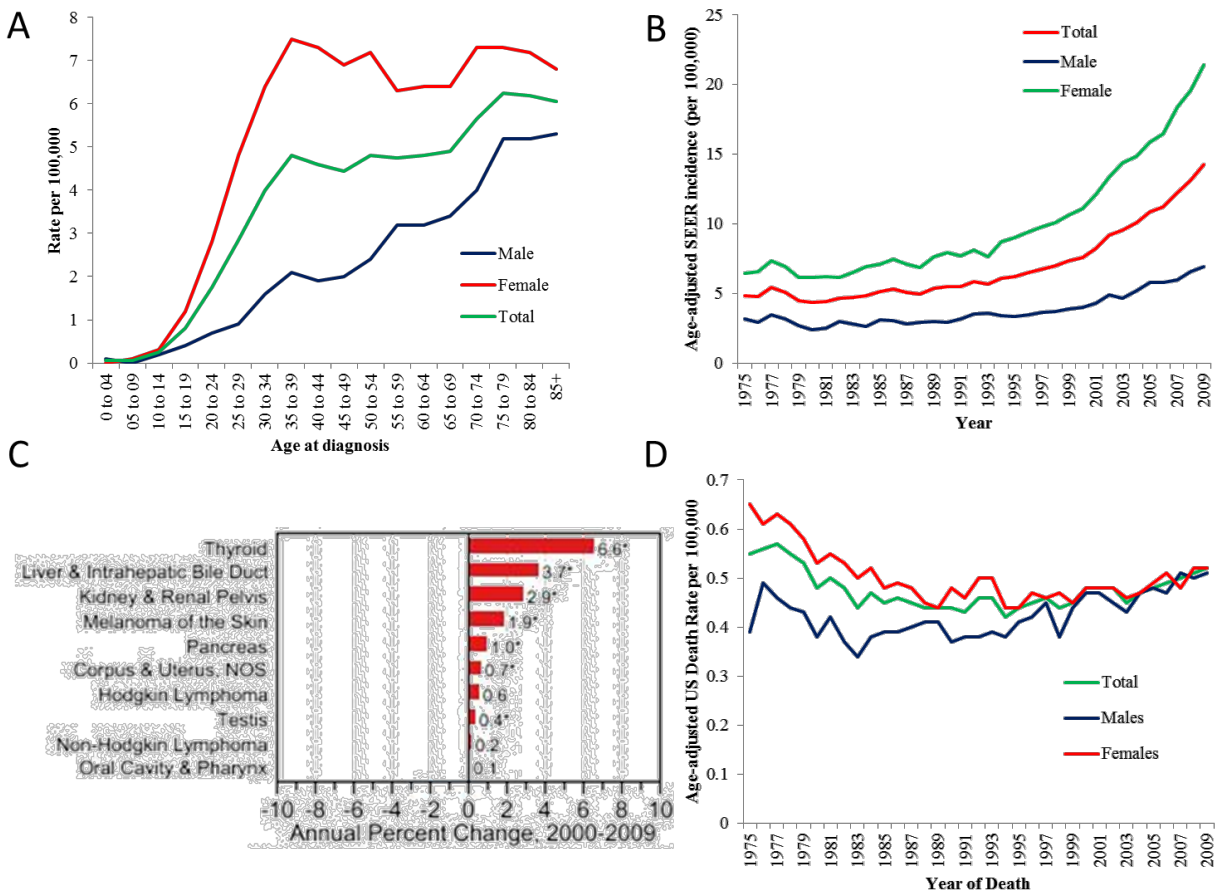

Figure 1.3 Thyroid cancer demographic data. A – Incidence of thyroid cancer per 100,000 across age groups by gender (CRUK 2013). B – USA age-adjusted incidence per 100,000 between 1975 and 2009. C – US annual percentage change in incidence of malignancy across all cancer sites. D – USA age-adjusted mortality rate per 100,000 between 1975 and 2009 (B – D from SEER data (Howlader N 2012)).

1.2.2 Risk factors for developing DTC

There are several well documented risk factors for developing thyroid cancer. One of the most widely studied is the effect of ionising radiation on the thyroid gland in childhood. First considered in a report of 28 childhood thyroid cancers, of whom 11 received radiation to the thymus for respiratory obstructive symptoms (Duffy and Fitzgerald 1950), the association was further explored over the subsequent decades (Kaplan et al. 2009). The atomic bomb

survivors of Hiroshima provided a long term cohort that have been extensively studied; a recent study has shown that the excess thyroid cancer risk of those exposed as children has continued for over 50 years after exposure (Furukawa et al. 2013). The more recent disaster at Chernobyl in 1986 led to a sharp increase in the number of cases of DTC in the surrounding areas (Stsjazhko et al. 1995). Papillary carcinomas are the most frequent DTC to be associated with radiation exposure, with chromosomal rearrangements (principally RET/PTC (35 %) and occasionally PAX8/PPARγ (3 %)) most common, and point mutations (BRAF (15 %) and RAS (8 %)) also present (Leeman-Neill et al. 2013). The effects of the Fukoshima disaster following the Japanese earthquake and tsunami on the health of the surrounding prefecture will be monitored closely over the following decades, with the World Health Organisation predicting a 70 % increase risk of thyroid cancer in females exposed as infants (WHO 2013).

A previous history of benign hyperplastic thyroid disease increases the risk of thyroid cancer (relative risk (RR) 14.5, $P < 0.01$) (Preston-Martin et al. 1987), as does a family history of thyroid cancer. The lifetime risk of thyroid cancer in a patient with a first degree relative diagnosed with a non-medullary thyroid cancer is 2 % (standardised incidence ratio (SIR) 2.9, 95 % CI 2.4 to 3.4, $p < 0.00001$) for women and 1 % (SIR 2.5, 95 % CI 1.9 to 3.3, $p < 0.00001$) for men. When 2 or more family members are affected, the SIR rises to 23.2 (95 % CI 10.6 to 44.0, $p< 0.00001$). The younger the family member was diagnosed with DTC, the higher the risk of developing the disease (Fallah et al. 2013).

Thyroid cancer is more common in association with certain hereditary diseases. Familial adenomatous polyposis coli (FAP) is an autosomal dominant pre-malignant disease caused by mutations in the tumour suppressor gene *APC*. Affecting 3 to 10 per 100,000 (Half et al. 2009), patients develop a large number of colonic polyps, and there is a 100 % progression to colorectal cancer. It is also associated with a number of extra-colonic manifestations, of which

the cribriform morular variant of papillary thyroid cancer is one. The rate of thyroid cancer amongst patients with FAP ranges from 0.4 to 11.8 % (Steinhagen et al. 2012), with a relative risk of 7.6 (95 % CI 2.5 to 17.7) (Giardiello et al. 1993). A specific mechanism for this association has not, as yet, been described. Cowden, and Cowden-like, syndrome, are characterised by the development of multiple cutaneous hamartomas, and due to autosomal dominantly inherited mutations in one or more of the *PTEN*, *SDHx* and *KLLN* gene. In a cohort of 2723 patients with the syndrome, for those with a *PTEN* mutation the SIR for thyroid cancer was 72 (95 % CI 51 to 99, $p < 0.001$) and this was disproportionally follicular thyroid cancer. The SIR for *SDHx* and *KLLN* mutations was 63 (95% CI 42 to 92, $p < 0.001$) for SDHx variants, and 45 (95% CI, 26 to 73, $p < 0.001$) respectively (Ngeow et al. 2011).

Chronic lymphocytic (Hashimoto's) thyroiditis leads to an increased risk of thyroid lymphoma (as well as systemic myeloproliferative and lympho-proliferative neoplasms generally) but not DTC, with an estimated relative risk of 67 ($p < 0.000001$) (Holm et al. 1985).

1.2.3 Types of thyroid cancer

The majority of thyroid cancers arise from follicular cells and are termed differentiated thyroid cancers (DTCs). The commonest sub-type is papillary thyroid cancer (PTC), which accounts for approximately 70 % of all thyroid cancer and is further split into pure papillary, follicular and mixed PTC. PTC metastasis is usually via lymphatic spread, and an involved cervical lymph node may be the first sign of the disease in some patients (Lim et al. 2012).

Follicular thyroid cancer (FTC) accounts for around 10 – 20 % of thyroid cancers. Unlike PTC, lymph node metastasis is rare, with blood borne spread to lungs and bone being more common. The 2 subtypes are Minimally Invasive Follicular Carcinoma (MIFC), which although macroscopically appearing the same as a follicular adenoma demonstrates capsular

and/or vascular invasion microscopically, and Widely Invasive Follicular Carcinoma (WIFC), which demonstrates diffuse infiltration of the thyroid gland, and a consequently poorer survival rate.

Medullary thyroid cancer (MTC) originates from the parafollicular cells and represents 5% of thyroid cancers. There is a strong hereditary component to the disease; 25% of MTC cases are caused by germline mutations in the RET proto-oncogene that result in multiple endocrine neoplasia (MEN) 2A (80%), MEN 2B (5%) and familial MTC (5-15%) (Ceolin et al. 2012). The cancers secrete calcitonin (used as a serum marker for the disease), which can cause the characteristic flushing and diarrhoea associated with the disease.

Anaplastic, or de-differentiated, thyroid cancer typically presents later in life and is associated with rapid mitosis and high rate of lympho-vascular invasion. It accounts for around 5 % of all thyroid cancers and is almost universally fatal (Ain 1998).

The histological distribution of thyroid cancers, as well as their mode of presentation and primary treatment is summarised in Table 1.2 .

Subtype	Proportion	Mode of presentation	Primary Treatment
Papillary	71.5 %	Thyroid mass or cervical lymphadenopathy	Surgery +/- ^{131}I
Follicular	19.6 %	Thyroid mass or distant metastases	Surgery +/- ^{131}I
Medullary	6.1 %	Thyroid mass or evidence of MEN	Surgery
Anaplastic	1.5 %	Rapidly enlarging thyroid mass	Palliative

Table 1.2 Subtypes of thyroid cancer including mode of presentation and primary treatment modality (British Thyroid Association and Royal College of Physicians 2007; British Association of Endocrine and Thyroid Surgeons 2009).

1.2.4 Diagnosing thyroid cancer

The commonest presentation of DTC is a solitary thyroid nodule (STN), which may have been identified by the patient or their general practitioner, or incidentally when the patient was being investigated for an unrelated problem. Once identified, the usual method of assessment of a STN is via ultrasonography and fine needle aspiration cytology (FNAC). There are a number of ultrasound characteristics that suggest a malignant nodule as opposed to a benign diagnosis: microcalcifications, irregular nodule margins, parenchymal hypoechogenicity, increased nodule vascularity and abnormal neck lymphadenopathy (Alexander 2008). However, none of these are definitive.

FNAC aims to provide a cellular sample from the nodule in question, thus allowing a cytological analysis with the aim of determining if the nodule is benign or malignant. FNAC can be performed using palpation alone or via ultrasound guidance; the latter is associated with higher "hit" rates and more reliable diagnosis, as the ultrasonographer is able to target the needle to the most suspicious area. FNAC results are split into 5 broad categories (see Table 1.3), known as the "Thy" classification.

RCPath modified BTA nomenclature	Description	Risk of malignancy (%)
Thy1	Non-diagnostic (virtually acellular)	0-10
Thy1c	Non-diagnostic- Cystic lesion	
Thy2	Non-neoplastic (Consistent with a benign follicular nodule or lymphocytic thyroiditis or subacute thyroiditis)	0-3
Thy 2c	Non-neoplastic, cystic lesion	
Thy3a	Neoplasm possible- atypia	5-15
Thy3f	Neoplasm possible- suggestive of follicular neoplasm	15-30
Thy4	Suspicious for papillary/ medullary/ metastatic/lymphoma/carcinoma	60-75
Thy5	Malignant	97-100

Table 1.3 Current recommendations for the reporting of thyroid FNAC specimens, with the associated risk of malignancy for each category (British Thyroid Association and Royal College of Physicians 2007; RCPath 2009).

In general, if a Thy2 result is obtained from FNAC, the patient will go on to have a repeat sample taken, usually at an interval of 3 to 6 months, and only if this is again benign will this be taken as a valid result. On the other end of the scale, a Thy5 result mandates at least a hemi-thyroidectomy (see section 1.2.5.2). Difficulties arise in the problematic area of the Thy3 result. It is not possible for a cytologist to determine whether follicular cells in a sample represent a benign follicular adenoma or the malignant follicular carcinoma, and therefore these results are classed as indeterminate. Most centres will proceed with a "diagnostic lobectomy", removing the half of the thyroid gland containing the suspicious nodule and thereby allowing a full histological diagnosis. The rate of malignancy in Thy3 FNACs is approximately 28 %, although the risk increases at ages less than 30 and greater than 60 years, in males, and for larger nodules (Mihai et al. 2009). This results in a large

number of patients undergoing surgery for what is in fact a benign disease, and over a quarter of patients requiring a second operation for what proves to be malignancy. At present, studies are underway to utilise biomarkers or mutation analysis of FNAC samples in an attempt to improve the diagnostic accuracy of these indeterminate results.

1.2.5 Management of differentiated thyroid cancer

1.2.5.1 Staging

In the UK, thyroid cancer is staged according to the TNM classification (Table 1.4), which takes into account **T**umour factors, **N**odal status and **M**etastases.

Stage	Description
TX	Primary tumour cannot be assessed
T0	No evidence of primary tumour
T1a	Tumour 1 cm or less in greatest dimension, limited to the thyroid
T1b	Tumour 1–2 cm in greatest dimension, limited to the thyroid
T2	Tumour more than 2 cm but not more than 4 cm in greatest dimension, limited to the thyroid
T3	Tumour more than 4 cm in greatest dimension, limited to the thyroid or any tumour with minimal extrathyroid extension (e.g. extension to sternothyroid muscle or perithyroid soft tissues)
T4a	Tumour of any size extending beyond the thyroid capsule and invading any of the following: subcutaneous soft tissues, larynx, trachea, oesophagus, recurrent laryngeal nerve
T4b	Tumour invades prevertebral fascia, mediastinal vessels, or encases carotid artery
NX	Regional lymph nodes cannot be assessed
N0	No regional lymph node metastasis
N1	Regional lymph node metastasis
N1a	Metastasis in Level VI (pretracheal and paratracheal, including prelaryngeal and Delphian lymph nodes)
N1b	Metastasis in other unilateral, bilateral or contralateral cervical or upper/superior mediastinal lymph nodes.
cM0	Clinically no distant metastasis
cM1	Distant metastasis clinically

Table 1.4 TNM staging classification for DTC (from AJCC Cancer Staging Manual, 2009).

In DTC, the disease is further staged by the patient's age to allow prognostication (see section 1.2.6).

1.2.5.2 Surgery

At present, the only definitive way of treating DTC is with surgery to remove all or part of the thyroid gland, affected lymph nodes and metastases. In the past, there was a tendency to perform sub-total thyroidectomy (leaving a significant portion of the gland behind in an attempt to preserve the recurrent laryngeal nerve (RLN)) but this was shown to increase recurrence rates when compared to total or near-total thyroidectomy. The main complications from the surgery are damage to the RLNs (resulting in voice change or in extreme cases airway compromise and respiratory embarrassment requiring tracheotomy) and/or parathyroid glands (resulting in temporary or permanent hypoparathyroidism); although in experienced hands these should occur in only a small number of cases. As more DTCs (in particular PTCs) with a diameter less than 10 mm are diagnosed, more centres are treating these with thyroid lobectomy. While this undoubtedly reduces complications, studies have shown that between 30 and 46 % of PTCs are multifocal and contralateral (Ricci and Alfonso 2012; Lee et al. 2013), meaning that some of these patients will have residual foci of malignancy in the neck following surgery.

1.2.5.3 Radioiodine ablation

Given the thyroid's ability to concentrate iodine, radioiodine ablative therapy has been used since the 1940s to treat thyroid disease (Miller and Soley 1948). The isotope used in thyroid cancer treatment is iodine-131 (I). This has a decay half-life of around 8 days, and emits both gamma (10 %) and beta (90 %) radiation. The isotope can therefore be imaged using gamma-readers, although it is not possible to detect the beta emissions. It is the latter that facilitates the death of thyroid tissue where it is taken up.

Over the past few years, there has been a move away from treating all thyroid cancers greater than 1 cm with post-operative I, instead only giving treatment to targeted patients who will show a predicted benefit (Table 1.5). There is still a group in whom there is no clear evidence one way or the other, and for these patients the decision to give or withhold treatment must be made on an individual basis by the multi-disciplinary team.

No indication for ^{131}I ablation (low risk of recurrence)	• Complete surgery • Favourable histology • No extra-thyroidal extension • PTC: unifocal. ≤ 1cm diameter, N0, M0. Minimally invasive FTC: no vascular invasion, ≤ 2cm diameter
Definite indications	• Distant metastases • Incomplete resection • High risk of tumour recurrence

Table 1.5 Indications for ^{131}I ablation post-surgery (British Thyroid Association and Royal College of Physicians 2007).

The efficacy of radioiodine treatment for thyroid cancer is directly related to the action of the sodium-iodide symporter, NIS. In well-differentiated malignancies with functioning NIS, I is concentrated within the gland at doses that ensure the destruction of any residual thyroid tissue. However, in tumours that show a lesser degree of differentiation, NIS is less active and the tumour cells therefore less susceptible to treatment. It is these cancers that are not only most likely to recur, but also less amenable to secondary treatments.

1.2.5.4 TSH suppression

In order to minimalise the risk of recurrence, most patients will require TSH suppression, regardless of initial surgical option or whether they have received I. By administering exogenous T4, the hypothalamic-pituitary-thyroid axis is supressed, thereby reducing TSH secretion from the anterior pituitary gland. This ensures that any remaining thyroid tissue is receiving little or no activating stimulus, therefore reducing the likelihood of further tumour growth. For most patients, doses of levothyroxine will be tailored to achieve a

serum TSH of less than 0.1 mIU/L, however for lower risk patients a measurable level below the reference range (i.e. 0.1 – 0.5 mIU/L) may be maintained with no increase in risk of recurrence.

1.2.6 Prognosis

The prognosis of appropriately managed DTC is favourable, with many patients being classed as "cured". Unfortunately, cancers have been known to recur many years following treatment and therefore lifelong surveillance is mandatory.

1.2.6.1 Recurrence

The American Thyroid Association stratifies patients into low, intermediate and high risk of recurrence (Table 1.6). Despite the generally good prognosis, the overall recurrence rate for DTC is 30 % at 30 years (Mazzaferri and Jhiang 1994), although this risk may be reduced by radioiodine ablation, TSH suppression and prophylactic central neck dissection (McLeod et al. 2013).

Low risk	Intermediate risk	High risk
• No metastatic spread (local/distant) • Full macroscopic resection • No locoregional invasion • Non-aggressive histology • No I uptake outside of the thyroid bed	• Microscopic invasion into perithyroidal soft tissues • Cervical lymph node metastases • Aggressive histology • Uptake of I outside of the thyroid bed	• Macroscopic tumour invasion • Incomplete resection • Distant metastases • Increase thyroglobulin out of proportion to post-treatment scan

Table 1.6 Factors influencing risk of recurrence (Cooper et al. 2009).

Recurrence is most often in the thyroid bed, although the exact cause is often unknown. Factors associated with recurrence include extra-thyroidal extension of the primary tumour, bulky nodal metastatic lesions, macroscopic local invasion, and aggressive histologic subtypes; inadequate primary surgery may also contribute (Shaha 2012). Although recurrent

DTC are less radioiodine avid than primary tumours, there is still a role for radioiodine, especially in combination with surgery, either as a pre-operative debulking tool or a post-operative ablative technique. Metastases are most common in the neck, either in the central and lateral compartment; distant metastases occur predominantly in the lung or bones (79 %) (Jin et al. 2013).

1.2.6.2 Mortality

The 5 year survival for thyroid cancer is 98.9 % below the age of 65 years, although this drops to 91.1 % after this; the mortality rate has risen slightly over the last 15 years in the USA from 0.44 to 0.51 per 100,000 per year (Howlader N 2012). The reason behind the relatively stable mortality rate despite the rising incidence is that DTC is being diagnosed much earlier, allowing more successful treatment. There are, however, a significant cohort of patients for whom the diagnosis is made after disease progression, and it is in this group that the majority of the early mortality (less than 5 years from diagnosis) occurs. Late mortality is often due to an increased aggressiveness, difficulty in resection and lack of response to adjuvant therapies of recurrent tumours.

1.3 The molecular basis of thyroid cancer

1.3.1 Oncogenes and thyroid cancer

Most malignant thyroid tumours are monoclonal in origin, meaning that genetic alterations in a single cell within an otherwise healthy thyroid gland are responsible for the disease. These alterations may reflect activating mutations of oncogenes or inactivation of tumour suppressor genes.

1.3.1.1 Mitogen-Activated Protein Kinase Pathway

The MAPK pathway, also known as the RAS-RAF-MEK-ERK pathway, is an important cascade that allows signalling from a cell surface receptor to trigger nuclear transcription, and thereby govern key cellular events (Figure 1.4).

Uncontrolled activation of the pathway is a feature of many cancers and this is often brought about by mutation of its constituent kinases. These mutually exclusive mutations are found in approximately 75 % of PTCs and 70 % of FTCs (Figure 1.5) (Bhaijee and Nikiforov 2011).

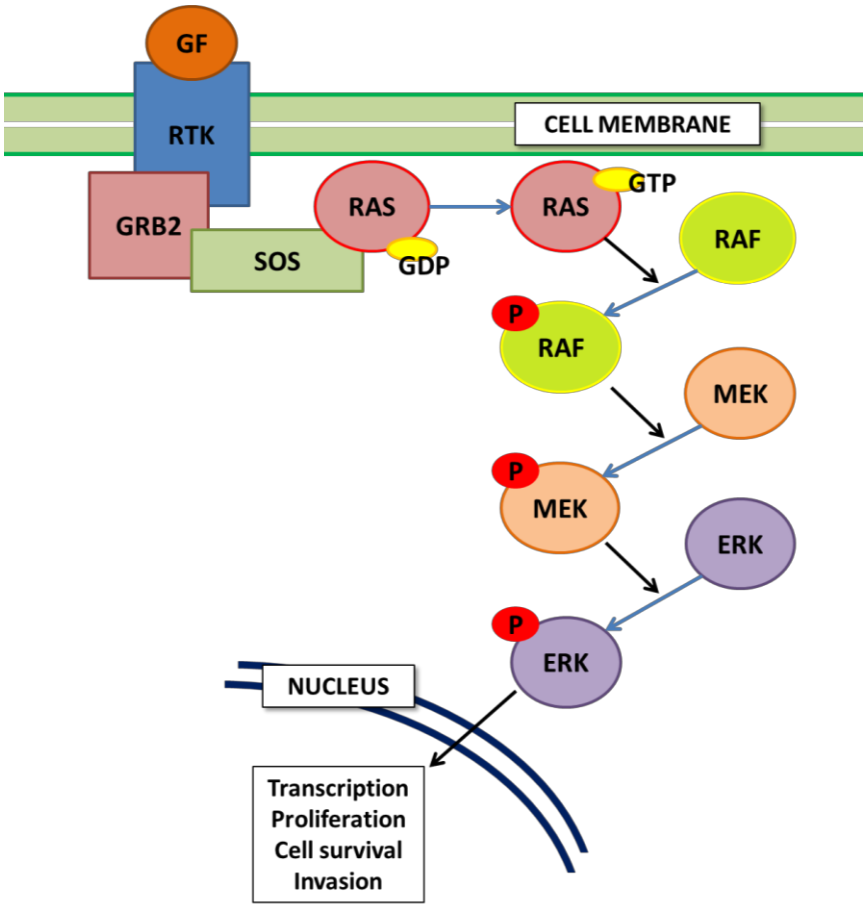

Figure 1.4 The Mitogen Activated Protein Kinase pathway. Binding of a growth factor (GF) to a receptor tyrosine kinase (RTK) leads to the subsequent interaction with Growth Factor Receptor Bound protein (GRB) 2 via its SH3 site. GRB2 then binds Son of Sevenless (SOS), which facilitates a guanine exchange, converting RAS-GDP to RAS-GTP. This triggers a cascade of phosphorylation reactions culminating in a number of key nuclear events.

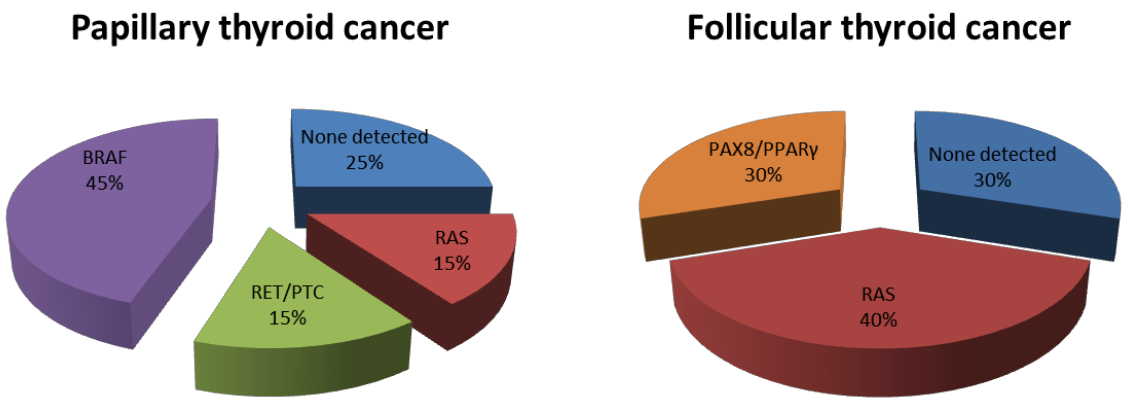

Figure 1.5 Frequency of genetic mutations in papillary and follicular thyroid cancer (Bhaijee and Nikiforov 2011).

1.3.1.2 Point mutations

1.3.1.2.1 BRAF

There are 3 *RAF* genes - *A*, *B* and *C* – the corresponding proteins of which are serine/threonine kinases. *BRAF* mutations have been identified in many human cancers (Davies et al. 2002), the commonest of which is the point mutation T1799A, which leads to the amino acid change V600E. This leads to oncogenic activation of the BRAF kinase. *BRAF* mutation occurs in 44 % of PTC and 24 % of papillary derived ATC, but does not occur in FTC, MTC or benign thyroid disease such as thyroid adenomas or hyperplasia (Xing 2005). PTCs displaying the *BRAF* mutation are more aggressive, showing lymph node spread, extra-thyroidal invasion, distant metastases (Xing 2007) (Table 1.7) and loss of radioiodine avidity (Xing et al. 2005).

Clinicopathologic characteristic	**Odds Ratio with *BRAF* mutation (95% confidence interval)**
Lymph node metastases	1.83 (1.58-2.13)
Extra-thyroidal invasion	2.50 (2.11-2.97)
Disease stage III or IV	2.14 (1.79-2.56)

Table 1.7 Association of BRAF mutation with the most aggressive characteristics of PTC (Xing 2007).

Recurrence is also more likely in the presence of *BRAF* mutation (odds ratio 2.65, $p < 0.001$ (Xing 2007)) and is associated with a reduced disease free survival (Figure 1.6) (Kim et al. 2006). The increased recurrence rates are valid even when taking into account the poor prognostic factors detailed above.

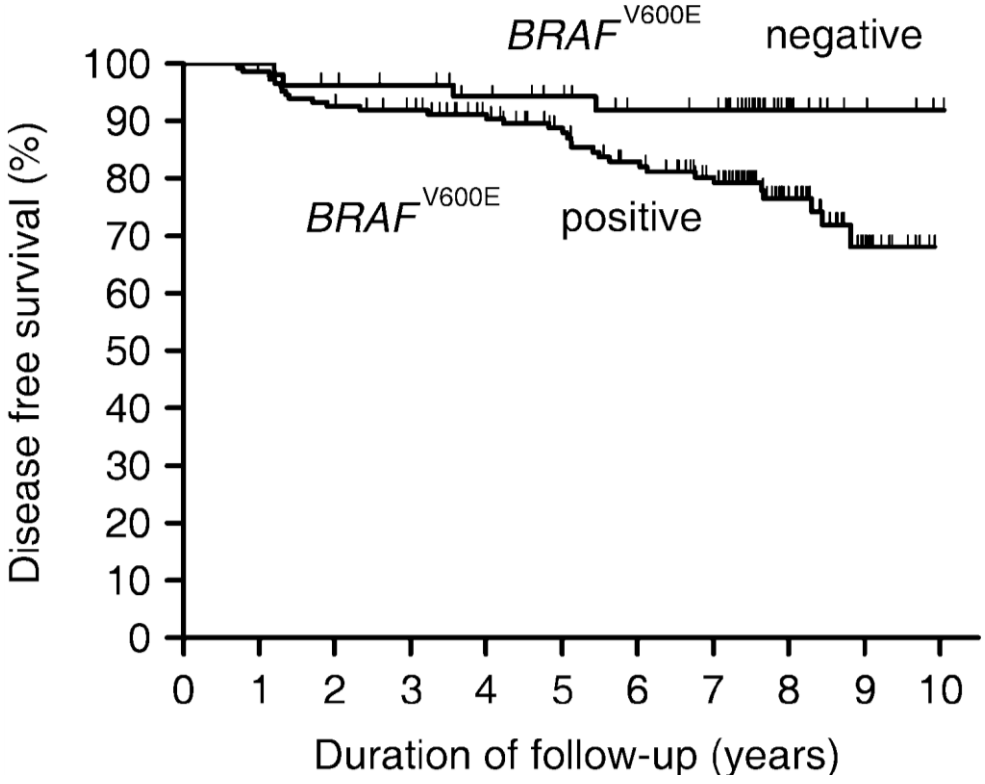

Figure 1.6 Disease free survival from time of diagnosis of thyroid cancer, depending on BRAF mutation status, taken from Kim et al. 2006.

In vivo work also confirms that $BRAF^{V600E}$ induces thyroid enlargement and PTC, with one study of transgenic mice expressing this mutation demonstrating carcinomas in 14 of 15 mice by 12 weeks, most with an aggressive phenotype (Knauf et al. 2005). Further work has suggested that TSH plays a key role in inducing $BRAF^{V600E}$ PTC, with oncogenic BRAF knock-in mice requiring the TSH receptor in order to transform thyroid follicular cells (Franco et al. 2011).

This link between *BRAF* mutation and aggressiveness of tumour phenotype has prompted research into both the therapeutic significance and diagnostic and prognostic value of the mutation. Using siRNA, *BRAF* knockdown in human ATC cell lines *in vitro* reduced the phosphorylation of downstream proteins in the MAPK cascade as well as significantly reducing their growth. This was then replicated using BAY 43-9006, a small molecule RAF kinase inhibitor (Salvatore et al. 2006), thus demonstrating that these compounds may be effective in treatment for ATC containing the $BRAF^{V600E}$ mutation. For diagnostic purposes, Xing et al used both direct DNA sequencing and a colorimetric mutation detection method to identify the $BRAF^{V600E}$ mutation in pre-operative FNAC samples from patients undergoing thyroidectomy for nodular thyroid disease (Xing et al. 2004). Of those patients with a final diagnosis of PTC, 50 % were positive for $BRAF^{V600E}$, whereas no patients with other malignancies or benign thyroid disease harboured the mutation. While this would not be useful for those patients in whom a follicular neoplasm is suspected (see Section 1.2.4), it may aid the planning of the extent of surgery in patients with a possible or confirmed diagnosis of PTC. Yip *et al* compared 106 BRAF-positive to 100 BRAF-negative PTC patients, the majority of which were identified post-operatively. Significantly more of the former group required further surgery for persistent/recurrent disease ($p = 0.04$), with the

authors suggesting that had the BRAF status been known pre-operatively, 24 % of patients would have had more extensive surgery at initial operation (Yip et al. 2009).

1.3.1.2.2 RAS

The RAS proteins are another family involved in cell growth and proliferation. Named after the "Rat sarcoma" virus, they were first discovered as proteins encoded by retroviral oncogenes. Subsequently, these were shown to be constitutively activated by point mutations. The RAS family are GTP-binding proteins, with different subsets controlling different aspects of cell behaviour. RAS carries out its normal functions when localised to the cytosolic surface of the cell membrane, and is involved in the MAPK cascade (see Figure 1.4). Inactive RAS is bound to guanosine diphosphate (GDP) and is converted to the active, GTP bound protein, by guanine nucleotide exchange factors, two of the most studied of which are Son of Sevenless (SOS) 1 and 2. Following the activation of receptor tyrosine kinases, GRB2 binds via its SH2 domain to the TKR and then via its SH3 domain to SOS1/2. This brings SOS1/2 into proximity with RAS and via nucleotide exchange brings about the conversion of GDP to GTP. Activated RAS then continues to signal downstream via the MAPK pathway.

Approximately 20 % of malignancies involve a mutation in one of the *RAS* genes (Bos 1989). The three *RAS* genes most frequently involved in human tumour formation are *HRAS*, *KRAS* and *NRAS*, with point mutations in codons 12, 13 or 61 leading to aberrant activation and uncontrolled stimulation of the cellular proliferation pathways. *RAS* mutations are found in both papillary and follicular thyroid cancers, although are more common in FTC. However, mutations are also found in almost 50 % of follicular adenomas (Nikiforova et al. 2003); in both carcinomas and adenomas the predominant mutation is in *NRAS* codon 61. This implies that RAS activation alone is insufficient to cause malignancy, but does sensitise the tumour to other genetic alterations. The high prevalence of *RAS* mutations in follicular adenomas may

also suggest that these tumours are not completely benign, but may represent a pre-cancerous stage in FTC development. A study of poorly-differentiated thyroid cancers reported that in a cohort of 65 patients, *NRAS* codon 61 mutations were the most common genetic alteration present (15/65, 23 %). This was in contrast to the PTC "markers": *BRAF* mutations (1/65, < 1 %), *PAX8*/*PPARγ* translocation (0/65, 0 %) and *RET*/*PTC* re-arrangement (0/65, 0 %) (Volante et al. 2009). The authors suggest that these findings indicate that *RAS* mutation is a key step in the progression to poorly-differentiated thyroid cancer, more so than the other well recognised mutations. However, in their cohort there were 49 patients in whom none of the above mutations was identified. This implies that their testing was limited, and that wider screening may identify an oncogene that is more important, and that again *RAS* mutation is merely acting as a sensitising precursor to progression.

Studies examining the RAS pathway as a therapeutic target in the treatment of cancer are on-going. Farnesyltransferase (FTase) adds the 15-carbon isoprenoid group to the C terminal of RAS, thus ensuring its localisation to the plasma membrane, and was therefore an obvious target for inhibition. Unfortunately, due to the ability of other transferases to modify RAS, inhibition of FTase alone did not result in an inhibition of tumour growth. However, when used in combination with the EGFR inhibitor Gefitinib, the FTase inhibitor Tipifarnib reduced the viability of C-643 cells (thyroid follicular cells with *HRAS* point mutations at codons 12 and 61), with a corresponding reduction in the phosphorylation of the downstream effector ERK (Frasca et al. 2013). As the majority of *RAS* mutations in thyroid tumours involve *KRAS* and *NRAS*, with only a few involving *HRAS*, the clinical relevance of this observation may be small.

1.3.1.3 Rearrangements

1.3.1.3.1 RET/PTC

RET (REarranged during Transfection) is a proto-oncogene located on chromosome 10q11.2 that encodes a receptor tyrosine kinase (RTK), which acts as a receptor for the glial cell line-derived neurotrophic factor (GDNF) family of ligands (GFLs). GFLs are involved in cell survival, differentiation and migration and specifically in neurite outgrowth. Alteration in *RET* can lead to thyroid cancers in 2 different ways. As wild-type RET in the thyroid gland is predominantly found in parafollicular C cells, it follows that activating mutations will result in C cell hyperplasia and ultimately medullary thyroid cancer (MTC). Indeed, point mutation in exon 16 is found in 95 % of patients with Multiple Endocrine Neoplasia type 2B (MEN 2B), of which MTC is a feature (Martucciello et al. 2012). The second mechanism is via chromosomal re-arrangement. Wild type RET harbours an extracellular, transmembrane, and intracellular tyrosine kinase domain. In *RET/PTC* rearrangements, chromosomal translocations in intron 11 fuse the kinase domain with an activating gene. There are three major types of RET rearrangement; RET/PTC1 and 3 are paracentric inversions involving another gene on chromosome 10q while RET/PTC2 is between chromosomes 10 and 17. An additional 8 rearrangements have been described, most of which are associated with radiation exposure (Table 1.8).

Name	Activating gene	Location
RET/PTC1	H4	10q21
RET/PTC2	RIα	17q23
RET/PTC3	ELE1	10q11.2
RET/PTC4	ELE1 (different breakpoint)	10q11.2
RET/PTC5	GOLGA5	14q
RET/PTC6	HTIF1	7q32
RET/PTC7	RFG7	1p13
RET/PTC8	KTN1	14q22.1
RET/ELKS	ELKS	12p13
RET/RFG8	RFG8	18q21-22
RET/PCM-1	PCM-1	8p21-22

Table 1.8 The range of described RET rearrangements, with corresponding activating gene and its chromosomal location (Nikiforov 2002).

As these re-arrangements are lacking the transmembrane domain of RET, the protein product can be located in different subcellular locations, and therefore can produce different effects. Of the three main re-arrangements, thyroidal over-expression of RET/PTC1 and 3 in mice has been shown to result in papillary thyroid cancer formation (Santoro et al. 1996; Powell et al. 1998). The prevalence of RET/PTC varies widely by location and this is compounded by differences in testing measures. In Caucasian adults and children with no history of radiation exposure, the prevalence of RET/PTC in papillary thyroid carcinomas is around 35 %, with RET/PTC1 being the most common. Both RET/PTC1 and 3 are present in PTCs associated with radiation exposure after the Chernobyl disaster (22 % and 13 % of tumours respectively (Leeman-Neill et al. 2013)). RET/PTC3 containing cancers are more likely to develop early than RET/PTC1, and are associated with more aggressive clinical behaviour (Ciampi and Nikiforov 2007).

Numerous strategies have been implemented to use RET as a therapeutic target, not just in thyroid cancer but in tumourigenesis in general. These have been developed to target different steps in the RET pathway, from ligand binding to recruitment of adaptor proteins (de Groot et al. 2006), but none are yet in clinical use.

1.3.1.3.2 PAX8/PPARγ

The Paired Box Gene 8 (PAX8) / Peroxisome proliferator-activated receptor gamma (PPARγ) fusion protein is brought about by a translocation between chromosomes 2 and 3 (t(2;3)(q13;p25)). It was identified first in 5 of 8 follicular thyroid cancers (Kroll et al. 2000), and the prevalence is thought to be approximately 20 – 60 % in FTC (Dwight et al. 2003; Bhaijee and Nikiforov 2011). The prevalence of the translocation in follicular adenoma is contentious, with reports ranging from 0 – 4 % (Nikiforova et al. 2002; French et al. 2003; Nikiforova et al. 2003; Hibi et al. 2004), although these tumours may represent pre-malignant FTCs, merely lacking capsular or vascular invasion (Dwight et al. 2003). FTCs expressing the PAX8/PPARγ fusion tend to affect younger patients, be smaller in size, and exhibit more vascular invasion compared to those without (French et al. 2003; Nikiforova et al. 2003). It is found in a small number of PTCs, possibly linked to radiation exposure (Leeman-Neill et al. 2013).

Given that PAX8/PPARγ is relatively specific to FTC, testing fine needle aspiration cytology specimens for the re-arrangement, with the aim of differentiating those patients with benign and malignant follicular lesions, has been attempted, with mixed results (Ferraz et al. 2012; Pauzar et al. 2012). While the absence of the re-arrangement does not denote benign disease, the presence indicates a much higher probability of malignancy, or at least atypical follicular adenoma, and therefore this strategy may prove useful in the future when deciding which patients should receive radical, as opposed to diagnostic, surgery.

As a therapeutic target, both PAX8 and PPARγ have shown promise, although the aim is restoration of function rather than inhibition as both proteins increase the degree of differentiation of thyroid follicular cells. In K1 and F133 thyroid cell lines, transfection with *PAX8* significantly increased ^{125}I uptake and reduced cell survival after radioiodine therapy (Mu et al. 2012). Treatment with PPARγ agonists increases anaplastic thyroid cancer differentiation *in vivo* (Aiello et al. 2006), and murine studies also support a potential *in vivo* application (Dobson et al. 2011)

1.3.1.3.3 TRK

TRK oncogenes are the result of mutation of the *NTRK1* gene. This encodes the neurotrophic tyrosine kinase receptor type 1 (TRK1), a receptor for nerve growth factor, NGF (Kaplan et al. 1991). This plays a role in cell differentiation and sensory neuronal pathway development, as well as proliferation of keratinocytes and lymphocytes (Di Marco et al. 1993). The oncogenes are the result of activating translocations and are associated with papillary thyroid cancer. There are 4 described re-arrangements, the most common of which is the fusion between *NTRK1* and *TPM3* (Greco et al. 2010).

Transgenic mice with the *Trk-T1* oncogene under the control of the thyroglobulin promoter have been shown to develop hyperplasia and papillary carcinoma at a young age (4 and 6 of 26 mice respectively under 7 months of age), with 100 % of older mice having either hyperplasia or PTC (2 and 7 of 9 mice) (Russell et al. 2000). Unfortunately this study did not comment on the frequency of disease in wild type mice. However, another group examined the effect on the thyroid when the *Trk-T1* mouse was crossed with the p27-null mouse strain (Fedele et al. 2009), which develop multi-organ hyperplasia, lung/GIT/gonadal tumours but no thyroid tumours (Fero et al. 1996). An increase in the percentage of papillary thyroid

carcinomas in both the p27 -/- and p27 +/- genotypes was observed, with a shorter latency period, when compared to wild type mice (Figure 1.7).

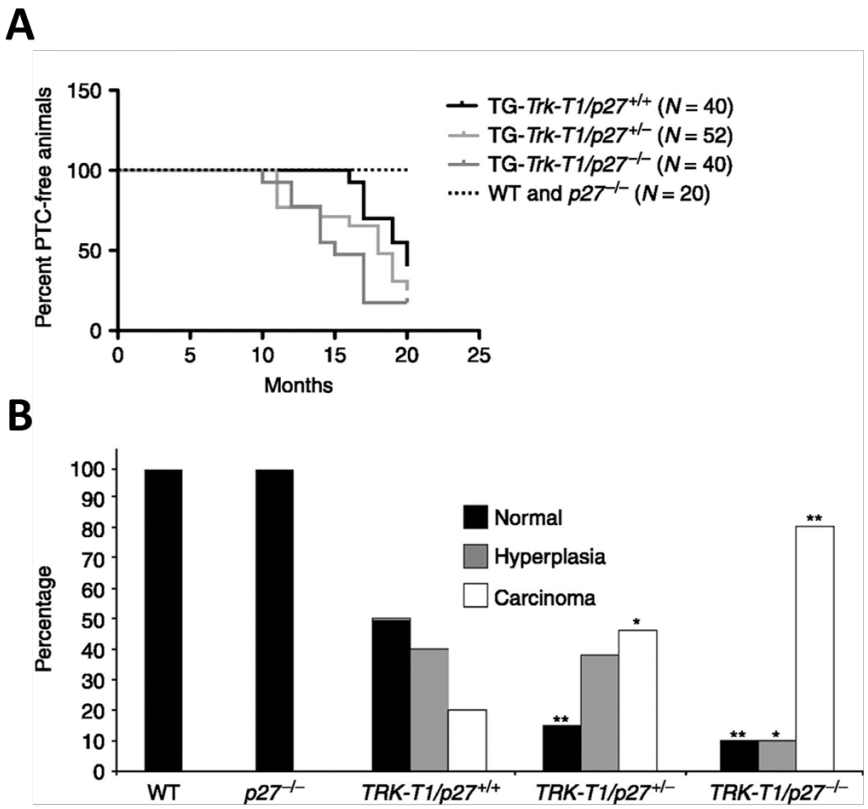

Figure 1.7 Trk-T1 mice are more prone to PTC, an effect enhanced by p27 knockout. A - Kaplan Meier analysis of latency period for developing PTC in Trk-T1 mice with variation in p27 genotype. p27 knockout reduces the latency period for developing PTC. B – The percentage of Trk-T1 mice developing PTC is incrementally higher for p27 heterozygotes and knockouts compared to wild type. Taken from (Fedele et al. 2009).

Numerous studies have examined *NTRK1* mutations in cohorts of patients with papillary thyroid cancer, with the reported prevalence varying depending on the population studied; however, the commonly accepted figure is in the region of 12 % (Beimfohr et al. 1999; Bounacer et al. 2000; Brzezianska et al. 2006; Greco et al. 2010). Unlike *RET*/*PTC*, there is no association with either environmental (e.g. Chernobyl) or therapeutic radiation exposure (Beimfohr et al. 1999; Bounacer et al. 2000).

There are no effective therapies targeting this gene in the treatment of thyroid cancer, and there is less focus on their development, likely due to the lower frequency at which it is found in both sporadic and radiation induced PTC when compared to *RET*/*PTC*. Studies have investigated the potential of *NTRK1* mutation testing to improve the detection of malignancy in thyroid nodule aspirates (Sapio et al. 2007; Cantara et al. 2010). While valid in theory, these have not translated into a clinical use due to zero pick up rate of the mutation in patient cohorts studied.

1.3.1.4 p53

In contrast to many other solid organ malignancies, the tumour suppressor gene *p53* is rarely mutated in well-differentiated thyroid cancer. It is, however, frequently mutated in poorly differentiated and undifferentiated (anaplastic) thyroid cancer (Donghi et al. 1993; Fagin et al. 1993). This loss of p53 function is thought to be a trigger of progression from well- to poorly-differentiated carcinoma (Nikiforov 2004) (especially if co-existing with a mutation such as *RET*/*PTC* (Quiros et al. 2005)). Reports are conflicted as to whether re-introduction of p53 into *p53*-mutant cells is able to rescue the phenotype (Moretti et al. 1997; Blagosklonny et al. 1998), and if not this suggests that other factors continue to drive tumour growth once de-differentiation has occurred.

1.3.1.5 PTEN

PTEN is a protein phosphatase and acts as a tumour suppressor by inhibiting the AKT/PI3K pathway. It dephosphorylates PIP3, an upstream effector in the pathway, thus preventing AKT induced cell growth and proliferation (Chu and Tarnawski 2004). Loss of PTEN function is associated with a wide range of human malignancies, including follicular thyroid cancer. A thyroid specific *Pten* knockout mouse model (*Pten* -/-) develops follicular adenomas by 10 months of age (Yeager et al. 2007), and when followed up half of all females

developed invasive follicular carcinomas, while the remainder had either follicular adenomas or hyperplasia (Antico-Arciuch et al. 2010). Methylation, and associated inactivation, of *PTEN* is linked with greater degrees of de-differentiation in human thyroid tumours (Hou et al. 2008), thus implicating PTEN in the progression of thyroid tumours.

1.4 PTTG-Binding Factor (PBF)

1.4.1 Physiology

PBF was first identified as a binding partner of the pituitary tumor transforming gene, PTTG (Chien and Pei 2000). PTTG acts as a securin, inhibiting separase activity and thus preventing sister chromatid separation during mitosis (Zou et al, 1999). PTTG stimulates expression of fibroblast growth factor 2 (FGF2) and vascular endothelial growth factor (VEGF) (McCabe et al. 2002). Given these functions, and that PTTG is involved in DNA repair mechanisms (Kim et al. 2005), it is unsurprising that PTTG over-expression has been described in several solid organ tumours, including thyroid cancer (Kim et al. 2005).

In order to determine the mechanism of PTTG action, yeast 2-hybrid assays were performed to identify potential binding partners, with PBF as one of the results (Chien and Pei 2000). In subsequent studies, it was established that PBF was a ubiquitously expressed 180 amino acid protein, with a mass of 22 kDa. *PBF* was subsequently matched to a previously cloned gene, *C21orf3*, located on the long arm of chromosome 22 at 22q22.3 (Yaspo et al. 1998). Although there is no significant homology with other human proteins, PBF is highly conserved across species (Figure 1.8). This implies not only a specific and unique function but also an evolutionary importance.

```
1   MAPGVARGPTPYWRLRLGGAALLLLLIPV-------AAAQEPPGAACSQNTNKTCEECLK  53  HUMAN
1   MASSGVRGPTPRWGPTLGSAALFLLLLPA-------AAAQ-----GCSQNTSRTCEECLK  48  BOVINE
1   -MAPANLGLTPHWVMLLGA--VLLLLLSG-------ASAQEPPRVGCSEYTNRSCEECLR  50  MOUSE
1   --------MMGKWAELPGTVALLLMLSLGMAGGSYTSAPVPPVTAACSFYSGRSCEECLK  52  FROG
1   ----------------------------MTEAFLATATPPAPAQACSEFSQRSCEECLR  31  CHICKEN

54  NVSCLWCNTNKACLDYPVTSVLPPASLCKLSSARWGVCWVNFEALIITMSVVGGTLLLGI  113 HUMAN
49  NVSCLWCNANKMCLDYPVTKVLPPSSLCRLSSARWGVCWVNFEALIIAMSVIGGSLLLGV  108 BOVINE
51  NVSCLWCNENKACMDYPVRKILPPASLCKLSSARWGVCWVNFEALIITMSVLGGSVLLGI  110 MOUSE
53  NVSCFWCITNNTCLDYPVRNILPPSSLCAMSAARWGACWINFEALIITISVVLGLILLST  112 FROG
32  NVSCLWCFTNNTCIDYPVRSILPPSSLCSLSNARWGVCWINFEALIITIAVIAGIILVSI  91  CHICKEN

114 AICCCCCCRRKR----SRKPDRSEEKAMREREERRIRQEERRAEMKTRHDEIRKKYGLFK  169 HUMAN
109 AICCCCCCRRSR----SRRPDKSEEKAIREREERRVRQEERRVEMKLRHDEIRKKYGLFK  164 BOVINE
111 TVCCCYCCRRKK----SRKPDKSDERAMREQEERRVRQEERRAEMKSRHDEIRKKYGLFK  166 MOUSE
113 TVCCCYCCYCRKRSNSLMRLEAEEENLMRERERRKQEALQRKNERTVKHNEIRKKYGLLQ  172 FROG
92  AVCCCYCCYCRRRFKS--RPDEEEEQLARKREERRLQSLQRKHERKQKHDEIRKKYGLLQ  149 CHICKEN

170 E-ENPYARFENN  180 HUMAN
165 E-ENPYARFENN  175 BOVINE
167 E-QNPYEKF---  174 MOUSE
173 DMDHPYSRYENE  184 FROG
150 ESDNPYSRFENE  161 CHICKEN
```

Figure 1.8 Amino acid sequence of PBF, demonstrating high conservation across species.

1.4.1.1 Structure

PBF is a type 1a transmembrane glycoprotein which, although thus far poorly characterised, has several putative functional domains (Figure 1.9). The N-terminal contains a 32 amino acid signal peptide region, within which exists a leucine rich putative nuclear export signal (la Cour et al. 2004). Between residues 40 and 95 is a plexin-semaphorin-integrin (PSI) domain. Typically, PSI domains consist of 8 cysteine residues in an approximately 50 amino acid section, between which disulphide bonds exist (usually between cysteines 2-4, 3-8, 5-7, and occasionally 1-6) (Bork et al. 1999). PSI domains are usually extracellular and involved in protein-protein interaction and cellular signalling (Bork et al. 1999; Kozlov et al. 2004). There then follows a transmembrane domain (residues 95 to 122).

Towards the C-terminal, there is a bipartate nuclear localisation signal and further sorting signal. This NLS plays a role in the translocation of PTTG into the nucleus; without this region PTTG is unable to regulate FGF-2 (Chien and Pei 2000).

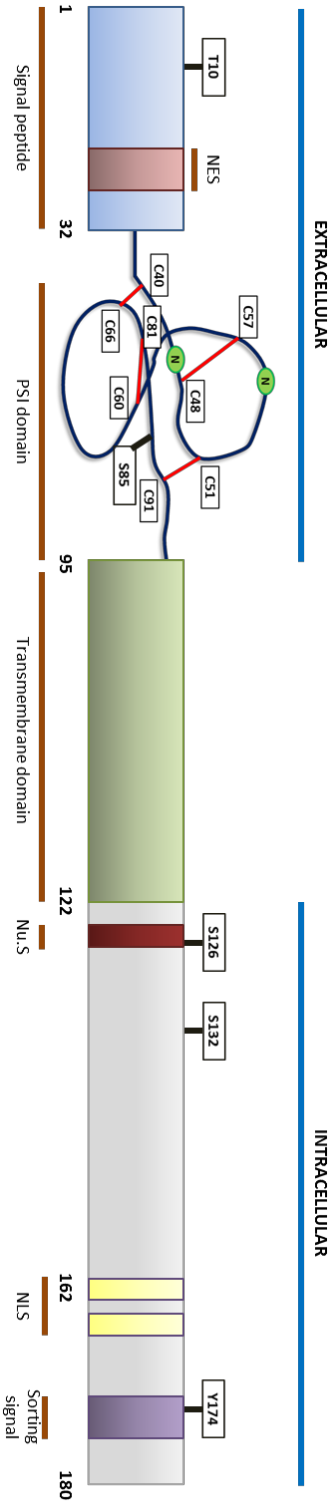

Figure 1.9 Putative structure of PBF. PBF contains an N terminal extracellular signal peptide with nuclear export signal (NES), alongside a cysteine rich region PSI domain, with di-sulphide bonds represented by red lines. The C-terminus contains a nuclear localisation signal and sorting signal and is necessary for the interaction with PTTG. A putative nucleolus signal (Nu.S) is also present in the intra-cellular region.

1.4.1.2 Expression and regulation

PBF is ubiquitously expressed in normal tissues (Yaspo et al. 1998; Chien and Pei 2000). The mechanism of its regulation is not yet understood; PTTG over-expression results in an increase in PBF mRNA (Stratford et al. 2005), although neither EGFR or TGF-α affected expression *in vitro* despite causing an increase in PTTG levels (Vlotides et al. 2006). The PBF promoter contains a variable number of oestrogen response elements (ERE), with oestrogen receptor α (ERα) binding to the promoter (Watkins et al. 2010). In MCF-7 breast cancer cells, treatment with both diethylstilbestrol and 17β-estradiol induced PBF mRNA and protein expression (Watkins et al. 2010). The *PBF* promoter was also identified as a transcriptional target for Runx2 during a differential hybridisation screen (Stock et al. 2004). PBF was up-regulated in Runx2-expressing cells, and the *PBF* promoter bound Runx2, with transactivation in MC3T3-El cells.

More recently, work on micro-RNAs in liver disease has shown that miR-122 may effect PBF expression (Li et al. 2013). Micro-RNAs are small segments of non-coding RNA which interact with complementary regions of a target mRNA, with subsequent repression of function (Krol et al. 2010); the group identified a predicted miR-122 complementary site in the 3'-untranslated region (UTR) of PBF, with repression of expression of GFP labelled PBF after treatment with miR-122 (Li et al. 2013).

1.4.1.3 Function and subcellular localisation

Despite the evidence for functional domains within the protein structure of PBF, the precise function of the protein is largely unknown beyond its interaction with PTTG. This interaction occurs at the C-terminus, allowing the nuclear translocation of PTTG (which does not contain an NLS) and facilitating the role of PTTG as a securin, and also a transcriptional activator of FGF-2. Both PTTG and PBF are required for the transactivation of FGF-2, with

expression of each alone having no effect on the FGF-2 promoter (Chien and Pei 2000). In addition to this nuclear localisation of PBF, it has also been identified in intracellular vesicles, where it co-localised with the late endosomal marker CD63, while a C-terminal deletion mutant accumulates at the cell membrane (Smith et al. 2009).

1.4.1.4 Post-translational modifications

Although still relatively poorly characterised, there are a number of residues in the PBF amino acid sequence that are likely sites of post-translational modification (PTM).

1.4.1.4.1 Glycosylation

Asparagine residues located at position 45 and 54 both fulfil the criteria for potential N-linked glycosylation sites. These are predicted when the local sequence reads Asp-Xaa-Ser/Thr, where Xaa is any amino acid except proline (Rao and Bernd 2010). For PBF, the consensus sequences are N-K-T (N45) and N-V-S (N54).

1.4.1.4.2 Phosphorylation

Phosphorylation is a key process in the regulation of function of many cellular processes and is carried out by kinases that have varying specificities for phosphorylation motifs. Phosphorylation prediction software highlights several potential sites for serine, threonine or tyrosine phosphorylation. These were identified using the NetPhos 2.0 Server from the Technical University of Denmark (available at http://www.cbs.dtu.dk/services/NetPhos/). Putative phosphotyrosine sites were identified at Y174, while phosphoserine/threonine sites were identified at S85, S126, S132 and T10 (Figure 1.10).

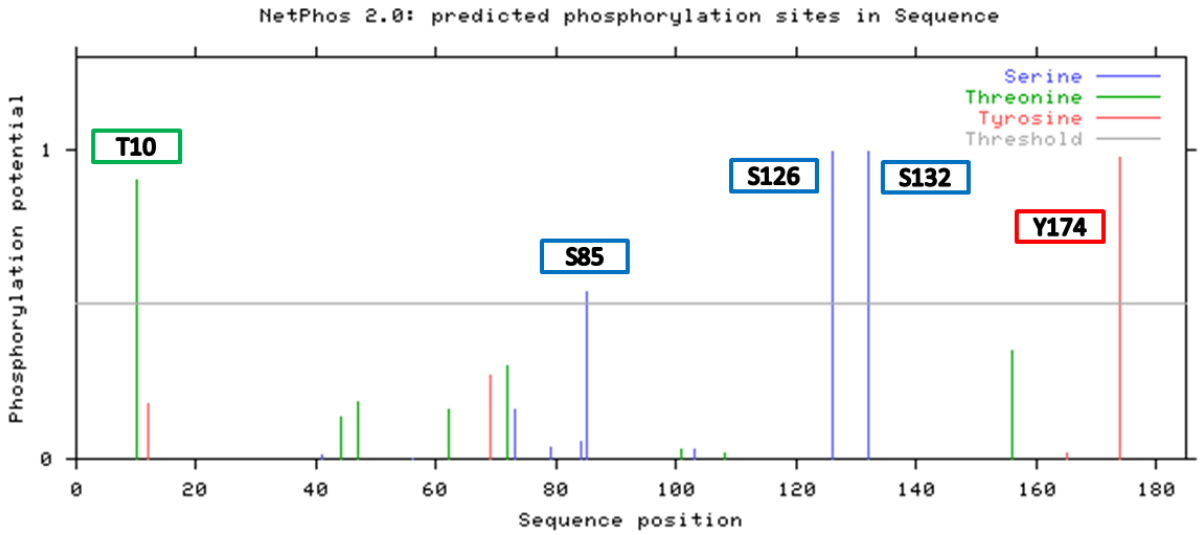

Figure 1.10 Predicted sites of serine, threonine and tyrosine phosphorylation within PBF. Scores are relative to 1, with a threshold set at 0.5 (from NetPhos 2.0, available at http://www.cbs.dtu.dk/services/NetPhos/).

Software is also available to predict which kinases may phosphorylate a given residue (e.g. www.phosphonet.ca).

1.4.1.4.3 SUMOylation

The Small Ubiquitin-Like Modifier (SUMO) protein, similar to ubiquitin, is covalently bound to many proteins with effects on their cellular function. PBF has one predicted SUMOylation site, at lysine 169 (Ren et al. 2009).

1.4.2 PBF in thyroid cancer

1.4.2.1 PBF has a significant role in thyroid cancer

The first description of the potential role of PBF in tumourigenesis identified increased levels of PBF mRNA in pituitary tumours compared to normal tissue, where a positive correlation was found between expression of PTTG and PBF in pituitary tumours (McCabe et al. 2003). A contemporaneous report described increased levels of PTTG and FGF-2 in follicular thyroid cancers compared to normal tissues, and suggested a potential role as

prognostic markers for the disease (Boelaert et al. 2003). This prompted investigation into the role of PBF in thyroid disease. PBF mRNA expression was 3.3 times higher in a cohort of differentiated thyroid cancers compared to normal controls, and multiple regression analysis demonstrated an independent association between PBF mRNA expression and early tumour recurrence (Figure 1.11 A and B) (Stratford et al. 2005). These findings have recently been confirmed, with high PBF expression identified in 61.4 % of differentiated thyroid cancers, which directly correlated with a reduced disease specific survival (Hsueh et al. 2013). To support the theory that PBF has an effect independent of PTTG expression, PBF over-expression in NIH3T3 cells (a standard fibroblast cell line (Todaro and Green 1963)) led to a 12-fold increase in colony formation compared to controls; additionally, the transforming effect of PTTG was shown to be dependent on an intact domain for binding PBF. *In vivo*, mice injected with NIH3T3 cells stably over-expressing PBF developed aggressive high grade invasive carcinomas (Figure 1.11 C) (Stratford et al. 2005).

These findings led to the further exploration of the role of PBF in the thyroid, in particular the mechanisms by which the above effects are mediated.

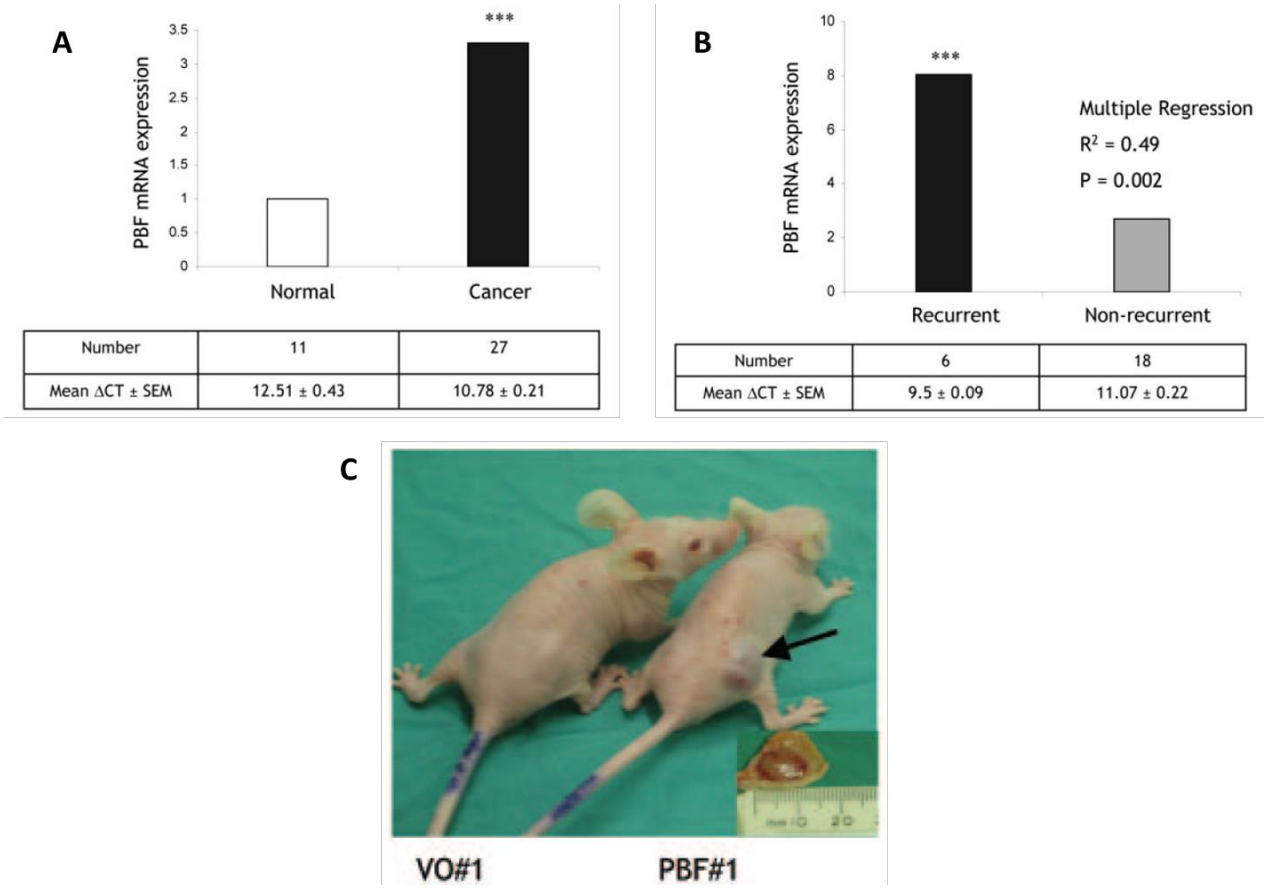

*Figure 1.11 A - PBF mRNA expression is significantly higher in thyroid cancer compared to normal thyroid tissue. B - Higher levels of PBF mRNA expression are associated with recurrent disease. C –Injection of NIH3T3 cells over-expressing PBF into nude mice induces tumour growth (black arrow) compared to controls (Stratford et al. 2005). *** = $p < 0.001$.*

1.4.2.2 Thyroidal effects of PBF *in vivo*

To further explore the role of PBF in thyroid disease, a transgenic mouse model exhibiting thyroid specific over-expression was generated (PBF-Tg) (Read et al. 2011). These mice over-expressed hemagglutinin (HA)-tagged PBF (PBF-HA) specifically in the thyroid gland. The HA tag is derived from the glycoprotein human influenza hemagglutinin, and is commonly used in molecular biology to facilitate protein detection. Thyroidal specific over-expression was achieved using the thyroglobulin promoter to drive PBF expression (Figure

1.12), thus ensuring that not only would PBF over-expression be limited to the thyroid, but that it would only be found in thyroid follicular cells.

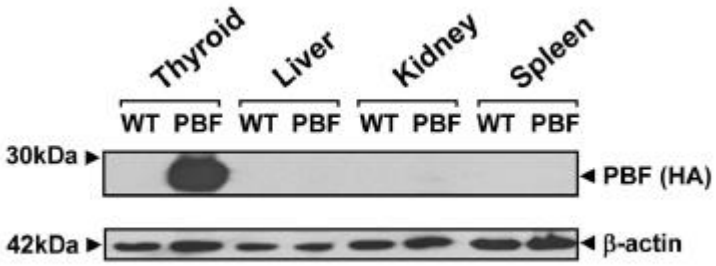

Figure 1.12 Western blot demonstrating thyroid specific over-expression of PBF-HA in the PBF-Tg mouse (Read et al. 2011).

The most characteristic phenotype of these mice was their significantly enlarged thyroid size. Compared to wild type littermates, the transgenic mice had thyroid glands 1.7 times heavier by week 7 and 3.2 times heavier by 52 weeks (Figure 1.13 A and B). In addition, the thyroids of the PBF-Tg mice were nodular and exhibited macro-follicles (Figure 1.13 C), suggesting that the over-expressed PBF may be altering the normal structural development of the thyroid. Another finding was that of both focal and nodular follicular hyperplasia. These lesions had large nuclei, and an increase in expression of phosphorylated AKT (a target of PI3 kinase (PI3K)) and cyclin D1 (a downstream proliferation marker) (Read et al. 2011). The PI3K pathway is a signalling cascade involved in cellular proliferation which is frequently dysregulated in cancer.

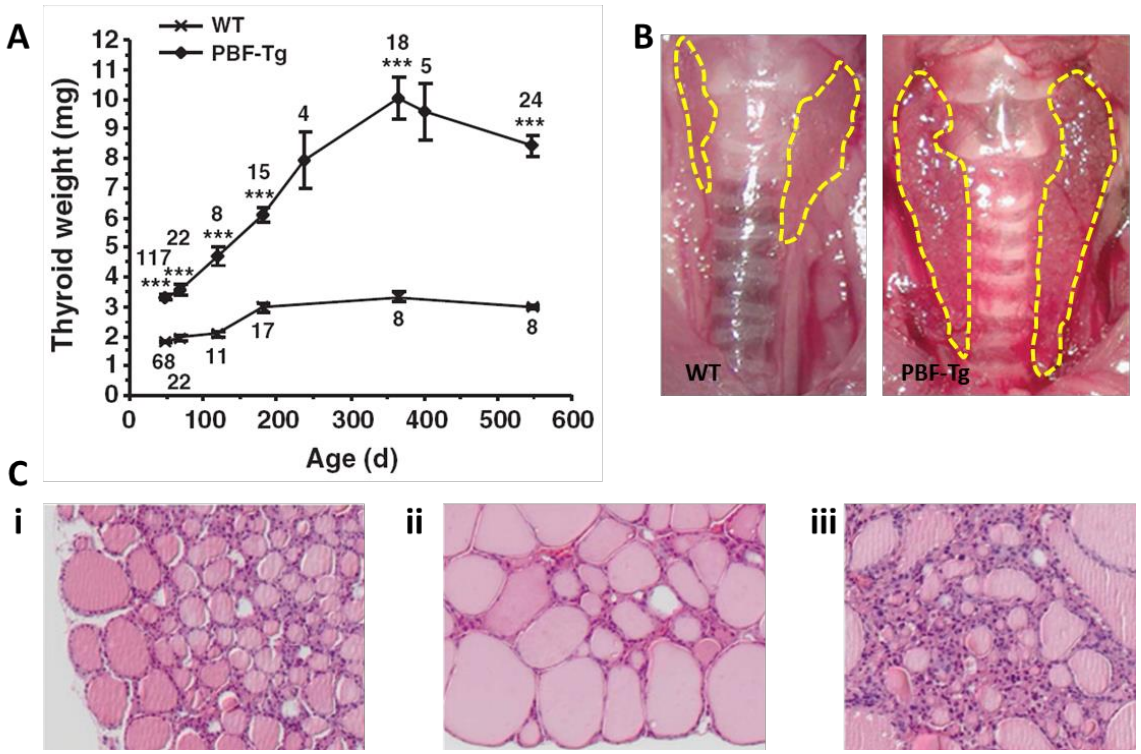

Figure 1.13 Thyroidal effects of PBF-HA over-expression. A - PBF-Tg mice developed significantly larger thyroid glands than their wild type (WT) litter mates. B- Representative image of thyroid glands from WT and PBF-Tg mice at 52 weeks (thyroid glands are outlined by dashed lines). C – H&E stained sections through mouse thyroid glands: Compared to WT (i), PBF-Tg mice developed macro-follicles (ii) and areas of hyperplasia (iii) (Read et al. 2011).

Given this phenotype, the potential impact of PBF on the thyroid hormone secretory pathway was investigated. PBF was found to sequester the thyroid hormone transporter MCT8 away from the plasma membrane and into the cell. Additionally, there was an increase in intra-thyroidal T3 and T4 levels (Smith et al. 2012). This did not, however, correspond to a difference in total serum T3 or T4, suggesting that although thyroidal MCT8 functional is repressed, there is compensation to maintain a steady state of thyroid hormone export. Subsequently, the hypothalamic-pituitary-thyroid negative feedback loop was not affected and there was no observed increase in serum TSH (Figure 1.14 A and B) (Read et al. 2011). There was, however, an increase in the expression of the TSH receptor (TSHR) (Figure 1.14 C) (Read et al. 2011) suggesting an increased responsiveness to TSH within the transgenic

thyroids, although from that it was not possible to say whether this was as a direct or indirect response to excess PBF and repressed MCT8 function. Interestingly, this increase in TSHR did not seem to have a functional effect. When the mice were administered 50 mU of TSH, the increase in serum T4 found in wild type was absent in the transgenic mice (Figure 1.14 D) (Smith et al. 2012).

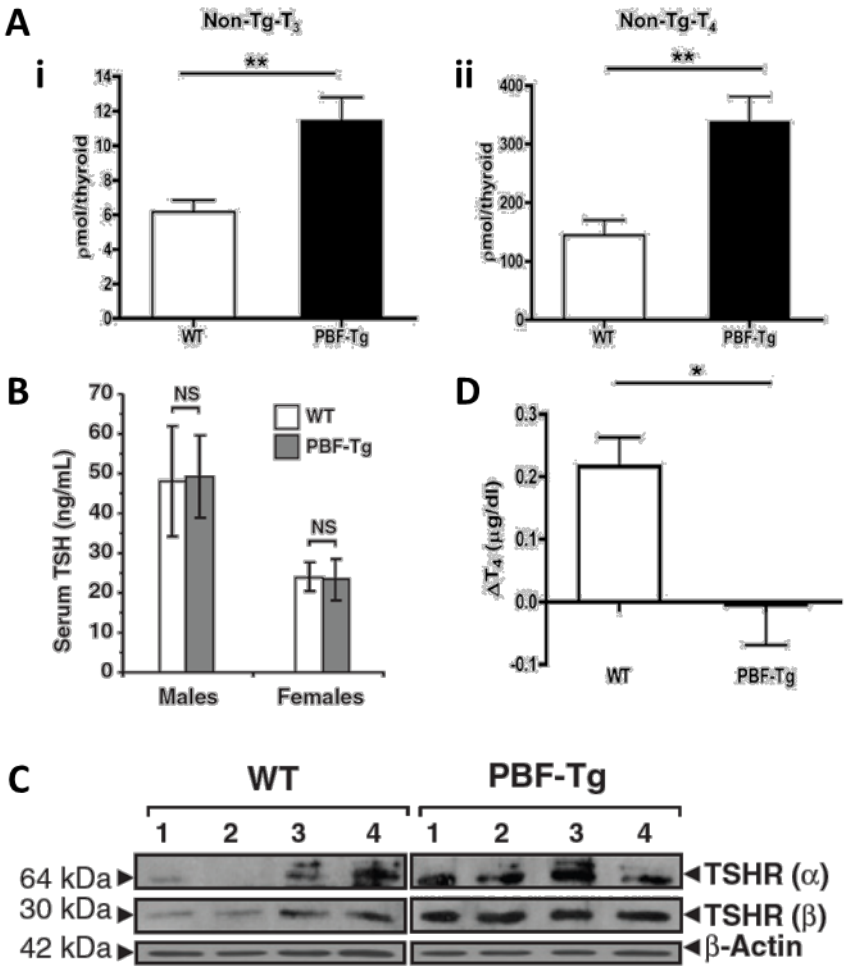

*Figure 1.14 Thyroid hormone profiles in the PBF-Tg mouse compared to WT. A - Intra-thyroidal levels of unbound T3 (i) and T4 (ii), demonstrating an increase in the PBF-Tg mouse. B – Serum levels of TSH in WT and PBF-Tg mice, demonstrating no significant difference between the two. C – Western blot demonstrating increased levels of thyroidal TSHR in the PBF-Tg mouse. D – Change in serum T4 levels following administration of 50 mU TSH in WT and PBF-Tg mice. No response to TSH was seen in the transgenic mouse ((Read et al. 2011; Smith et al. 2012). WT = wild type, Non-Tg = non-thyroglobulin bound, TSH = Thyroid stimulating hormone. TSHR = TSH-receptor, NS = not significant, * = $p < 0.05$, ** = $P < 0.01$.*

Taken together, these data imply that excess PBF is causing a sequestering of thyroid hormone within the thyroid gland, while preventing the hormones from being transported to the blood stream. To maintain a steady state level of serum T3 and T4, the amount of TSHR expressed by follicular cells is increased. However, this appears to be at a maximum capacity for responsiveness given that any further increase in TSH has no effect on serum thyroid hormone.

No thyroid malignancies were observed in the transgenic mice, a fact which is potentially at odds with the finding that PBF is significantly over-expressed in human thyroid cancer. However, these data demonstrate a role for PBF in the proliferation of thyrocytes via the activation of AKT. In addition, these events may well provide the first "hit" in the steps towards thyroid carcinogenesis. Therefore, while over-expression of PBF in isolation may not be sufficient to cause carcinogenesis, a second hit in combination could be.

1.4.2.3 PBF and the sodium iodide symporter

FGF2 had been shown to reduce iodide uptake in thyroid follicular cells (Cocks et al. 2003), and both PBF and PTTG are required for the transcription of FGF2 (Chien and Pei 2000). Given that PBF levels are higher in thyroid cancer compared to normal tissue, and that over-expression of PBF is associated with a poorer prognosis in thyroid cancer, experiments were performed to assess the effect that PBF (and PTTG) may have on the sodium iodide symporter, NIS. As described in Section 1.2.5.3, NIS is vital to the uptake of radioiodine into thyroid follicular cells, and it follows that any disruption to this function would lead to a poorer response to treatment.

PTTG and PBF over-expression were shown to reduce NIS mRNA in primary thyrocytes (86 % and 95 % reduction respectively), with similar levels seen when co-transfecting the two together, and also when transfecting a mutated PTTG which lacked the

ability to transactivate FGF2 (Figure 1.15 A). This also had a functional effect, with PBF over-expression leading to a reduction in ^{125}I uptake by 68 %, while PTTG over-expression resulted in a fall of 59 %. Here, co-transfection led to a greater reduction (83 %), while transfection of the mutant PTTG resulted in a fall of only 34 % (Figure 1.15 B). Together, these data indicated that while the suppression of NIS function by PTTG occurs mostly via FGF2, PBF mediates its effect via an independent mechanism. Promoter studies examined the effect of PBF and PTTG on the NIS promoter. Both proteins caused transcriptional repression via a PAX8/USF1 site within the human NIS upstream enhancer element, while PBF also repressed the basal NIS promoter, which harbours the transcriptional activation site (Boelaert et al. 2007).

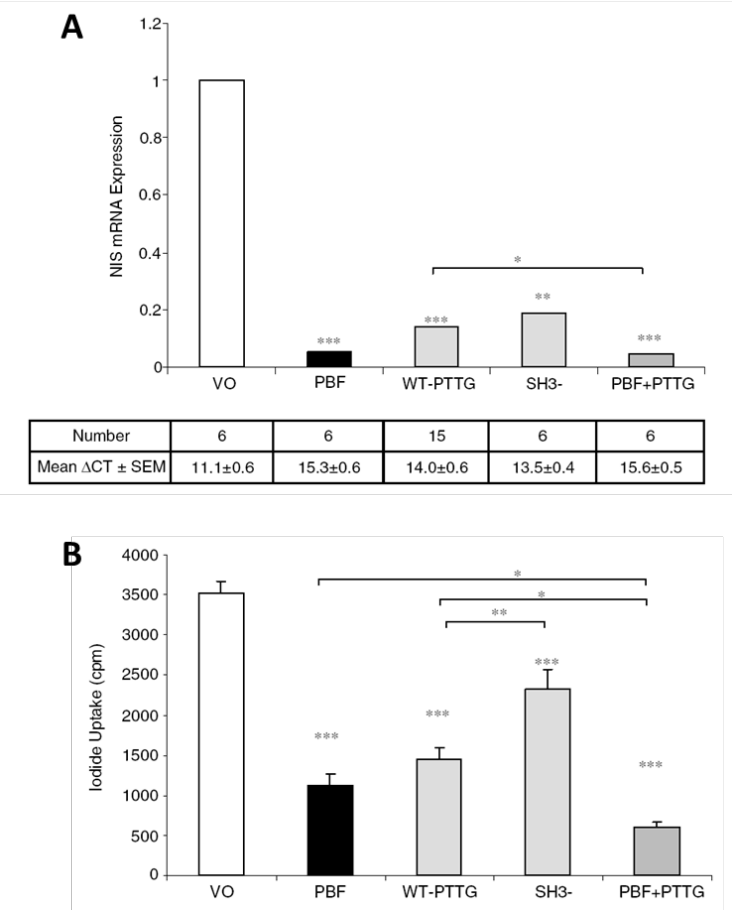

*Figure 1.15 PBF and PTTG inhibit NIS expression and activity in primary thyroid cultures. A – NIS mRNA expression is reduced by PBF and PTTG transfection alone and in combination, and also with the SH3 deletion mutant of PTTG (SH3-). B – Iodide uptake in primary thyrocytes after transfection with PBF/PTTG/SH3- * = p < 0.05, ** = p < 0.01, *** = p < 0.001 (Boelaert et al. 2007).*

The mechanism by which PBF repressed NIS function was examined in further studies. Interaction between PBF and NIS was confirmed by glutathione-S-transferase (GST) pull-down and co-immunoprecipitation assays. PBF over-expression was shown to alter the sub-cellular localisation of NIS, internalising it away from the plasma membrane and into intracellular vesicles (Figure 1.16), a process mediated via clathrin-dependant endocytosis due to strong co-localisation with CD63, a marker for late endosomes (Smith et al. 2009).

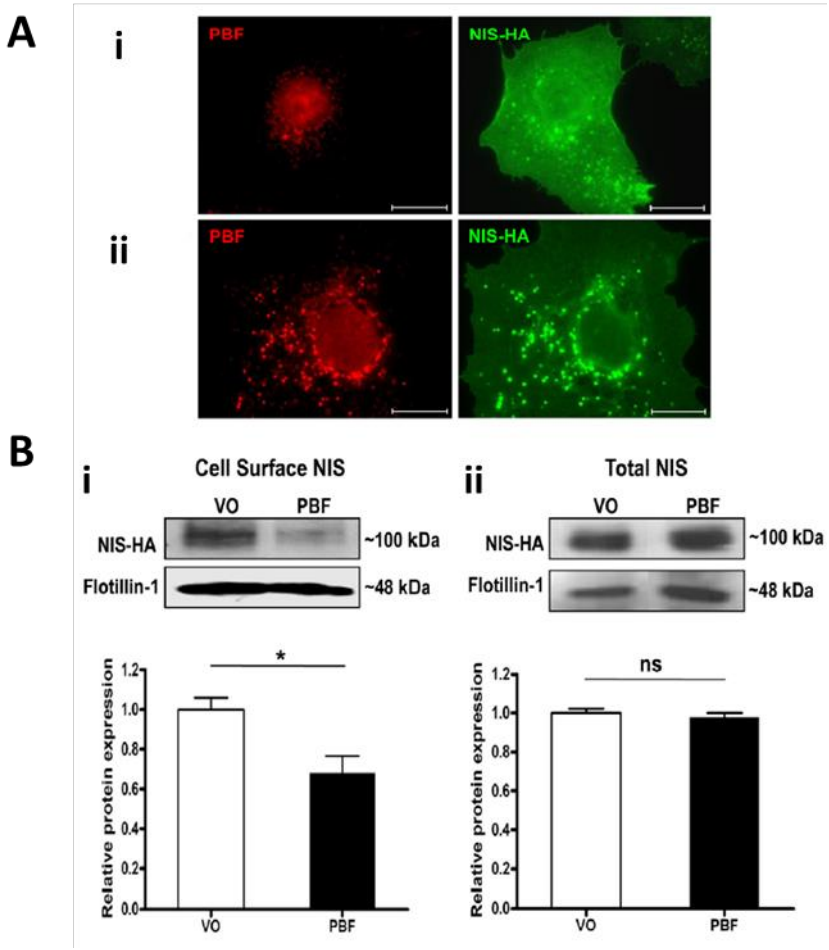

Figure 1.16 Effect of PBF over-expression on NIS in COS-7 cells. A – Immunofluorescence in the presence of wild type (i) or over-expressed (ii) PBF, with NIS localising to intracellular vesicles with increased PBF. B – Corresponding cell surface biotinylation study demonstrating reduced cell surface NIS (i) but no change in total NIS (ii) with over-expressed PBF compared to WT levels (Smith et al. 2009).

PBF-induced NIS repression was also observed in the PBF-Tg mouse model. In a similar effect to that apparent in the *in vitro* model, for age and sex-matched mice, NIS mRNA expression was reduced by approximately 50 % in the PBF-Tg mouse compared to wild type, and immunohistochemistry demonstrated a marked reduction in NIS staining in the transgenic thyroids (Figure 1.17 A and B) (Read et al. 2011). Primary cultures from these murine thyroids showed a 70 % repression of iodide uptake in the transgenic thyroids compared to wild type. Perhaps most importantly, this effect could be completely reversed by knocking

down PBF using siRNA (Figure 1.17 C) (Read et al. 2011). This demonstrated that PBF is able to repress NIS, leading to a direct decrease in iodide uptake, both *in vitro* and *in vivo*, and that targeting this process may provide a potential therapy to increase iodide uptake in radioiodine refractory thyroid cancers.

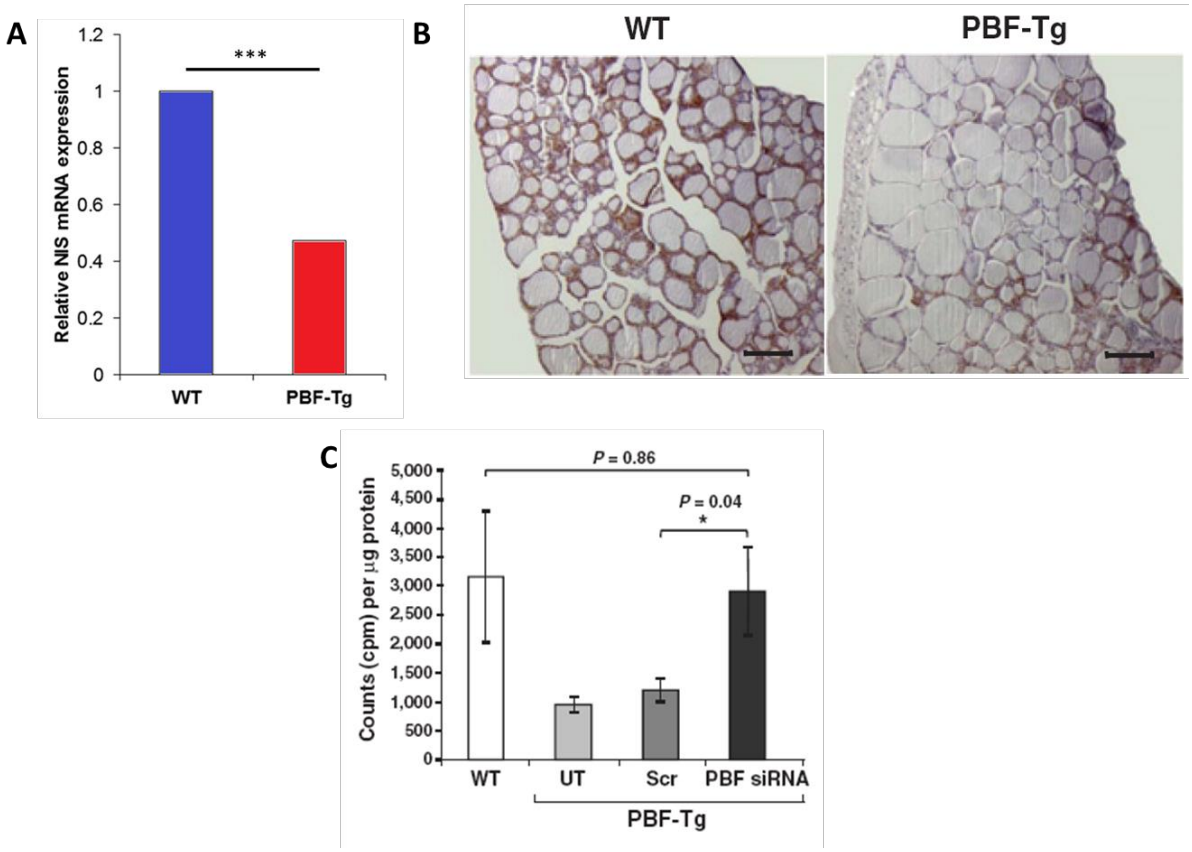

Figure 1.17 A - NIS mRNA expression in wild type (WT) and PBF transgenic (PBF-Tg) mice. B - NIS expression demonstrated by immunohistochemistry in WT and PBF-Tg mice. C – Iodide uptake in primary murine thyrocytes; PBF knockdown reversed the PBF-mediated repression of NIS function (Read et al. 2011).UT = untransfected, Src = scrambled siRNA.

While the above studies have shown PBF to directly affect a number of key cellular processes, including NIS expression and function, the full range of functions that PBF has within the thyroid remain unknown. Additionally, there is still as yet no clear way to target PBF in the treatment of thyroid cancer. Further elucidation of the range of interactions PBF has within the cell may help determine potential therapeutic strategies, with the study of a

protein's range of interactions being recognised as an important pre-requisite to the development of novel treatments for cancer. Mass spectrometry (MS) plays an ever increasing part in this process, and techniques to improve accuracy and combat technical difficulties are evolving. There is an increasing body of evidence demonstrating that MS has important and wide ranging applications to endocrine and thyroid cancer. As discussed above, thyroid cancers are often difficult to distinguish from benign tumours during initial investigation, and in some cases present late with a consequently worse prognosis. In addition, there is often a complex interplay between the on-going normal physiology of the thyrocyte, aberrant production of secreted hormones and disordered cellular function. Together, this results in thyroid cancer research being particularly amenable to mass spectromtery.

1.5 Mass spectrometry and protein-protein interactions

1.5.1 Role of protein-protein interactions in the cell

Proteins do not exist in isolation in a cell, and each protein will have many other proteins with which it interacts (its "interactome" (Sanchez et al. 1999)). These interactions are key to all cellular processes; understanding and mapping these is taking on an increasing importance in the field of translational molecular biology. The consequences of these include altered kinetic properties, substrate channelling, formation of new binding sites, inactivation of one or both proteins and a change in specificity for a given substrate (Phizicky and Fields 1995).

In general, interactions can be classified as either stable or transient. Stable interactions are found in complex, multi-protein molecules such as haemoglobin. Transient interactions form the backbone of most cellular processes. The transient nature is brought about by the fact that a specific condition, for example a particular sub-cellular localisation or post-translational modification, may be required for the interaction to occur and persist.

Despite the variety of potential binding sites with a protein, which may change depending on cellular conditions, there are some domains which are associated with protein-protein interaction. Examples of this include the leucine zipper (involved in stable interactions) and SH2/SH3 domains. The latter 2 are named for their homology to sections of the *SRC* oncogene in which they were first identified and are frequently involved in signal transduction and tyrosine kinase binding.

As a translational approach, studying the expression and interactions of proteins in both normal and malignant tissues significantly enhances the understanding of the mechanisms of disease progression and pathogenesis. By mapping the human interactome, new therapeutic targets may be identified which can lead to the development of novel cancer treatments.

1.5.2 General principles

The principle behind protein identification by tandem mass spectrometry (MS/MS) lies in the fact that every protein has a predictable fragmentation pattern ("peptide fingerprint") when cleaved by a digestive enzyme (Steen and Mann 2004). The most commonly used enzyme is trypsin, which cleaves peptide chains at the carboxyl side of lysine and arginine residues. An efficient, reproducible digestion is essential to generate worthwhile data and strategies include solubilising using 4 % SDS, which is removed by centrifuging the sample through a 35 kDa cut-off filter where the unfolded proteins are retained and the detergent removed in the filtrate. After concentration and purification, samples are digested using endoproteinase Lys C and / or trypsin and the peptides harvested for analysis (Wisniewski et al. 2009). Another common approach is the digestion of proteins in gel slices following separation of the proteins using SDS PAGE. This process is also reliable as once again the protein substrates are denatured and unfolded.

Tryptic digestion will often generate very complex peptide mixtures that are usually analysed by liquid chromatography (LC) MS/MS, where the peptides are separated using reverse phase HPLC prior to mass spectrometry. The peptides are eluted using a gradient of acetonitrile where the rate of the gradient is matched to the sample complexity. There has been considerable improvement in the design and performance of HPLC instrumentation and columns, allowing routine implementation of nano-bore (sub-μm / min flow rate) methods using columns with internal diameters of 50-100 μm. Therefore, peptides elute from these columns in a very small volume, meaning that the actual concentration of peptides in the HPLC eluate is relatively high (Steen and Mann 2004).

The mass spectrometric analysis of the HPLC-resolved peptides typically utilises two basic approaches; electrospray ionisation (ESI), or matrix assisted laser desorption/ionisation with a time of flight mass spectrometer (MALDI ToF/ToF). In the case of a MALDI instrument, a defined time period of HPLC column outflow is automatically spotted onto a MALDI target plate. Typically, several hundred or more spots are generated for a complex sample. In electrospray ionisation the column eluate is sprayed into the mass spectrometer source via an emitter (a fine needle that can conduct an electrical current) which is spatially isolated from the actual mass spectrometer. A high charge (1-5 kV) is applied to the emitter which ionises the peptides in the acidified HPLC solvent. As this liquid exits the fine tip, small droplets are generated and manipulated by electric fields according to their mass to charge ratio (*m*/*z*). The ions reach a detector and a mass spectrum is generated. By examining the separation pattern of the peaks produced, the specific *m*/*z* of each ion can be calculated. Tandem mass spectrometry (MS/MS) refers to the further fragmentation of the most abundant precursor ions using an inert gas. These are then passed through the spectrometer again and

the individual product ions assigned further peaks based on their *m*/*z*. Each product ion is the result of the loss of one or more amino acid residues from the precursor ion; by examining the population of peaks and their *m*/*z* (the peptide "tandem mass spectrum") it is therefore possible to determine the amino acid sequence of the ion, and therefore the structure of the precursor ion. Once the mass spectrum has been matched to a peptide sequence, computer databases use the predictable cleavage sites of trypsin to match the peptide to a parent protein.

1.5.3 Protein complexes

The isolation of proteins using affinity purification of a target (bait) protein has allowed the detection of novel protein-protein interactions in many studies. Antibodies to native or tagged proteins have been used extensively in this work and efforts to decrease the detection of non-specific binding partners have utilised tandem affinity tags (TAP-TAG) (Rigaut et al. 1999). However the protein complex is isolated, it is usual that the proteins are identified following resolution of the proteins using SDS-PAGE, band excision, and tryptic digestion. It is important to perform suitable controls to detect non-specific interactions and it is particularly useful if some interactions with the target protein are already known as these can act as positive controls, as does the detection of the target. As well as individual protein-protein interactions, the duration of these interactions and their relation to cellular function can also be determined, mapping out cell signalling pathways (Bisson et al. 2011).

1.5.4 Protein quantitation

Initially, the analysis of complex samples (often termed "shot-gun proteomics") focussed on identifying as many peptides/proteins as possible in complex samples such as blood serum and plasma, urine, CSF or tissue and cell lysates. However, it soon became clear that it is more relevant to determine either the absolute or relative abundance of proteins,

particularly in biomarker discovery. Several approaches have been developed and the actual protocol utilised is usually limited by the sample type, cost, mass spectrometer available and by the quality of data required. All of the methods have advantages and disadvantages compared to the other protocols and the choice of approach can be affected by the experience and personal preferences of the group performing the analyses.

Currently the most common approaches use stable isotope labelling strategies such that 2 (or more) isotopically labelled versions of each peptide are produced (Elliott et al. 2009). These molecules are identical chemically and behave in exactly the same way during purification steps but vary by a known mass. Therefore, since they are analysed under identical conditions, differences in the peak intensities of the isotopic versions represent an accurate estimation of the relative abundance of the isotopic species.

The vast majority of quantitative proteomic methods attempt to determine the relative amount of large numbers of different peptides or proteins in complex samples without any prior knowledge of the proteins under investigation. However, a focussed analysis of specific proteins can be performed if the protein of interest is known and if preliminary analysis can determine which unique tryptic peptides are consistently observed in LC MS/MS of digests of the target protein. Then, an isotopically labelled version of the peptide is synthesised and a known amount spiked into samples. When analysed by LC MS/MS, the natural and isotopic versions co-elute meaning that their relative MS spectra intensities can be used to calculate the concentration of endogenous peptide in the original sample (Gerber et al. 2003; Elliott et al. 2009). More recently the approach has been improved, to a large extent because of improvements in the performance of “triple quad” mass spectrometers, which generate a

"cleaner" spectrum by selecting for specific *m/z* values. This facet can be used to not only quantify potential biomarkers, but also to identify the gene products of specific mutations that are known to be tumourigenic (Wang et al. 2011). These techniques are summarised in Figure 1.18.

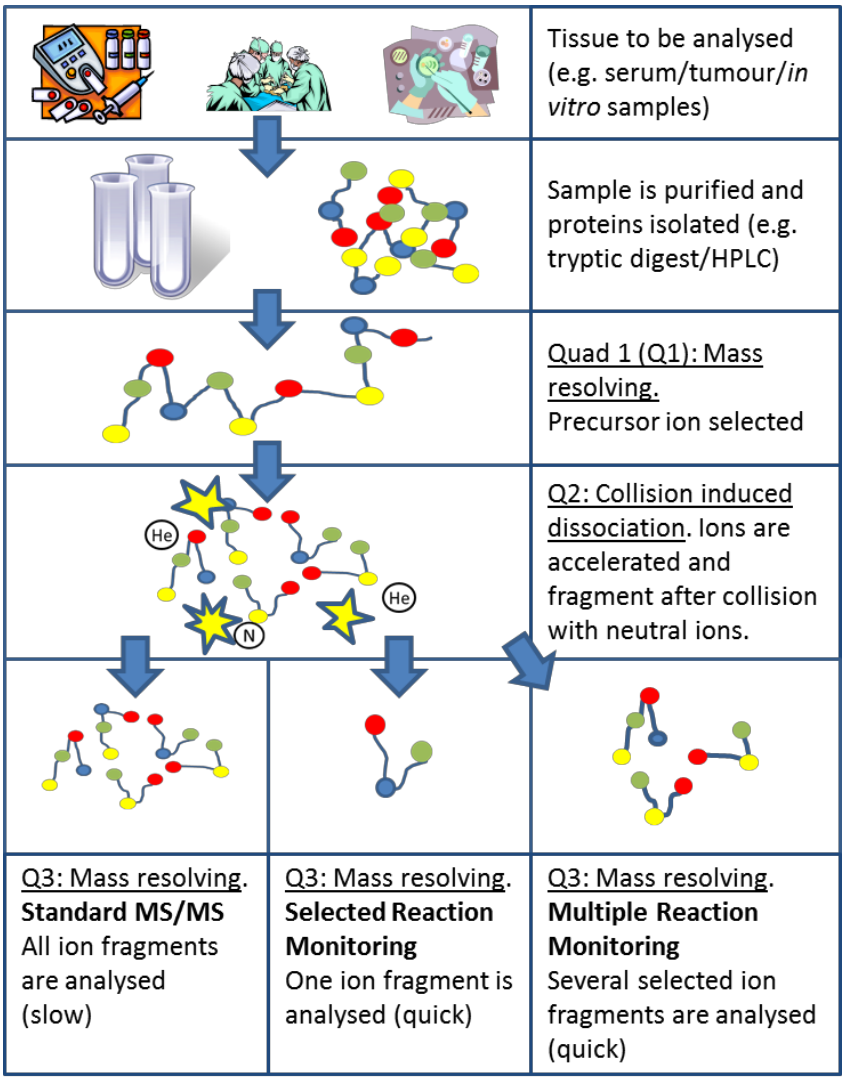

Figure 1.18 The process of triple quadrupole mass spectrometry. Two quadrupole mass spectrometers are in series (Q1 and Q3), with a third non-mass filtering spectrometer in-between (Q2). Q1 selects an ion of a specific mass, which is then fragmented in Q2 by collision with inert gases. In standard MS/MS, all fragments are analysed. In selected and multiple reaction monitoring only one, or a specific number, of the fragment ions is analysed, allowing for much quicker sample processing (Sharma et al. 2012).

Stable Isotope Labelling by Amino acid in Culture (SILAC) is a method of isotopically labelling proteins metabolically, where 2 (or more) cell types, or the same cell type under different conditions, are grown in either "heavy" or "light" media (Ong et al. 2002). In the "heavy" media either the naturally occurring ^{12}C-arginine and/or the ^{12}C-lysine is/are replaced by ^{13}C versions. When the cells grow and use the amino acids from the media to make new proteins, the cells grown in the "heavy" media isotopically label their own proteins and if sufficient rounds of cell division are allowed the labelling will approach equilibrium. An attempt to extend the SILAC approach for the quantitation of proteins in tissue samples has been reported (Geiger et al. 2010). This "super SILAC" approach is relatively expensive as several cell lines have to be grown in ^{13}C labelled amino acid containing media.

1.5.5 Mass spectrometry and thyroid cancer

In the field of thyroid cancer research, MS/MS has several distinct applications, including identifying biomarkers, facilitating personalised medicine and also in developing novel therapies.

1.5.5.1 Identification of biomarkers

One of the most significant areas of cancer biology in which MS/MS has had an impact is the identification of biomarkers. These are used in pre-diagnosis screening as well as prognostication of cancers and identification of recurrence. Standard molecular biology techniques such as immunohistochemistry and quantitative PCR remain in routine use to identify genes that may serve to stratify a tumour into a particular sub-group. However, using MS/MS, plasma and urine can be analysed as well as tumour tissue, enabling the detection of circulating proteins that have been either secreted by the cancer or have "leaked" out (Manne et al. 2005; Ward et al. 2008; Turtoi et al. 2011). The application of this to the field of cancer

research raises some exciting possibilities. The identification of a thyroid cancer biomarker that would allow the differentiation between a follicular adenoma and carcinoma may prevent a significant number of patients undergoing surgery. In addition, determining which tumours are more likely to de-differentiate or metastasise would clearly be invaluable when planning treatment.

Despite thyroid cancer being the commonest endocrine malignancy, there remains a lack of reliable markers available that predict cancer within a thyroid nodule. The two most commonly used serum markers, thyroglobulin for differentiated thyroid cancer and calcitonin for medullary cancer, both have their disadvantages, and there is a continued need for further development. Genetic mutations such as *RET*/*PTC*, *BRAF* and *RAS* have all been identified in thyroid cancer specimens (Namba et al. 2003; Carta et al. 2006; Stanojevic et al. 2011), but these again require a tissue sample in order to identify them. While Fine Needle Aspiration Cytology (FNAC) can be useful for this, the amount of material obtained is often minimal and, even with ultrasound guidance, not necessarily fully representative of the tumour. As an alternative approach, a number of studies over the past decade have examined the proteome of thyroid samples. Initially, 2D electrophoresis was used to identify protein spots from normal, goitrous, hyperplastic, adenomatous and malignant thyroid specimens followed by sequencing from polyvinylidene difluoride (PVDF) membranes and MS/MS to determine which proteins were most abundant (Srisomsap et al. 2002). Cathepsin B was reportedly over-expressed in thyroid cancer and ATP synthase and prohibitin were specifically over-expressed in the papillary variant; proteins that had not been previously linked to thyroid cancer. Although this first study used both MS/MS and traditional methods, as MS/MS technology has advanced, the need to run synchronous techniques has diminished. Later, proteins over-expressed in 29 thyroid tumour samples when compared with normal thyroid were identified using SELDI-

TOF MS/MS (Sofiadis et al. 2010). When the spectra produced from nuclear and cytosolic fractions of cell lysates were analysed, the Ca^{2+} binding ion S100A6 was over-expressed in PTC compared to FTC and normal thyroid, which was confirmed by Western blotting and immunohistochemistry (Sofiadis et al. 2010). Additionally, 2-hydroxyglutarate levels have been shown to be elevated in PTC compared to both normal thyroid and hyperplastic nodules (without the IDH1 and IDH2 mutations usually seen in gliomas and myeloid leukemias), although these results are yet to be validated (Rakheja et al. 2011).

Characterisation of a thyroid tumour, then, may prove useful in further stratifying tumour tissue post-biopsy/surgery. However, it is the high-throughput analysis of serum and urine for secreted proteins that may serve as biomarkers which highlights the potential of MS/MS as a vital tool in cancer proteomics. Two recent studies have taken different approaches to the identification of the thyroid cancer secretome. The first utilised an *in vitro* model of TPC-1 (PTC) and CAL62 (ATC) cell lines (Kashat et al. 2010). After culturing cells in serum free conditions, media was collected, trypsinised and run through LC MS/MS. Proteins were classed as high-confidence if identified by 2 or more peptides with ≥95% confidence. Forty six proteins were shortlisted; the mean number of peptides identified was 4.82 with average sequence coverage of 12.5%. After further validation, 6 proteins were determined to be present in the thyroid cancer secretome; biotinidase, nucleolin, enolase1, PTMA, CYR61 and clusterin. The expression of these proteins in the serum of patients with thyroid cancer was then examined but unfortunately none of the proteins were proven to be over-expressed in this setting. This inability to translate results from an *in vitro* to an *in vivo* setting is a shortcoming observed in a number of MS/MS studies. However, identifying those proteins selectively secreted by thyroid tumours remains a fundamental imperative. Using human serum directly to identify secreted proteins has the advantage of being applicable to a

large number of patients and also being representative of the *in vivo* setting. SELDI-TOF MS/MS was employed to study the serum protein profile of 224 patients, 108 with PTC and 116 normal controls (Fan et al. 2009). Haptoglobin alpha-1 was found to be up-regulated in PTC while apolipoproteins CI and CII were down-regulated. Further, as the stage of tumour increased, there was a corresponding rise in haptoglobin alpha-1 and fall in the apolipoproteins. Further work is now needed to consolidate these observations and to determine if these proteins may be of use in the initial investigation of patients with suspected thyroid cancer. To differentiate PTCs from both nodular goitres and normal thyroids, a metabolomic approach comparing the three groups found that the greatest difference occurred in lipid metabolism, with 3-hydroxybutyric acid expression much higher in the PTC group compared to the others (Yao et al. 2011). The authors suggest that this may therefore be a potential marker to distinguish between PTC and benign nodular lesions.

1.5.5.2 Personalised medicine

The search for biomarkers for thyroid cancer does not seek to find a way of tailoring treatment, rather identifying novel proteins that can then be studied in a more translational context. When treating patients with cancer, future therapies are likely to evolve away from protocol driven management strategies to a more tailored, individual approach (Pirmohamed 2010). In this respect, MS/MS can be used to identify proteomic differences between different groups of cancer patients and although not yet widespread in the field of thyroid cancer, has been used to study other malignancies. While most ovarian cancers will be initially susceptible to platinum based chemotherapy, many will eventually become resistant (Cho and Shih Ie 2009). Using ESI-MS/MS to examine the proteome of primary and post-chemotherapy ovarian cancers, 11 proteins were identified that were expressed at higher levels in the recurrent group, all of which were confirmed by RT-PCR (Jinawath et al. 2010).

By knocking down 2 of these (RELA (NF-κB p65) and STAT5), carboplatin-resistance *in vitro* was reversed. Most importantly, by treating the cells with either a NF-κB or STAT5 inhibitor, their sensitivity to carboplatin was significantly enhanced. A similar study compared the proteome of paclitaxel-resistant and -sensitive cell lines, using both MALDI-TOF and LC-MS/MS (Di Michele et al. 2009). A number of proteins that showed significant differential expression between the two were demonstrated and grouped into those related to stress response, metabolism, protein biosynthesis and apoptosis. Collectively, these studies provide a possible way of determining whether a patient will benefit from a particular chemotherapeutic agent prior to its delivery, potentially avoiding both unnecessary side effects and cost.

Previous techniques have performed proteomic analyses on either serum or fresh tissue, but in some cases the specimen may have already been paraffin embedded and examined by a pathologist. Several methods exist for carrying out HPLC-MS/MS on formalin fixed and paraffin embedded (FFPE) tissue, which is much more applicable to a hospital setting (Gustafsson et al. 2010; Paulo et al. 2011). In this way, previously archived samples could be revisited in certain cases or as new discoveries regarding treatment are made, allowing a patient's treatment to remain contemporary, regardless of when the original diagnosis was made or surgery performed. As mentioned above, statistical analysis is often hampered by insufficient sample numbers for what are often rare or unusual malignancies and by the short follow up time that the patients recruited to current studies have available. By using FFPE tissue, which has been archived and for which long term patient outcomes are known, studies will be able to compare larger numbers of samples and correlate different proteomic measures to specific patient factors, such as recurrence and response to treatment.

1.5.5.3 Interaction proteomics

MS has enabled the large scale identification of protein-protein interactions (Downard 2006; Volkel et al. 2010), and from these large interaction networks have been generated. Tyrosine kinase inhibitors (TKIs) are promising agents in the treatment of many cancers (Raymond et al. 2011; Verbeek et al. 2011), and proteomic analysis of interactions can identify more accurately specific kinases to target (Gorla et al. 2009). Directly related to this, MS/MS allows the identification of post-translational protein modifications (Chung et al. 2011), including phosphorylation, which can lead to further therapeutic insight. However, if high molecular weight proteins are examined, the presence of post-translational modifications may obscure the data; analyses must therefore be tailored to specific events, such as phosphorylation or glycosylation. It has been demonstrated that resistance to the TKI lapatinib in breast cancer cell lines is linked to increased phosphorylation of Src family kinases (Rexer et al. 2011). Further, by treating these cells with Src inhibitors the sensitivity to lapatinib is restored. Similarly, LC-MS/MS has been utilised to explore the phosphorylation of the epidermal growth factor receptor (EGFR) (Zhang et al. 2011). Thirty phosphorylation sites were documented and were related to activating mutations in cancer cell lines as well as sensitivity to the EGFR inhibitor erlotinib. These strategies thus highlight the potential to target treatment for specific cancers based on the proteomic profile of the tumour tissue, and to monitor and address disease progression in the light of the on-going treatment regimen.

1.6 Hypothesis and aims

Over recent years, PBF has been shown to have transforming effects *in vitro*, and tumourigenic effects *in vitro*. Specifically in relation to thyroid disease, PBF over-expression

leads to a macro-follicular goitre with areas of hyperplasia. High levels of PBF are found in thyroid cancer when compared to normal tissue, and the amount of PBF present within thyroid tissue has a positive correlation with thyroid cancer recurrence. At a cellular level, PBF binds to both NIS and MCT8, internalising them away from the cell membrane, with a direct functional response in terms of iodide uptake and thyroid hormone transport. This has important consequences for the treatment of thyroid cancer and implications on prognosis.

The hypothesis of this thesis is that in addition to those described, PBF has a range of interactions with the thyroid cell, and that increased levels of PBF, as observed in thyroid cancer, lead to a disruption of cellular processes key to normal thyrocyte function and, by extension, to the treatment of thyroid cancer.

From this, the aims of this thesis were:

1. *Identification of potential novel binding partners of PBF*. Tandem mass spectrometry was used to identify potential binding partners of PBF. From the large list of potential proteins, scoring systems and validation strategies were employed to generate a shortlist of most likely interactors, and from this 3 were chosen to be further validated based on predicted function.
2. *Validation of binding partners*. GST-tagged pull down assays and co-immunoprecipitation were used to validate the potential binding partners identified by MS/MS.
3. *Functional assessment of the significance of interactions*. Functional studies, including iodide uptake and secretion assays, were used to investigate the

functional significance of the interactions, and the potential to utilise them as targets for future therapies for thyroid cancer were assessed.

Chapter 2 Materials and Methods

Unless otherwise stated, all reagents described were obtained from Sigma-Aldrich (Poole, UK).

2.1 Cell lines

K1 cells were obtained from the European Collection of Cell Cultures (Salisbury, UK). The K1 line is a moderately-well differentiated human papillary thyroid carcinoma cell line displaying the V600E BRAF mutation (Meireles et al. 2007), but expressing wild-type p53. The TPC-1 cell line is a moderately differentiated human PTC line expressing wild type p53 and BRAF, but with the *RET*/*PTC1* re-arrangement on chromosome 10 (Ribeiro et al. 2008). They were kindly provided by Dr Rebecca Schweppe (Division of Endocrinology, Metabolism, & Diabetes, University of Colorado Denver, Aurora, Colorado). Both cell lines were cultured from passage 7 (P7) as a monolayer in 75 cm^2 flasks in RPMI with L-Glutamine (Life Technologies, Grand Island, NY, USA), 10^5 U/L penicillin, 100 mg/L streptomycin (Invitrogen, Paisley, UK) and 10 % fetal bovine serum (FBS) (Invitrogen). Cells were passaged twice weekly, using a 10 % (K1) and 5 % (TPC1) division and kept in a 37 °C incubator with 5 % CO_2, with fresh P7 cells re-cultured every 6 to 8 weeks.

The FRTL-5 cell line is a rat thyroid cell line derived from normal rat thyroid tissue, and displays normal thyroid cellular functions, including iodide uptake and thyroglobulin synthesis (Ambesi-Impiombato 1986). Cells were cultured from P10 in 1 x Coon's modified Hamm's F-12 medium (Biochrom AG, Berlin, Germany) with 30 mM sodium bicarbonate made up to 1 litre with H_2O then sterilised through a 0.22 μm pore 54.5 cm polyethersulfone membrane (Corning Ltd, Ewloe, UK), with 10^5 U/L penicillin, 100 mg/L streptomycin, 300 U/L thyroid stimulating hormone and 300 μg/L insulin) with 5 % FBS.

HeLa cells, a malignant epithelial cell line derived from a cervical epidermoid carcinoma (Scherer et al. 1953), were used as a non-thyroid cell line due to their ease of transfection and well characterised phenotype. Cells were cultured from P5 in Dulbecco Modified Eagle's Media (DMEM) (PAA, Pasching, Austria), supplemented with 4.5 g/dL glucose, 10^5 U/L penicillin, 100 mg/L streptomycin and 10 % FBS. Cells were passaged twice weekly and split at 20 %.

2.2 Transfection

2.2.1 Plasmid purification

2.2.1.1 Vectors

Over-expression of protein was achieved through transfection with mammalian expression vectors containing the complete coding sequence for the gene of interest. Plasmids used were pCI-Neo (Promega, Madison, WI, USA), pcDNA3.1+ (Invitrogen), pCMV6-XL (Origene, Rockville, M, USA). All contained the cytomegalovirus promoter and sites for antibiotic resistance.

2.2.1.2 Restriction digest and ligation

The Invitrogen Restriction Digest kit was used to digest a cDNA sequence from a vector according to the manufacturer's instructions. Unique restriction enzymes were chosen as described in relevant chapters. 4 μg of insert and vector DNA were combined with the restriction enzymes (each at 10% of digest mixture), 10 % 1 x BSA, 10 % Buffer H and incubated at 37 °C for 2 hours. The digest solution was combined with DNA loading dye (0.042 % bromophenol blue, 0.042 % Xylene cyanol FF, 2.5 % Ficoll) and run through a 1 % agarose gel in 1 x TAE buffer (40mM Tris, 20mM acetic acid, 1mM EDTA) at 100 V for 1

hour. Using ultraviolet light, the DNA bands corresponding to the insert and the linearised vector were excised with a clean scalpel.

DNA was extracted using the QIAquick Gel Extraction Kit (QiaGen) according to the manufacturer's instructions, with all centrifugation steps carried out at 17,900 x g in a table top microcentrifuge. Briefly, Buffer QG was added to the gel slice in a ratio of 3:1 (v:w) in a microcentrifuge tube and then incubated at 50 °C for 10 minutes with regular vortexing. Once completely dissolved, 10 µL of 3 M sodium acetate pH 5.0 were added before adding 1:1 isopropanol and mixing. The sample was then centrifuged in a spin column for 1 minute to bind the DNA and the flow through discarded. After adding 0.5 ml Buffer QG the sample was spun again for a further minute and flow through again discarded. The DNA was washed with 0.75 ml Buffer PE for 1 minute and the spun again for a further minute to remove any residual wash solution. The DNA was eluted with Buffer EB by spinning for 1 minute, collecting the supernatant in a clean microcentrifuge tube. DNA purity was assessed using the NanoDrop© ND-1000 Spectrophotometer (NanoDrop), with a pure sample having a 260/280 ratio between 1.8 and 2 : 1. Where indicated, samples were purified using the Macherey Nagel PCR Clean Up Kit (Macherey Nagel), according to manufacturer's instructions. All steps were at room temperature with all centrifugation at 11,000 x g for 30 seconds unless otherwise stated. One part DNA was combined with 2 parts Buffer NTI and transferred to a Clean-up Column. After centrifugation to bind the DNA, the sample was washed twice with 700 µL Buffer NT3. The membrane was then dried by centrifuging for 2 minutes and the DNA eluted in 35 µL of Buffer NE for 1 minute, then re-assessed using the NanoDrop as above.

Ligation of the 2 digest products was performed using DNA ligase (Invitrogen). Equal molar quantities of linearised vector and insert were incubated with 10 % DNA Ligase and 10 % 10 x Buffer for 16 hours at 6 °C. The samples were then incubated at 22 °C for 3 minutes

then 70 °C for 10 minutes to heat inactivate the DNA Ligase. The DNA samples were then used to transform bacteria as described below.

2.2.1.3 Bacterial transformation

Transformation was carried out using Subcloning Efficiency™ DH5α™ Competent E. Coli Cells (Invitrogen) according to the manufacturer's instructions. 10 ng of plasmid DNA were added to 50 µL of DH5α™ cells in a 1.5 ml microcentrifuge tube. After incubation on ice for 30 minutes to increase the permeability of the cell membrane, cells were heat shocked at 42 °C for 20 seconds and then incubated on ice for a further 2 minutes. 950 µL of Lysogeny Broth (LB) were added and the samples incubated at 37 °C for 1 hour with shaking. Bacterial cells were pelleted by centrifugation on at 13,000 rpm on a bench top centrifuge and the supernatant discarded. The cells were then re-suspended in the remaining LB (approximately 100 µL). This suspension was plated on warmed LB-Agar (1 % Agar) containing antibiotics. Plates were incubated at 37 °C for 16 hours.

2.2.1.4 DNA purification and sequencing

Purification was performed using the Wizard® Plus SV Miniprep DNA Purification System (Promega) according to manufacturer's instructions. Following incubation, a single colony was selected from the plate and incubated in 5 ml LB with antibiotics at 37 °C for 16 hours with shaking. All subsequent steps were carried out at room temperature. The bacterial suspension was centrifuged at 10,000 x g for 5 minutes and the supernatant discarded. Cells were re-suspended in 250 µL of Cell Resuspension Solution by vortexing and transferred to a 1.5 ml microcentrifuge tube. A cleared lysate was then prepared by the addition of 250 µL of Cell Lysis Solution and incubating the suspension until it had cleared. 10 µL of alkaline protease were added to inactivate any endocucleases released during cell lysis and the lysate incubated for 5 minutes. Finally, 350 µL of neutralisation solution were added to terminate

the lysis and the tube inverted 4 times before centrifuging for 10 minutes at 14,000 x g. Subsequent centrifugation was carried out at 14,000 x g for 1 minute. After transferring to a spin column, the cleared lysate was centrifuged and the eluate discarded. Plasmid DNA was washed twice by centrifugation with Column Wash Solution (750 µL wash 1, 250 µL wash 2) by centrifugation. Finally, the DNA was eluted with 100 µL of nuclease free water (NF-H_2O). DNA quantification was carried out using the NanoDrop© ND-1000 Spectrophotometer (NanoDrop) and accompanying ND-1000 v3.3 software on the DNA-50 setting.

To sequence the plasmid DNA, 250 ng of DNA were combined with 3.2 pmol of forward or reverse primer and made up to 10 µL with NF-H_2O. Primers for pcDNA3.1+ were T7 forward (TAATACGACTCACTATAGGG) and BGH reverse (TAGAAGGCACAGTCGAGG).

Samples containing bacteria that had incorporated the plasmid DNA were used to prepare a glycerol stock, which was then used to re-amplify the DNA as needed. 0.5 ml of 30 % filter-sterilised glycerol were mixed with 0.5 ml of the bacterial culture. After incubation on ice for 30 minutes, the stock was stored at -80 °C.

2.2.1.5 DNA Amplification

Once the sequence of the plasmid DNA had been verified as correct, amplification of plasmid DNA was performed using the GenElute™ HP Plasmid Maxiprep Kit (Sigma) according to the manufacturer's instructions. 5 ml of LB with antibiotics were inoculated with a pipette dipped in the appropriate glycerol stock for 8 hours at 37 °C with shaking. This was then transferred to 150 ml of LB with antibiotics and cultured overnight at 37 °C on an orbital shaker. All subsequent steps took place at room temperature unless otherwise stated. After transferring to 50 ml centrifuge tubes, the culture was then centrifuged at 5000 x g for 10 minutes and the supernatant discarded. The bacterial pellet was re-suspended thoroughly with

a total of 12 ml chilled resuspension solution, following which 12 ml of lysis buffer were added, the tube inverted 6 times and left to stand for 5 minutes. The solution was then neutralised by adding 12 ml neutralisation solution and inverting 4 times. DNA was bound using 9 ml binding solution and after inverting twice the mixture was transferred to the barrel of a filter syringe and incubated for 5 minutes. During this period, a spin column was prepared by centrifuging 12 ml of Column Preparation Solution at 3000 x g for 2 minutes. The DNA solution was then filtered through the syringe into the spin column and centrifuged for 2 minutes at 3000 x g. The DNA was then washed by centrifuging first with 12 ml Column Wash Solution 1 for 2 minutes at 3000 x g then 12 ml of Column Wash Solution 2 for 5 minutes, again at 3000 x g. Finally, DNA was eluted using 3 ml Elution Buffer and centrifuging for 5 minutes at 1000 x g. Sequencing was performed as above to verify the plasmid as well as additional purification steps, if necessary, as described.

2.2.2 Transfection of bacterial plasmids

Cells were seeded into 6 well plates 10 x 10^4 cells per well. After 24 hours incubation at 37 °C, transfection was carried out using Fugene6 (Roche, Indianapolis, USA), or polyethylenimine (PEI). All quantities refer to transfection per well of a 6 well dish. Fugene6 transfection was carried out according to the manufacturer's instruction using an optimised ratio of 6 µL Fugene6 : 2 µg plasmid DNA.

PEI facilitates high transfection efficiencies with low toxicity in cells that had previously been difficult to transfect (Neu et al. 2005). PEI was used at 3 mM in 20 mM HEPES buffer (4-(2-hydroxyethyl)-1-piperazineethanesulfonic acid), with 150 mM NaCl, allowing for 20 µL per well. As for Fugene6 transfection, plasmid DNA was used at 2 µg per well, made up to the same volume as PEI with 20 mM HEPES buffer and 150 mM NaCl. After 5 minutes incubation at room temperature, PEI and DNA were combined and incubated for a further 20

minutes. Immediately prior to transfection, the well medium was changed for 1 ml of SFM. Forty microliters of transfection mix per well were then added and the plates returned to the incubator for 4 hours. After this time, the medium was replaced with 2 ml of fresh media supplemented with 10^5 U/L penicillin, 100 mg/L streptomycin and 10 % FBS.

2.2.3 siRNA transfection

Short interfering RNA (siRNA) was used to activate the RNA interference pathway, thereby reducing specific gene expression. siRNA transfection was facilitated by Lipofectamine 2000 (Invitrogen). Scrambled siRNA was used as a control transfection. Cells were cultured as described in Section 2.2.2 and incubated for 24 hours. Gene specific siRNA (see relevant chapters) or scrambled siRNA was transfected to deliver a concentration of 100 nM in serum free Opti-MEM (Invitrogen). Thirty minutes prior to transfection, media was changed to 1 ml of serum free (SF) Opti-MEM. Six microliters of Lipofectamine and siRNA were prepared in separate aliquots of 100 µL SF Opti-MEM and incubated for 5 minutes at room temperature. The two solutions were then combined and incubated for a further 15 minutes, before drop-wise addition into the culture wells.

2.3 Western blotting

2.3.1 Protein Extraction and quantification

Twenty-four hours following transfection (72 hours for siRNA transfection), cells were washed in phosphate buffered saline (PBS) then lysed in Radioimmunoprecipitation Assay (RIPA) buffer (50 mM Tris pH 7.4, 150 mM NaCl, 1 % v/v Igepal CA-630, 6 mM sodium deoxycholate, 1mM ethylenediaminetetraacetic acid (EDTA)), with 60 µL/ml Protease Inhibitor Cocktail (containing 104 mM 4-(2-aminoethyl)benzenesulfonyl fluoride (AEBSF),

80 µM Aprotinin, 4 mM Bestatin, 1.4 mM E-64, 2 mM Leupeptin, 1.5 mM Pepstatin A, in dimethyl sulfoxide (DMSO)) (Sigma), which specifically inhibits serine, cysteine and aspartic proteases, and amidopeptidases. Lysis was completed by a 20 minute freeze-thaw cycle followed by 30 seconds vortex mixing.

Protein concentration was measured using the bicinchoninic acid (BCA) colorimetric assay kit (Pierce), with cell lysates compared to bovine serum albumin (BSA) standards of 0, 0.125, 0.25, 0.5, 0.75, 1 and 2 mg/ml in RIPA buffer. Both lysates and standards were measured in duplicate, with 78.4 µL Reagent A and 1.6 µL Reagent B added to each sample. After incubation for 30 minutes at 37 °C, absorbance was measured at 560 nM using the Victor3 1420 Multilabel Counter (PerkinElmer). The standard curve produced from the BSA concentrations was then used to determine the sample concentration.

2.3.2 Western blotting

Western blotting was performed as previously described (Smith et al. 2009; Watkins et al. 2010; Read et al. 2011). 15-30 µg of protein was incubated for 5 minutes at 95 °C with 40 % v/v loading buffer (Laemmli buffer (Biorad) with 0.105 g/ml dithiothreitol (DTT, Sigma)). The samples were then pulse centrifuged at 13,000 rpm on a bench-top centrifuge. Resolving gel (375 mM Tris (from 1.5 M, pH 8.8 stock), 12 % acrylamide (from 30 % (w/v) acrylamide : 0.8 % (w/v) bis-acrylamide stock (Geneflow)), 3.5 mM sodium dodecyl sulphate (SDS), 0.1 % (v/v) tetramethylethylenediamine (TEMED, Sigma), 4.4 mM ammonium persulphate (APS)) and stacking gel (375 mM Tris (from 1.5 M, pH 6.8 stock), 5 % acrylamide, 7 mM SDS, 0.2 % TEMED, 8.8 mM APS) were made and wells rinsed using running buffer (24.8 mM Tris, 192 mM glycine, 3.47 mM SDS). Protein samples were then separated by SDS-Polyacrylamide Gel Electrophoresis (SDS-PAGE) in running buffer as above, with 5 µL Precision Plus Protein Standard (Biorad) used as a molecular weight marker.

Following separation, proteins were transferred onto previously activated (immersion in 100 % methanol for 30 seconds) PVDF membrane in transfer buffer (25.0 mM Tris, 192 mM glycine, in 20 % methanol) at 360 mA for 1 hour. PVDF membranes were then blocked in 5 % w/v non-fat milk (Marvel) in Tris-buffered saline with Tween (TBS-T) (20 mM Tris (from 1 M, pH 7.6 stock), 137 mM NaCl, 0.00025 % v/v Tween 80) for a minimum of 1 hour at room temperature. Primary antibodies were prepared in either 5 % w/v milk or 5 % w/v Bovine Serum Albumin (BSA) in TBS-T. Primary antibodies were used at (v/v ratios): polyclonal rabbit anti-human PBF 1:300, anti-Cortactin 1:1000, anti-HA (mouse) 1:2000, anti-HA (rabbit) 1:1000, anti-Src 1:1000, suppliers are listed in individual chapters. The membranes were incubated with 5 ml of the primary antibody on a rocker overnight at 4 °C. Excess antibody was eliminated by washing membranes 4 times for 15 minutes in TBS-T at room temperature before incubating with secondary antibody (horse radish peroxidase (HRP)-conjugated polyclonal goat anti-rabbit immunoglobulin or HRP-conjugated polyclonal rabbit anti-mouse immunoglobulin (both at 650 ng/ml) made in 5 % w/v milk in TBS-T) on a rocker for 1 hour at room temperature. Following 6 ten minute washes with TBS-T, antigen-antibody complexes were detected using ECL (Pierce) according to the manufacturer's instructions.

2.4 Co-immunoprecipitation

Cells were cultured in T25 flasks and treated as required by the specific experiment. Cells were harvested using 500 µL RIPA / 30 µL PI cocktail as above. After end-over-end rotation at 4 °C for 10 minutes, cells were sonicated for 30 seconds (medium setting, Bioruptor Standard, Diagenode, Liège, Belgium) before undergoing end-over-end rotation for a further 10 minutes at 4 °C. The samples were then centrifuged at 12,000 g for 10 minutes at 4 °C and the cell lysate transferred to a clean micro-centrifuge tube. Thirty micrograms of

protein (as determined by BCA assay, above) were retained and the samples incubated with primary antibody overnight at 4 °C with end-over-end rotation. Protein G sepharose beads (GE Lifesciences, Little Chalfont, Buckinghamshire, UK) were pulse washed with RIPA buffer before a 1:1 (v:v) bead slurry was prepared with RIPA. Fifty microliters of slurry were added to the samples and incubated for 2 hours at 4 °C with end-over-end rotation. Pulse centrifugation precipitated the beads and the supernatant was discarded. The beads were washed in 500 μL RIPA by pulse centrifugation 4 times. Bound proteins were then eluted with loading buffer (1:20 β-mercaptoethanol and 1 % SDS in Laemlli buffer and incubated at 37 °C for 30 minutes). Loading buffer was added to the retained cell lysates and both these and the samples were analysed by Western blotting as described above.

2.5 GST-tagged pull down assays

2.5.1 Expression of GST-tagged PBF

The pGEX plasmid (Amersham, Biosciences, Little Chalfont, Buckinghamshire, UK) was used to express PBF as a fusion protein with a GST tag as previously described (Turnell et al. 2000; Smith et al. 2009). This was expressed from overnight cultures of E. Coli; After induction with isopropyl β-D-1-thiogalactopyranoside for 3 hours, the culture was centrifuged at 5000 rpm for 5 minutes. The pellet was re-suspended in 14 ml lysis buffer (8 M urea, 15 mM Tris–HCl, pH 7.4, 15 mM beta-mercaptoethanol), with the remainder of the process carried out on ice. After sonicating 4 times for 1 minute, the solution was centrifuged twice at 18,000 rpm for 20 and 5 minutes, preserving the supernatant. The supernatant was again preserved and combined with 1 ml of packed agarose beads, before being incubated on a rotating mixer at 4 °C overnight. The beads and bound protein were isolated by centrifugation at 3000 rpm for 5 minutes, and subsequently washed 4 times by centrifugation in 50 ml GST

lysis buffer (50 mM Tris pH 7.5, 150 mM NaCl, 0.05 % NP-40) and in 50 ml then 15 ml EDTA buffer (50 mM Tris-HCl pH 7.4, 0.5 M NaCl, 5 % sucrose (w/v), 1 mM EDTA and 1 % NP-40). GST-PBF was eluted from the beads with 3 ml elution buffer (40 µl of 25 mM glutathione in 50 mM Tris-HCl, pH 8,) for 3 hours at 4 °C. The protein was finally purified by dialysis tubing in EDTA buffer with a cut off of 12-14 kDa.

2.5.2 Translation of L-α-[^{35}S]-methionine labelled protein

The TNT Couples Reticulocyte Lysate System (Promega) was used to translate and [^{35}S]-methionine label each protein of interest from the relevant plasmid, according to the manufacturer's instructions. The reaction consisted of: 25 µL rabbit Reticulocyte lysate, 2 µL TNT buffer, 1 µL amino acid mixture (minus methionine), 0.5 µL RNAsin Ribonuclease Inhibitor, 2 µg plasmid DNA, 2 µL [^{35}S]-methionine, 1 µL TNT RNA polymerase and 17 µL nuclease free water. This was then incubated for 2 hours at 30 °C.

2.5.3 Binding assay

Twenty micrograms of GST-PBF (and separately 20 µg GST only control) were combined with 10 µL [^{35}S]-methionine labelled protein and incubated on ice for 30 minutes. After the addition of 500 µL low salt buffer (50 mM Tris pH 7.4, 150 mM NaCl, 1 % NP-40), 50 µL packed glutathione agarose beads were added to each sample and incubated at 4 °C for 2 hours with end over end rotation. The beads were then pulsed and the supernatant discarded before washing 4 times with low salt buffer. GST-PBF was then eluted with 40 µL of 25 mM glutathione in 50 mM Tris pH 8 for 1 hour at 4 °C. Subsequently, 40 µL of loading buffer (Laemmli sample buffer with 5% (v/v) β-mercaptoethanol) were added to each sample and analysed by SDS-PAGE. 1 µL [^{35}S]-methionine labelled protein was combined with 20 µL

loading buffer and run as a 10 % input control. Following electrophoresis, the gel was dried and exposed to radiographic film for between 1 and 24 hours at –20 °C.

2.6 Fluorescence immunocytochemistry

Glass cover slips were washed in 100 % ethanol, rinsed in PBS and placed in 34.8 mm diameter cell culture plates. Cells were seeded into the wells at a varied concentration depending on cell type: K1 – 75,000 / well, TPC1 and HeLa – 50,000 / well.

After 24 hours growth, transfection was carried out as described previously. After a further 72 hours, medium was removed and the wells rinsed with 1 ml PBS. The following steps took place at room temperature unless otherwise stated. The coverslips were fixed for 20 minutes in 800 µL fixing solution (0.1 M phosphate buffer (from 0.2 M Na_2HPO_4 pH corrected to 7.4 using 0.2 M NaH_2PO_4), 0.2 % paraformaldehyde, 0.2 % glucose, 0.02 % sodium azide). After rinsing twice with PBS, cells were permeabilised with 800 µL of chilled 100 % methanol for 20 minutes. Cells were rinsed again twice with PBS and then blocked with 800 µL 10% newborn calf serum (NCS) in PBS. After blocking, the coverslips were placed face down onto 80 µL of 1 % BSA in PBS with primary antibody, on parafilm and incubated in the dark for 1 hour. Specific antibody concentrations are detailed in the relevant chapters. Subsequently, the coverslips were rinsed 3 times with PBS, then placed face down onto 80 µL of 1 % BSA in PBS with 1 % NCS, 1:250 Alexa Fluor® 488 Goat Anti-Mouse IgG (H+L) (Invitrogen), 1:250 Alexa Fluor® 594 Goat Anti-Rabbit IgG (H+L) (Invitrogen) and 1:1000 Hoechst stain 33258 (Sigma) and incubated for 1 hour in the dark. The coverslips were again rinsed 3 times in PBS and after removing any excess liquid were mounted on to slides using Fluorescent Mounting Medium (Dako) and air dried in the dark. Coverslips were

then fixed to the slides using nail varnish (Monsoon Accessorize, London, UK) and slides stored at 4 °C.

2.7 Human primary thyroid cultures

Fresh thyroid tissue was obtained from patients undergoing thyroidectomy (hemi/total/completion) with the approval of the Local Research Ethics Committee. All patients gave written informed consent for their tissue to be collected. Collected thyroid tissue was surplus to histological requirements, and was taken from an area of macroscopically normal tissue in the contra-lateral lobe to the site of disease. Thyroid tissue was collected from patients with diagnoses of multinodular goitre, suspicious thyroid nodules and thyroid cancer.

Thyroid specimens were prepared as described previously (Eggo et al. 1996). Thyroid tissue was extensively macerated under sterile conditions until a smooth consistency was obtained. The tissue was then digested in 0.2 % collagenase Type 2 (Worthington Biochemicals, NJ, USA) in Hanks' Balanced Salt Solution (HBSS) (Sigma) (filter sterilised through a 0.22μm pore 54.5 cm polyethersulfone membrane (Corning)) for 16 hours at room temperature or 3 hours at 37 °C. The resulting tissue was further filtered through a 1 ml sieve and the pellet washed in HBSS. The pellet was re-suspended in primary thyroid media as described previously (Ambesi-Impiombato 1986; Eggo et al. 1996): 1 x Coon's modified Hamm's F-12 modified medium (Biochrom AG) with 30 mM sodium bicarbonate made up to 1 litre with H_2O then sterilised as above, supplemented with 10^5 U/L penicillin, 100 mg/L streptomycin, 300 U/L thyroid stimulating hormone, 300 μg/L insulin and 5 % fetal bovine serum, and, after plating, incubated at 37 °C. After 72 hours, serum was omitted. Cells were considered ready for experimentation between days 9 and 11.

2.8 Statistical analysis

Data were analysed using IBM SPSS Statistics Version 19 (IBM, UK). Normal distribution of data was determined and parametric data groups were analysed by student's t-test. Significance was taken as $p < 0.05$. ImageJ (public domain software, available at http://rsb.info.nih.gov/ij/) was used to calculate scanning densitometry results.

Chapter 3 Optimisation of tandem mass spectrometry

3.1 Introduction

Despite being first described over 10 years ago (Chien and Pei 2000), relatively little is understood regarding the precise role of PBF within the cell, certainly compared to its named binding partner PTTG. The majority of the work concerning PBF has focussed on its involvement with thyroid disease, and specifically thyroid cancer (see section 1.4.2). PBF over-expression has a diverse range of effects within the cell, interacting with NIS and internalising it from the cell membrane (Boelaert et al. 2007; Smith et al. 2009), with a similar effect observed in relation to the thyroid hormone transporter MCT8 (Smith et al. 2012). PBF is transforming *in vitro*, tumourigenic *in vivo*, and over-expression is found in thyroid cancers and is associated with early cancer recurrence (Stratford et al. 2005). It has recently been shown to be additionally related to the presence of metastases, advanced stage, multicentricity and increased mortality; acting as an independent prognostic indicator (Hsueh et al. 2013). PBF also increases the invasiveness of breast cancer cells *in vitro* (Watkins et al. 2010), an observation which may underlie the increased recurrence observed in thyroid cancer.

To help explain this diversity of effect it is important to understand the breadth of PBF relationships within the cellular interactome. Currently described interactors with PBF are PTTG (Chien and Pei 2000), NIS (Smith et al. 2009), MCT8 (Smith et al. 2012) and p53 (unpublished data) but these are insufficient to fully explain the range of effects PBF is involved in. Key areas of interest include proteins involved in the movement of PBF around the cell, allowing it to reach the cell membrane and internalise the membrane transporters. Given the association with early cancer recurrence, another is any role of PBF in pathways associated with invasion or metastasis. A final area of specific interest is the identification of the serine/threonine or tyrosine kinases which may be responsible for phosphorylating PBF.

MS/MS is a tool that is developing momentum as the optimum method of identifying protein-protein interactions. Although several variations exist, one of the most straightforward is the analysis of samples that have been immunoprecipitated with the protein of interest. With the powerful detection that is inherent in MS/MS also come limitations. The first of these is the contamination of test samples by material exogenous to the experimental process (i.e. dust, skin etc.). Where small amounts of target protein are present, these additions can significantly hamper results. The second is the software used to analyse the mass spectra. Each protein has a unique fingerprint, based on the position of trypsin digestion sites and the subsequent chains of amino acids generated. When a peptide chain is analysed, the resulting mass spectrum, caused by the ionisation and fragmentation of the peptide, is assigned by the software to a protein. If the spectrum contains all possible fragments of the peptide (therefore scoring highly), and the protein is identified by several such peptide spectra, it can be assumed that it is genuinely present in the sample. Unfortunately, where the spectrum is ambiguous, containing some identified and some unidentified peaks, it may be assigned incorrectly to a protein. In these cases it is likely that only 1 peptide will be assigned to this protein, and it can therefore be discarded from further analysis. A difficulty arises where a protein that *is* present, but in low quantities, is only identified by 1 peptide and is therefore wrongly excluded. A way to account for this is to either examine the spectra for these proteins manually to determine if it is accurate, or to match those proteins identified by 1 peptide across several experiments, lending credibility to what may otherwise have been a discarded result.

The aim of this chapter, therefore, was to establish the optimal conditions for MS/MS, from cell culture, transfection and immunoprecipitation to gel digest, MS/MS and data

analysis. Key contaminants and non-specific interactions would be identified and spreadsheet templates to facilitate the fast analysis of the large amounts of data would be produced.

3.2 Methods

3.2.1 Cell culture

K1 and TPC1 cells were maintained in RPMI as described in Section 2.1. For analysis by Western blotting, cells were seeded onto 6 well plates; for immunoprecipitation, T25 and T75 flasks were used.

3.2.2 Bacterial plasmids

PBF-HA in pci-Neo was sublcloned into pcDNA3.1+ using the restriction enzymes EcoR1 and Xba1 as described in Section 2.2.1. Transfection was carried out using Fugene6 or PEI as described in Section 2.2.2.

3.2.3 Fluorescence-activated cell sorting (FACS)

K1 and TPC1 cells were transfected with the pMax-GFP plasmid (Amaxa, Cologne, Germany). After 24 hours, cells were processed as described in Section 2.3.1, with 1 % paraformaldehyde instead of RIPA / PI. After transferring to a test tube, samples were analysed using the FACSCalibur 4-colour flow cytometer (BD Biosciences, Oxford, UK). GFP was detected in the FL1 channel with settings calibrated using mock-transfected cells as a negative control. FL1 was set to log 400 with an amplification gain of 400. Forward and side scatter were set to linear. The M1gate was set at approximately 2.5×10^{1}.

3.2.4 Western blotting

Western blotting was performed as described in Section 2.3. Primary antibodies were anti-HA (mouse monoclonal, HA.11 Clone 16B12, Covance, UK) 1:2000 and monoclonal anti-β-actin (clone AC-15, Sigma-Aldrich), 1:10000.

3.2.5 Tandem mass spectrometry (MS/MS)

3.2.5.1 Immunoprecipitation

K1 and TPC1 cells were cultured in T75 flasks and transfected with *PBF-HA* or blank vector using PEI, as described in Section 2.4. Cells were washed 4 times with 10 ml cold PBS then scraped into a 50 ml centrifuge tube, combining samples from several T75 flasks in each tube. The samples were spun for 5 minutes at 1200 rpm and the supernatant discarded. The cells were re-suspended in 1ml of high salt lysis buffer (50 mM Tris pH 7.4, 1% v/v Igepal CA-630, 400 mM NaCl) / PI cocktail (ratio 1 ml lysis buffer:60 µl PI) and the resultant suspension transferred to a micro-centrifuge tube. Subsequent steps were as described in Section 2.4, using anti-HA (above) as primary antibody and high salt lysis buffer instead of RIPA.

Proteins were separated using the NuPage Bis-Tris electrophoresis system (Invitrogen) as per manufacturer's instructions, using 1x running buffer with 500 µl NuPage antioxidant. Under positive pressure in dust-free conditions, the gels were removed from the casing and incubated in Colloidal Coomassie Blue stain (0.08 % Coomassie Brilliant Blue G250 (Sigma), 1.6 % Orthophosphoric Acid, 8 % Ammonium Sulphate, 20 % Methanol) with gentle agitation overnight at room temperature. Gels were de-stained with 4 to 5 washes in 1 % acetic acid and stored in 1 % acetic acid at 4 °C until digest.

3.2.5.2 Gel digest

All steps were undertaken in a positive pressure hood to minimize keratin contamination and all washes and incubations carried out at room temperature with gentle agitation unless otherwise stated. Gels were scanned and processed to allow identification of visible bands.

The gels were then placed onto a clean glass slide and each lane excised and divided into sections approximately 2 mm in height. Gel pieces were washed twice with 500 µl 50 % acetonitrile / 50 mM ammonium bicarbonate for 45 minutes. They were then incubated for one hour at 56 °C with 50 µl of 50 mM DTT in 10 % acetonitrile/50 mM ammonium bicarbonate and the supernatant discarded. After adding 50 µl of 100 mM iodoacetamide in 10 % acetonitrile with 50 mM ammonium bicarbonate, samples were incubated in the dark for 30 minutes and the supernatant removed. A further three washes with 500 µl 10 % acetonitrile in 40 mM ammonium bicarbonate for 15 minutes were undertaken and the bands subsequently dried down using a vacuum centrifuge for 60 minutes. 200 µg / ml trypsin solution were prepared using Sequencing Grade Modified Trypsin (Promega) according to the manufacturer's instructions and diluted to 12 µg / ml with 10 % acetonitrile with 40 mM ammonium bicarbonate. 30 µl of this were added to the dried gel pieces and the samples incubated for 60 minutes. 40 µl of 10 % acetonitrile with 40 mM ammonium bicarbonate were added and the samples incubated at 37 °C overnight. The supernatant was collected and the samples incubated in 60 µl of 3 % formic acid for 60 minutes. After collecting the supernatant, a further 60 µl of formic acid were added to the gel pieces and incubated for 60 minutes. The supernatant was again retained and combined with the previous sample collected.

3.2.5.3 Sample processing

100 µl of sample were loaded into clean sample tubes. These were then loaded into the Ultimate 3000 High Performance Liquid Chromatography (HPLC) unit (Dionex, California, USA) as per manufacturer's instructions. An acetonitrile gradient was used as advised. Following HPLC, the samples were run in continuity through the AmaZon ETD ion trap and tandem mass spectrometer (Bruker Daltronics, Coventry, UK).

3.2.5.4 Data analysis

Mass spectrographs were analysed using a pan-mammalian database via the Mascot search engine (v2.2.06, Matrix Science Ltd, London, UK), with results generated by ProteinScape (v3.0.0.446, Bruker, Coventry, UK).

3.3 Results

3.3.1 Optimisation of transfection efficiencies for K1 and TPC1 cells

3.3.1.1 Subcloning *PBF-HA* into pcDNA3.1

Full length *PBF-HA*, already in use within our group in the mammalian expression vector pCI-Neo, was subcloned into pcDNA3.1+, using the restriction enzymes EcoR1 and Xba1, as described in section 2.2.1.2. Correct insertion was confirmed by sequencing using the T7 and BGHrev primers. Transfection was confirmed by Western blotting (Figure 3.1).

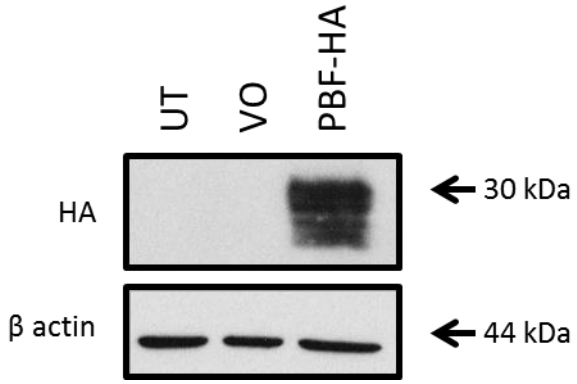

Figure 3.1 Western blot demonstrating PBF-HA transfection in K1 cells, compared to untransfected (UT) and vector only (VO) transfected cells. β actin is shown as a loading control.

3.3.1.2 Polyethylenimine results in the greatest transfection efficiencies

In order to obtain the greatest transfection efficiency (TE) for the thyroid cancer cell lines, Fugene6 – the transfection reagent used for transfection of K1 and TPC1 cells within our group, was compared with polyethylenimine (PEI, Sigma). Cells were transfected with a Green Fluorescent Protein (GFP) -tagged vector (pMax-GFP (Amaxa, Cologne, Germany)) and, after trypsinisation, were analysed by Fluorescence-Activated Cell Sorting (FACS). K1 and TPC1 cells were transfected under a number of conditions, with varying amounts of transfection reagent, plasmid DNA and agitation. Untransfected cells were used as a negative control – as they demonstrated only base line fluorescence, a cut off could be set above which the cells were classed as "transfected" (the "M1 gate", Figure 3.2A). When transfected cells were analysed under the same conditions, the percentage of cells that fell within the M1 gate, and could thus be classed as transfected, was determined (Figure 3.2B).

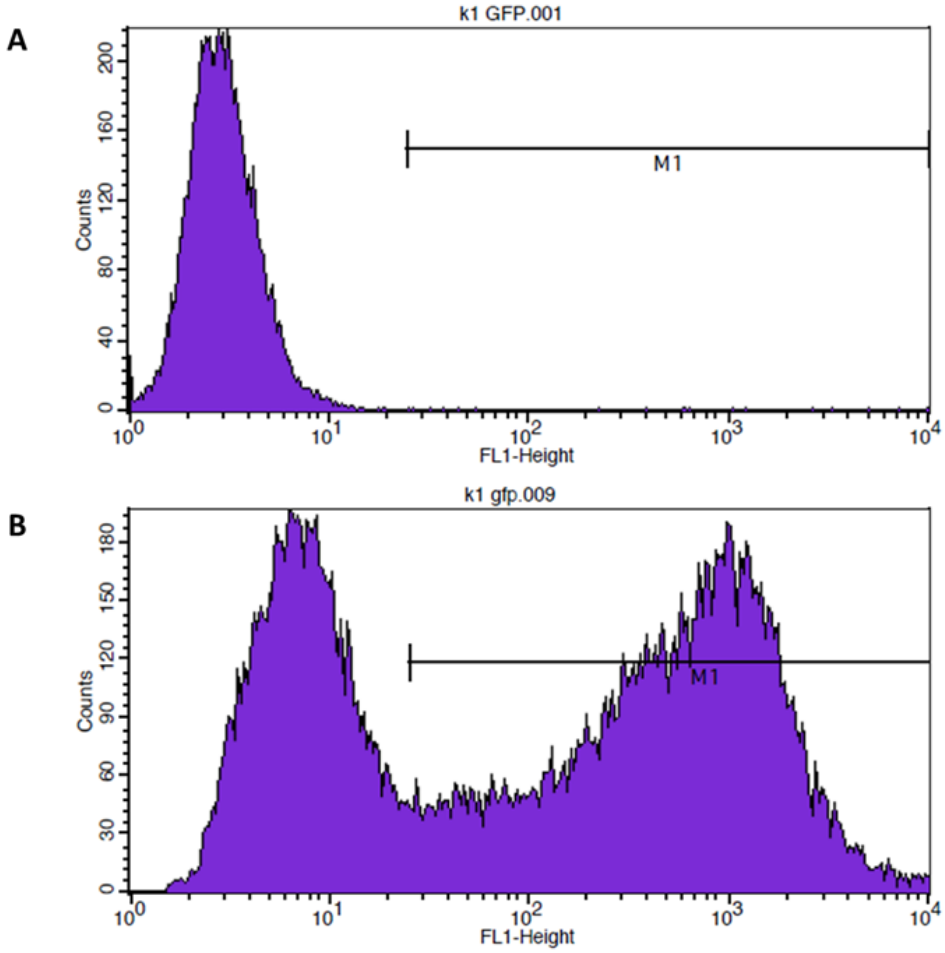

Figure 3.2 Representative FACS output from cells untransfected (A) and transfected (B) with pMax-GFP. The FL1 axis indicated the degree of fluorescence, with the y axis representing the number of cells. The percentage of M1 gated cells was substantially higher for the transfected sample compared to the untransfected cells.

Each set of transfections was carried out in triplicate and repeated on 3 occasions with a different passage of cells. For PEI transfection, using NaCl supplemented serum-free media improved transfection (data not shown). Centrifuging the plates after transfection had a negative effect on transfection of K1 cells (many cells became detached) but in the TPC1 cell line, although a negative trend was seen, variability was such that no significance could be attributed to this. The optimum ratio of PEI to DNA was 10:1, using 2 µg DNA for K1s and 4 µg DNA for TPC1s (for a 6 well plate transfection). The maximum TE was 81.4 ± 1.6 % for K1s and 55.5 ± 4.8 % for TPC1s (Figure 3.3).

For Fugene transfection, 65.6 ± 10.4 % TE was reached in the K1s using 2 µg DNA with a Fugene to DNA ratio of 3:1. In the TPC1 cell line, the maximum reached was 23.4 ± 7.4%, with 4 µg DNA in a ratio of 3:1. In this cell line, centrifuging the plates after transfection had a positive effect; at the lower concentration of DNA, TE was significantly increased to 37.5 ± 3.1 % (p = 0.02), whereas at 4 µg DNA, there was no significant change in TE (25.4 ± 7.4 %, p = 0.9) (Figure 3.3). A summary of the optimum conditions for transfection in the cell lines is given in Table 3.1.

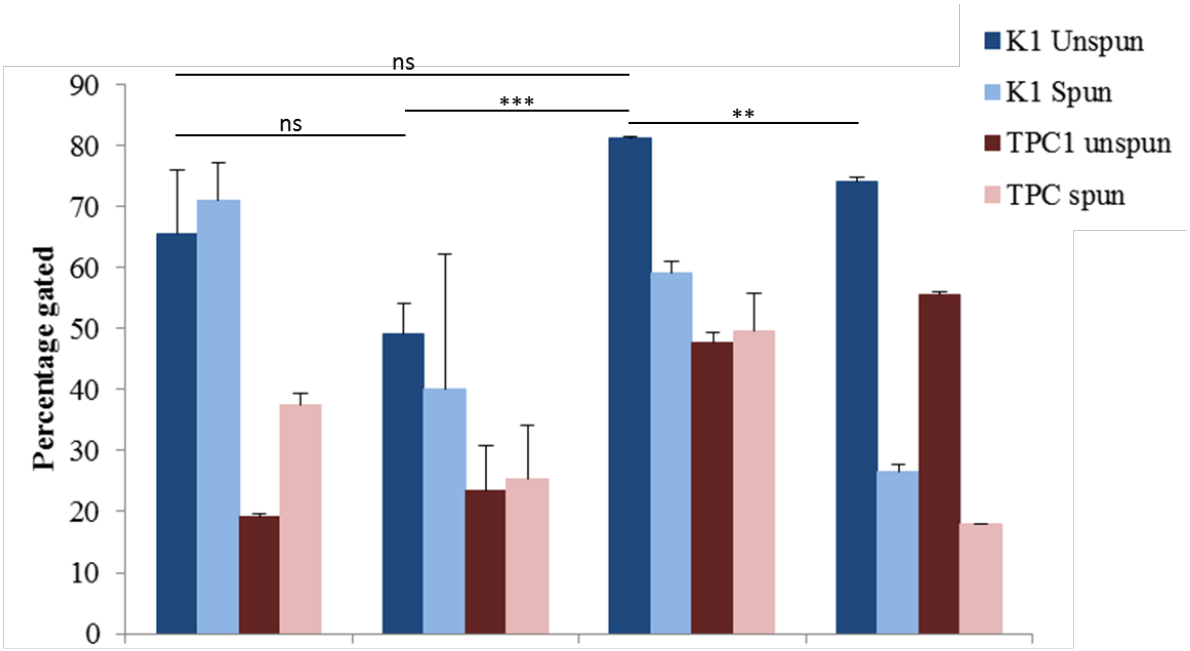

Amount of DNA (µg)	2	4	2	4
Transfection reagent	Fugene 6		Polyethylenimine	

*Figure 3.3 Transfection efficiencies (TEs) of K1 and TPC1 cells for differing transfection reagents. TEs are given as percentage of gated cells relative to untransfected cells (n = 3).ns = not significant, ** = p < 0.01, *** = p < 0.001*

		Fugene 6	**Polyethylenimine**
K1	**DNA (μg)**	2	2
	Reagent:DNA ratio	3:1	10:1
	Spun/Unspun	NSD	Unspun
TPC1	**DNA (μg)**	2	4
	Reagent:DNA ratio	3:1	10:1
	Spun/Unspun	Spun	Unspun

Table 3.1 Optimum transfection conditions for K1 and TPC1 cells. NSD = No significant difference.

3.3.2 Optimisation of MS/MS

3.3.2.1 Volume of culture and negative control

In order to determine the optimum amount of cell lysate to use in the MS/MS process, K1 cells were cultured in T25 plates and transfected with *PBF-HA*, using PEI, as described above. The cell lysate was harvested and immunoprecipitated using an anti-HA antibody (as above). A different negative control was used in each experiment; in the first an additional flask was cultured and transfected as before but no antibody was used to precipitate the lysate (this ensured that any peptides identified in the negative control were the result of non-specific binding between proteins and the protein G coated sepharose beads), while in the second the cells were transfected with blank vector and immunoprecipitated with antibody, thus revealing the extent of non-specific binding to the antibody as opposed to PBF-HA. The immunoprecipitant was run through SDS-PAGE using pre-cast gels to reduce the risk of contamination, and following this the gels were stained with colloidal Coomassie blue in a negative pressure fume hood. This demonstrated the predominant protein bands present in the sample while again reducing the risk of contamination.

Using the protein ladder as a guide for molecular mass, both the test and control lanes were divided into a number of small gel pieces, again under negative pressure. A representative gel image with markers to demonstrate cut locations is shown in Figure 3.4.

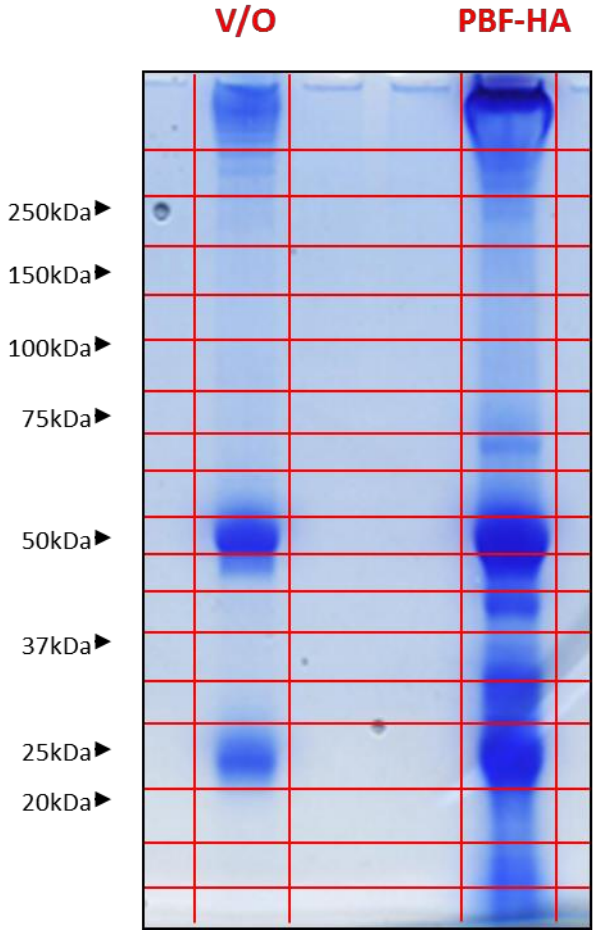

Figure 3.4 Representative scan of polyacrylamide gel stained with colloidal Coomassie blue after SDS-PAGE. Dominant protein bands stained blue. La - Ladder used to determine molecular mass of gel segments. PBF-HA - Cells transfected with PBF-HA. V/O - Cells transfected with blank vector.

Bovine serum albumin was used to calibrate both the HPLC and tandem mass spectrometer, and following this the samples were then passed through MS/MS; the resulting peptides were identified using a pan-mammalian database. The predominant proteins identified for the test and control samples were different types of keratin and porcine trypsin. While the latter was to be expected given that this was used to digest the proteins during the

extraction process, the former were all due to contamination of the samples at one, or several points, of the process from gel staining to entry into HPLC. There were several other proteins identified in all samples across both experiments, again most likely resulting from contamination, and these are summarised in Table 3.2.

Contaminant	
Collagen	Dermcidin
Desmoglein	Desmoplakin
Dynein	Hornerin
Junction plakoglobin	Keratin
Kinesin	Laminin
Myosin	Vimentin

Table 3.2 Proteins identified as contaminants in both experiments and in multiple samples.

Once these contaminants had been discounted, the control samples were examined to identify those proteins present due to non-specific binding, either to the anti-HA antibody or to the sepharose beads. This was determined to be any protein identified by greater than 2 peptides in either of the control samples, which was not in the contaminant list above. In general, the number of peptides by which these were identified ranged from 3 to 8, while the contaminants were identified by > 30 peptides. The other group of proteins were those that had been carried over to MS/MS during the preceding steps. These included trypsin, as mentioned above, immunoglobulins and proteins likely remaining from the culture process (e.g. bovine albumin). A list was thus developed of proteins whose presence in a test sample was unlikely to be attributable to interaction with PBF, and could therefore be discounted, the highest ranking of which are listed in Table 3.3.

Non-specific interacting proteins	**Experimental contaminants**
Nebulin	Albumin
Dystrophin	Trypsin
E3 ubiquitin-protein ligase UBR1	Immunoglobulins
Histone-lysine N-methyltransferase	Alpha-S1/2-casein
DNPK1	Beta-lactoglobulin
Kinase suppressor of Ras 2	

Table 3.3 Table detailing the highest ranking non-specific interactions identified by MS/MS, and those proteins carried over as a result of experimental process.

This list would be updated with each experiment and included subunits of proteins where applicable, as these could be identified separately by the database. The process by which the original list of proteins was reduced to a final shortlist is summarised in Figure 3.5. Run 2 had a greater number of proteins in the original list (before contaminants, non-specific interactions and experimental carry-over results were removed). The final step in the process, removing any proteins identified in the control samples by 2 peptides (not already covered in one of the previous steps) and then any identified by 1 peptide only in the test sample, yielded a final shortlist that contained similar numbers of proteins.

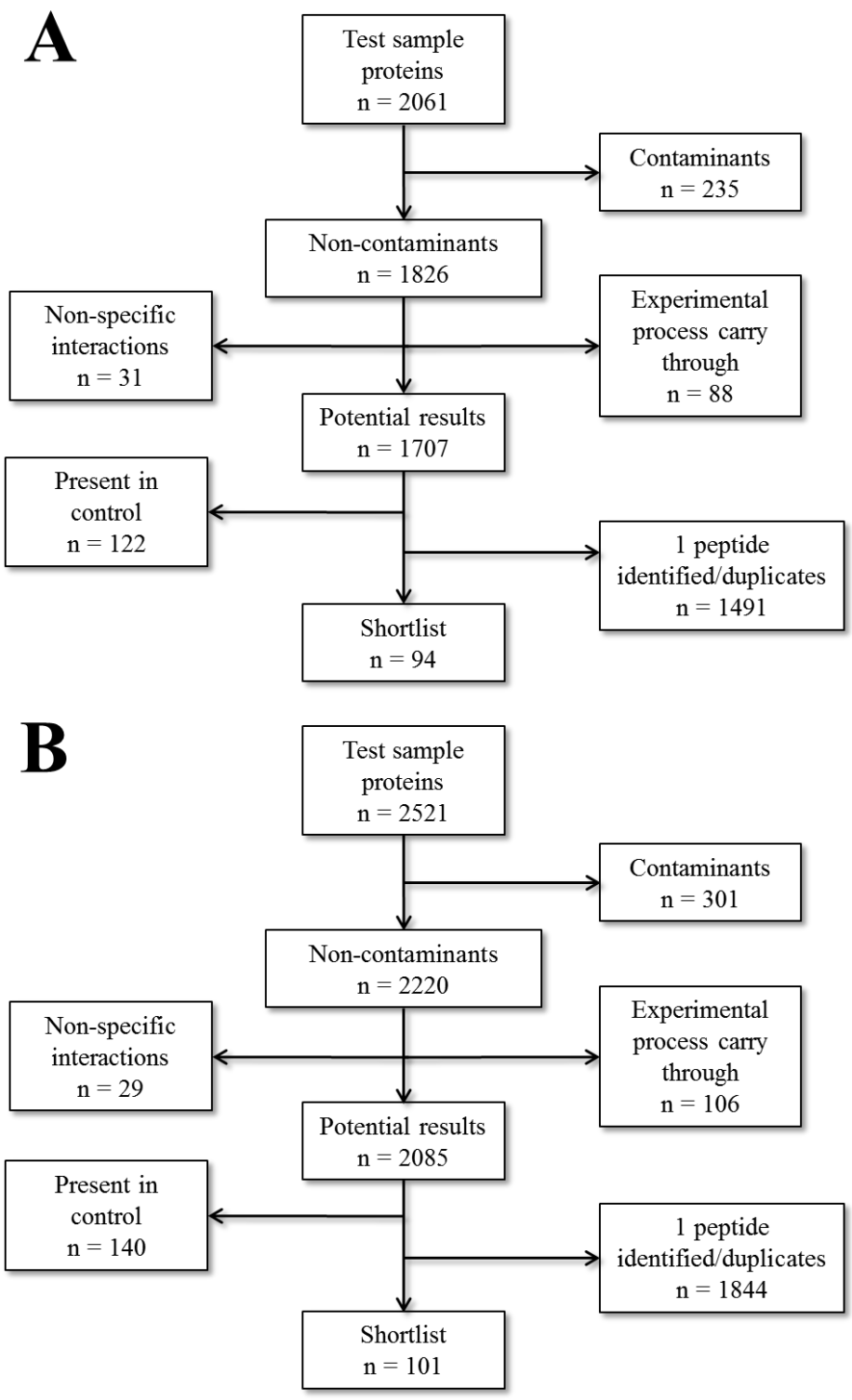

Figure 3.5 Flowcharts demonstrating the process by which the original list of proteins identified by MS/MS was reduced to give a final shortlist of potential interacting proteins. A - Experiment 1 (no antibody used as negative control). B - Experiment 2 (blank vector transfection used as negative control).

From these first two experiments, therefore, a number of limitations were identified which had to be addressed prior to proceeding with further MS/MS and determination of potential binding partners.

Contamination

Contamination by large amounts of keratin was significantly impeding the results. Of all peptides identified, 53.9 % were assigned to contaminants (Table 3.4). The mass spectrometer is only capable of analysing one compound of a particular *m*/*z* at a time; therefore if a large number of contaminant peptides were passing through the analyser this would be at the expense of other proteins. This was demonstrated by the poor yield of PBF in the test results. In the first experiment, PBF was only identified by 1 peptide (sequence coverage (SC) 6.7 %), and although 3 peptides were identified in the second experiment (SC 23.3 %) this was still fewer than expected.

Sample	n = 1		n = 2		Total
	Test	Control	Test	Control	
Total peptides	4267	3910	6085	7044	21306
Contaminants peptides	2176	1990	3393	3916	11475
Percent contamination	51.0 %	50.9 %	55.8 %	55.6 %	53.9 %

Table 3.4 Number of peptides attributed to contaminants in both test and control samples, across both experiments.

Non-specific interactions

A significant number of peptides resulted from presumed non-specific interactions. While the purpose of the control samples was to identify these, large numbers would have a similar effect to the contaminants in swamping the true values and therefore where possible should be reduced.

Low peptide yield

As well as reducing swamping, increasing the amount of lysate present would improve the average peptide yield per protein, helping to identify the true binding partners.

To manage these limitations, the following conditions were changed:

- Cell culture was carried out in T75 flasks, increasing the seeding area and cell count at confluency by 3 fold.
- High salt lysis buffer reduces non-specific interactions when immunoprecipitating for mass spectrometry (Shimwell et al. 2009) and this was therefore used in place of RIPA buffer. Additional wash steps were performed prior to cell lysis to remove as many residual proteins as possible.
- All steps of the procedure were undertaken in negative pressure conditions, using unopened, sealed microcentrifuge tubes for each experiment to reduce the risk of external contamination.

For the third experiment, again using K1s, the negative control used was blank vector transfected cells, with an additional list of control proteins transferred from the first 2 experiments. The process by which the shortlist of proteins was generated is described in Figure 3.6.

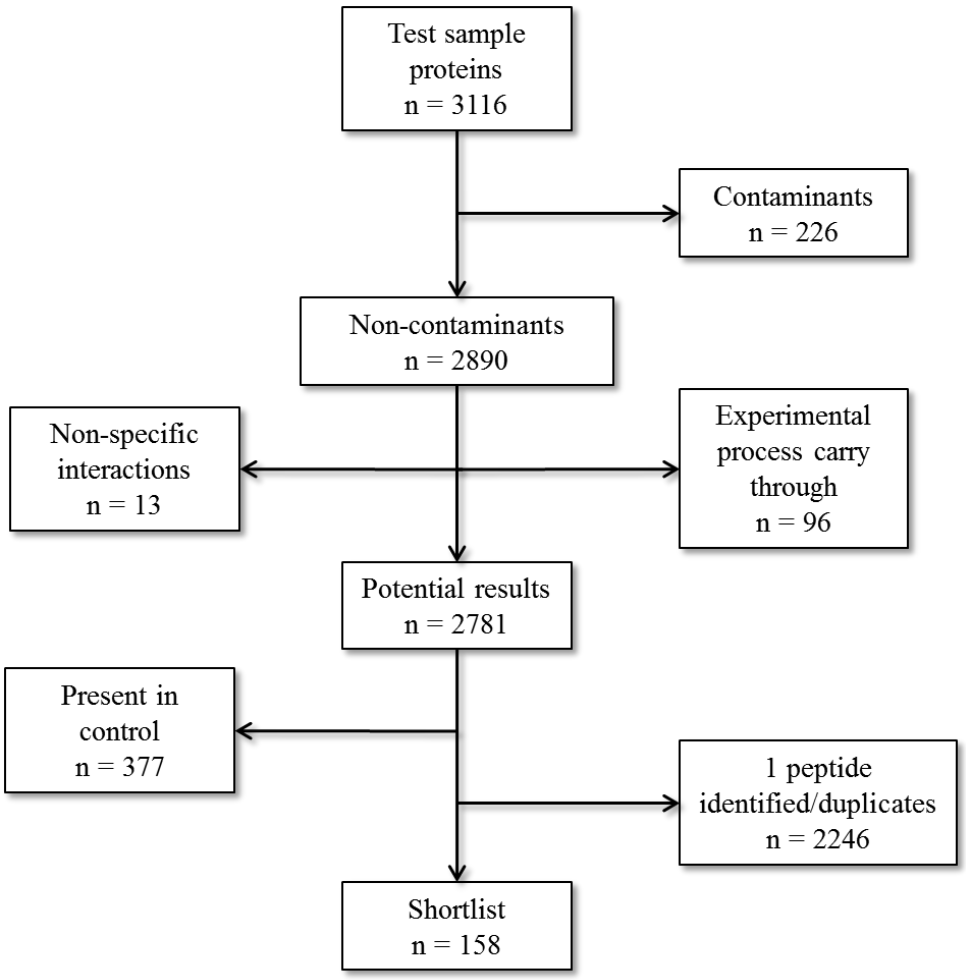

Figure 3.6 Flowchart demonstrating the process by which the shortlist of potential binding partners was generated.

There was less contamination, with 25.9 % of peptides belonging to contaminants (as opposed to 50.9 % and 55.7 % in the first 2 experiments) (Table 3.5).

Sample	n = 1	n = 2	n = 3	
			Test	Control
Total peptides	8177	13129	6522	9452
Contaminants peptides	4166	7309	1307	2998
Percent contamination	50.9 %	55.7 %	20.0 %	31.7 %

Table 3.5 Comparison of the number of peptides attributed to contamination. Experiment 1 (no antibody negative control) and Experiment 2 (blank vector negative control) show totals for both test and control results.

The number of proteins identified that could be attributed to either non-specific interaction or experimental carry-over was slightly reduced (13 and 96 respectively, compared to 30 and 97 on average from the first 2 experiments), although the reduction in the number of peptides attributed to these showed a greater reduction (7.5 % vs. 11.8 % and 14.6 %). Importantly, significantly more peptides were identified as belonging to PBF under the new conditions. In total, 45.6 % of the PBF sequence was covered by identified peptides (Figure 3.7), compared with 6.7 % and 23.3 % as described above.

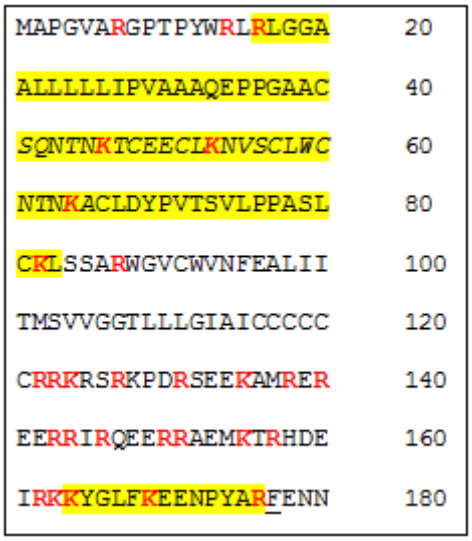

Figure 3.7 Amino acid sequence for PBF. Amino acids identified by MS/MS are highlighted in yellow. Trypsin digest sites are printed in red.

3.3.3 Optimum conditions for MS/MS

Based on the above results, a number of conditions were deemed to be necessary in order for MS/MS to identify potential binding partners with the greatest degree of accuracy, with minimal contamination and false positive results, and these are listed in Table 3.6.

Co-immunoprecipitation	Culture K1 cells in a T75 flask
	Transfect 15 μg DNA
	Transfect using PEI at 10:1
	Lyse and wash using high salt lysis buffer
	Use sterile, new microcentrifuge tubes for each step
Gel staining and digest	Work in negative pressure hood for all steps
Analysis of output	Discard all contaminants Discard proteins identified as non-specific interactors Produce a shortlist based on proteins not found in a control sample and identified by ≥ 2 peptides

Table 3.6 Summary of the optimum conditions needed for MS/MS.

3.4 Discussion

MS/MS provides a valuable method of identifying small amounts of protein from within a complex sample, although it is prone to misleading results due to contamination and non-specific interactions in the case of immunoprecipitated proteins. The aim of this chapter was to define the optimum conditions for co-immunoprecipitation and MS/MS, in order to develop a protocol that would allow for the accurate identification of potential binding partners of PBF.

Once the PBF-HA cDNA had been successfully sub-cloned into the vector pcDNA3.1+, optimum transfection conditions were determined using FACS. It was essential that a high level of transfection was achieved; the immunoprecipitation step relied on the transfected HA tag, therefore low levels of transfection would result in a smaller amount of PBF-HA immunoprecipitating and with that a smaller number of interacting proteins. By using K1 and TPC1 cells transfected with pMax-GFP, FACS identified those cells that had undergone transfection by their degree of fluorescence. Altering the amount of plasmid DNA as well as

transfection reagent allowed for multiple conditions to be assessed, with TEs of 81.4 % for K1 and 55.5 % for TPC1 cells achieved.

Once the optimal conditions for transfection had been established, the cells were lysed and passed through MS/MS. In the two initial experiments, 2 different negative controls were implemented. The first, using cells that had been transfected with PBF-HA as for the test samples but immunoprecipitated without the anti-HA antibody, identified those proteins present in the output data as a result of binding to the protein G sepharose beads and any that had been carried across as a result of the experimental process. In the second, the negative control was treated in exactly the same way as the test sample, but the cells were transfected with blank vector only. This had the advantage of identifying the same group of proteins as the first control, but with the addition of any proteins that had been carried through as a result of non-specific binding to the anti-HA antibody. Together, these 2 controls were able to provide a list of contaminants, non-specific interactors and carry-through proteins that could be discarded from future results.

The above measures removed many proteins from the output data, but there were still 1707 in the first and 2085 in the second to be analysed. The next step of the process removed any proteins that had been identified by 2 peptides in either of the control samples. The principle behind this step were that there would be many peptides/proteins that were identified that were not the result of true interaction between themselves and PBF-HA, and not identified by enough peptides to be placed on the previous list of exclusions. Using spreadsheet analyses, these lists could be compared easily and any peptide that met the criteria removed. Finally, only proteins that had been identified by more than one peptide were included in the shortlist of potential binding partners.

This method of shortlisting did have shortcomings. It is possible that some interacting proteins were discarded due to a chance/false finding in the control sample. Similarly, one may have been overlooked as it was only identified by one peptide, either due to a small amount of protein present or as a result of swamping by a more abundant peptide.

Another limitation of the process was that PBF was only identified by one peptide in the first and 3 peptides in the second experiment. It was not possible to determine whether this was a result of swamping by other peptides or a lack of protein brought forward to MS/MS.

To improve on these results, a number of conditions were changed to address the potential and definite problems. Firstly, cells were cultured in larger quantities, which increased by three-fold the amount of lysate used for immunoprecipitation. More wash steps were undertaken, using a high salt lysis buffer, with the aim of both reducing the number of non-specific interactions and reducing the amount of protein brought through from cell culture. Finally, all steps were undertaken in a negative pressure fume hood with a clean filter, to reduce the amount of dust contamination.

The following results were much improved, contamination by keratin and similar proteins was reduced by 50 – 60 %, and although the number of proteins from the non-specific and carry-over lists remained similar, the proportion of peptides attributed to them was reduced by almost a half. Additionally, PBF was strongly identified in this experiment, adding credibility to other strongly identified proteins.

Concluding remarks

This chapter has described the process by which the optimal conditions for identification of potential binding partners of PBF have been determined. The process involved keeping contamination by keratin and other dust based contaminants to a minimum, while also

reducing the amount of non-specific interactions using high salt lysis buffer and stringent wash steps.

Although the final shortlist from the first two experiments would not be used in further analysis, they provided important information as to the proteins that could be discarded from analysis.

Chapter 4 Novel binding partners of PBF identified by MS/MS

4.1 Introduction

Chapter 3 discussed the optimisation of the MS/MS process to achieve the greatest possible sensitivity for the detection of potential binding partners of PBF. This was an important step as although MS/MS is an exceptionally sensitive tool, it is also undiscriminating and will therefore "identify" a very large number of proteins, which will include the true interactors as well as contaminants, non-specific interactors and those proteins inherent to the experimental process. A number of experimental conditions and analysis parameters were therefore set which limited the results to those proteins most likely to represent true interacting partners. Although there may be some valid results that would be discounted as a result of this, as well as many false positives that would be carried forward, these would be minimised.

The aim of this chapter, therefore, was to generate a shortlist of likely binding partners and, from these, select three to take forward to validation experiments and functional studies. In addition, a secondary aim was to determine a larger list of potential binding partners that could be used in further studies of PBF function.

4.2 Methods

4.2.1 MS/MS protocol

Mass spectrometry was carried out as described in Section 3.2.5. K1 and TPC1 cells were used for transfection, co-immunoprecipitation and generation of gel fragments for use in HPLC and MS/MS. Anti-HA was used to immunoprecipitate lysates from cells transfected with *PBF-HA*, while our polyclonal rabbit anti-human PBF (Eurogentec, Seraing, Belgium,

(Smith et al. 2009)) was used for cells transfected with untagged PBF or untransfected cells. Analysis was as described in Section 3.2.5.4.

4.2.2 Statistical methods

Full lists of protein hits from both test and control samples were exported to MS Excel. Contaminants, non-specific interactions, carry over proteins and duplicates were deleted (see section 3.3.2). Any protein identified in the control samples by 3 peptides once, or 1 or 2 peptides more than once, was also removed. The resulting long-list was used to compare results across the different runs, with protein hits assessed on the number of peptides identified, the number of runs the protein was found in, and the score for each protein.

4.3 Results

4.3.1 Immunoprecipitation with anti-HA

Using the protocol optimised in Chapter 3, potential binding partners of PBF were identified using K1 cells. Despite variation in the total number of proteins identified in each run, the final shortlist number was similar, with most variation occurring in the number of proteins identified by one peptide only or with duplicated proteins assigned to different species (Table 4.1). The amount of contamination varied across experiments, despite strict adherence to dust free protocol; the major contributor to this was keratin (Table 4.2).

	R3	**R4**	**R5**
Test sample proteins	3166	2677	3784
Contaminants	*226*	*352*	*273*
Non-contaminants	2890	2325	3511
Non-specific interactions	*13*	*14*	*22*
Experimental carry through	*96*	*123*	*135*
Potential results	2781	2188	3374
Present in control	*377*	*617*	*683*
1 peptide/duplicates	*2246*	*1432*	*2502*
Shortlist	**158**	**139**	**189**

Table 4.1 Table demonstrating elimination process for proteins identified by MS/MS runs R3 to R5.

	R3	**R4**	**R5**
Total peptides	6522	6180	6070
Contaminants	1307	3428	1886
Percent contamination	**20.0 %**	**55.5 %**	**31.1 %**

Table 4.2 Contamination of MS/MS samples in runs R3 to R5.

4.3.2 Binding partners identified in TPC1 cells

To provide another cell line representative of thyroid cancer with which to validate and compare potential binding partners, TPC1 cells were used. This was another model of moderately differentiated thyroid cancer, but one displaying the RET/PTC re-arrangement as opposed to *BRAF* mutation. The protocol was identical to that used for K1 cells. The number of proteins identified was comparable to the K1 cells (Figure 4.1), while contamination was 27.9 %.

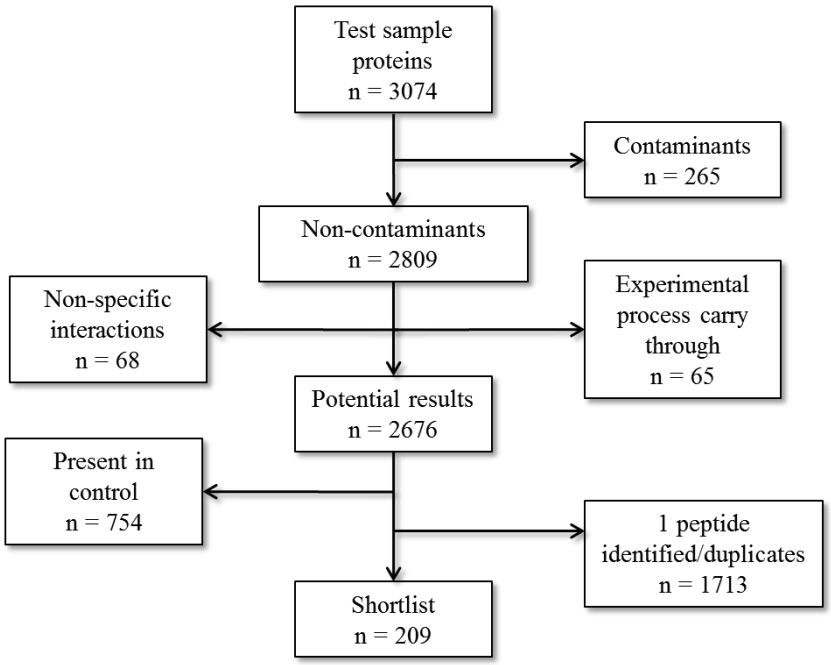

Figure 4.1 Flowchart demonstrating protein elimination process for TPC1 cells.

4.3.3 Immunoprecipitation using an anti-PBF antibody

The above experiments sought to identify potential binding partners of PBF using a tagged protein; the final experiment involved immunoprecipitating using an anti-PBF antibody, with K1 cells either transfected with PBF, or left untransfected. As a percentage of total peptides, contamination was higher in both of these experiments. The number of shortlisted proteins was again comparable to previous runs (Figure 4.2). However, one limitation of these experiments was that PBF was not identified in the untransfected run. This may have been due to the excess contamination; however it is possible that the anti-PBF antibody was not strong enough to ensure sufficient pull back of protein-protein complexes to allow detection of these lower levels of PBF, especially in the presence of other swamping proteins.

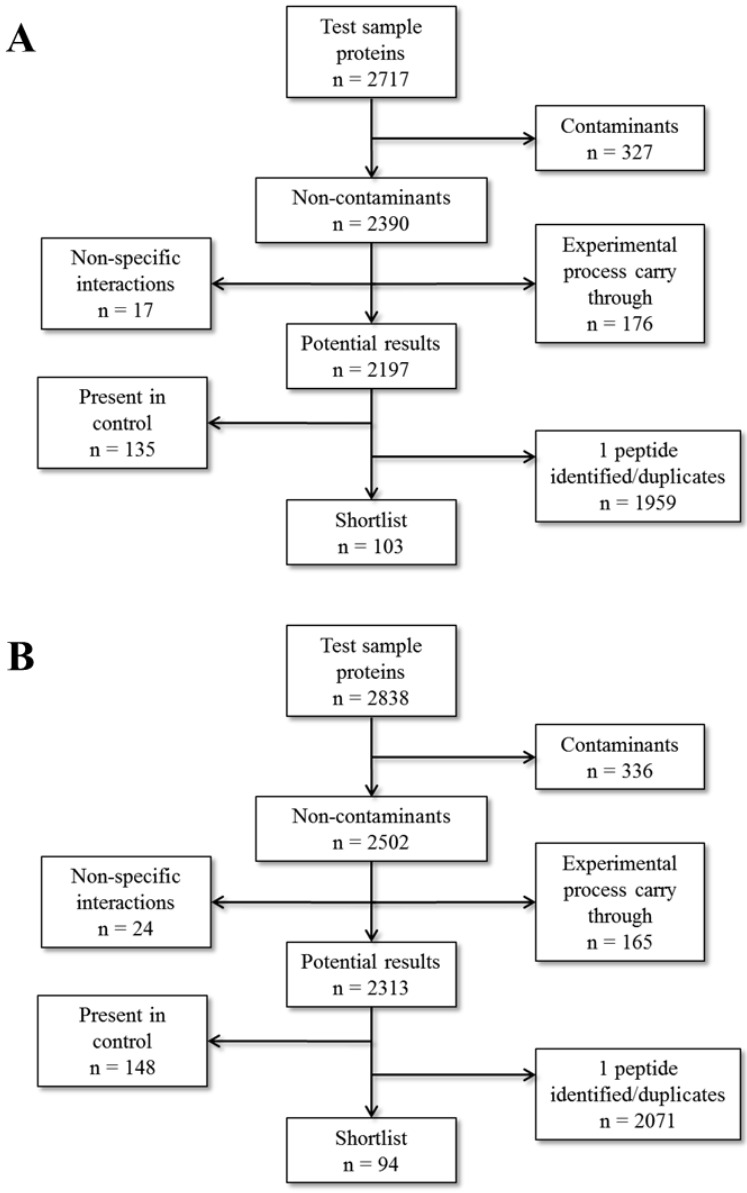

Figure 4.2 Flowcharts detailing analyses of a PBF transfected run (A) and an untransfected run (B).

4.3.4 Shortlisting of potential binding partners

To draw up a final list of potential binding partners, the shortlist from each experiment was compared, with those proteins scoring highest across several runs being included. Following this, the full list of proteins (i.e. including those identified by 1 peptide only) was

compared across each experiment, to identify any proteins that may have been excluded based on a lower score that were actually present in multiple runs, thus representing potential true positives. This list is documented in Appendix 1. Finally, a search was carried out for any proteins that had been predicted as potential binding partners based on analysis of PBF structure. Ranking of this final shortlist was carried out by assessing the total score assigned to the protein across all experiments by the Mascot search engine, and factoring in the total number of peptides identified. The final list of 9 proteins is shown in Table 4.3. After assessing the scores and potential relevance to PBF physiology as well as practicality of future experiments, three proteins were chosen for validation: thyroglobulin, cortactin and src / src-family kinases.

Protein Name	R3		R4		R5		TPC		PBF o/e		Untrans		Total peps	Total sc	Average score per peptide
	Peps	Sc	Peps	Sc	Peps	Sc	Peps	Sc	Peps	Sc	Peps	Sc			
Cortactin	10	413.3	-	-	-	-	2	66.9	-	-	-	-	12	480.2	40.0
Heat shock protein 90-beta	18	752.8	2	52.2	4	149.0	4	127.3	-	-	-	-	28	1081.3	38.6
Thyroglobulin	-	-	-	-	6	221.3	1	15.3	2	57.6	3	107.8	12	402.0	33.5
Src family kinases (Lyn/Src)	-	-	-	-	2	58.5	1	16.7	1	41.2	-	-	4	116.4	29.1
Leucine-rich rpt flightless-interacting protein 1/2	2	50	1	35.6	3	62.4	4	127.3	-	-	-	-	10	275.3	27.5
Focal adhesion kinase 1	-	-	1	17.4	-	-	2	54.2	1	25.4	-	-	4	97.0	24.3
Uveal autoantigen with coiled-coil domains	3	47.0	-	-	2	42.1	-	-	1	35.6	1	23.4	7	148.1	21.2
Adenomatous polyposis coli protein	1	17.6	2	36.8	1	28.3	-	-	2	38.3	1	26.7	7	147.7	21.1
Citron Rho-interacting kinase	-	-	-	-	3	39.2	2	34.7	1	39.9	2	39.9	8	153.7	19.2

Table 4.3 Table listing the proteins identified by MS/MS as most likely to interact with PBF. Score was assigned by Proteinscape for each experiment. Ranking was based on average score per peptide across the experiments (n=6). Peps = Number of peptides, Sc = Score, Untrans = Untransfected, "-" = no peptides found.

4.4 Discussion

In chapter 3, the optimum conditions for MS/MS were described, and in this chapter these were used to generate a list of proteins that may interact with PBF. Initially, 3 experiments were performed utilising HA-tagged PBF and immunoprecipitating with an anti-HA antibody. Each provided a similar number of proteins for consideration. A further 3 experiments were then carried out with varied conditions; in the first, the K1 cell line was substituted for the TPC cell line. Although both represent papillary thyroid carcinoma, the genotype of the two varies and there may have been proteins identified in the TPC1 line that were missed in the K1 cells. Similarly, should a protein be found in both cell lines, this would lend credibility to the potential interaction. Finally, K1 cells were again used but immunoprecipitation was carried out using an anti-PBF antibody, with both over-expressed and endogenous levels of PBF. In the former, this would hopefully identify any proteins in which an interaction with PBF was disrupted by the HA tag, and the latter would provide strong evidence for an interaction as only those proteins present in abundance in the immunoprecipitant would be picked up by MS/MS.

To develop a final shortlist, the results from all experiments were compared on an Excel spreadsheet. It was not practical to validate all potential interactions, or even all those that appeared most likely, and therefore a number of strategies, both objective and subjective, were employed to generate a list of proteins for validation. Firstly, the elimination protocol described in Chapter 3 was used on each list of proteins, although in this case those identified by 1 peptide only were retained. Filters were then used to remove all proteins identified by only 1 peptide in 1 run, and proteins identified by a total of 2 peptides were manually searched and eliminated if their scores were low. In the next stage, the number of peptides each protein was identified by in each run was combined, as was the score assigned by

Mascot. This then allowed a "score per peptide" to be generated, and the remaining proteins ranked by this result. The list was again manually searched, and a shortlist of 9 proteins was generated, based on both final score and also potential relevance. Each of these proteins would benefit from further study, but due to restraints on time and resources, 3 were chosen for further validation and, if proven as true interacting partners, functional studies.

Cortactin: Average score per peptide (ASP) – 40.0

Cortactin was first described in the early 1990s as a Src substrate that bound to filamentous actin and was present in lamellipodia; cytoskeletal actin projections from the mobile edge of a cell which aid movement (Wu and Parsons 1993). The *CTTN* gene is located at 11q13, which is a region amplified in a number of cancers, including breast and head and neck (Schuuring et al. 1993). Cortactin has seen been implicated in a number of processes key to cancer progression: invadopodia formation (protrusions from the cell membrane associated with invasion), cell migration, stabilising of branched actin networks and membrane trafficking (Weaver 2008; Kirkbride et al. 2011). Cortactin had the highest score of all the shortlisted proteins, and was identified in both K1 and TPC1 cells. Given that PBF is a protein that is shuttled to and from the cell membrane, and that over-expression leads to an increase in cell invasion, an interaction with cortactin may serve to further explain these effects. This, combined with its high score, led to cortactin being chosen for validation.

Thyroglobulin: ASP 33.5

Thyroglobulin is the essential pre-cursor to thyroid hormone and is present in abundance in the thyroid follicle. Although at first it was thought possible that its presence may have been due to the high quantity present and therefore a non-specific binding/carry over, none

was identified in any of the control samples and therefore it could not be discounted. Additionally, when the data generated from the first 2 experiments (carried out in T25 flasks) was searched, thyroglobulin was identified by 2 peptides in each, lending further credence to the result. Given that the PBF-Tg mice displayed macro-follicular, hyperplastic goitres with deranged thyroid hormone content, this potential interaction may provide clues as to the mechanism by which this occurs.

Src family kinases: ASP 29.1

A number of Src family kinases (SFKs) were identified, including Lyn, Src and Yes; the former of which had the highest score. The SFKs have significant homology and it is possible that peptides assigned to one member actually belonged to another. These proteins were of particular interest, as kinase prediction software had identified Src as a potential kinase for PBF. Given this fact, and that there are a number of cancer therapies currently being trialled using Src as a target, it was felt appropriate to shortlist the SFKs as potential binding partners. The parent member of the group - and the kinase with the highest predicted score on phosphorylation prediction software - was Src, and these factors led to its inclusion in the validatory group.

The remaining proteins were from a variety of functional classes, and future research will focus on defining these in more detail.

Heat shock protein 90 – beta: ASP 38.6

Hsp90 is a 90 kDa protein which is ubiquitoiusly expressed and plays a key role in protein homeostasis. It is a chaperone protein involved in protein folding as well as

intracellular trafficking (Pearl and Prodromou 2006). Expression of Hsp90 is abundant, and this rises 2 to 3 fold in tumours compared to normal tissue (Moulick et al. 2011). Inhibition of Hsp90 has been the subject of clinical trials for some time (Barrott and Haystead 2013), although none are in regular oncological use. The protein scored highly in MS/MS, and it will certainly warrant further investigation.

Leucine-rich repeat flightless-interacting protein 1 / 2: ASP 27.5

LRRK1 is a large, 225 kDa protein which is thought to function as a GDP/GTP-binding protein (Korr et al. 2006). Although its paralogue, LRRK2, is associated with Parkinson's disease (Lu and Tan 2008), very little is known regarding the function of LRRK1. Mutations have been described in both LRRK1 and 2; a barrier to clear functional work on either protein is the lack full length recombinant proteins, with either truncated or tagged proteins being used (Civiero and Bubacco 2012). LRRK1 scored highly, however despite this the lack of commercially available materials with which to perform validatory experiments meant that it would not have been feasible to pursue it at this stage and LRRK1 and 2 were therefore discarded.

Focal Adhesion kinase 1: ASP 24.3

FAK is a non-receptor tyrosine kinase with important roles in normal human development, as well as cell migration (via the actin cytoskeleton) and proliferation (Schaller 2010). Perhaps most importantly in relation to this thesis, FAK phosphorylates Src, and in doing so increases its kinase activity (Aleshin and Finn 2010). It is possible that FAK was identified through indirect interaction with PBF, with a complex forming between activated Src, FAK and PBF at the cell periphery. Another possibility is that FAK is the kinase

responsible for phosphorylating PBF. Given the limited time available for this PhD, and the strength of data suggesting Src as the principle kinase for PBF (both with phosphorylation prediction software and MS/MS), only Src was taken further for validation.

Uveal autoantigen with coiled-coil domains and ankyrin repeats: ASP 21.2

UACA is an autoantigen initially identified in thyroid tissue and shown to be upregulated by TSH (Wilkin et al. 1996). Most studied in relation to its role in panuveitis (Ohkura et al. 2004), it has recently been shown to be upregulated in a lung and prostate cancer, with the proposed mechanism being inhibition of apoptosis (Burikhanov et al. 2013). How this would correlate with the effects of PBF is unclear, and while a potential interaction with UACA is interesting and will warrant further study in the future, the paucity of evidence regarding its structure and function at the current time led to its exclusion from further study.

Adenomatous polyposis coli protein: ASP 21.1

The APC gene encodes a protein that down-regulates the Wnt signalling pathway through interaction with β-catenin, and thereby inhibits tumourigenesis (Yokoyama et al. 2011). Mutations in APC result in Familial Adenomatous Polyposis (FAP), a hereditary disorder of multiple colonic polyps with a 100 % progression to malignancy. There is a 1-6 % lifetime risk of thyroid cancer with FAP, usually papillary (Steinhagen et al. 2012). In addition, β-catenin mutations are observed in anaplastic thyroid carcinomas (Yokoyama et al. 2011), further indicating that aberrant activation of this pathway is important in thyroid cancer. However, its contribution outside of FAP / specific ATC studies is as yet unknown. An interaction between APC and PBF could, therefore, provide an explanation for the tumourigenic effects of PBF, and will be an exciting avenue for further research.

Citron Rho-interacting kinase: ASP 19.2

Citron kinase is a serine/threonine kinase first identified as a binding partner of Rho (a small GTP-ase from the same family as the proto-oncogene Ras) (Zhao and Manser 2005). Having been mainly studied in the context of neuronal growth, it has a role in the contractile process of cytokinesis (Madaule et al. 2000). Mice deficient in the *CRIK* gene display abnormal cytokinesis and apoptosis of neuronal precursors (Di Cunto et al. 2000). The relevance of citron kinase to PBF physiology is not readily apparent. While it is known to phosphorylate MLC (Yamashiro et al. 2003), further studies have not been carried out to identify other substrates, and whether it was identified due to direct or indirect interaction with PBF will prove interesting for further research in the future.

Concluding remarks

This chapter has described the generation of a shortlist of potential binding partners of PBF, and also provided a longer list (Appendix 1), both of which will serve as a resource for further research beyond the scope of this thesis. Three proteins have been highlighted for validation and functional experiments: Thyroglobulin, cortactin and src, all of which have the potential to provide further insight into the mechanisms by which PBF has its effects of the cell.

Chapter 5 PBF and thyroglobulin interact in thyroid cells

5.1 Introduction

The first of the 3 proteins chosen for validation, thyroglobulin is a large, 660 kDa dimeric molecule that is a vital component of the thyroid follicle. It is synthesised within the thyroid follicular cell via a complex series of steps, increasing in size until the final product is fully assembling immediately prior to secretion into the colloid (Malthiery and Lissitzky 1987). Thyroglobulin (Tg) was identified in 3 of the main experiments and also in the initial, standard setting experiments and was therefore one of the stronger results produced. This was especially interesting as the thyroid glands of the PBF-Tg mice displayed macro-follicular goitres with higher intra-thyroidal levels of T3 and T4 (Read et al. 2011; Smith et al. 2012); it is conceivable, therefore, that an interaction between PBF and Tg might contribute to this phenotype. The aim of this chapter was thus to validate the interaction between PBF and Tg, and if proved, to assess its functional significance.

5.2 Methods

5.2.1 Cell culture and transfection

K1 and TPC1 cells were maintained in RPMI as described in section 2.1. *PBF-HA* was transfected into K1, TPC1 and primary thyrocytes as described in Section 2.2.2.

5.2.2 GST pull-down assay

GST-tagged PBF was translated as described in 2.5.1. [^{35}S]-methionine labelled thyroglobulin was prepared using the TNT® T7/SP6 Coupled Reticulocyte Lysate System (Promega, as described in Section 2.5) from the full length *Tg* cDNA in the vector pCR-XL-TOPO (IMAGE clone 9056745, Source Biosciences). The assay was performed as described in Section 2.5.

5.2.3 Co-immunoprecipitation and Western Blot

Protein was extracted from cell lysates as described in section 2.3.1. Co-immunoprecipitation was performed as per Section 2.4, with anti-Tg (Dako UK Ltd, Ely, UK) used at concentrations of 1:10, 1:7.5 and 1:5 to immunoprecipitate thyroglobulin. For Western blotting, anti-Tg was used at 1:500, anti-HA at 1:2000 and anti-PBF at 1:500. Anti-β actin was used as a loading control as described above.

5.2.4 Primary thyroid culture

Human thyroid tissue was obtained and cultured as described in Section 2.7 with the approval of the Local Ethics and Research Committee.

5.2.5 Homogenisation of thyroid tissue

Human thyroid tissue was obtained from macroscopically normal thyroid tissue after thyroidectomy with approval of the Local Ethics Research Committee. Tissue was snap frozen in liquid nitrogen and stored at -80 °C. Thyroid tissue was homogenised in 300 µL RIPA / PI (described in Section 2.3.1). Prior to analysis, the homogenate was diluted with RIPA in to final concentrations of 12.5 %, 33.3 %, 50 % and 100 % homogenate.

5.2.6 Fluorescence immunocytochemistry

Samples were prepared as described in Section 2.6. Primary antibodies were anti-Tg (EPR3614, Abcam, Cambridge, UK) (1:100) and anti-HA (1:200).

5.2.7 Statistical analysis

Statistical analysis was performed as described in 2.8.

5.3 Results

5.3.1 Translation of [^{35}S]-methionine labelled thyroglobulin and GST pull-down assay

Despite scoring highly in MS/MS, the interaction between PBF and Tg needed to be validated by at least one other independent technique. The first to be implemented was the GST pull-down assay. In this experiment, GST-tagged PBF and [^{35}S]-methionine labelled Tg were translated and analysed in a cell free setting. GST-tagged PBF was first generated and found to run at the predicted size of 42 kDa when probed with our anti-PBF antibody (Figure 5.1A). Tg was translated but when run on SDS-PAGE, no band was seen at the predicted mass of 330 kDa (for the monomeric molecule). Instead, a number of bands were observed at lower masses, as indicated in Figure 5.1B by asterisks. It was thought possible that these may represent sub-units of Tg, and therefore the pull-down assay was run to test if any of these fragments bound to GST-PBF. No evidence of an interaction was evident for any of these bands (Figure 5.1C, n = 3), and given the difficultly in translating such a large molecule *in vitro*, further attempts at pull-down were not attempted.

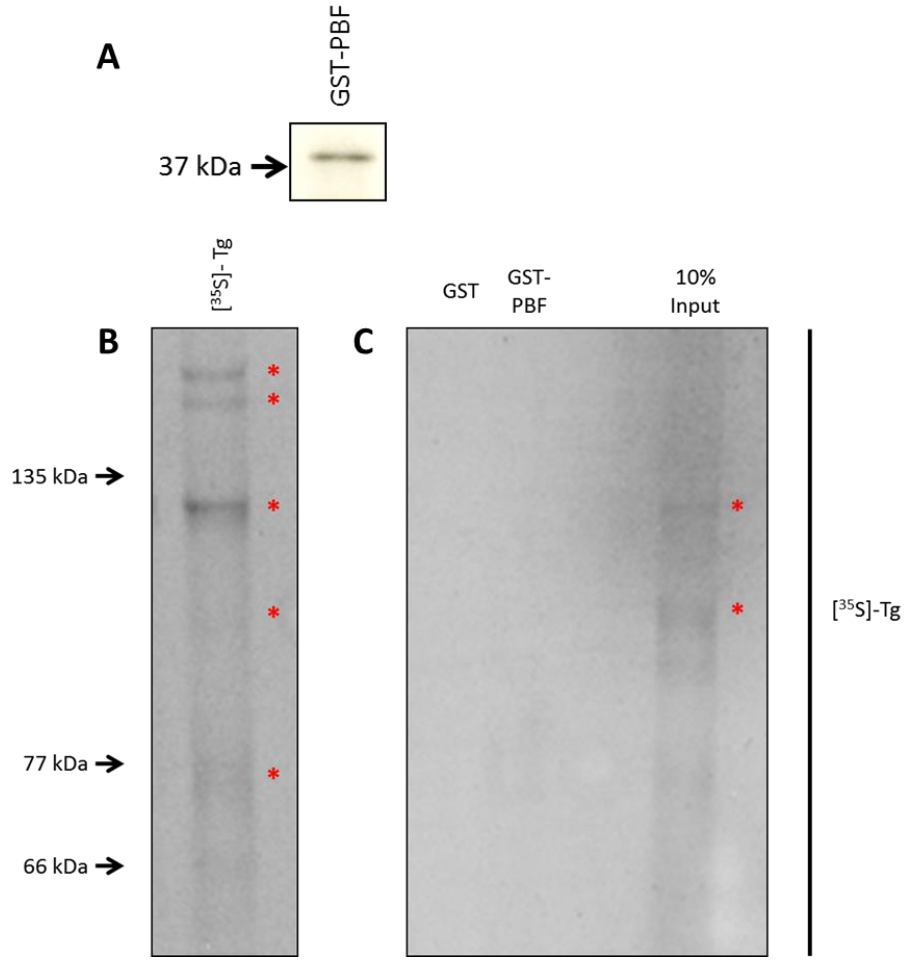

Figure 5.1 GST tagged pull-down assay to investigate an interaction between PBF and thyroglobulin. A: GST-tagged PBF ran at the expected size of 42 kDa. B: [^{35}S]-methionine Tg translation produced a number of bands of differing molecular weight (indicated by asterisks). C: No evidence of an interaction between GST-PBF and Tg was observed (n = 3).

5.3.2 Co-immunoprecipitation

Due to the large size of the Tg molecule and the difficulties encountered during the pull-down assay with translation of the protein from cDNA, an assessment of binding of endogenous Tg to PBF was made, the first step of which involved determining the expression of Tg within the thyroid cell lines used in this thesis.

5.3.2.1 Thyroglobulin expression in transformed cell lines

In the first instance, untransfected K1 and TPC1 cells were assessed by Western blotting for their endogenous Tg content. In both of these cell lines, there was a predominant band at approximately 140 kDa, with some fainter bands evident at lower masses (Figure 5.2A). No bands were observed above 140 kDa that could be attributed to the full length monomeric or dimeric molecule. A similar picture was observed when 6 % acrylamide gels were used as opposed to 12 %, although the gels were more difficult to work with and as no additional information was gained they were not used further (data not shown). These bands may have represented denatured sub-units (see Discussion, Section 5.4), as peptide chains were identified by MS/MS at these levels (approximately 150, 50 and 30 kDa) and some binding to PBF should therefore be evident.

Given the altered thyroid hormone content of the PBF-transgenic mouse thyroids, the effect of over-expressing PBF-HA on Tg content was assessed prior to co-immunoprecipitation to identify if there was a potential alteration in expression which would hinder interpretation of results. There was no significant difference in Tg levels between cells transfected with *PBF-HA* and those transfected with vector only (105.7 ± 33.6 % of control, p = ns, n = 3) (Figure 5.2).

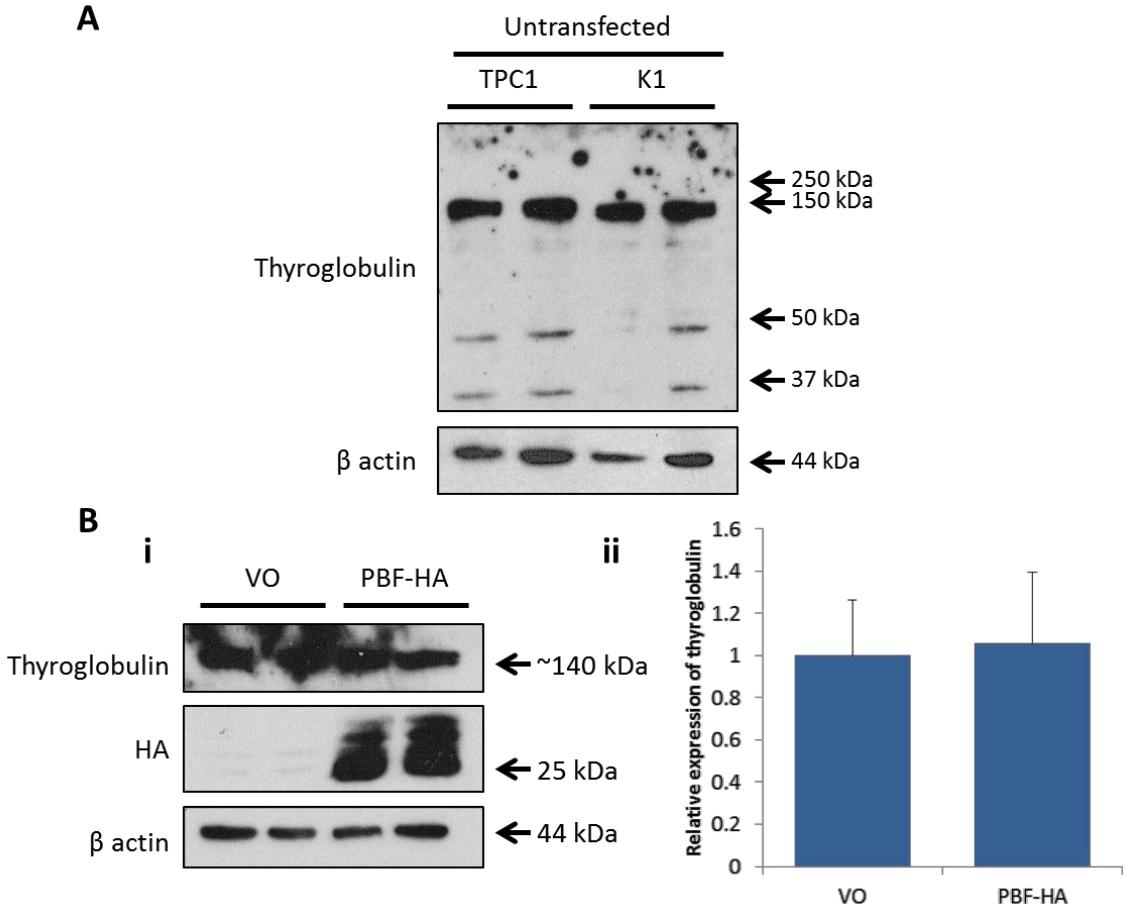

Figure 5.2 Thyroglobulin expression in K1 and TPC1 cells. A: In TPC1 and K1 cells, Tg was identified predominantly as a band at 140 kDa. B: Representative Western blot demonstrating no change in Tg with PBF-Ha transfection (i), and scanning densitometry showing relative value with VO vs. PBF-HA transfection (n = 3). β actin is shown as a loading control.

5.3.2.2 Co-immunoprecipitation in cell lines

Having established that thyroglobulin levels were not altered by the over-expression of PBF-HA, K1 cells were transfected with *PBF-HA* and the lysates immunoprecipitated with an anti-HA antibody. The subsequent solution was run through SDS-PAGE and probed for Tg. There was no evidence of interaction between the two proteins in this assay (Figure 5.3, n = 3). The reverse co-immunoprecipitation, in which lysates were immunoprecipitated with anti-Tg and probed for PBF-HA, did not demonstrate an interaction (data not shown).

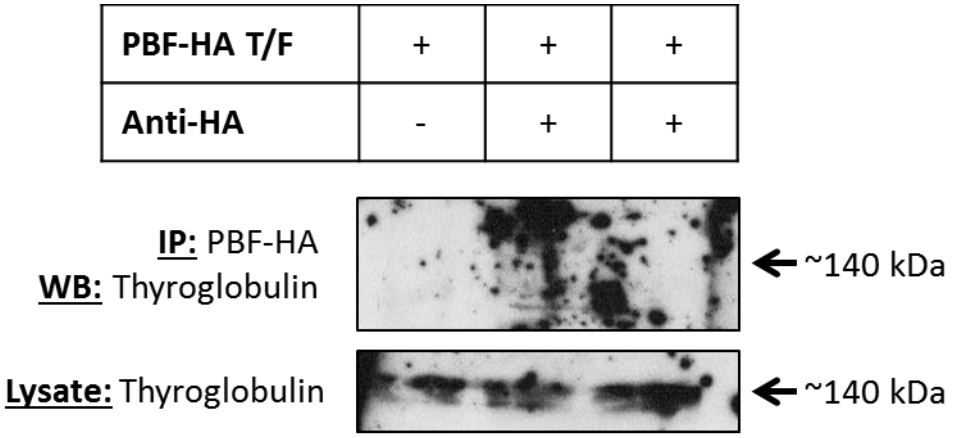

Figure 5.3 Attempted co-immunoprecipitation of PBF and Tg in K1 cells. K1 cells were transfected with PBF-HA and immunoprecipitated with an anti-HA antibody. No evidence of interaction was demonstrated in this assay. T/F = transfection, IP = immunoprecipitate, WB = Western blot

5.3.2.3 Thyroglobulin expression in human primary thyrocytes

This lack of evidence of an interaction in the cell free setting and in transformed cell lines led us to assess whether Tg would be more appropriately assessed in primary thyroid cultures, in which the processes for generation of the final molecule would be potentially more intact. Human primary thyroid cultures from macroscopically normal thyroid tissue were assessed by Western blot and compared to the 2 cell lines. In all cases, there were many more bands of varying sizes present in the samples from primary culture; the dominant bands were around 140 kDa and above, which were more likely to represent the monomeric molecule, although lower bands were also observed, including a band at approximately 25 - 30 kDa (Figure 5.4, indicated by red asterisks).

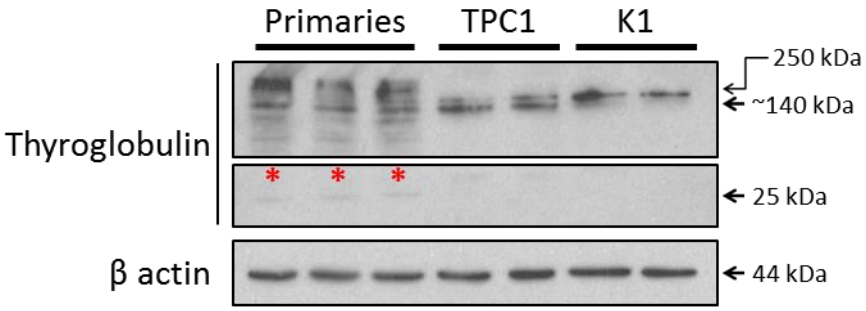

Figure 5.4 Western blot of human primary thyrocytes, TPC1 and K1 cells to demonstrate the expression of Tg. In addition to the bands ≥ 140 kDa, a smaller band at 25 kDa was observed in the primary cells (red asterisk). β actin is included as a loading control.

5.3.2.4 Co-immunoprecipitation using human primary thyrocytes and thyroid tissue

Due to the large number of bands observed when probing for Tg, the decision was made to immunoprecipitate with the anti-Tg antibody and probe for PBF in an attempt to detect an interaction. There was however still concern that the full length Tg molecule was not present in thyroid cultures, and that this would only be fully formed within the thyroid gland itself. Therefore, alongside co-immunoprecipitation using primary thyroid cultures, macroscopically normal thyroid tissue was homogenised and immunoprecipitated with anti-Tg.

In the former experiment, un-transfected cells were used to ensure as little disruption to the culture as possible. Immunoprecipitation of the lysates was carried out with differing concentrations of anti-Tg antibody. PBF was successfully co-immunoprecipitated with all concentrations, compared to no detectable PBF in the no-antibody control sample. The highest yield of PBF was with an antibody to lysate ratio of 1:5 (Figure 5.5).

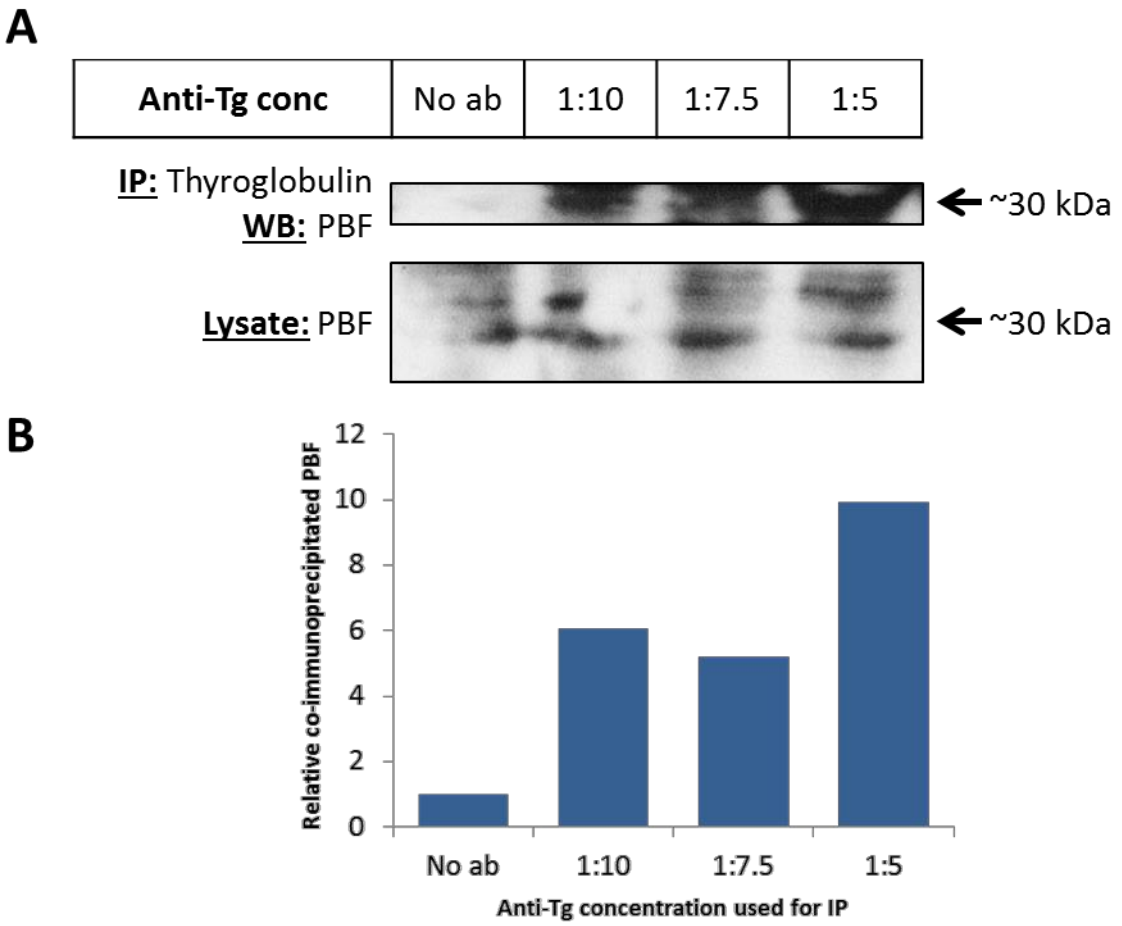

Figure 5.5 Co-immunoprecipitation of PBF and Tg in human primary thyroid cells. A: Untransfected cell lysates were immunoprecipitated with differing concentrations of anti-Tg and probed for PBF, with evidence of interaction compared to the no-antibody control ("No ab"). B: Scanning densitometry analysis of PBF Co-IP relative to PBF lysate.

Using this antibody ratio, co-immunoprecipitation was performed on homogenised human thyroid tissue. In this experiment, the homogenate was diluted with decreasing quantities of RIPA buffer prior to immunoprecipitation, and as expected this led to an increase in the amount of PBF detected, although this was not significant (Figure 5.6) ($R^2 = 0.44$, $p = 0.36$), providing further evidence to support the interaction between PBF and Tg.

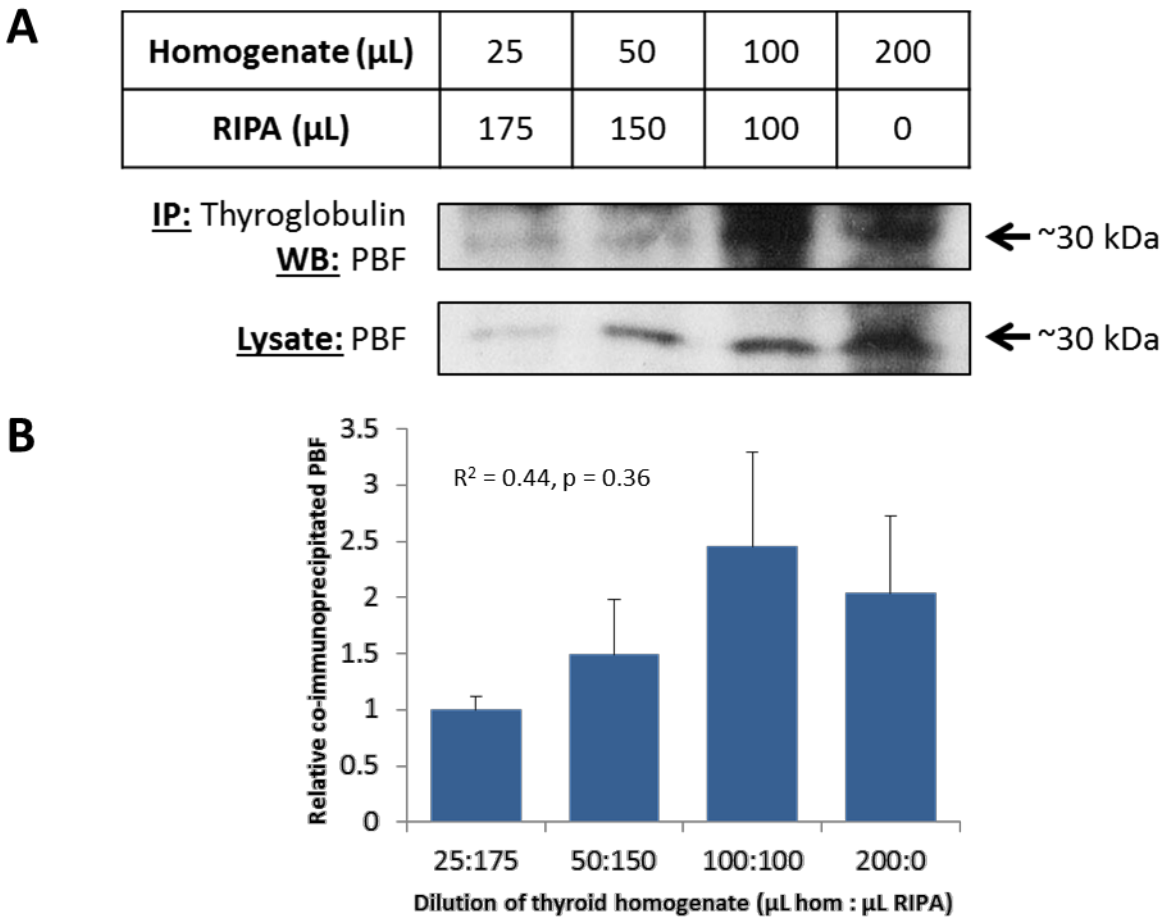

Figure 5.6 Co-immunoprecipitation of PBF and Tg in homogenised human thyroid tissue. A: Homogenised tissue was diluted with differing amounts of RIPA buffer and immunoprecipitated with anti-Tg then probed for PBF. B: Scanning densitometry analysis of the amount of co-immunoprecipitated PBF (n = 3).

5.3.3 Fluorescence immunocytochemistry

5.3.3.1 Thyroglobulin and PBF co-localise in intra-cellular vesicles

Having validated the MS/MS findings, fluorescence immunocytochemistry was undertaken to assess in what areas of the cell PBF and Tg interact. Initially, this was performed in K1 and TPC1 cells, and a small degree of co-localisation was observed within intra-cellular vesicles in the peri-nuclear region, with some co-localisation also apparent at the cell membrane (Figure 5.7).

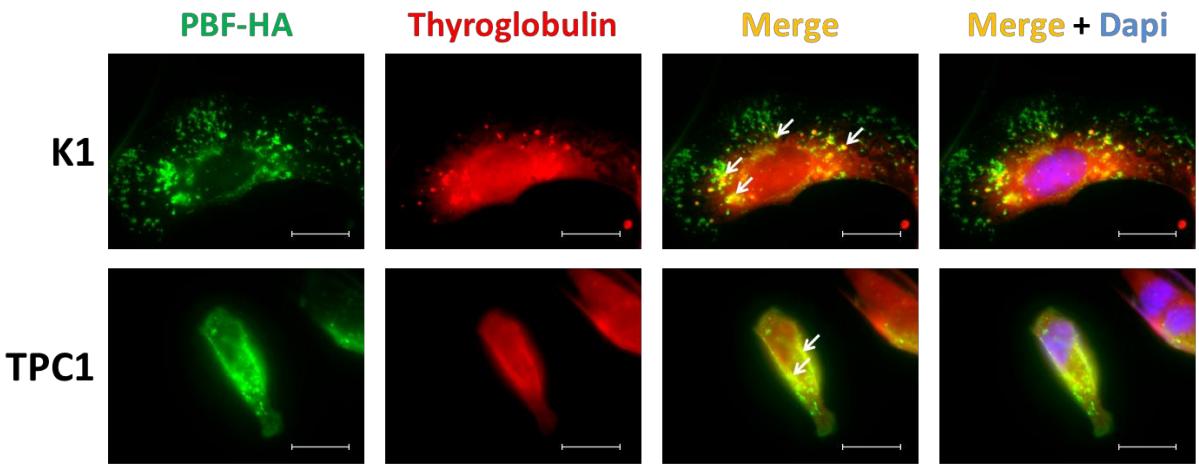

Figure 5.7 Fluorescence immunocytochemistry of K1 and TPC1 cells. PBF-HA is shown as green, Tg in red, with areas of co-localisation in yellow. Nuclear staining (DAPI) is blue. PBF and Tg appear to co-localise in intra-cellular vesicles as well as in the peri-nuclear region (white arrows). Bars, 20 µm.

Given the differences in band size detected by Western blotting between the transformed cell lines and primary thyrocytes, further immunofluorescence studies were performed on the human primary thyroid cultures. These cells were more confluent as a result of their culture conditions, and in places congregated into 2D follicle-like structures (Figure 5.8).

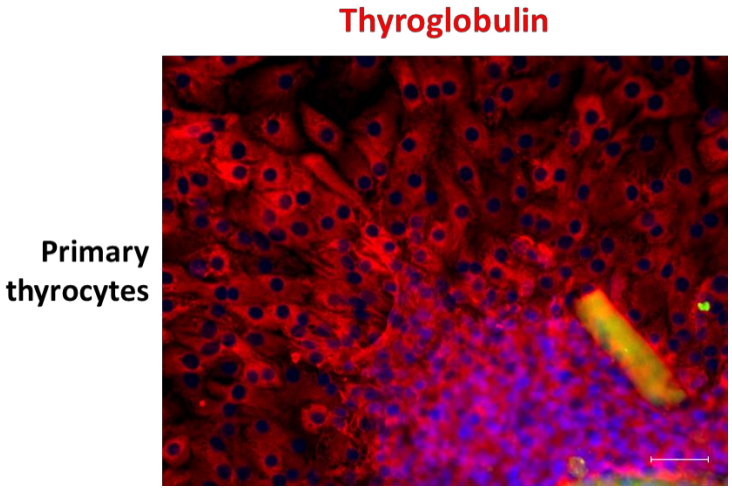

Figure 5.8 Immunofluorescence of untransfected primary human thyroid culture. Tg was stained red. A 2D follicle-like structure is evident in the bottom right of the image. Bars, 20 µm.

When these cells were transfected with *PBF-HA* and stained for both HA and Tg, some co-localisation was again seen in vesicles, but this was not a consistent finding, and there were examples of cells where there was no evidence of co-localisation (Figure 5.9). Due to the high density and overlap of cells, it was not possible to determine the precise intracellular nature of any co-localisation within the follicle-like structures.

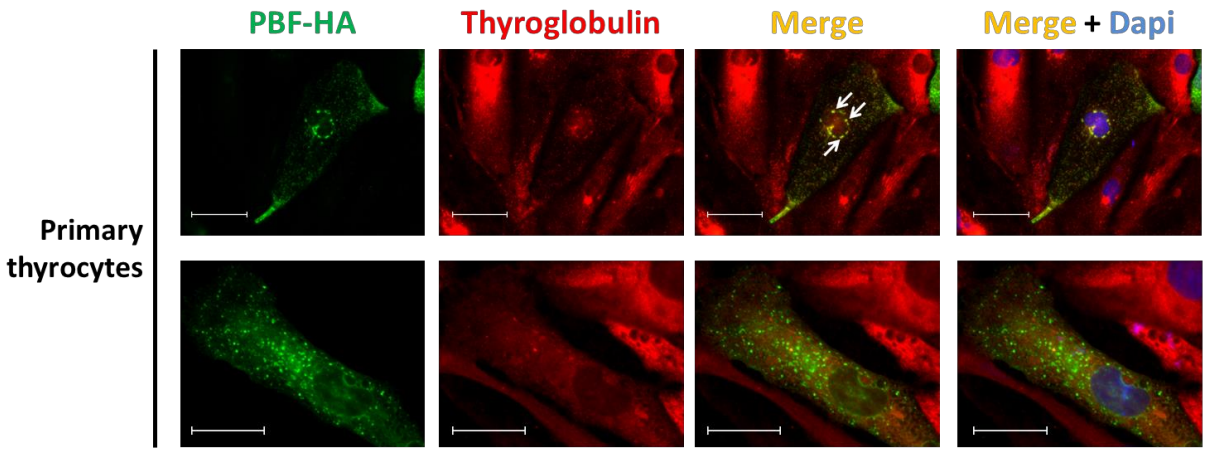

Figure 5.9 Immunofluorescence of primary human thyroid cells transfected with PBF-HA. PBF-HA was shown as green, Tg in red with areas of co-localisation in yellow. Nuclear staining (DAPI) is blue. As for the cell lines, possible co-localisation of PBF and Tg is observed in intra-cellular vesicles (white arrows). Bars, 20 µm.

5.4 Discussion

Thyroglobulin, in its most stable form, exists as a 660 KDa dimeric protein made up of 2 identical peptide chains of 2748 amino acid each (Dunn and Dunn 1999). It is the most abundant protein within the thyroid gland and essential for the synthesis of thyroid hormone. It is in this respect that Tg is most studied, as the clinical effects of deranged thyroid hormone synthesis can be profound. There is, however, significantly less evidence regarding the synthetic pathway of the protein itself, and how aberrations in this pathway may arise.

Initial studies focussed on attempting to validate the MS/MS findings using GST pull-down assays. In these, no interaction was observed between PBF and Tg; the [^{35}S]-methionine labelled Tg also produced bands of differing sizes and none at the expected masses of 330 kDa or 660 kDa. When Tg expression was determined in TPC1 and K1 thyroid cancer cell lines, again no large size band was detected, but rather a strong band at 140 kDa, as well as other, fainter, lower mass bands. The potential explanation for these findings lies in the synthesis of Tg and also its sub-unit structure.

Tg polypeptide chains undergo glycosylation in the rough endoplasmic reticulum, and the process of dimerization begins here. Chaperone proteins prevent the progression of Tg synthesis unless all aspects of post-translational modification are met, and therefore the final molecule (as exported into the colloid) will only be present in the cell should the pre-existing conditions be favourable (den Hartog et al. 1995; Miot et al. 2012). Clearly, in a cell free setting this is not possible and it is likely, therefore, that precursor peptides were detected. The GST pull-down assay, therefore, would not appear to be the best method with which to test an interaction with Tg.

The banding pattern demonstrated on Western blotting is most likely due to the breakdown of protein structure during denaturing prior to SDS-PAGE. The weight of Tg sub-units has been described (Spiro 1973) (Table 5.1), and several of the bands observed, including the major band at 140 kDa, are documented. The authors of this study used a variety of gels of differing concentration to fully assess the sub-units; however, in these experiments the lower percentage gels did not yield additional data, and given their difficult handling and lack of reliable results, 12 % acrylamide was used. This also correlated with the MS/MS

findings: Tg peptides were identified in gel bands corresponding to several different molecular weights, and it is likely that these were the result of breakdown during the denaturing process. Unfortunately, there is no description as to the composition or source of the bands identified by Spiro's group; therefore it is not possible to correlate the peptide chains determined by MS/MS to any particular subunit.

Component	Molecular Weight (kDa)
A	235
B	215
C	190
D	175
E	150
F	140
G	100
H	75
I	45
J	30

Table 5.1 Molecular weights of known sub-units of Tg following denaturing (Spiro 1973).

Accepting for the purposes of these experiments that the Tg subunits would be analysed as a surrogate marker for total Tg, TPC1 and K1 cells were transfected with *PBF-HA* to determine if this altered the quantity of Tg within the lysate. No difference was observed, suggesting that the mechanism by which PBF alters both the size and thyroid hormone content of the thyroid gland (Read et al. 2011) is not via a change in cellular Tg. Co-immunoprecipitation of Tg and PBF was attempted in the cell lines, but no reliable Tg band could be identified, either at 140 kDa or elsewhere on the gel. This may have been due to the

smaller quantities of Tg sub-units present after Co-IP which, while identified by MS/MS, were not detectable on Western blotting.

To over-come the difficulties observed with studying Tg in cell lines, human primary thyroid cultures were used. *TG* gene expression is controlled by a number of thyroid specific transcription factors, of which TTF-1, TTF-2 and Pax-8 are the most important (Fayadat et al. 1998). Cultures from macroscopically normal human thyroid tissue contain a more differentiated phenotype than transformed cell lines. Although the Tg content of TPC1 and K1 cells has not been investigated, studies have shown that transfecting *PAX-8* into K1 cells increased the expression of Tg (Mu et al. 2012). Primary thyrocytes subjected to the same protein extraction conditions as K1 and TPC1 cells demonstrated a similar band pattern, although there was an increase in high molecular weight bands compared to the cell lines. These bands correlated more closely with the bands described in Table 5.1. Immunoprecipitation was performed with the anti-Tg antibody, therefore ensuring that any intact Tg would be precipitated. To determine if there was an optimum concentration of antibody to use, 3 conditions were used, as well as a no-antibody control. While the latter lane remained empty, co-immunoprecipitated PBF was identified in each of the other samples, supporting the interaction first identified by MS/MS. For the higher concentration of anti-Tg, there was an increase in the amount of PBF detected relative to the quantity in the cell lysate which would again support that PBF was detected as a specific binding partner to Tg.

The final step in the binding analysis was to use homogenised thyroid tissue. The vast majority of Tg in the thyroid gland is situated within the colloid. These structures are not present in two dimensional cell cultures and therefore cells grown *in vitro* (either cell lines or

primary culture) lack the final element of Tg synthesis and transport: the movement across the apical membrane into the colloid. The human thyroid gland specimens were homogenised and further diluted with RIPA to differing concentrations. Immunoprecipitating with anti-Tg and probing for PBF again identified the two as interacting, although a direct comparison between this and primary culture was not appropriate due to the very different conditions. However, work carried out within our group by Dr V Smith on the transgenic mouse thyroid gland has demonstrated that PBF is present not only within the thyroid epithelial cell, but also at the apical membrane and within the colloid itself (Figure 5.10). Combining this with the data obtained from the above experiments suggests that PBF may interact with Tg both within the cell and in the colloid, and this interaction could perhaps explain the phenotype seen in our transgenic mouse model.

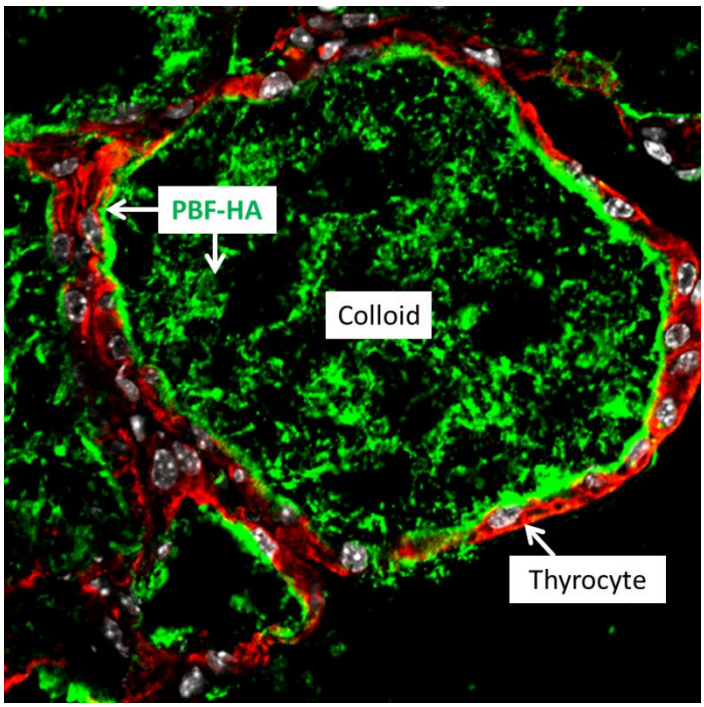

Figure 5.10 Confocal microscopy of a cross section through a PBF-transgenic mouse thyroid. PBF-HA is shown in green and localised within the colloid as well as at the apical membrane. Thyroid epithelial cells are shown via MCT8 staining in red. Courtesy of Dr V Smith, University of Birmingham.

Preliminary experiments into the co-localisation of Tg and PBF identified intra-cellular vesicles as well as the peri-nuclear region as potential sites of interaction, both in cell lines and human primary thyrocytes. The significance of this remains to be determined; whether PBF is transported with Tg to the cell membrane, or if the interaction is only transient within the cell will be the focus of further study. In addition, techniques such as 3D cell culture, which allow the formation of functional colloid units within primary thyroid cultures *in vivo*, will be essential to assess the functional significance of the interaction.

Concluding remarks

This chapter has investigated the potential interaction between PBF and thyroglobulin. Due to its large size and the requirement for a number of physiological conditions to be met in order for the full length protein to be assembled, studies using the transformed cell lines did not generate conclusive data. However, co-immunoprecipitation of PBF with Tg was demonstrated in primary thyroid cultures and homogenised thyroid tissue. In addition, fluorescence immunocytochemistry identified potential co-localisation sites within intracellular vesicles and the peri-nuclear region of the cell. These preliminary observations, therefore, provide a basis on which to further investigate the interaction and assess its functional significance, particularly in light of the transgenic mouse phenotype.

Chapter 6 Investigating the interaction between cortactin and PBF

6.1 Introduction

In Chapter 4, cortactin was identified by MS/MS as a protein highly likely to interact with PBF. Cortactin interacts with filamentous actin and thus regulates the actin cytoskeleton, in particular the stabilisation of the branched actin assembly (Weaver et al. 2001). It is also found in the leading edge of migrating cells, with over-expression of cortactin leading to increased cell mobility and knockdown reducing it (Bryce et al. 2005).While this is part of the normal physiological process of the cell, cortactin has also been shown to play a role in cancer, including in the formation of invadopodia and podosomes (Artym et al. 2006), and in the membrane trafficking of proteins to and from the cell surface (Cao et al. 2003). Cortactin also has a role in the secretion of certain proteins, and this is important in the Extra Cellular Matrix (ECM)-degrading properties of invadopodia (Clark and Weaver 2008). To date, cortactin over-expression has been found in head and neck squamous cell carcinoma, as well as cancers of the breast, ovary, stomach, liver, colon and oesophagus (Kirkbride et al. 2011).

Thus, the finding of cortactin as a possible binding partner of PBF had the potential to explain some of the effects previously observed with PBF over-expression. PBF is a protein present within the cytoplasm of the cell as well as at the cell membrane (Smith et al. 2009), and it is possible that cortactin may be key to this membrane trafficking. In addition, work within our group has shown that PBF is a secreted protein (Watkins et al. 2010), a process cortactin might influence. Finally, the link between PBF over-expression and increased cell invasiveness could potentially be mediated by cortactin.

The initial aim of this chapter, therefore, was to attempt to validate the interaction between PBF and cortactin. If confirmed, the effect of changes in cortactin expression on PBF physiology would be assessed. Specifically, these experiments would address PBF localisation, secretion and membrane transport.

6.2 Methods

6.2.1 Cell lines and transfection

K1, TPC1 and HeLa cells were maintained as described in Section 2.1 and transfected with PBF-HA, pCDNA3.1+, or Myc- and FLAG-tagged cortactin (Cambridge Bioscience, Cambridge, UK). Cortactin knock-down was achieved with siRNA transfection, carried out as described (Section 2.2.3) using ON-TARGETplus Human *CTTN* siRNA (Thermo Scientific).

6.2.2 GST pull down assays

GST-tagged PBF was translated as described in 2.5.1. [^{35}S]-methionine cortactin was prepared using the TNT® T7/SP6 Coupled Reticulocyte Lysate System (Promega; as described in Section 2.5) from the full length *CTTN* cDNA (in the bacterial vector POTB7 (IMAGE clone 3637586, Source Biosciences). The assay was performed as described in Section 2.5.

6.2.3 Western blotting and co-immunoprecipitation

These were carried out as described in Section 2.3. Antibodies used were anti-cortactin, 1:1000 for Western blotting, 1:10 for immunoprecipitation (clone 4F11, Millipore, UK), anti-HA (see Section 2.3.1), anti-Myc Tag, 1:2000 for Western blotting, 1:50 for immunoprecipitation (clone 9B11, Cell Signalling), anti-FLAG (Agilent Technologies, Wokingham, UK), 1:2000 for Western blotting, 1:50 for immunoprecipitation.

6.2.4 Fluorescence immunocytochemistry

This was performed as described in Section 2.6, using K1, TPC1 and HeLa cells.

6.2.5 Secretion assay

6.2.5.1 Cell seeding and transfection

Cells were seeded into 6 well plates and transfected as described in section 2.2.2. For cells undergoing knockdown and over-expression, siRNA transfection took place at 24 hours after seeding, and plasmid transfection a further 24 hours later. Medium was changed to 1 ml RPMI as above with 5% FBS at either 24 or 48 hours after initial transfection. At 72 hours, media and cells were harvested for analysis.

6.2.5.2 Confirmation of transfection

Cells were harvested in RIPA/protease inhibitor as described previously and protein concentration determined by Bradford assay. Thirty micrograms of protein were assessed by Western blotting to determine over-expression/knock down prior to further analysis.

6.2.5.3 Assessment of secretion by Western blotting

The medium was transferred to a 1.5 ml microcentrifuge tube and spun at 12,000 rpm on a benchtop centrifuge for 5 minutes to separate cell debris. The supernatant was then transferred to a 15 ml centrifuge tube, and protein precipitated by the addition of 2 ml 100 % ethanol and centrifuging for 15 minutes at 1000 rpm. The pellet was then re-suspended in RIPA with protease inhibitor. Protein concentration was quantified using the Bradford assay; 30 µg of protein was then separated by SDS-PAGE and Western blotting performed as per section 2.3.

6.2.5.1 Enzyme-Linked Immunosorbent Assay (ELISA)

Secretion of PBF was determined using the PTTG1IP ELISA kit (USCN Life Science Inc., China), as per manufacturer's instructions: Standards were prepared from serial dilution of the provided stock standard, to dilutions ranging from 0.156 to 50 ng / mL. 100 µL of

standards and samples (n = 2) were loaded in duplicate onto the plate. The plate sealer was applied and the plate incubated for 2 hours at 37 °C, allowing any PBF present to be bound to the anti-PBF antibody adherent to the well. The supernatant was discarded before adding 100 µL of Detection Reagent A (biotin conjugated anti-PBF) to each well and incubating for a further 1 hour at 37 °C. The supernatant was again discarded and the wells washed 3 times with 350 µL Wash Solution. One hundred microliters of Detection Reagent B (avidin conjugated to Horseradish Peroxidase (HRP)) were then added and the plate incubated for 30 minutes at 37 °C to allow binding of avidin to biotin. A further 5 washes were carried out with 350 µL of Wash Solution. After the addition of 90 µL of TMB Substrate Solution, the plate was incubated in the dark for 20 minutes at 37 °C, causing a colour change in those wells containing PBF, biotin-conjugated antibody and HRP-conjugated Avidin. The reaction was stopped with 50 µL of sulphuric acid Stop Solution and absorbance at 450 nm measured using the Victor3 1420 Multilabel Counter. Concentration was calculated from a standard curve generated by the standards.

6.3 Results

6.3.1 Validation of the interaction between cortactin and PBF

6.3.1.1 GST pull-down assay

As discussed in Section 5.3.1, before commencing any functional experiments it was necessary to validate the MS/MS interaction using glutathione-S-transferase (GST) pull-down assays and co-immunoprecipitation. GST-tagged PBF was translated as described in 5.2. The resulting band ran at the expected size of approximately 42 kDa (Figure 6.1A). [^{35}S]-methionine labelled cortactin was translated using a cell free system and detected at approximately 80 kDa (Figure 6.1B). However, the pull down assay failed to show a

difference in detection of cortactin between samples incubated with GST-PBF and GST alone (n = 3) (Figure 6.1C). Therefore this technique was unable to validate an interaction between the two.

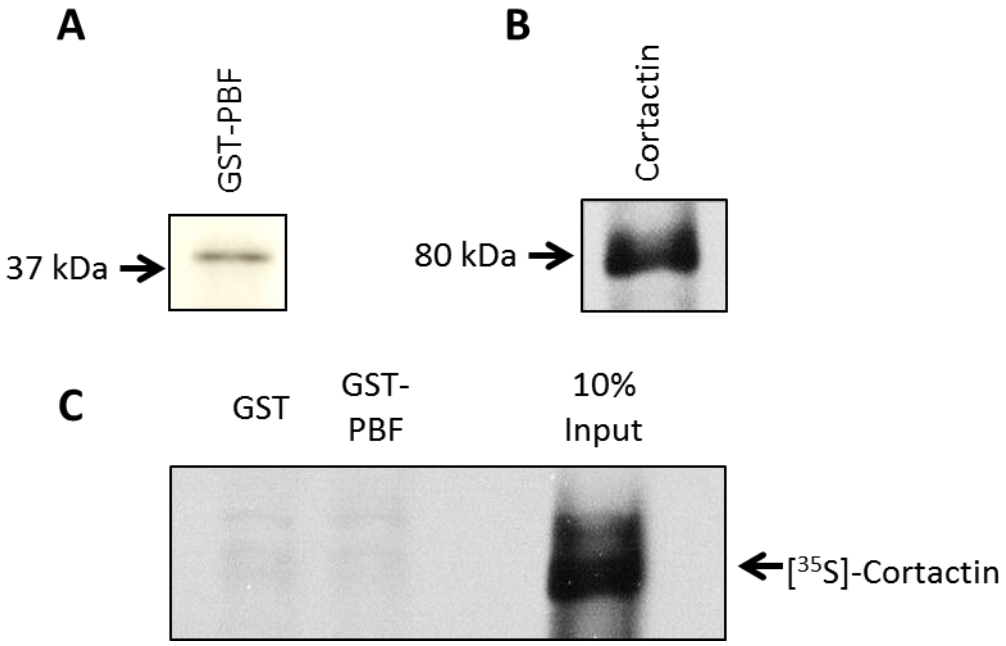

Figure 6.1 GST pull down assay investigating an interaction between PBF and cortactin. A: GST-tagged PBF ran at the expected size of 42 kDa. B: [^{35}S]-methionine labelled cortactin was translated and ran at 80 kDa. C: No evidence of an interaction was observed when comparing GST-PBF to GST alone (n = 3).

6.3.1.2 Co-immunoprecipitation

Given that GST pull-down assays had failed to demonstrate an interaction between cortactin and PBF, co-immunoprecipitation was used to assess whether a more physiological setting was necessary for the two to bind. The endogenous expression of cortactin in K1, TPC1 and HeLa cells was examined and shown to be similar (data not shown). Following this, K1 and TPC1 cells were transfected with *PBF-HA* and immunoprecipitated with an anti-cortactin antibody before being run through SDS-PAGE. Due to a strong light chain band from the anti-cortactin antibody at 25 kDa, it was not possible to reliably identify PBF on

immunoblotting. When the reverse experiment was performed, i.e. immunoprecipitating with an anti-HA antibody, any cortactin band was hidden again by immunoglobulin bands.

It was decided, therefore, to transfect cortactin into the cells. Given that cortactin was potentially hidden during Western blotting by non-specific antibody bands, a tagged vector was used for transfection, containing full length cortactin cDNA as well as an N-terminal Myc and FLAG tag ("Cort-Myc-FLAG"). This would allow a highly specific antibody to be used to immunoprecipitate cortactin and might therefore permit more efficient PBF detection by Western blotting. The tag would also help detect cortactin in the reciprocal experiment. In order to ensure the validity of the tagged protein, Western blotting was performed on the lysate of cells transfected with Cort-Myc-FLAG. The same samples were run in triplicate, and transfected cortactin was detected using an anti-cortactin antibody as well as ones directed to Myc and FLAG epitopes (Figure 6.2), demonstrating that this over-expressed protein could be detected by any of the three antibodies. Cortactin exists in predominantly two isoform within the cell, p80/85 (Buday and Downward 2007); over-expression resulted in an increase in both forms, although only the larger isoform was detected by the anti-Myc antibody.

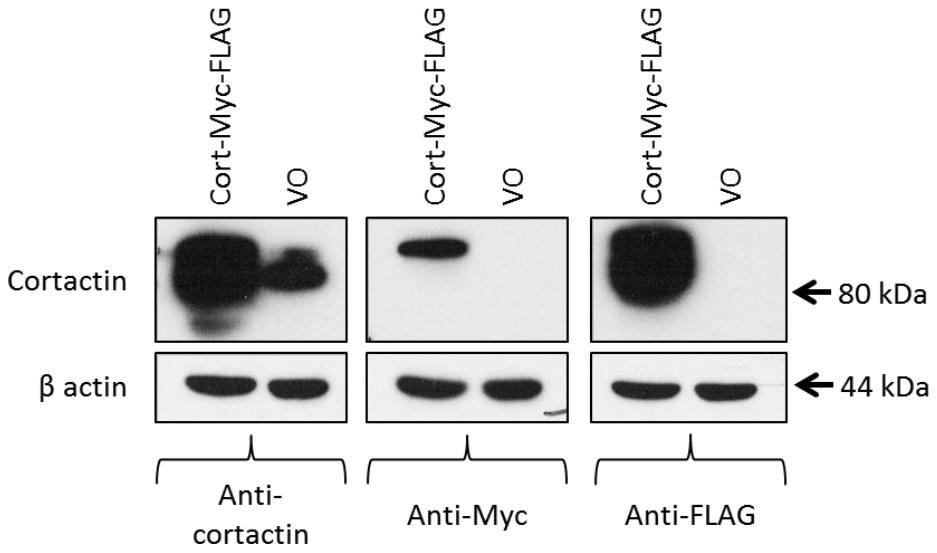

Figure 6.2 Western blot of HeLa cells demonstrating transfection with Cort-Myc-FLAG, with detection by 3 different antibodies. β actin is included as a loading control.

Using this plasmid, HeLa cells were transfected with both cortactin and PBF-HA and the resulting cell lysate immunoprecipitated using the anti-Myc antibody. After running these through SDS-PAGE, immunoblotting showed a clear interaction between PBF-HA and Cortactin-Myc, when compared to cells transfected with PBF-HA only, or in the no-antibody control (Figure 6.3). The reverse experiment, in which lysates were immunoprecipitated using anti-HA, and immunoblotted for anti-Myc, could not be interpreted again due to interference from non-specific / immunoglobulin bands at 75 kDa (data not shown).

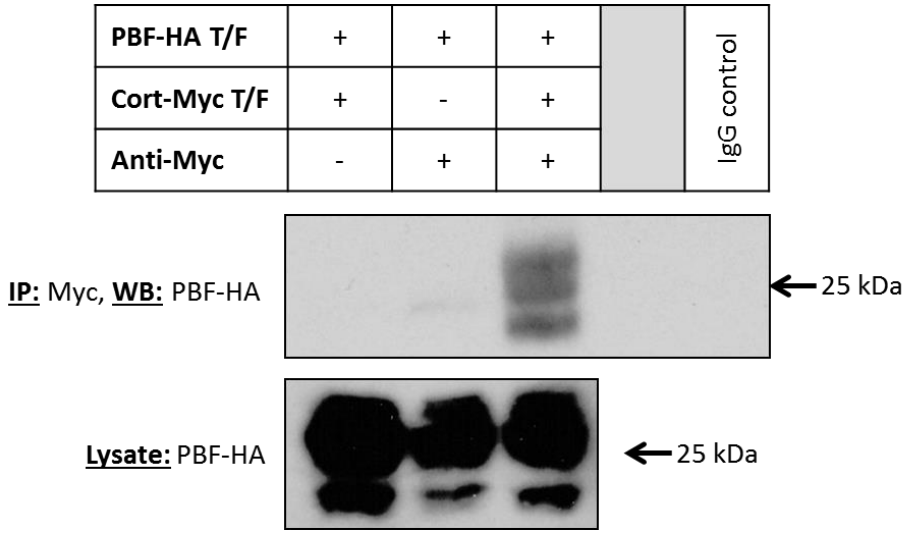

Figure 6.3 Cortactin-Myc-FLAG interacts with PBF-HA as demonstrated by co-immunoprecipitation. Western blot showing co-immunoprecipitation of PBF-HA after immunoprecipitating with an anti-Myc antibody. T/F = transfection, IgG control = immunoglobulin only control, IP = immunoprecipitation, WB = Western blot.

6.3.2 Cortactin has no effect on PBF expression

Before proceeding to functional studies, HeLa cells were again used to establish if over-expression of one protein had an effect on the amount of the other within the cell. When PBF-HA was over-expressed, there was no significant difference in the amount of cortactin compared to vector only controls (76.2 ± 7.1 % of control, p = ns, n = 3) (Figure 6.4A). Similarly, over-expression of Cort-Myc-FLAG had no effect on PBF-HA levels (123.4 ± 17.3 % of vector only controls, p = ns, n = 3) (Figure 6.4B)

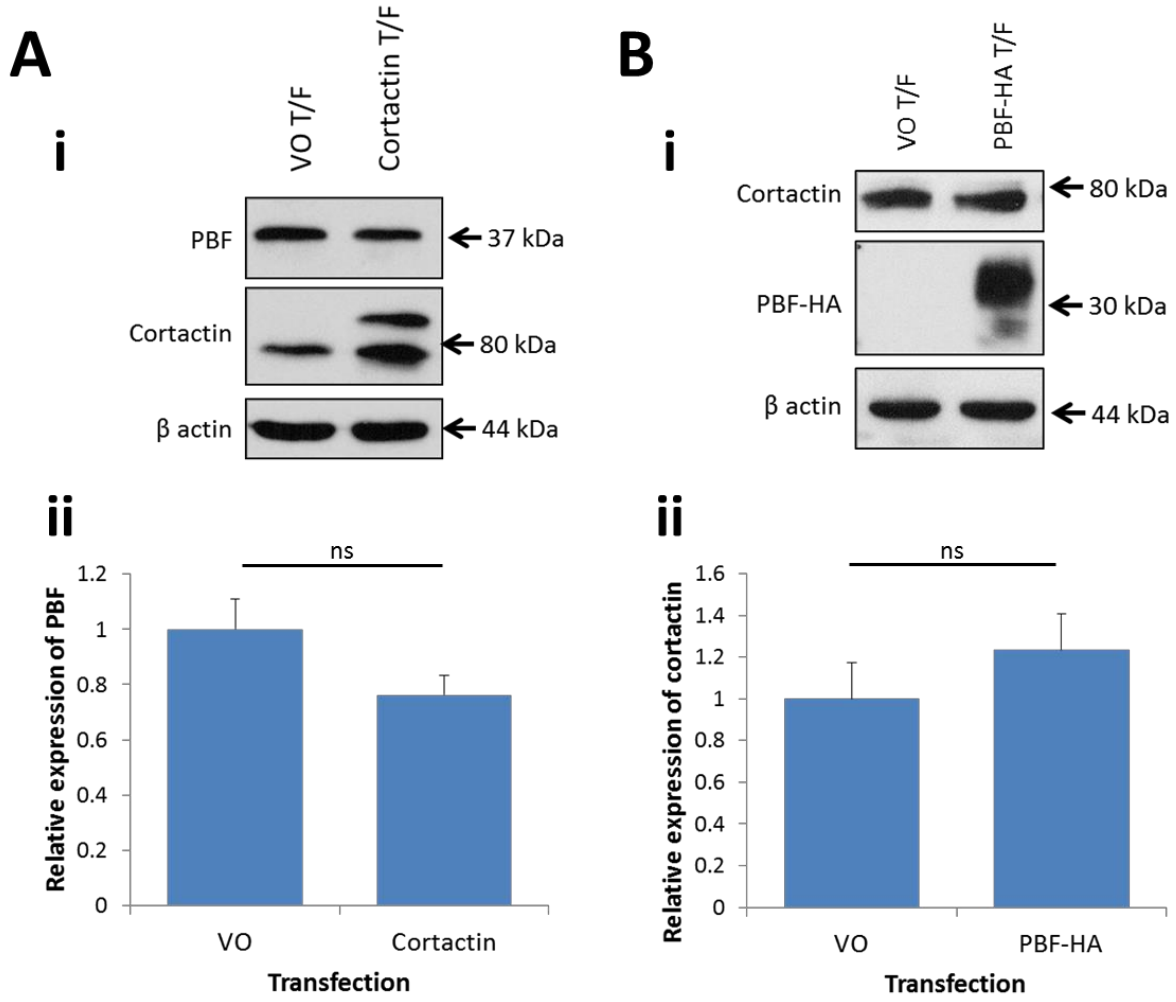

Figure 6.4 PBF and cortactin do not affect expression of each other. A: i - Western blot of HeLa cells transfected with either vector only (VO) or Cort-Myc-Flag. ii – Scanning densitometry did not show a significant difference in PBF-HA levels between the 2 conditions. B: i - Western blot of HeLa cells transfected with either vector only (VO) or PBF-HA. ii – Scanning densitometry demonstrated no difference in cortactin with either VO or PBF-HA transfection. Cortactin was detected using an anti-cortactin antibody. β actin is shown as a loading control.

6.3.3 Cortactin and PBF may co-localise in intra-cellular vesicles

The localisation of cortactin and PBF was examined in both K1 and TPC1 cells as well as HeLas. In some cells, PBF-HA appeared to co-localise with cortactin in intracellular vesicles (Figure 6.5).

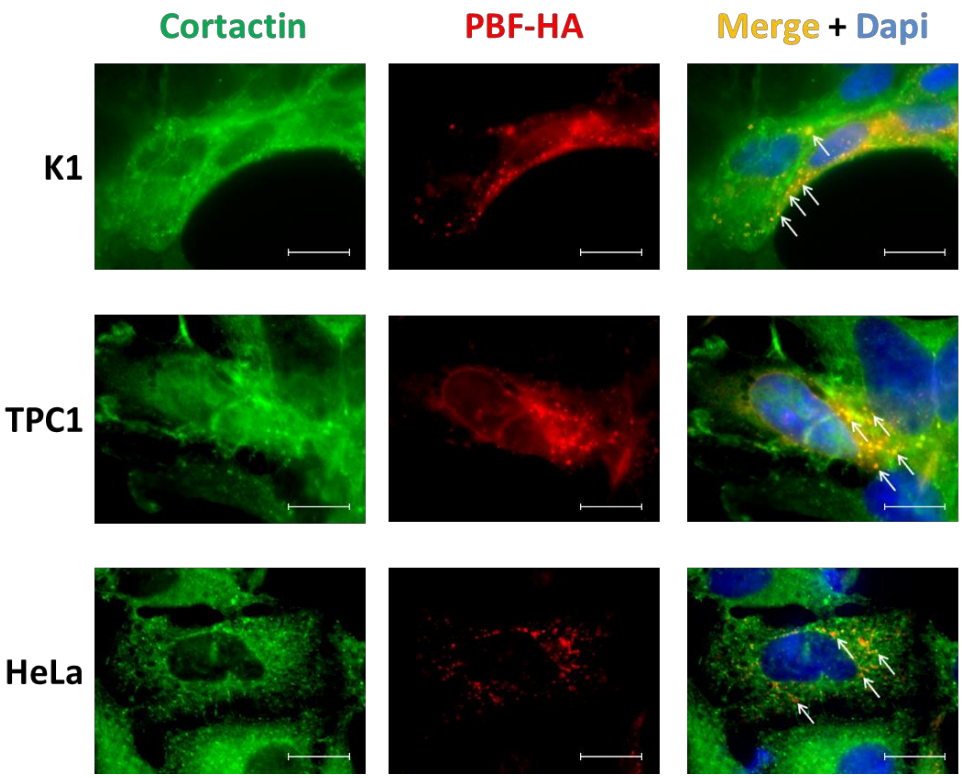

Figure 6.5 Fluorescence immunocytochemistry demonstrating possible co-localisation of PBF-HA and cortactin in K1, TPC1 and HeLa cells. PBF-HA was identified in red using an anti-HA antibody, Cortactin was identified in green and nuclear staining (DAPI) was shown in blue. Areas of potential co-localisation between PBF-HA and cortactin were shown in yellow, and occurred predominantly within intra-cellular vesicles (white arrows). Bars, 20 µm.

6.3.4 PBF is present in membrane projections

Given the role of cortactin in invadopodia formation, and the increase in invasiveness of cells over-expressing PBF (Watkins et al. 2010), immunofluorescence was undertaken to determine if PBF was present in membrane projection or invadopodia-like structures. No membrane projections were apparent in cells stained for both cortactin and PBF-HA; however, when a more effective anti-HA antibody was used (and cortactin not stained for) membranous projections were observed, albeit faintly (Figure 6.6). This suggests a possible

role for PBF in invadopodia, although further experiments will be required to elucidate any potential mechanism.

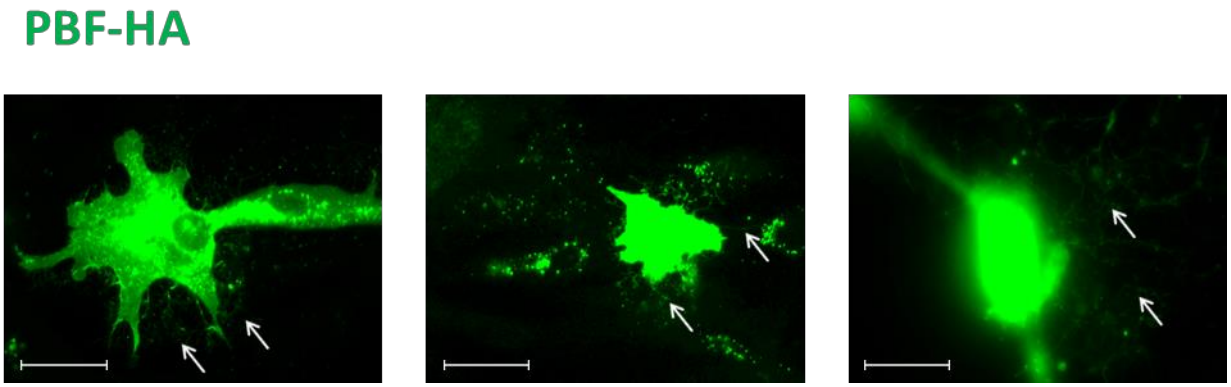

Figure 6.6 Fluorescence immunocytochemistry of three different HeLa cells. PBF-HA is stained green and over-exposed to demonstrate membrane projections (white arrows). Bars, 20 µm.

6.3.5 Investigations into the effect of cortactin on PBF secretion

PBF is a secreted protein (Watkins et al. 2010), although the mechanism for this has not yet been established. Given the known role of cortactin in protein export, its effect on PBF secretion was assessed using 2 assays: Western blotting and ELISA. Cortactin was over-expressed as described above. In order to determine if a lack of cortactin had a detrimental effect on the secretion of PBF, siRNA targeting cortactin was transfected into HeLa cells. This led to a substantial knock down of cortactin expression when compared to transfection of scrambled siRNA. A representative Western blot demonstrating cortactin over-expression and knockdown is shown in Figure 6.7.

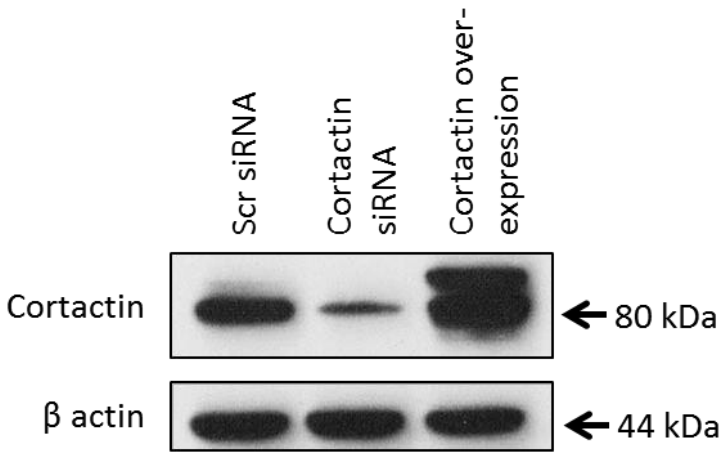

Figure 6.7 Representative Western blot demonstrating knock down and over-expression of cortactin in HeLa cells. Scrambled siRNA (Scr siRNA) was used as a negative control and β actin as a loading control.

6.3.5.1 Endogenous PBF secretion is not detectable by Western blotting

HeLa cells were transfected with Myc-tagged cortactin or blank vector to test the effect of over-expression, and with cortactin siRNA or scrambled siRNA to test the effect of knockdown. Cells and media were harvested at 24 and 48 hours. The cell lysates were subjected to Western blotting to demonstrate that the transfection had been successful, following which the media was assessed for PBF content by Western blotting. Previous work performed by our group using this technique has shown that over-expressed PBF-HA is secreted, and that glycosylation and/or the N terminal signal peptide was essential for this (Watkins 2010). However, when media were analysed by Western blotting, no PBF was detected at its expected size (Figure 6.8). Therefore using this technique, it was not possible to establish whether PBF secretion was dependent on cortactin expression within the cell.

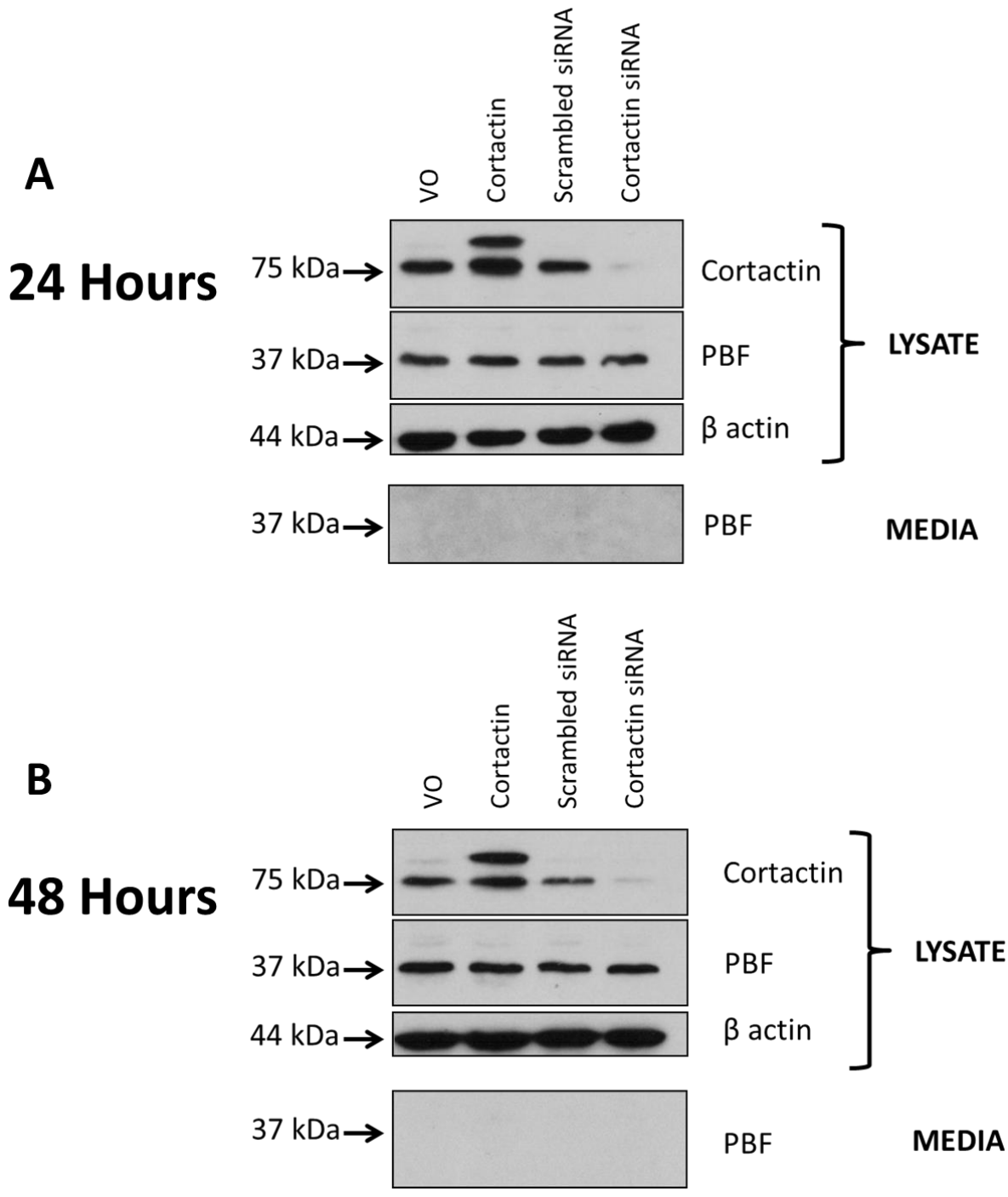

Figure 6.8 Assessment of the effect of cortactin on PBF secretion by Western blotting. Media were analysed at 24 (A) and 48 (B) hours post-transfection. Efficacy of transfection and knockdown were demonstrated by Western blot of the cell lysate. PBF was not detected in the media at either timepoint.

6.3.5.2 Cortactin does not affect PBF secretion as demonstrated by ELISA

Due to the failure to detect secreted PBF by Western blotting, a separate, independent experiment to assess PBF secretion was performed using Enzyme-Linked Immunosorbent Assay (ELISA). Transfection of HeLa cells was performed as described in Section 2.2.2; at both 24 hour and 48 hour timepoints, media and cells were harvested, and cell lysates analysed to ensure adequate transfection and knockdown of cortactin. As demonstrated previously, the cell lysates exhibited a marked increase in cortactin with over-expression, and no detectable cortactin when siRNA was used. At the 24 hour timepoint when cortactin was over-expressed, there was no significant difference in the amount of secreted PBF (99.5 ± 38.9 % of control, p = ns); a similar effect was observed at the 48 hour timepoint (92.2 ± 29.9 % of control, p = ns). For cortactin knockdown, a greater drop was observed for both timepoints (79.9 ± 37.1 % at 24 hours, 80.5 ± 32.6 % at 48 hours) although neither of these differences were significant (Figure 6.9). Of note, there was a wide variability in the amount of secreted PBF detected, and this contributed to the large inter-experimental error.

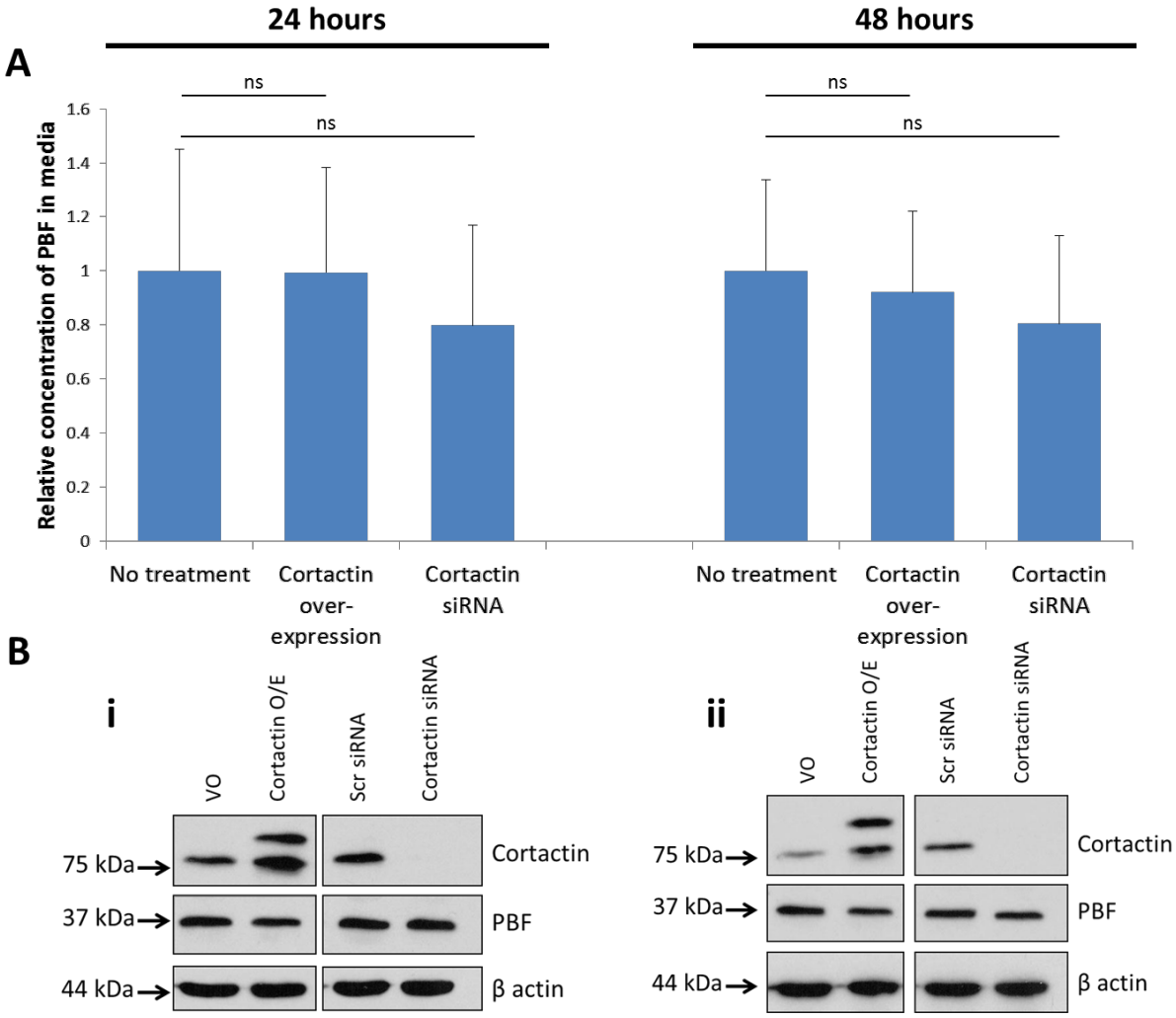

Figure 6.9 Assessment of the effect of cortactin on PBF secretion by ELISA. A: Relative concentrations of PBF detected in media at 24 and 48 hours post transfection with either cortactin or siRNA targeting cortactin. Standard error of the mean is plotted as error bars. B – Western blots demonstrating over-expression and knockdown of cortactin at 24 (i) and 48 (ii) hours post transfection. β actin is shown as a loading control. VO = Vector Only, O/E = over-expression, ns – not significant.

6.4 Discussion

Cortactin was identified as a potential binding partner of PBF in Chapter 4, scoring the highest of all the shortlisted proteins. Cortactin has been studied for its role in normal cellular physiology, where it is involved in cell structural maintenance via the actin cytoskeleton,

membrane trafficking of proteins and cell mobility via lamellipodia. In addition to this, cortactin has a clear role in the development of malignancy. It is over-expressed in a number of cancers, and *in vitro* studies have demonstrated that cortactin is involved in the formation of invadopodia; membranous protrusions that promote invasion by secreting enzymes which can break down the extra-cellular matrix (Kirkbride et al. 2011).

To determine whether the interaction identified by MS/MS was valid, GST pull-down studies were first undertaken to assess binding in a cell-free setting. Although [^{35}S]-methionine labelled cortactin was successfully translated at the predicted molecular mass, no binding was identified in the assay. While this did not support the MS/MS findings, it was possible that binding could only occur within the cell once a particular post-translational modification had taken place, to either cortactin or PBF, or required the presence of a binding partner to facilitate the interaction.

Co-immunoprecipitation was therefore performed, immunoprecipitating lysates from cells transfected with PBF-HA with either an anti-HA or anti-cortactin antibody. Unfortunately, both of these experiments were hindered by non-specific immunoglobulin bands obscuring the target areas on the Western blot (25 kDa for PBF-HA and 75 kDa for cortactin). To counter this, cells were transfected with cortactin which had been tagged with Myc and FLAG epitopes. Both these tags were small, and had well established antibodies suitable for co-immunoprecipitation. By also increasing the amount of cortactin within the cell, this allowed the amount of antibody used in the immunoprecipitation step to be reduced, and also reduced the exposure time needed for Western blot detection of protein. This plasmid was successfully validated, showing a significant increase in the amount of cortactin following transfection. Importantly, when anti-Myc and anti-FLAG antibodies were used, there was no non-specific interaction identified. Interestingly, expression of the p85 isoform

of cortactin was greater than the p80. The significance of the ratio of the 2 isoforms has not been established, although it has been suggested that the p85 is associated with tumour invasiveness (Zhang et al. 2006). Using this plasmid for over-expression, PBF-HA was successfully co-immunoprecipitated with Myc-tagged cortactin; no non-specific binding was identified and due to the lower amount of antibody used and short exposure time, there was no contamination by light chain immunoglobulin. While this provided good evidence for an interaction between the 2 proteins, the reverse experiment remained problematic, due to the large immunoglobulin band at 75 kDa. Methods exist to counter this problem, such as using magnetic beads, and are currently being used within our group to further investigate this angle.

PBF is known to have a direct effect on the expression of NIS via the *NIS* promoter (Boelaert et al. 2007). Therefore, before any functional studies were performed, experiments were undertaken to ascertain whether the over-expression of either PBF or cortactin had any effect on expression of the other. When analysed by Western blotting, there was no difference in the amount of either protein detected when the other was over-expressed.

Having established that the 2 proteins interact, fluorescence immunocytochemistry was performed to identify areas of co-localisation within the cell. The resulting data were inconclusive, however in both the thyroid cell lines (K1 and TPC1) and also in the HeLa cells, cortactin demonstrated potential co-localisation with PBF-HA in intra-cellular vesicles, although further experiments would be needed to explore this observation. PBF has been shown to internalise the membrane proteins NIS (Smith et al. 2009) and MCT8 (Smith et al. 2012), although the exact mechanism of this remains unclear. PBF co-localises with the late endosome marker CD63, suggesting that this may be mediated by clathrin-dependant endocytosis (Smith et al. 2009). Cortactin regulates both clathrin-dependent and –independent

endocytosis (Cao et al. 2003; Sauvonnet et al. 2005), and this may therefore be key in understanding and potentially preventing the reduction and subsequent repression of these membrane bound transporters by PBF.

As cortactin plays a role in invadopodia formation and function, a feature which is directly related to tumour invasiveness, and PBF increases invasiveness (Watkins et al. 2010), as an additional preliminary study the potential role PBF in invadopodia was then assessed. No co-localisation between PBF and cortactin was observed in cell membrane projections, although when cells stained only for PBF-HA were over-exposed, membrane protrusions staining for PBF-HA were apparent. These invadopodia-like structures were visible in a number of cells types with *PBF-HA* transfection. These preliminary data are currently the focus of study within our group to further define the potential role of PBF in invadopodia function, using specific invadopodia assays.

The invasive potential of PBF is reliant on its secretion (Watkins 2010); the above studies have suggested a role for cortactin in the transport of PBF to and from the cell membrane, and also a link between PBF and invadopodia. The final area assessed was to determine whether cortactin had a role in the secretion of PBF. As well as stabilising invadopodia, cortactin regulates the secretion of matrix metalloproteases (MMPs) which degrade the ECM (Clark and Weaver 2008), and therefore may also provide the mechanism for PBF secretion. Two separate assays were performed to investigate a link between PBF secretion and cortactin. For both, secretion was assessed with over-expression of cortactin (using blank vector transfection as a control) and cortactin knockdown. Loss of cortactin results in a reduction in invadopodia number as well as reduced ECM degradation (the latter through reduced secretion of MMPs) (Clark et al. 2007). The first method used - assessment by Western blotting - had been successfully implemented to demonstrate that PBF was a

secreted protein previously by our group (Watkins 2010). However, in this experiment, no PBF was detected in the media at 24 and 48 hours, although the cells themselves had transfected successfully as indicated by Western blotting of the cell lysates. Given that endogenous as opposed to over-expressed PBF was used, the concentration of any PBF within the media would have been significantly lower than identified in previous studies (Watkins et al. 2010), potentially below the detection limit of Western blotting.

This led to the second method, Enzyme-Linked Immunosorbent Assay (ELISA), which utilised an antibody to immobilise PBF to a plate, with subsequent detection being potentially more sensitive than Western blotting. There was significant variability in the output generated from the ELISA, which led to high standard errors and the results not reaching significance. There was a trend towards reduced secretion of PBF with cortactin knockdown, however.

These 2 experiments, therefore, should be seen as preliminary studies on which to base future research. Questions that will need to be addressed include the validity of co-transfecting *PBF* alongside either cortactin or siRNA, and also (perhaps most importantly) the timing at which analysis should be performed. In addition, cell surface biotinylation assays will allow the quantitative assessment of the effect of cortactin on PBF membrane trafficking. These experiments are on-going within our group.

Concluding remarks

This chapter has validated the interaction between PBF and cortactin, and suggested that they may co-localise in intra-cellular vesicles, which may explain the membrane trafficking of PBF as well as its secretion. PBF is found in protrusions from the cell membrane when over-expressed; preliminary studies have identified potential ways of studying the effects of

cortactin knockdown and over-expression on PBF secretion, and will provide a starting point for future work researching this interaction and its functional significance.

Chapter 7 Validation of the interaction between SRC and PBF

7.1 Introduction

The SRC tyrosine kinase family are non-receptor tyrosine kinases, members of which are SRC, LYN, YES, FYN, FGR, LCK, HCK, BLK and FRK. Two members of this group, LYN and SRC, were identified by MS/MS. The two proteins share 78 % homology (BLAST analysis, available at http://blast.ncbi.nlm.nih.gov/Blast.cgi?PAGE=Proteins), which includes the sections of the peptide chains identified by MS/MS. As phosphorylation prediction software had identified SRC as a potential kinase for PBF, and as the most well studied member of the group, SRC was chosen for validation studies and potential functional work.

c-SRC is regarded as the first identified oncogene, and is the cellular homologue of *v-SRC*, the oncogenic component of the Rous sarcoma virus, which causes tumours in chicken. c-SRC, henceforth referred to as SRC, contains four SRC homology ("SH") domains, of which SH2 and SH3 are key to its regulatory mechanism (Figure 7.1A) (Bjorge et al. 2000). Inactivation of SRC is brought about by phosphorylation at Y530; this then interacts with the SH2 domain to bring the protein into a closed configuration, thereby inactivating it. In addition, the SH3 domain interacts with a proline rich segment within the kinase domain causing further de-activation. When de-phosphorylated at Y530, the molecule opens to allow auto-phosphorylation at Y419 and subsequent activation (Figure 7.1) (Anbalagan et al. 2012). Activated SRC is involved in cellular proliferation, survival, migration and angiogenesis, and it follows that an aberrant increase in SRC expression is associated with many human malignancies.

The aim of this chapter was to independently validate the binding between SRC and PBF, an essential process prior to functional studies exploring the interaction.

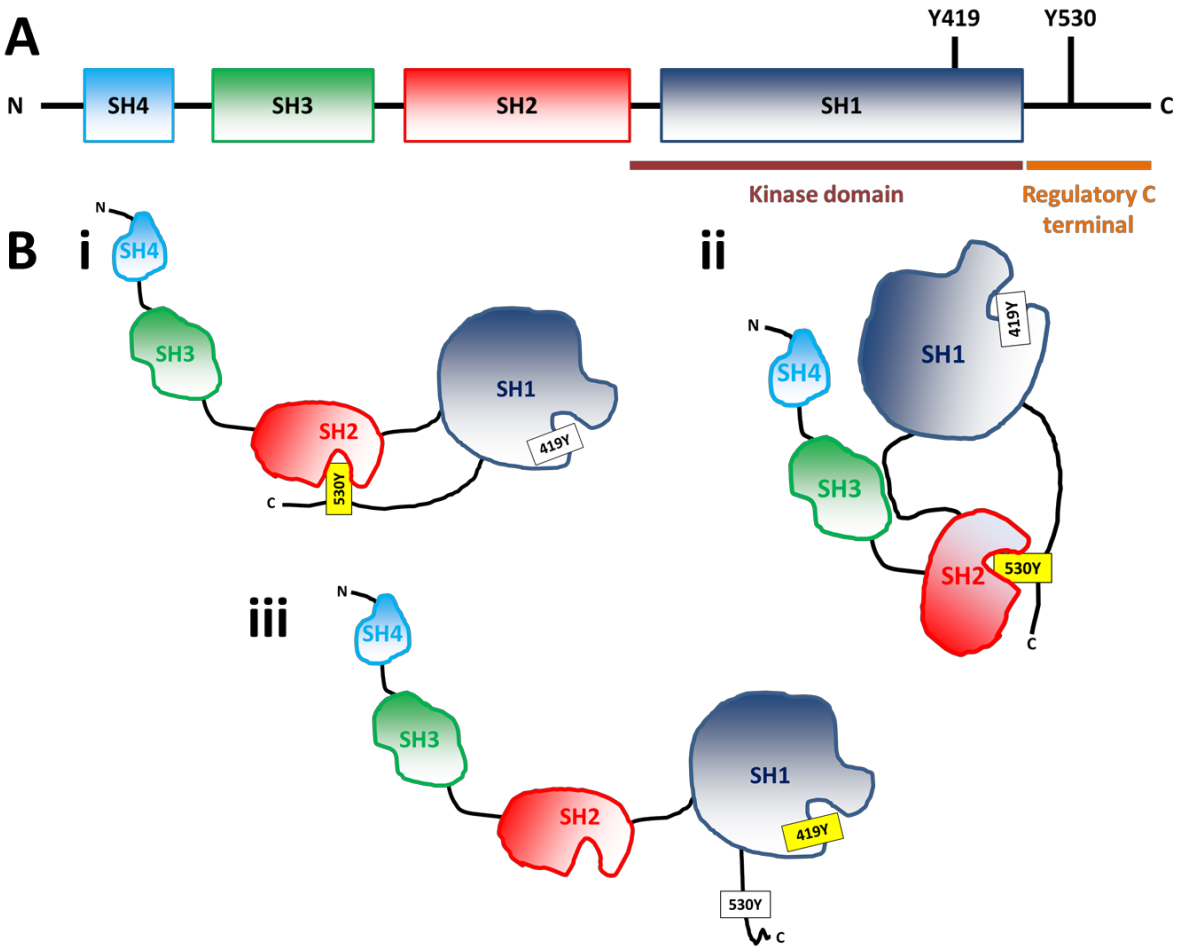

Figure 7.1 Diagrammatic representation of SRC. A: The protein consists of four SH domains, with SH1 responsible for kinase activity. Negative regulation is through phosphorylation at Y53 (yellow). Loss of this C terminal region leads to mutant activation, as seen in v-SRC. B: Inactivation and activation of SRC. i. Phosphorylation at Y530 allows coupling to the SH2 domain. ii. This allows interaction between SH3 and the kinase domain to bring the molecule into a closed, inactive position. iii. De-phosphorylation at Y530 and auto-phosphorylation at Y419 open the molecule resulting in activation.

7.2 Methods

7.2.1 Cell culture and transfection

K1, TPC1 and HeLa cells were maintained as described in Section 2.1. Transfection was carried out with PBF-HA and SRC in pcDNA3.1+ using Fugene6 as previously detailed.

7.2.2 GST pull-down assay

GST-tagged PBF was translated and [^{35}S]-methionine labelled SRC was translated from full length *SRC* cDNA (kindly provided by Dr Yotis Senis, University of Birmingham, in the bacterial expression vector pOTB7) as described in Section 2.5.

7.2.3 Subcloning of *SRC* cDNA into pcDNA3.1+

In order to allow transfection of cell lines, *SRC* was subcloned into pcDNA3.1+, using the restriction enzymes EcoR1 and Xba1, as described in Section 2.2.1.2. Correct insertion was confirmed by sequencing using the T7 and BGHrev primers.

7.2.4 Western blotting and co-immunoprecipitation

Western blotting and co-immunoprecipitation was performed as previously described in 2.4. Monocloclonal rabbit anti-human SRC (Cell Signalling, Danvers, MA) was used at 1:1000 for Western blot and 1:10 for immunoprecipitation. Anti-HA and anti-β actin were used as previously described.

7.2.5 Fluorescence immunocytochemistry

This was carried out as described in Section 2.6. Anti-Src was used at 1:100. Other antibodies were used as previously described.

7.3 Results

7.3.1 Validation of the interaction between SRC and PBF

7.3.1.1 GST pull down assay

Before examining the functional significance of a potential interaction between SRC and PBF, the putative interaction was investigated using glutathione-S-transferase (GST) pull

down assays and co-immunoprecipitation. In a cell-free setting, GST-tagged PBF was translated and its size determined by SDS-PAGE with the resulting band running at the expected (Figure 7.2A). [^{35}S]-methionine labelled SRC was translated using a cell free system and detected at 60 kDa (Figure 7.2B). To test for an interaction, GST-tagged PBF was incubated with [^{35}S]-methionine labelled SRC, using GST alone as a negative control. After eluting, the samples were run through SDS-PAGE with 10% [^{35}S]-methionine labelled SRC as a positive control. When compared to GST alone, GST-PBF appeared to bind SRC in this cell free setting (Figure 7.2C), although a small degree of binding was apparent in the GST-only control lane.

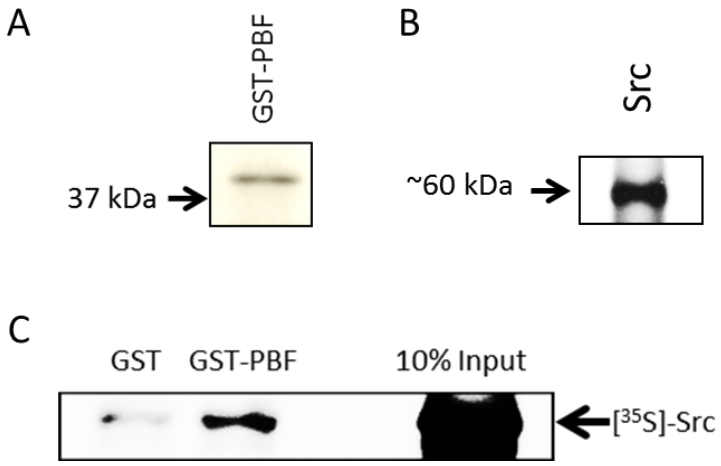

Figure 7.2 GST pull down assay. A: Western blot of translated GST-PBF. B: [^{35}S]-methionine labelled SRC detectable at approximately 60 kDa. C: GST pull-down assay demonstrating binding between SRC and GST-PBF when compared to GST alone.

7.3.1.2 Co-immunoprecipitation

As well as examining the interaction in a cell free system, co-immunoprecipitation was performed to establish if the interaction occurred in a more physiological setting. As the endogenous expression of SRC in TPC and K1 cells is low, over-expressed SRC was used. The full length human cDNA for *SRC* was sub-cloned into the mammalian expression vector pcDNA3.1+ from the bacterial vector pOTB7. The resulting plasmid was sequenced and

shown to contain the full length *SRC* cDNA. When transfected into TPC1, K1 and HeLa cells, SRC was over-expressed as expected (Figure 7.3).

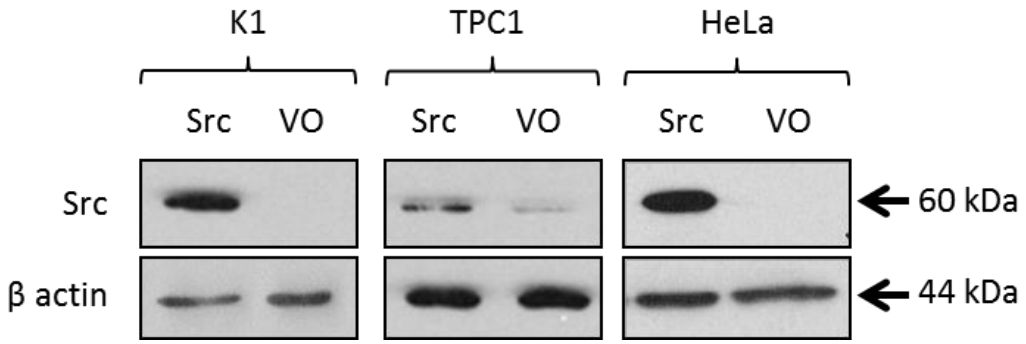

Figure 7.3 Over-expression of SRC in K1, TPC1 and HeLa cell lines demonstrated by Western blot.

Due to the high transfection efficiency of HeLa cells, they were used for co-immunoprecipitation, and were transfected with both *PBF-HA* and *SRC*. Western blot analysis was performed and demonstrated that PBF-HA expression was not affected by SRC over-expression (n = 3, Figure 7.4).

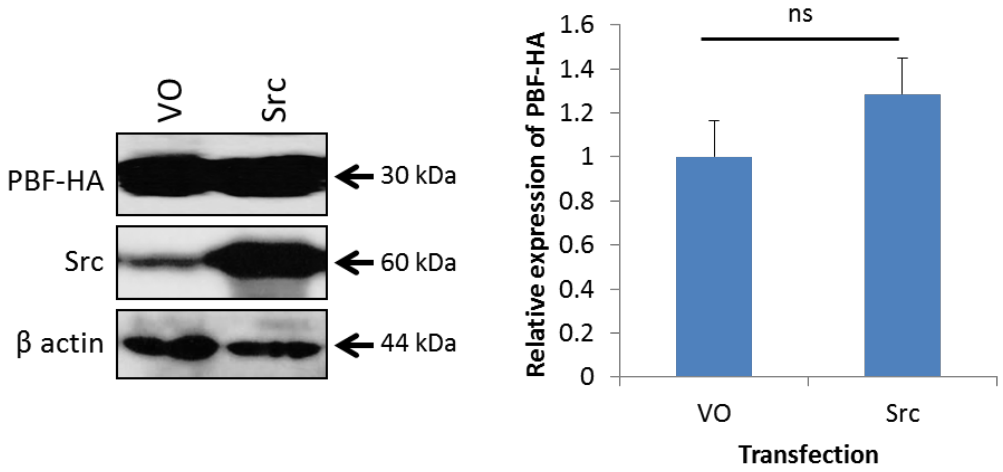

Figure 7.4 Over-expression of SRC does not affect PBF-HA expression. A: i.) Western blot analysis of HeLa cells transfected with either VO or SRC. There was no significant difference between the two conditions in terms of PBF-HA expression as demonstrated by scanning densitometry (ii.) (28.6 ± 16.4% of control, n = 3, p = ns).

Subsequently, after immunoprecipitating PBF-HA with an anti-HA antibody, SRC was detected, whereas in control lanes no SRC was identified (Figure 7.5A). In the reciprocal experiment, PBF-HA was co-immunoprecipitated with SRC using a SRC antibody (Figure 7.5B). Together with the GST-pull down and MS/MS data, this demonstrated an interaction between the two.

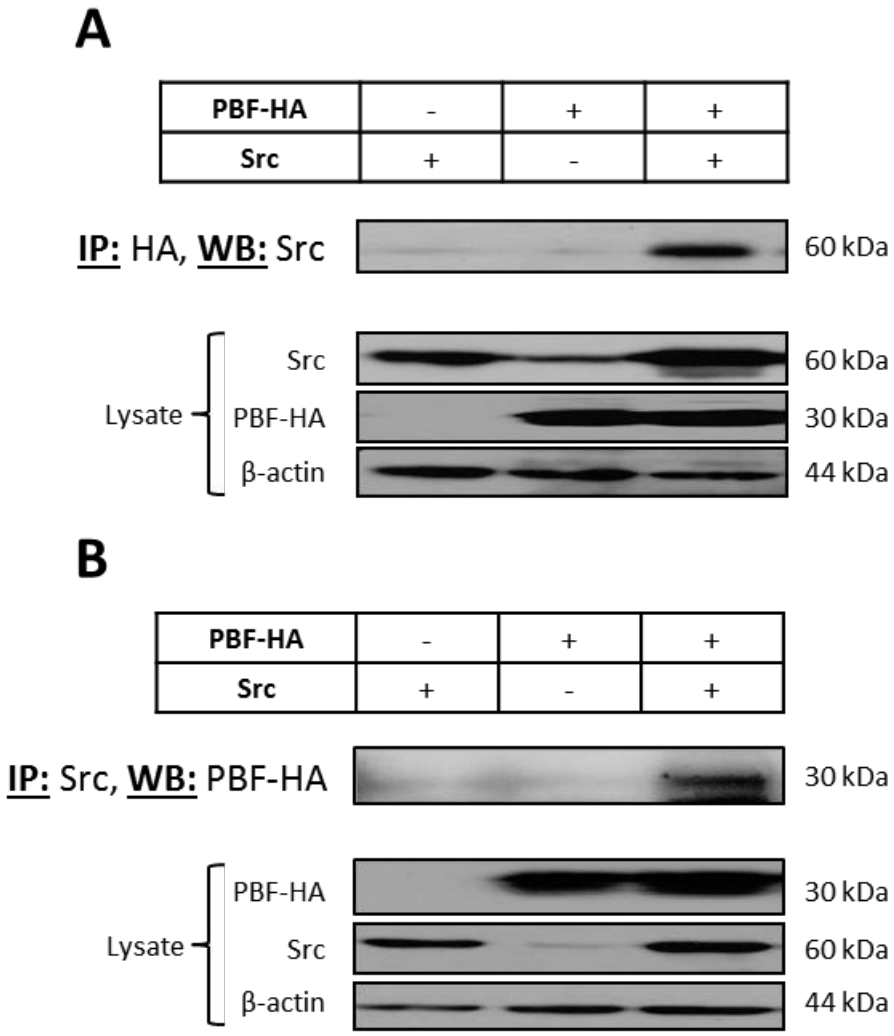

Figure 7.5 PBF-HA binds to SRC in HeLa cells in forward and reverse co-immunoprecipitation assays. A: Western blot showing co-immunoprecipitation of SRC after immunoprecipitating with an anti-HA antibody. B: Western blot showing co-immunoprecipitation of PBF-HA after immunoprecipitating with an anti-SRC antibody.

7.3.2 PBF and SRC co-localise

Having confirmed the interaction between SRC and PBF, their cellular localisation was then examined using fluorescence immunocytochemistry in K1, TPC1 and HeLa cells transfected with *PBF-HA* and *SRC*. In all 3 cell lines, the distribution of both PBF-HA and SRC was similar; both were found in the cytoplasm and at the cell membrane (Figure 7.6).

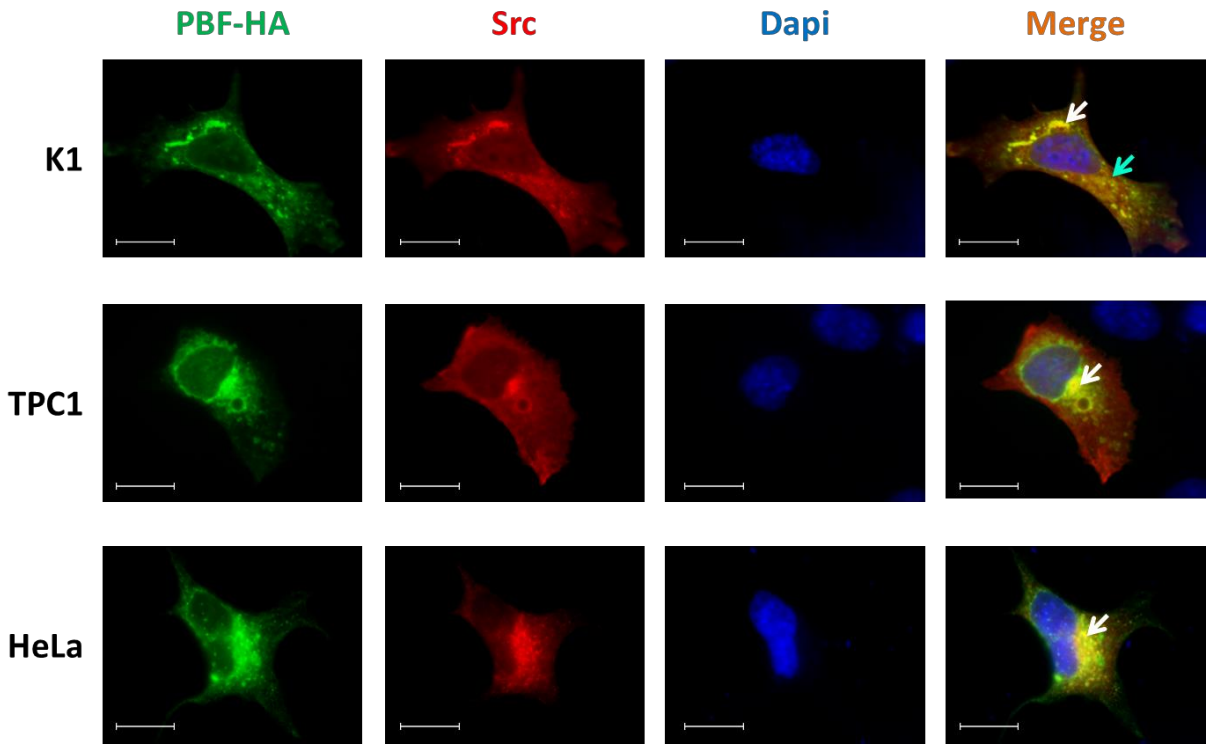

Figure 7.6 Fluorescence immunocytochemistry demonstrating co-localisation of PBF-HA and SRC in K1, TPC1 and HeLa cells. PBF-HA was identified in green using an anti-HA antibody, SRC was identified in red, nuclear staining was shown in blue. Areas of co-localisation between PBF-HA and SRC were shown in yellow, and occur within intra-cellular vesicles (white arrows) and at the cell membrane (blue arrow). Bars, 20 µm.

7.3.3 SRC does not alter the sub-cellular localisation of PBF-HA

The final analysis performed was to assess the effect of Src over-expression on PBF sub-cellular localisation. An increase in SRC expression did not have an effect on PBF sub-cellular localisation, as apparent in Figure 7.7, where 2 adjacent cells are displayed. The lower right cell is co-transfected with *PBF-HA* and *SRC*, while the upper cell is transfected with *PBF-HA* only. It is readily apparent that PBF-HA has a similar distribution in both cells.

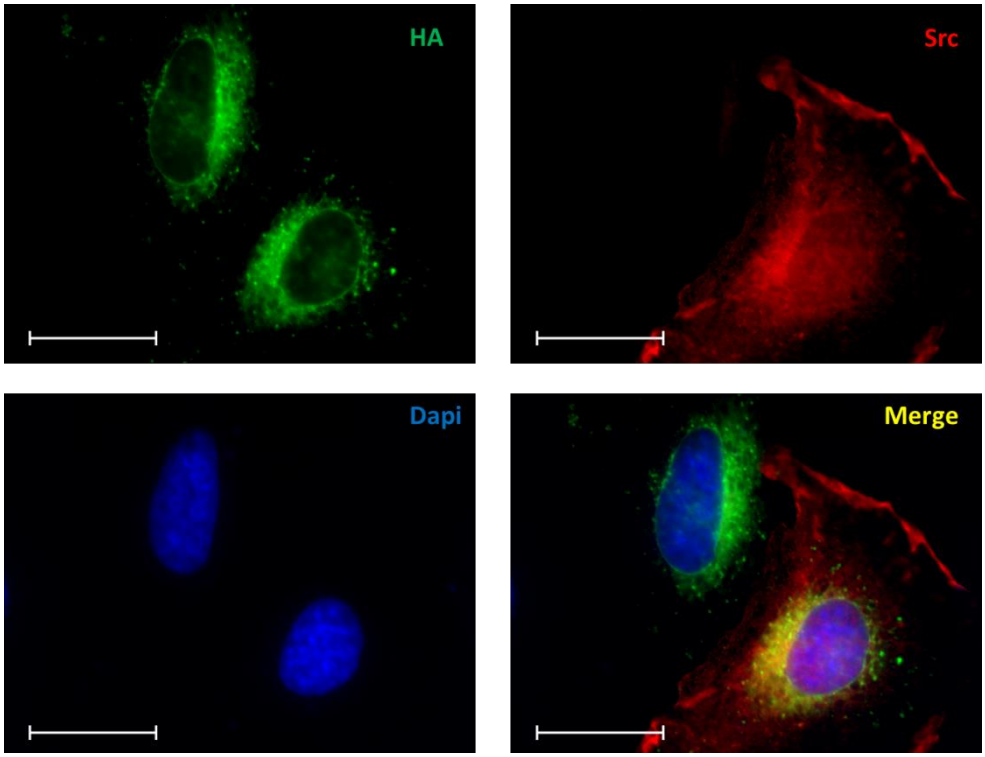

Figure 7.7 Fluorescence immunocytochemistry demonstrating that SRC does not affect PBF sub-cellular localisation. HeLa cells were transfected with SRC (red) and PBF-HA (green), areas of co-localisation are shown in yellow and nuclear staining in blue. In the 2 cells, only the lower cell has been transfected with SRC; however PBF-HA distribution is similar in both. Bars, 20 µm.

7.4 Discussion

The SFKs were identified by MS/MS as potential interacting partners of PBF, and SRC had been identified as a potential kinase for PBF. These factors led to the decision to include SRC in the final shortlist of proteins to take on for further experiments. As in previous chapters, the first step in this process was to independently validate the interaction between PBF and SRC, using GST-tagged pull down assays and also co-immunoprecipitation. The GST pull-down assay demonstrated an interaction in a cell-free setting, but initial attempts at co-immunoprecipitation were unsuccessful (data not shown) as the expression of SRC was not sufficient for detection by Western blotting. MS/MS is significantly more sensitive than co-immunoprecipitation, with the capability of detecting femtomolar concentrations of peptides, hence the identification of SRC in those assays when compared to co-immunoprecipitation. The c-DNA for SRC was subcloned into a mammalian expression vector, which facilitated its transfection into the cell lines used in previous chapters. The over-expression was confirmed in all cell lines on Western blotting. Using this model, SRC was over-expressed in HeLa cells and an interaction was confirmed by forward and reverse co-immunoprecipitation. Taken together, these data validated the interaction between PBF and SRC first identified by MS/MS.

Finally, fluorescence immunocytochemistry was performed to investigate any co-localisation of the two proteins. Western blot analysis demonstrated no change in PBF-HA expression when SRC was over-expressed. Immunofluorescence indicated co-localisation at both the cell membrane and within intra-cellular vesicles in HeLa cells. The location of SRC within the cell is important to understanding any potential kinase role it may have regarding PBF. Usually, cytoplasmic SRC is in the pY530 inactive state; de-phosphorylation here leads

to translocation to the cell membrane where full activation is achieved through phosphorylation at Y419 (Anbalagan et al. 2012). The findings above indicate co-localisation at the cell membrane, where active SRC may be able to phosphorylate PBF, and also within intra-cellular vesicles, the consequences and reasons for which are as yet unknown and are the focus of on-going study.

Concluding remarks

This chapter has validated the interaction between PBF and the tyrosine kinase SRC using two independent binding assays. Co-localisation was observed within intra-cellular vesicles and also at the cell membrane, and it is at this location that SRC is active as a protein kinase. These data, taken together with phosphorylation prediction, suggest that SRC may be the kinase responsible for phosphorylating PBF. The following chapter further explores this interaction, and the functional implications of targeting it.

Chapter 8 The role of SRC and its inhibition on PBF-induced NIS repression

8.1 Introduction

The previous chapter validated the interaction between SRC and PBF using GST pull-down assay and co-immunoprecipitation. Additionally, co-localisation was observed in intra-cellular vesicles and at the cell membrane. These data were important preliminary steps prior to any investigation into the kinase role of SRC within PBF physiology, and what effect SRC may have on PBF function and thyroid cancer development.

SRC lies downstream of a number of cell membrane receptor tyrosine kinases, and thus plays a vital part in many of the key cellular process they govern (Figure 8.1). In human malignancies such as breast, gastrointestinal, lung, ovary and lymphomas, SRC is overexpressed, with its effects on adhesion, cell growth and angiogenesis contributing to metastasis formation (Alvarez et al. 2006). However, over-expression of SRC alone is insufficient to act as a transforming event in these cells, rather depending on the mutation of the c-terminal part of the protein, as seen in v-SRC, which constitutionally activates the kinase (Shalloway et al. 1984). A truncated version of the protein lacking the c-terminal regulatory mechanism was found in 12% of advanced colorectal carcinomas, demonstrating a direct role in disease progression (Irby et al. 1999).

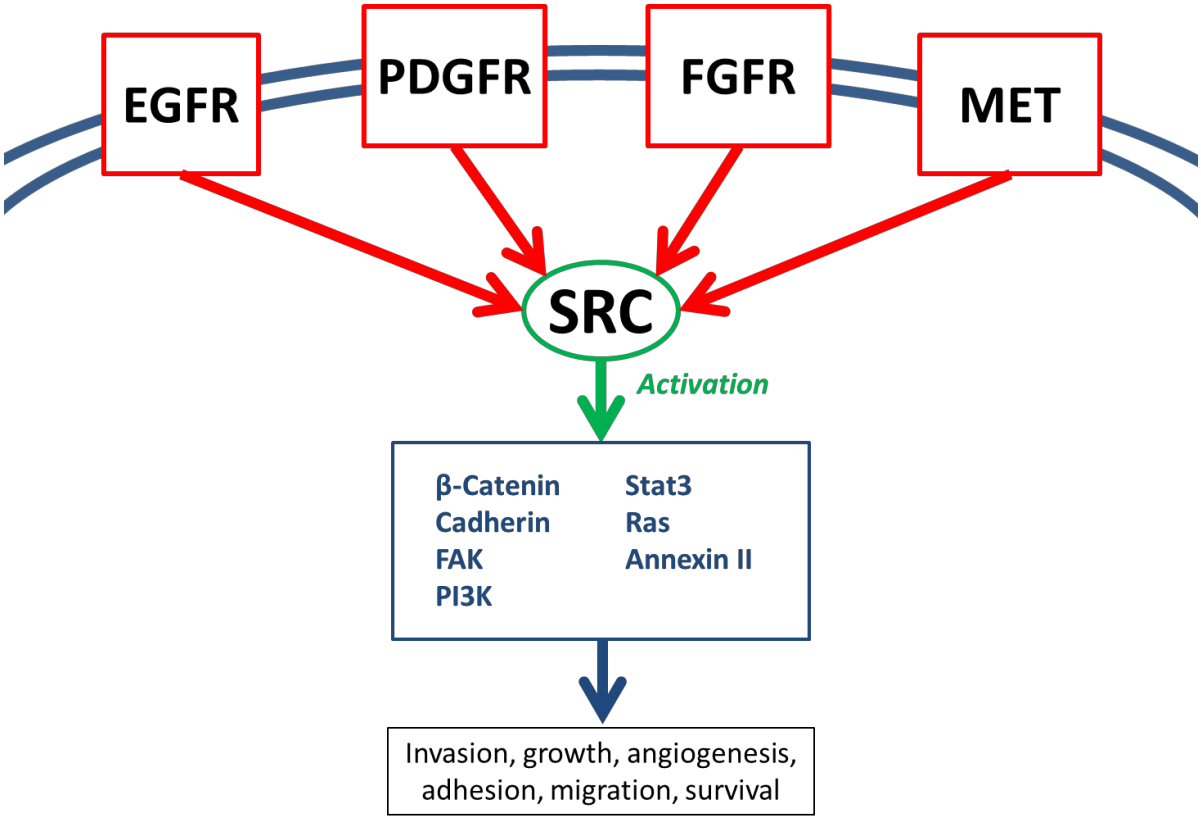

Figure 8.1 SRC lies downstream of several receptor tyrosine kinases. Activation of SRC leads to activation of other pathways which in turn control key cellular events. Increased activation of these physiological processes can lead to increased invasiveness and metastasis of cancer. EGFR – epidermal growth factor receptor, PDGFR – platelet derived growth factor receptor, FGFR – fibroblast growth factor receptor, MET – hepatocyte growth factor receptor. Adapted from (Irby and Yeatman 2000).

Despite a potential link between SRC activity and medullary thyroid cancer being put forward in 2004 (Liu et al. 2004), the relationship between SRC and differentiated thyroid cancer was not described until 2009 where a SRC inhibitor was shown to reduce growth and invasion in a number of thyroid cancer cell lines, although this was thought to be due to inhibition of SRC phosphorylating Focal Adhesion Kinase (FAK) (Schweppe et al. 2009). Since then, SRC has been identified as up-regulated in invasive thyroid cancers (Cho et al. 2012), with inhibition of SRC reducing metastases and tumour growth (Chan et al. 2012). Total SRC is not increased in thyroid cancers, therefore it is the phosphorylation, and

consequently the activation, of SRC that promotes this aggressive tumour behaviour, although the exact pathway by which this effect is mediated remains unknown.

Tyrosine phosphorylation is a post-translational modification that is often key to controlling a protein's activity within a cell. Unpublished data within the McCabe group have recently shown PBF to be phosphorylated at Y174, although the kinase responsible was unknown. Phospho-site prediction software identified SRC as a potential kinase for this residue. The aims of this chapter were therefore to determine whether SRC, which was confirmed to bind PBF in Chapter 7, was responsible for phosphorylating PBF. This interaction could then be targeted with a variety of inhibitors, with the aim of reducing phosphorylation and potentially increasing iodide uptake in radioiodine refractory, PBF over-expressing, thyroid cells.

8.2 Methods

8.2.1 Cell culture and transfection

K1, TPC1, HeLa and FRTL-5 cells were maintained as described in 2.1. Human primary thyroid tissues were cultured with approval of the Local Ethics and Research Committee as described in Section 2.7.

8.2.2 Western Blotting

Western Blotting was performed as described in Section 2.3.2. In addition to antibodies previously described, a PBF phospho-specific antibody to residue Y174 ("anti-Y174") (CovalAb, Villeurbanne, France) was kindly provided by Dr V Smith, University of Birmingham, and was used at 1:500.

8.2.3 Fluorescence immunocytochemistry

Immunofluorescence was carried out as described in Section 2.6. In addition to previously described antibodies, anti-Y174 was used at 1:100.

8.2.4 Assessment of phosphorylation status

8.2.4.1 Treatment with a phosphatase inhibitor

In order to preserve the phosphorylation status of proteins, cells were harvested using the irreversible tyrosine phosphatase inhibitor sodium orthovanadate (Na_3VO_4). Prior to harvesting, cells were treated for 15 minutes with 100 μM pervanadate (from a 30 mM stock solution: 951.1 μL PBS, 6 μL hydrogen peroxide, 42.9 μL Na_3VO_4, incubated in the dark at room temperature for 15 minutes). The medium was then removed and the cells washed with 1 ml cold PBS before adding 100 μL modified RIPA (50 mM Tris, 150 mM NaCl, 1 % Igepal, 6 mM sodium deoxycholate, 1 mM ethylene glycol tetraacetic acid (EGTA), buffered to pH 7.4) with 1 mM Na_3VO_4 and 6 % protease inhibitor cocktail. Cells were scraped into a microcentrifuge tube, sonicated for 30 seconds and spun on a benchtop centrifuge at 12,000 rpm for 20 minutes. The supernatant was then stored at -20 °C.

8.2.4.2 Treatment with tyrosine kinase inhibitors (TKIs)

In an attempt to alter the phosphorylation of PBF, cells were treated with a panel of TKIs. The different TKIs used, with their known targets and dose, are shown in Table 8.1. Thirty minutes prior to harvesting, appropriate TKIs were added to the media and plates returned to the incubator. Protein was then harvested as described above.

TKI	Dose (nM)	Target(s)
Gefitinib	10	Epidermal growth factor receptor (Ciardiello 2000)
Imatinib	10	Abl, c-kit α, platelet derived growth factor receptor (Buchdunger et al. 1996)
PD173074	10	Fibroblast growth factor receptor, Vascular endothelial growth factor receptor (Mohammadi et al. 1998)
SU11274	10	c-MET (Sattler et al. 2003)
PF573228	10	Focal adhesion kinase (Slack-Davis et al. 2007)
PP1	2 – 10	Src (Hanke et al. 1996)
PP3	2 - 10	Src family negative control (Liu et al. 1999)

Table 8.1 Dose and target(s) of tyrosine kinase inhibitors (TKIs) used.

8.2.5 Iodide uptake assays

8.2.5.1 TSH responsiveness

Prior to uptake analysis, functionality of primary thyrocyte cultures were assessed. Primary human thyrocytes are able to remain functional for several weeks when cultured as described in Section 2.7, although this decreases with time (Eggo et al. 1996). In addition, cultures from some patients may not exhibit functions associated with differentiated thyroid follicular cells. This may be due to the specimen originating from macroscopically normal, but histologically abnormal, thyroid tissue. The response to TSH by primary thyrocytes is a reliable marker of thyroid cell function, with increasing concentrations of TSH resulting in an increase in iodide concentration by the cell. However, at super-physiologic doses of TSH, iodide uptake falls (Eggo et al. 1996). For each prep, half of a 24 well plate was kept in TSH and serum free medium from day 4 (the other half being maintained in serum-free medium only). On day 7, the cells were treated (in duplicate) with 0.01, 0.1, 0.3, 1 and 10 U of TSH.

On day 9 the ability of the cells to take up ^{125}I was measured as described below; any preparations that did not show the anticipated TSH response were discarded.

8.2.5.2 Iodide uptake

Primary thyroid cells were treated with sodium iodide (NaI) containing 100,000 cpm ^{125}I (Hartmann Analytic, Braunschweig, Germany) to give a final concentration of 10^{-7} NaI. This concentration of iodide ions had been optimised to ensure maximal uptake by thyrocytes (Eggo et al. 1996). The cells were returned to the incubator for 3 hours to allow the uptake of ^{125}I by the thyrocytes. Subsequently, the cells were washed rapidly twice with HBSS to remove any residual ^{125}I and lysed in 200 µL 2 % SDS. After transferring to a test tube, ^{125}I uptake was assessed by analysing the gamma emissions as measured on a LKB Wallac 1260 Multi gamma II gamma counter for 1 minute. To standardise the results between wells, the amount of protein present was quantified using the BCA assay as described in Section 2.3.1, with BSA standards made in 2 % SDS. In addition, transfection was determined by running 25 µL of the lysate through SDS-PAGE and immunoblotting with antibodies targeting the transfected protein.

Iodide uptake was also measured in HeLa, TPC1 and K1 cells. Cells were seeded in 9.5 cm^2 tissue culture wells and transfected as previously described. After 48 hours further incubation at 37 °C, cells were treated with NaI containing ^{125}I and iodide uptake measured as described above.

8.3 Results

8.3.1 SRC over-expression leads to phosphorylation of PBF

As work within our group has shown that PBF is a phospho-protein, the above model of SRC over-expression was used to determine the effect of SRC on the phosphorylation status of PBF. An antibody specific to Y174- phosphorylated PBF (pY174) was kindly provided by Dr Vicki Smith. Having been previously validated by Dr Smith to demonstrate specificity in Western blotting, fluorescence immunocytochemistry also validated its use in identifying PBF-HA phosphorylated at Y174 (Figure 8.2).

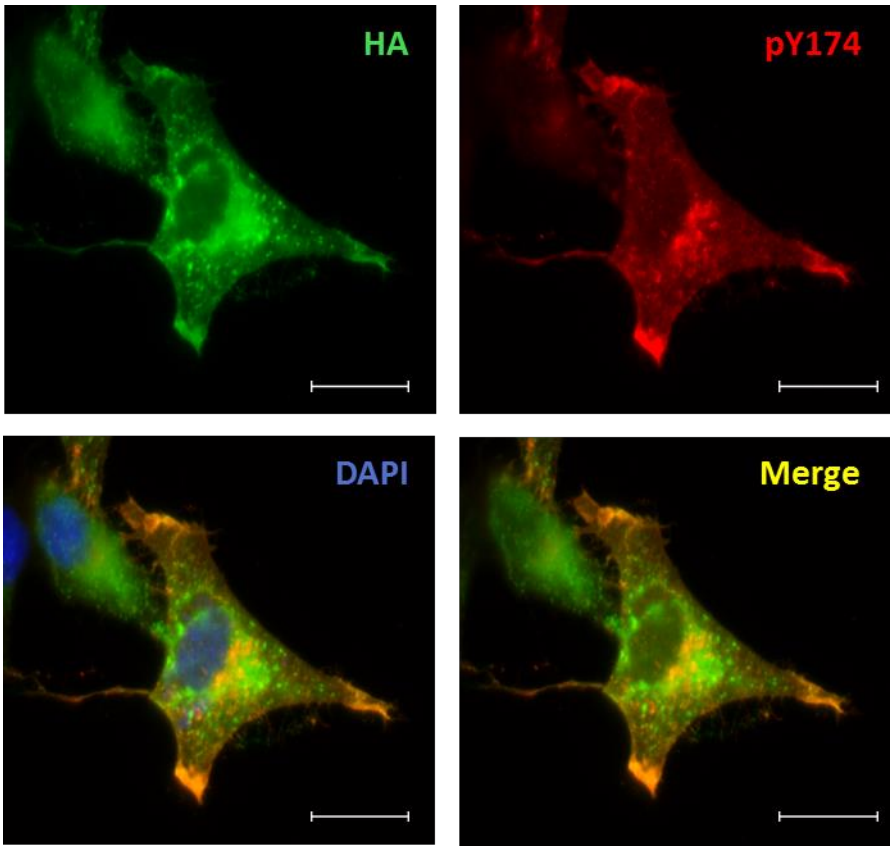

Figure 8.2 Detection of pY174 by fluorescence immunocytochemistry. HeLa cells were transfected with PBF-HA and stained for HA (green) and pY174 (red). Yellow staining indicated both HA and Y174, demonstrating that exogenous PBF was phosphorylated and detectable by IF. Bars, 20 µm.

HeLa cells were transfected to transiently over-express PBF-HA, and co-transfected with either *SRC* or blank vector. As phosphorylation is a post-translational modification that can easily be disrupted by the process of harvesting and lysing cells, the phosphatase inhibitor pervanadate was added 30 minutes prior to harvesting in order to preserve the phosphorylated state of PBF, with vehicle-only treatment as a control. With vector only transfection, pY174 was apparent at low to undetectable levels; however, SRC was shown to significantly increase the amount of pY174 (n = 3) (Figure 8.3). Cells transfected with the *Y174A* mutant of *PBF* (which cannot be phosphorylated at residue 174) were used as a negative control and did not demonstrate detectable phosphorylation. In addition, using pervanadate increased the yield of pY174 as would be expected.

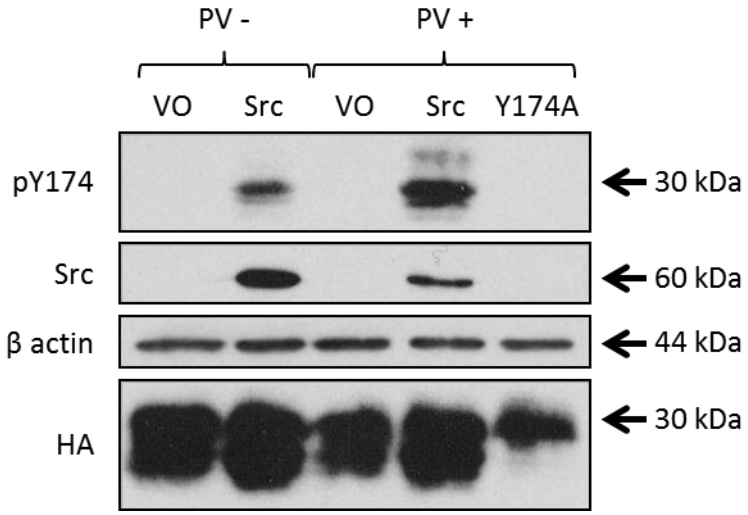

Figure 8.3 SRC over-expression leads to increased phosphorylation of PBF at Y174 (pY174). Western blot analysis of HeLa cells co-transfected with PBF-HA and either SRC or VO. Treatment was either with (PV+) or without (PV-) pervanadate. Y174A was a mutant of PBF which could not be phosphorylated at Y174. β actin shown for loading control and HA to demonstrate transfection.

8.3.2 TKIs affect pY174 in a time and dose dependent manner

Phosphorylation is a key post-translational modification that frequently governs a protein's function within a cell, and having demonstrated that PBF is a phosphorylated at Y174, the effect of a small panel of tyrosine kinase inhibitors (TKIs) on pY174 was assessed. HeLa cells transfected to over-express PBF-HA were treated with pervanadate as described above, following which 10 nM aliquots of gefitinib, imatinib, SU11274 and PD173074 were added. SU11274 led to an 89 ± 2.6% reduction in pY174 ($p < 0.05$, $n = 3$) (Figure 8.4).

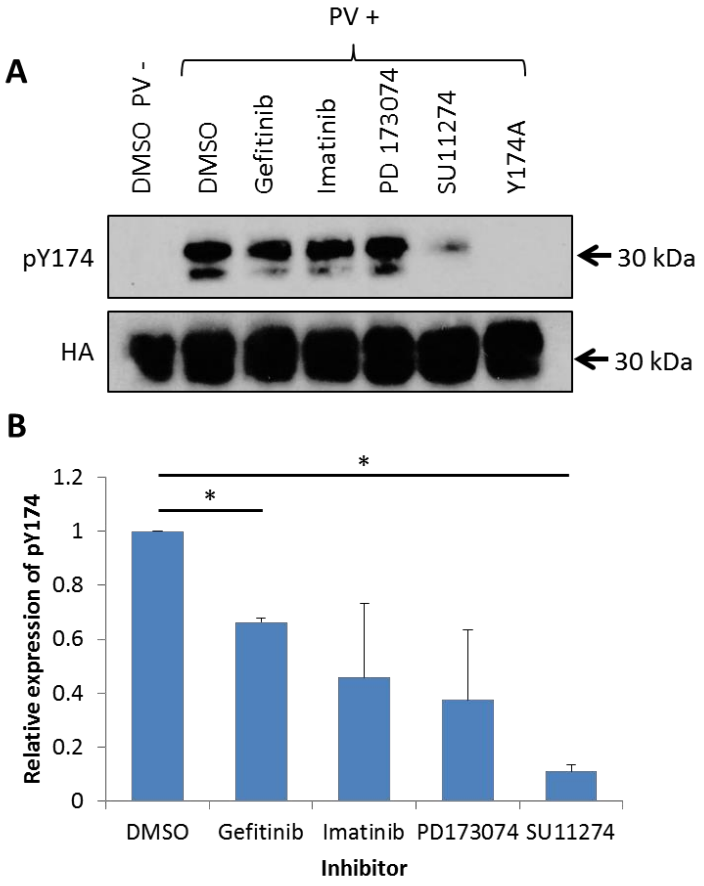

Figure 8.4 Western blot analysis of the effect of various TKIs on pY174 expression. A: Representative Western blot of HeLa cells treated with either vehicle (DMSO) or TKI demonstrated some degree of reduction in pY174 with all TKIs, although imatinib and PD1736 did not have a significant effect. Y174A indicates non-phosphorylatable PBF mutant. PV+ indicates treatment with pervanadate. B: Scanning densitometry revealed a significant reduction for gefitinib (34 ± 1.6%, $p < 0.05$, $n = 3$) and SU11274 (89 ± 2.6%, $p < 0.05$, $n = 3$).

Given that SU11274 led to the greatest response of the panel of TKIs, this was used to determine the optimum dose that could be applied in order to demonstrate an effect. Using concentrations varying from 0 to 10 μM, SU11274 was applied to HeLa cells over-expressing PBF-HA. A reduction in pY174 was observed with the lowest dose, 0.5 μM (79.5 ± 2.1% of control, $p < 0.05$, $n = 3$) (Figure 8.5). There was a significant difference between the reduction observed with 0.5 μM and concentrations of 2 μM (95.2 ± 1.5%), 5 μM (95.5 ± 1.2%) and 10 μM (96.4 ± 1.4%) (all $p < 0.01$, $n = 3$). The optimum dose was therefore taken to be 2 μM.

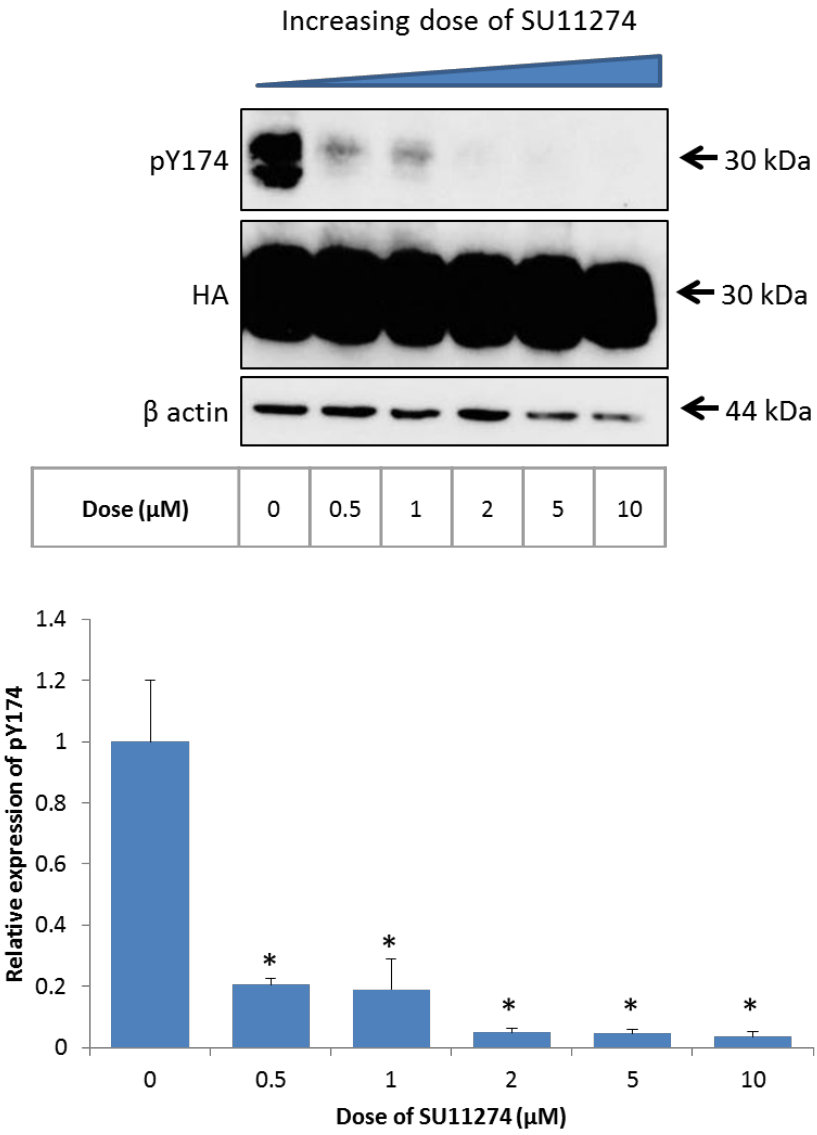

Figure 8.5 SU11274 reduces pY174 expression in a dose dependent manner. Representative Western blot showing a reduction in pY174 with increasing concentrations of SU11274. Below, scanning densitometry demonstrated a significant reduction compared to control with all concentrations used ($p < 0.05$, $n = 3$).

Once the optimum dose of TKI had been determined, the optimum treatment time was assessed. HeLa cells were again transfected with *PBF-HA*, and all treated with 2 µM SU11274. In these experiments, treatment time ranged from 0 minutes to 24 hours. All cells were treated with pervanadate as above to preserve phosphorylation after cell harvest. In Western blot, a decrease in pY174 expression was observed at all timepoints when compared

to the 0 minutes negative control (Figure 8.6A). However, the change across the range was small and therefore it was decided to use the 30 minute timepoint for subsequent experiments, given the potential cytotoxicity of the inhibitor.

Fluorescence immunocytochemistry across the same timepoints was also performed. Interestingly, for all timepoints there appeared to be a fall in the amount of pY174 associated with the cell membrane, with more being located in intracellular vesicles. However, this was not quantified directly (Figure 8.6B).

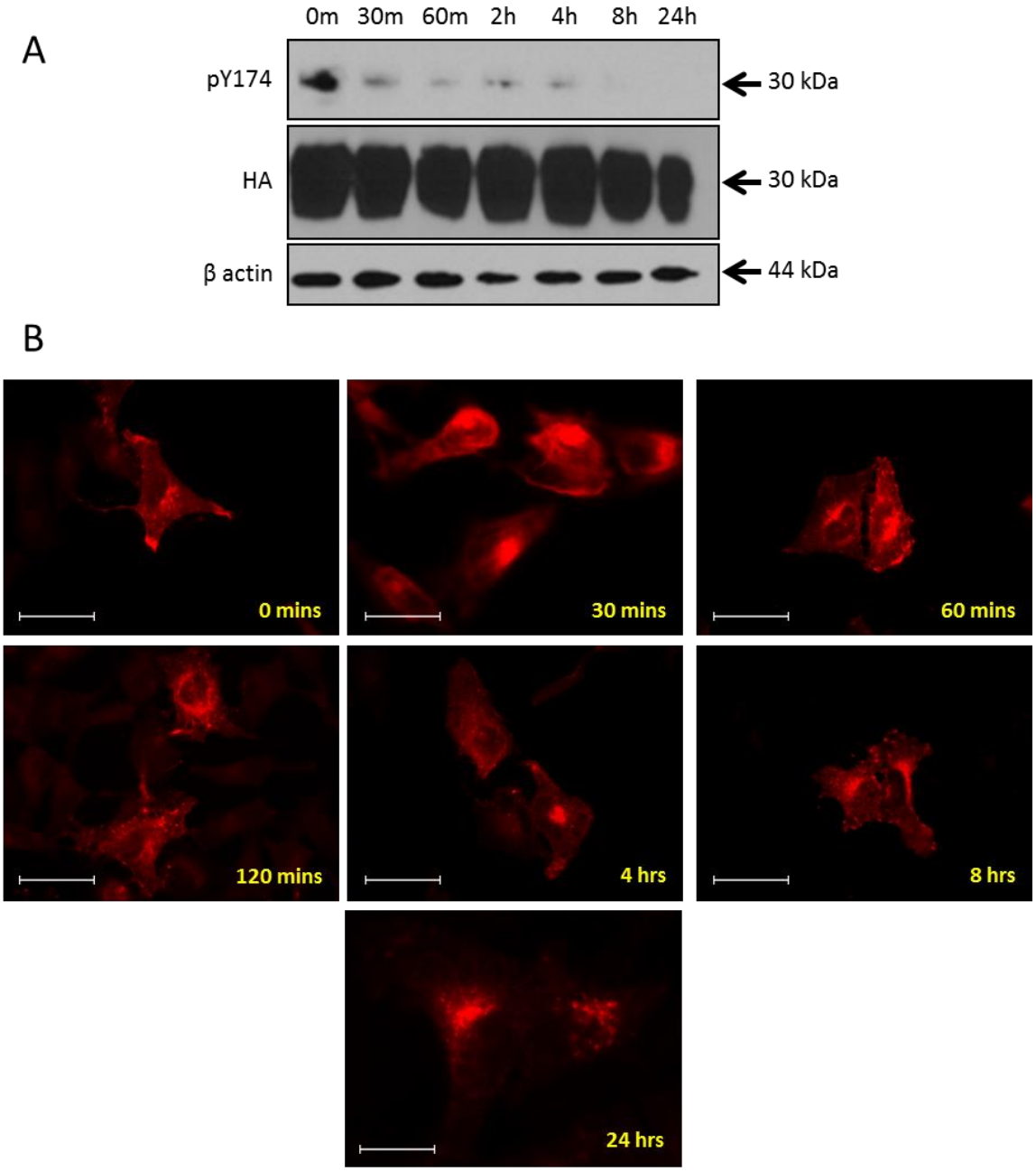

Figure 8.6 Time course treatment of HeLa cells with SU11274. A: Representative Western blot demonstrating a time-dependent reduction in pY174 with SU11274 treatment (2 µM). B: Fluorescence immunocytochemistry of HeLa cells treated for differing time periods with SU11274, with pY174 staining in red. With increasing treatment time, there was less membrane localisation observed. Bars, 20 µm.

8.3.3 Inhibition of SRC by PP1 leads to reduced pY174 expression

Given that the panel of TKIs was shown to differentially affect PBF phosphorylation, and that SRC is involved in the process, a specific SRC inhibitor was used to determine whether SRC was an essential or contributory kinase in the process. The SRC specific inhibitor PP1 (a cell-permeable pyrazolopyrimidine compound) was used. PP3, which is a non-functioning analogue of PP1, was used as a negative control. PP1 was able to reduce pY174 levels significantly compared to both DMSO and PP3 (which exhibited similar levels) in HeLa cells co-transfected with *PBF-HA* and *SRC* (Figure 8.7). This response was a partial reversal of the increase apparent with over-expressed SRC.

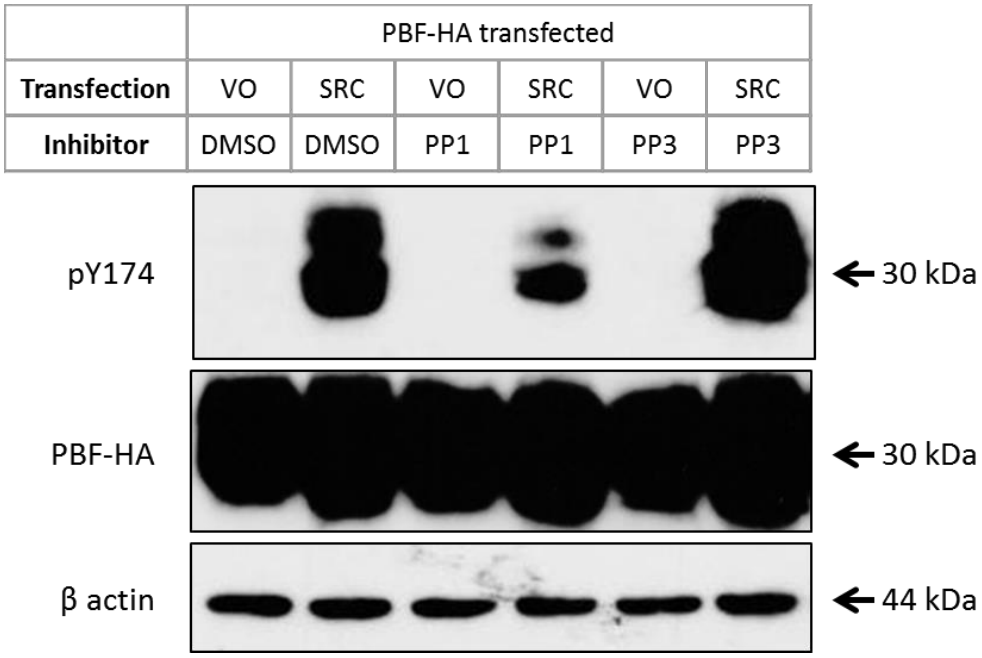

Figure 8.7 Western blot analysis of HeLa cells transfected with PBF-HA*, demonstrating an increase in pY174 with SRC over-expression and also a reduction in pY174 when treated with the SRC inhibitor PP1 when compared with DMSO alone. There was no change in pY174 when the inactive version of the inhibitor, PP3, was used. VO = vector only.*

This demonstrated that PP1 was able to reduce the effect that over-expressed SRC had on PBF phosphorylation, but as yet the effect of inhibitors on pY174 in the presence of endogenous SRC was undetermined. Following on from this, the effect of PP1 when

compared to the other TKIs was assessed in cells with endogenous levels of SRC and PBF. K1, TPC1 and HeLa cells were again treated with the panel of inhibitors, but were untransfected. Understandably, in these circumstances pY174 was significantly harder to detect. K1 and TPC1 cells both showed a reduction in pY174 with PP1 treatment, and in K1 and HeLa cells gefitinib also had an inhibitory effect on phosphorylation. These data demonstrated that pY174 could not only be detected in the presence of endogenous levels of SRC, but also that PP1 still had an effect on the amount of phosphorylation.

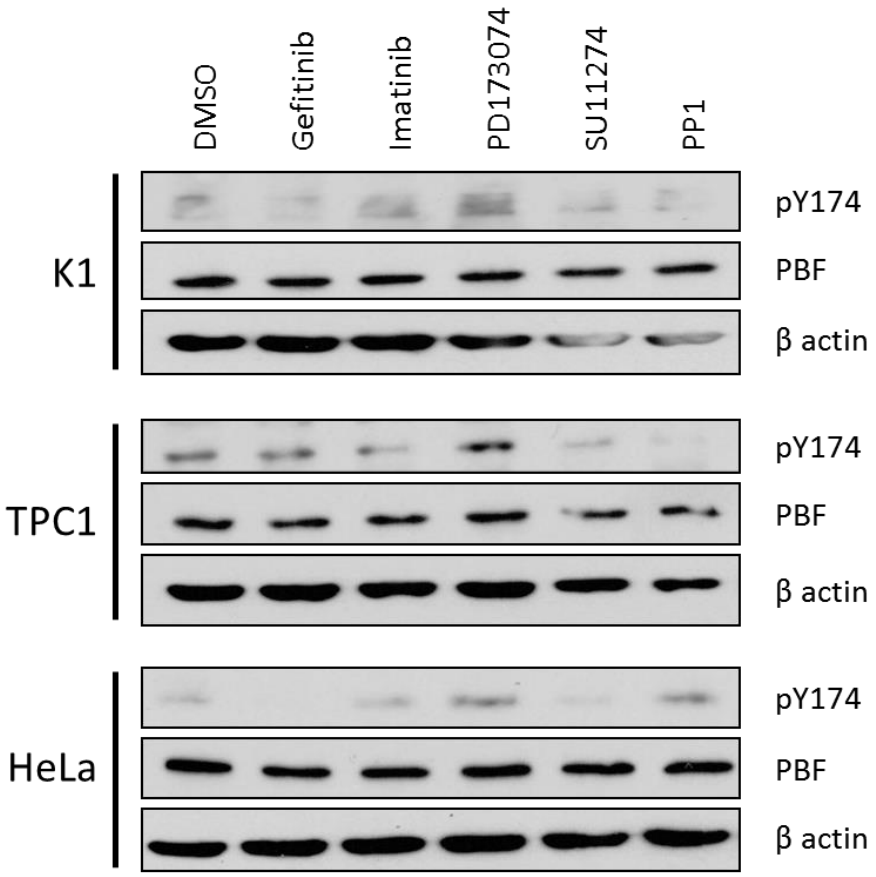

Figure 8.8 Western blot analysis of K1, TPC1 and HeLa cells and the effect on pY174 of various tyrosine kinase inhibitors. In untransfected cells, PP1 reduced pY174 in K1 and TPC1, while gefitinib also reduced pY174 in K1 and HeLa cells. β actin is shown as a loading control.

8.3.4 PP1 treatment leads to a significant reduction in pY174 expression in human primary thyroid cultures

The above experiments were carried out on transformed cells lines, all of which behave in different ways depending on their particular cancer genotype, and may have aberrantly activated kinase pathways. While this is useful for initially testing hypotheses, a more physiological model is to use normal human thyroid tissue. The inhibitor experiments were therefore repeated using human primary thyroid cultures, where the tissue was taken from macroscopically normal thyroid. As pY174 was easier to detect in primary thyroid tissue, these cells were left untransfected in order to reduce the amount of cell death and therefore maximise yield. As would be expected, human thyroid tissue demonstrated a large variation in culture across different preps, which affected statistical analysis. However, across a number of cultures, gefitinib and PP1 yielded the greatest reduction in pY174, with PP1 having the largest effect (Figure 8.9A). PP1 was therefore examined in isolation compared to treatment with DMSO alone. PP1 led to an 81.1 ± 7.8% reduction in pY174 ($p < 0.001$, $n = 5$), demonstrating that in both transformed cell lines and primary cultures, it is the most potent inhibitor of PBF phosphorylation at Y174 (Figure 8.9B).

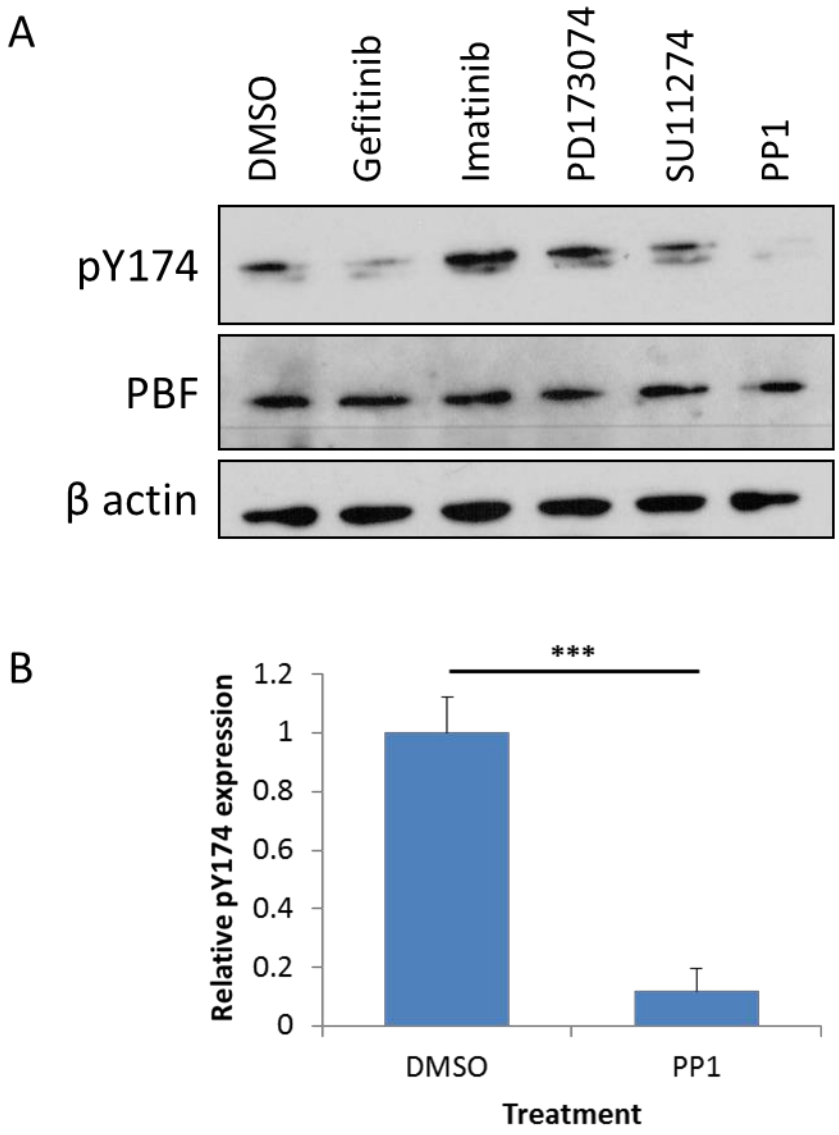

Figure 8.9 Effect of TKIs on pY174 in human primary thyroid cultures. A: Western blot analysis demonstrating that treatment with gefitinib and PP1 led to a reduction in pY174. B: Scanning densitometry revealed an 81.1 ± 7.8% reduction in pY174 ($p < 0.001$, $n = 5$) with PP1 treatment compared to DMSO alone (n=3).

8.3.5 Effect of PBF and SRC on ^{125}I uptake

8.3.5.1 Determination of uptake efficiency in different cell lines

Work within our group has demonstrated that over-expression of PBF significantly reduces ^{125}I uptake in both murine and human primary thyroid cultures (Read et al. 2011). In order to explore the relationship between PBF phosphorylation and ^{125}I uptake, the human primary thyroid model was validated and the cell lines assessed for uptake experiments. When measured on a gamma counter, untransfected and untreated human primary thyrocytes and FRTL5 cells both had counts in excess of 15,000 cpm per 3.7 cm^2 of culture. The K1, TPC1 and HeLa cells all had low counts, the highest being in the TPC1 cells where the average count was just over 500 cpm (n = 3) (Figure 8.10). While this was to be expected in the HeLa cells which do not express NIS, the low uptake in the thyroid cell lines was an indicator of their degree of de-differentiation from normal thyroid tissue and their lack of functional NIS. Given that these counts were low in the absence of treatment or transfection, it was thought unlikely that they would be suitable for further uptake experiments as the cell death that inevitably occurs would render the counts too low to be meaningful, and further uptake experiments were subsequently conducted on the primary cultures and FRTL5s, discounting the other cell lines.

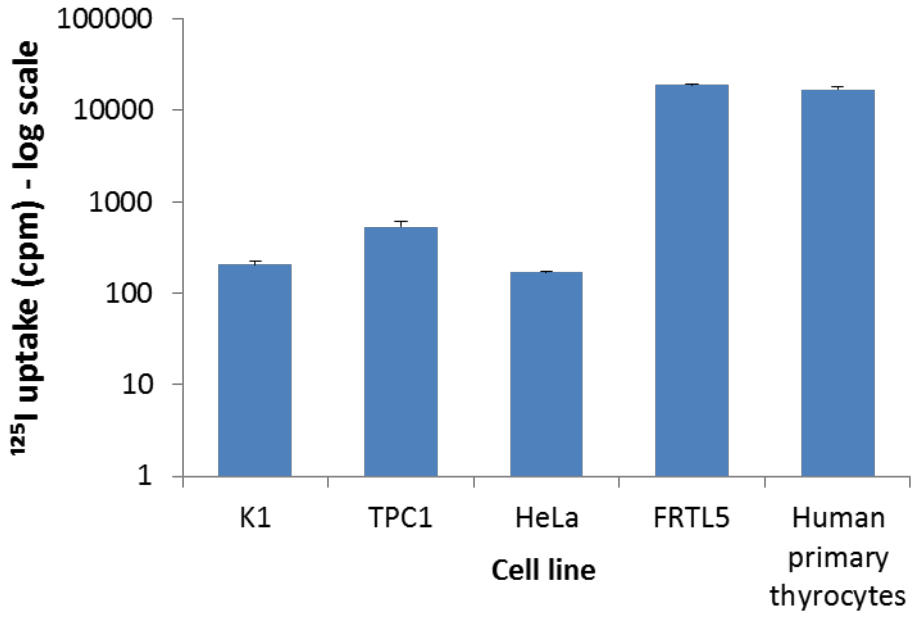

Uptake (cpm)	206	535	169	18949	16901
SEM	19	75	3	470	1473

Figure 8.10 3 hour ^{125}I uptake in cell lines. FRTL5 and human primary thyrocytes exhibit significantly higher uptake when compared to K1, TPC1 and HeLa cells (SEM = standard error of the mean, uptake in counts per million counted over 60 secs).

8.3.5.2 There is significant variation in ^{125}I uptake between primary thyroid cultures

Although from macroscopically normal thyroid tissue, each primary thyroid culture came from a different patient, yielding significant variation in the behaviour of the cells. Therefore, for each preparation the culture had to be assessed to ensure that it was functional in terms of iodide uptake. Untransfected cells showed wide variation; although most cultures had uptake counts of greater than 15,000 cpm, some exhibited little or no uptake and these were discarded from subsequent analysis. In addition, cells should exhibit the typical dose-response effect with TSH, whereby uptake increases up to around 0.3 Units, then falls off as the dose increases further (Pratt et al. 1989). In Figure 8.11A and C, this was demonstrated across 4 cultures. Figure 8.11A demonstrates the uptake of the preps, and it can be seen that

Prep 1 has a much lower uptake that the other 3, therefore would not be usable once transfected and treated. Despite this, Prep 1 showed a typical TSH response, although Prep 3 did not show any change in uptake with changing TSH concentration (Figure 8.11B). Therefore, of the 4 preps, only Preps 2 and 4 would be used in uptake experiments.

The response of preps to transfection was also varied; Figure 8.11C shows the different uptake profile of 3 separate cultures, all of which were transfected with blank vector, with average counts ranging from 700 to 2450 cpm. Cultures where the average count after transfection with blank vector was less than 300 cpm were not used for analysis, as at these lower values the intra-culture variation meant that significant results were unlikely to be obtained.

To eliminate variation caused by errors inherent to the gamma counter itself, each sample was counted at least twice in different wells of the counter, and the machine calibrated on a regular basis. The variation between counts in a representative prep is shown in Figure 8.11D; although most samples had a less than 15% difference between the 2 counts, those exhibiting a greater variation were re-counted twice in different wells. If the variation was still greater than 15% the samples were discounted.

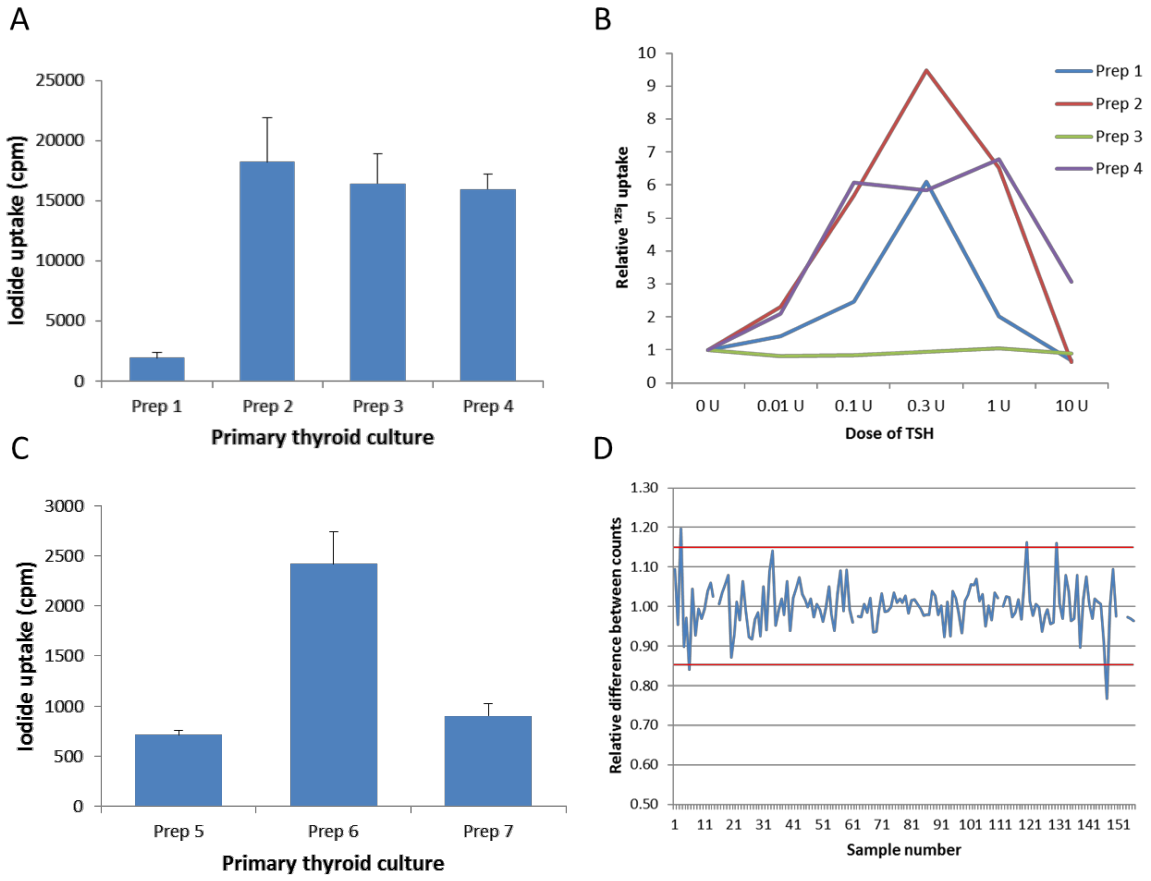

Figure 8.11 Variation in iodide uptake between different patient cultures. A: Uptake from 4 preps demonstrated poor uptake in Prep 1, and some variation in the uptake in the other preps. B: TSH response curves for the same 4 preps; Prep 3 did not exhibit the physiologically correct response and was therefore discarded. C: Iodide uptake in a separate 3 preps following transfection with blank vector; uptake was generally lower than observed in untransfected preps - Preps 5 and 7 demonstrated a more marked reduction. D: Variation in count obtained when measuring the same sample in different wells of the gamma counter. Red lines indicate a 15% difference between the 2; results outside these lines were re-counted and if still variable then discarded.

Provided the samples met the initial criteria for uptake and TSH response, they were then assessed for their response to PBF over-expression. Some cultures did not show any change in ^{125}I uptake with PBF over-expression. In some cases this was due to lack of transfection, although in others it appeared that PBF did not affect ^{125}I uptake at all (Figure 8.12). As the aim of these experiments was to attempt to modulate the effect that PBF had on

^{125}I uptake, and because several publications have now confirmed that PBF represses iodide uptake *in vitro* and *in vivo* (Smith et al. 2009; Read et al. 2011), only those that demonstrated a significant reduction in uptake with PBF over-expression were used.

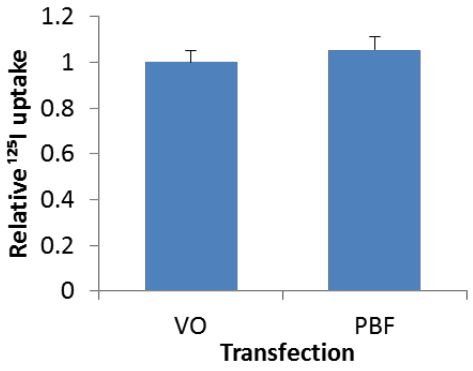

Figure 8.12 Relative ^{125}I uptake by human primary thyrocytes in a single prep. This prep did not demonstrate any change in uptake with PBF transfection and was therefore not used (1.05 ± 0.05 fold change, p = ns).

8.3.5.3 PBF and SRC inhibit ^{125}I uptake in human primary thyroid cultures

For those thyroid cultures which adhered to the criteria described in the previous section, over-expression of PBF-HA led to a 60 ± 8% reduction in iodide uptake ($p < 0.05$, $n = 4$). When untagged *PBF* was transfected, there was a similar, albeit smaller, reduction in uptake (45 ± 17% decrease compared to VO, p = ns, n = 4), although there was no significant difference between the two (Figure 8.13A). This was in keeping with previously published data from our group (Smith et al. 2009; Read et al. 2011).

To assess the relationship between SRC over-expression and ^{125}I uptake in the context of PBF expression, *PBF* and *SRC* were co-transfected into human primary thyroid cultures, with blank vector used as a control (n = 3) (Figure 8.13B). Despite the fact that when co-transfecting, half the amount of cDNA was used for each vector, there was still a 52.4 ± 16.4% reduction in ^{125}I uptake when PBF was over-expressed compared to blank vector at 48 hours post-transfection. When *SRC* alone was transfected, a similar reduction in uptake was

seen (48.6 ± 16.7%), although interestingly when *PBF* and *SRC* were co-transfected the subsequent reduction in ^{125}I uptake was no different (46.2 ± 9.8%), i.e. there was no cumulative effect of the dual transfection. Unfortunately, given the variable nature of thyroid preps, in particular the variability when transfecting in blank vector, none of these results reached statistical significance (Figure 8.13B).

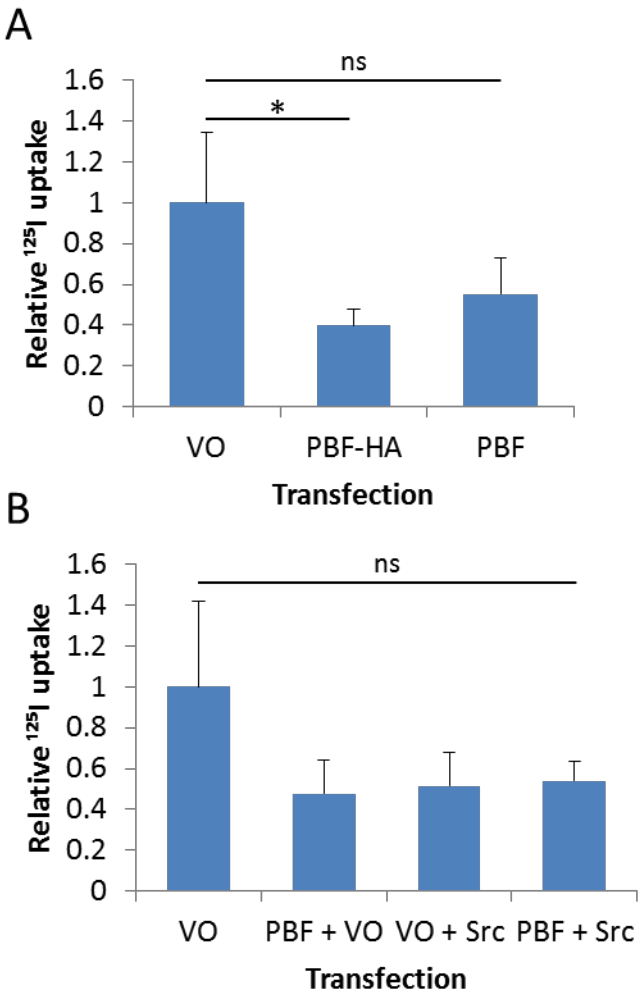

*Figure 8.13 Iodide uptake in human primary thyrocytes following transfection. A: Transfection with PBF-HA resulted in a 60 ± 8% fall in uptake ($p < 0.05$, $n = 4$); untagged PBF transfection resulted in a 45 ± 17% fall (p = ns, $n = 4$). B: Co-transfection of PBF and SRC caused uptake to fall by 46.2 ± 9.8%, which was no different to when PBF and VO (52.4 ± 16.4%) or SRC and VO (48.6 ± 16.7%) were transfected (for all compared to VO: p = ns, $n = 3$). * = $p < 0.01$, ns = not significant.*

8.3.6 Effect of TKIs on iodide uptake

8.3.6.1 Treatment for 30 minutes does not alter ^{125}I uptake

Having demonstrated that PBF and SRC both cause a reduction in ^{125}I uptake in human primary thyrocytes, and having previously shown that SRC leads to an increase in pY174, experiments were performed to determine if this reduction in uptake could be reversed by targeting the phosphorylation of PBF at Y174. The uptake in primary thyrocytes transfected with *PBF*, *SRC*, or both was measured after 30 minutes treatment with the inhibitors previously shown to have the most effect on PBF phosphorylation: SU11274, gefitinib and PP1, with PP3 acting as a negative control. As previously observed, both PBF and SRC over-expression led to a reduction in ^{125}I uptake when compared to blank vector transfection, both independently and when co-transfected, although this did not reach statistical significance (Figure 8.14). However, following treatment with the panel of TKIs for 30 minutes, there was no difference in the uptake when compared to either DMSO or PP1 treatment, thus indicating that treatment with these inhibitors and for this time period had no effect on the PBF induced repression of iodide uptake.

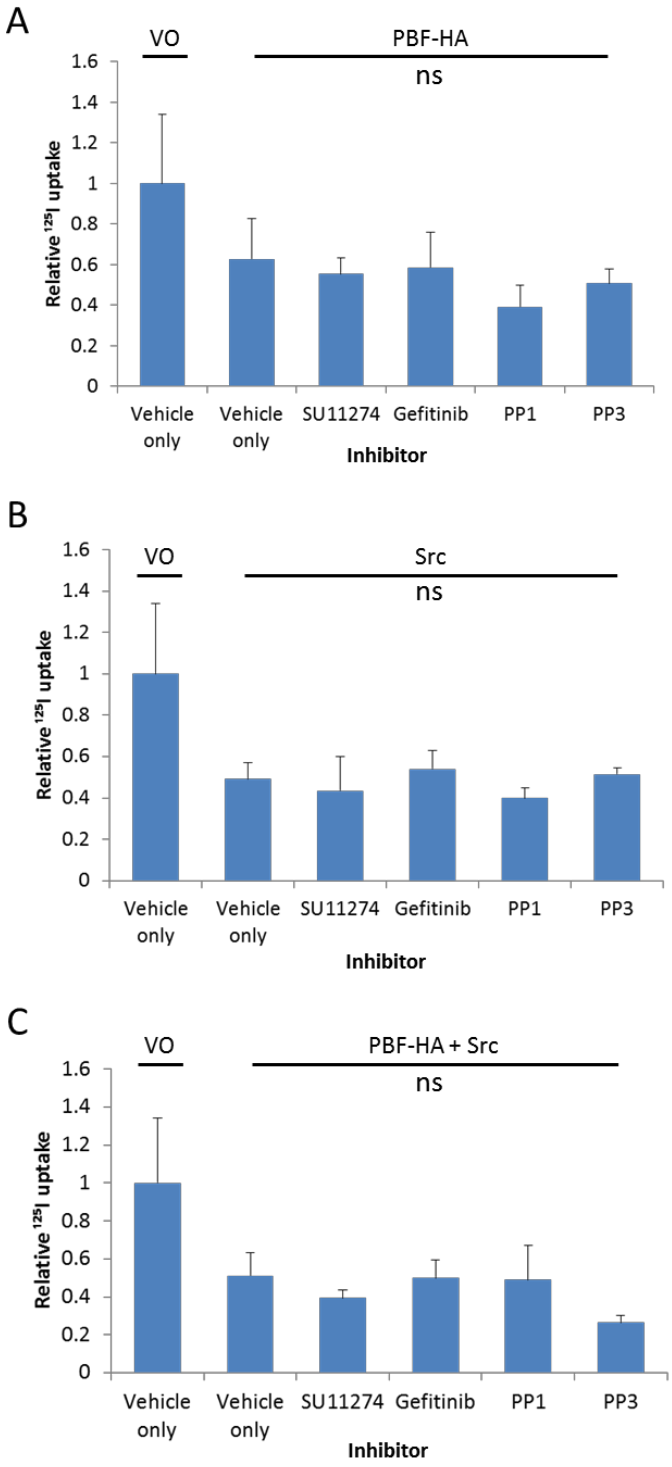

Figure 8.14 ^{125}I uptake of human primary thyrocytes after treatment with 10 µM TKI for 30 minutes. A: Cells transfected with PBF-HA showed a reduction in uptake but no reversal after treatment with TKIs. B: Cells transfected with SRC also exhibited a reduced ^{125}I uptake which was not reversed by any TKI. C: The reduced uptake observed after co-transfection with PBF-HA and SRC was not reversed by treatment with TKIs. There was no statistically significant difference between these results (n = 3).

8.3.6.2 PP1 increases ^{125}I uptake

Despite the fact that PBF phosphorylation was significantly reduced by the TKIs (Figure 8.4), there was no apparent effect on ^{125}I uptake after 30 minutes treatment (Figure 8.14). Given that we have shown PBF to internalise NIS and reduce its expression (Smith et al. 2009), it was felt likely that 30 minutes treatment may be too short a time to reverse this process and therefore facilitate an increase in uptake.

To test this theory, untransfected human primary thyrocytes were treated with PP1 for 24 hours, with control wells treated with DMSO only. The PP1-treated cells demonstrated a 65% ± 15% increase in ^{125}I uptake compared to DMSO treated cells ($p < 0.001$, $n = 3$) (Figure 8.15).

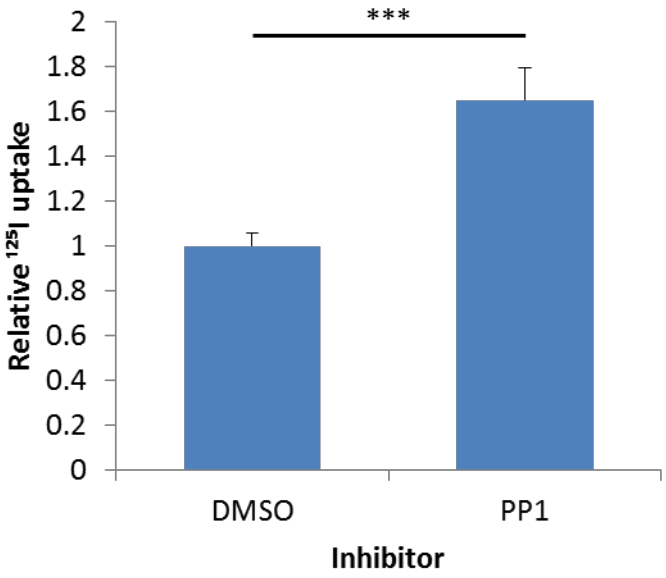

Figure 8.15 ^{125}I uptake in untransfected human primary thyrocytes treated with DMSO or PP1 for 24 hours. PP1 treatment resulted in a 65 ± 15% increase in iodide uptake ($p < 0.001$, $n = 3$).

Alongside this experiment, FRTL5 cells were transfected with *PBF* or blank vector and treated with PP1 or DMSO for 24 hours. In both the *VO* and *PBF* samples, uptake was increased by PP1 treatment (19.1 ± 5.2%, $p < 0.05$ and 31.1 ± 9.2%, $p < 0.01$ respectively, n =

3). However, no difference was observed between the *VO* and *PBF* transfected cells as a whole (Figure 8.16). When examined by Western blotting, the FRTL5 cells were shown not to have transfected efficiently, essentially leading to no genotypic difference between the two groups and hence the similarity in uptake profile (data not shown). Despite this lack of transfection, these data again pointed to PP1 as an agent that could increase ^{125}I uptake in thyroid cells.

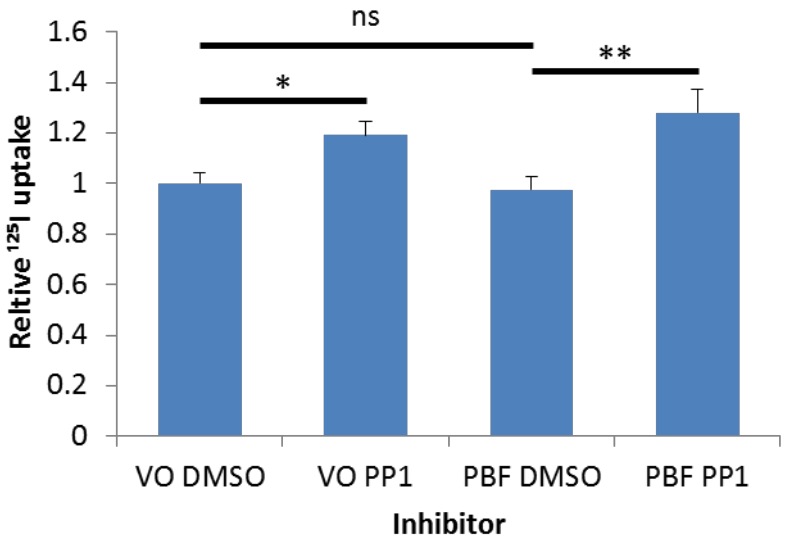

Figure 8.16 ^{125}I uptake in FRTL5 cells treated with either DMSO or PP1 for 24 hours. PP1 increased uptake in both VO and PBF *transfected cells (19.1 ± 5.2%, $p < 0.05$ and 31.1 ± 9.2%, $p < 0.01$ respectively). There was no difference in uptake between the DMSO treated VO and* PBF *transfected cells (2.4 ± 5.1%, p = ns), although subsequent analysis showed that these cells had not taken up the transfection (n = 3).*

8.3.6.3 PP1 reverses the PBF induced repression of iodide uptake

To examine the effect of PP1 in the most physiologic *in vitro* setting, primary human thyrocytes were transfected with either blank vector or *PBF-HA*, and subsequently treated for 24 hours with PP1 or DMSO (n = 5). In these cultures, treating blank vector transfected cells

with DMSO made no difference to the iodide uptake (7.4 ± 9.9% increase, p = ns). Transfection with *PBF-HA* resulted in a 47.3 ± 7.3% reduction in ^{125}I uptake compared with blank vector ($p < 0.01$). Most importantly, this effect was completely reversed by treatment with PP1, with *PBF-HA* transfected cells treated with PP1 showing no significant difference to blank vector transfected cells receiving only DMSO treatment (4.1 ± 17.7% difference from VO, p = ns) (Figure 8.17). Therefore, treatment of human primary thyrocytes with PP1 for 24 hours led to a full recovery from PBF-mediated iodide uptake repression.

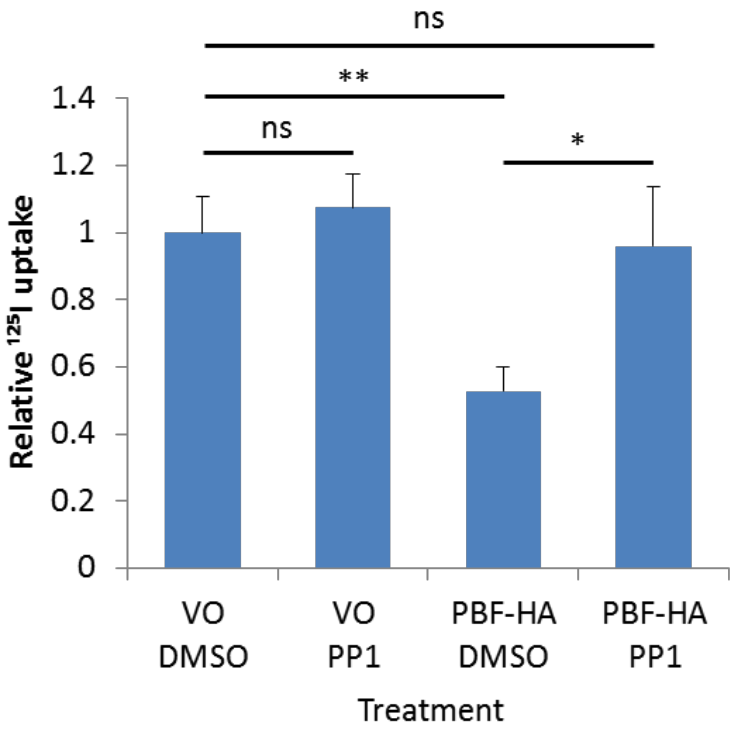

Figure 8.17 ^{125}I uptake in human primary thyrocytes transfected with either VO or PBF-HA and treated for 24 hours with DMSO or PP1. PBF-HA transfection led to a 47.3 ± 7.3% ($p < 0.01$, $n = 5$) reduction in uptake compared to VO transfection. PP1 treatment was able to reverse this, with PBF-HA transfected cells treated with PP1 having a significantly higher uptake than those treated with DMSO (82.8 ± 33.6%, $p < 0.05$, $n = 5$). This abrogation of the PBF response resulted in treated cells exhibiting no differnce in uptake compared to VO untreated cells (4.1 ± 17.7% reduction compared to VO, p = ns, n = 5).

8.4 Discussion

PBF is a phosphoprotein, with a potential site of tyrosine phosphorylation identified as Y174 (see Section 1.4.1.4.2). Phosphorylation prediction software identified SRC as a potential tyrosine kinase at this site, and the identification of SRC in the MS/MS dataset of Chapter 4 was therefore interesting, especially as targeting tyrosine kinases is a rapidly emerging field in the treatment of aggressive cancers. The previous chapter validated the interaction between PBF and SRC, with evidence of co-localisation within intra-cellular vesicles and at the plasma membrane; this chapter sought to further explore this interaction in relation to PBF phosphorylation and implications for iodide uptake in thyroid cells.

A specific antibody to pY174 PBF was already in use within our group and had recently been validated by Western blotting (data not shown); Chapter 7 validated its use for fluorescence immunocytochemistry. Using this antibody, SRC over-expression was shown to significantly increase the amount of pY174 in HeLa cells, although not to alter the sub-cellular localisation of PBF. SRC acts within a number of signalling networks and therefore it could not be determined from this experiment whether SRC was acting as the kinase itself or if it was part of a cascade that resulted in PBF phosphorylation. Given the multiple ways SRC may affect PBF, a panel of inhibitors that are currently in use in trials/clinical care was tested to determine whether any of these (which all target a kinase linked to SRC) could reduce PBF phosphorylation. The most successful of these was SU11274, a potent and selective inhibitor of MET (Wang et al. 2003). MET is the receptor for hepatocyte growth factor (HGF), activation of which leads to increased cellular proliferation, survival, motility and invasion. Inhibition of MET using small molecule inhibitors has been shown to reduce SRC phosphorylation and kinase activity in breast cancer cells (Mueller et al. 2008), and this corresponds well with the observed result. Having identified SU11274 as the most potent

inhibitor of the panel in HeLa cells, the optimum dose and treatment time was then established. Various studies using TKIs have reported results with concentrations ranging from 0.5 to 10 μM and treatment times from 15 minutes to 24 hours. In these experiments, no further reduction in pY174 was identified on Western blotting with a treatment time of longer than 30 minutes and an inhibitor concentration greater than 2 μM, and therefore these were the conditions used.

In addition to the panel of TKIs tested, the SRC family kinase specific inhibitor PP1 was also tested for its ability to inhibit pY174. PP1, first described in 1996 (Hanke et al. 1996) is a potent selective inhibitor for the SRC family, and is often used when studying both SRC individually as well as the family as a whole. As a negative control, PP3 (which has a similar structure to PP1 but does not affect SRC kinase activity) was used. If SRC was part of a kinase cascade that at some point resulted in PBF phosphorylation, then given the overlaps that exist in such pathways, inhibition of SRC would not result in a complete loss of pY174. However, if SRC was the kinase responsible for Y174 phosphorylation it would be expected that levels of pY174 would be almost undetectable. In the first experiments, PP1 was assessed with both endogenous and over-expressed SRC. When the two conditions were directly compared, SRC once again led a large increase in pY174, and this could be reversed to some extent by PP1 (although not by PP3). pY174 was not reduced to the levels observed with endogenous SRC, which was most likely due to the excess of SRC resulting from transfection. To compare the effect of PP1 with the other TKIs, in particular SU11274, and also to assess its efficacy with endogenous levels of SRC, pY174 was measured in K1, TPC1 and HeLa cells. In all 3 cell lines, PP1 had an effect on pY174 expression. In TPC1 and K1 cells, PP1 inhibited pY174 the most, although in HeLas SU11274 and gefitinib appeared the most potent. The reason for the discrepancy in the HeLa results is unclear; and may be a

consequent of constitutively altered and therefore different kinase activation in this cell line. This is a problem that is inherent to using transformed cancer cell lines, as each will have varying mutations that affect the cell's basic physiological processes.

To combat this factor, human primary thyrocytes were used. These cultures were taken from macroscopically normal thyroid tissue and were therefore as close to physiologically normal cells as possible. As *in vivo*, there were differences in the behaviour of the cultures between different patients. This, at times, resulted in wide variation and therefore reduced the significance of some results.

With normal human tissue now the subject of analysis, the panel of inhibitors was once again tested in untransfected cells. pY174 was much easier to detect in primary cells than for the cell lines, which resulted in the ability to assess the response of pY174 to the TKIs in a more physiological setting, as a precursor to the model of PBF over-expression found in thyroid cancers. In these circumstances, PP1 resulted in an almost complete abrogation of pY174, with reduction also observed with gefitinib and SU11274. A second experiment, treating cells with only PP1 or DMSO, confirmed this as a significant 81% reduction.

Having established that PBF phosphorylation was modulated by SRC, and that phosphorylation could be affected by PP1, the next process was to assess the physiological impact of both this phosphorylation and its inhibition in the context of radio-iodide uptake. Iodide uptake is a key feature of thyroid epithelial cells, and forms an essential aspect of post-surgical treatment of thyroid cancer. Previous work within our group had demonstrated that PBF represses NIS and thereby reduces iodide uptake (Smith et al. 2009), and that the murine transgenic model of thyroidal over-expression of PBF similarly demonstrates reduced iodide uptake *in vivo* (Read et al. 2011). Vitally, this phenotype could be rescued by PBF knockdown in primary cultures of murine thyrocytes (Read et al. 2011). The aim of these

experiments was thus to further elucidate a mechanism for this process, and if possible to target PBF-induced repression using a chemical inhibitor.

Firstly, it was necessary to select the most appropriate model for experimentation. Both TPC1 and K1 cell lines had a low ^{125}I uptake. Both cell lines are de-differentiated to a degree; the K1 line is known to have poor NIS expression (Petrich et al. 2002) and both have low expression of TSHR, which in turn reduces NIS expression (Meireles et al. 2007), and therefore these cell lines would not be suitable. The uptake in the non-thyroidal HeLa cell line was, as expected, poor and all three cell lines were therefore discounted from iodide uptake studies.

As a result, human primary thyroid cultures were deemed to be the most appropriate cells on which to examine iodide uptake in the context of PBF phosphorylation, despite the high degree of variation between individual cultures. A number of validatory steps had to be performed for each culture before it was included in iodide uptake assays. The cells had to be shown to respond to TSH in the physiologically normal manner, indicating that the cellular processes governing TSH response, iodide uptake and thyroid hormone synthesis were functioning correctly. In addition to these normal functions of thyrocytes, the cells had to demonstrate a reduction in ^{125}I uptake with *PBF* transfection. The purpose of these experiments was to attempt to reverse the reduction in iodide uptake demonstrated by tumours with high levels of PBF. Experiments on thyroid cancers not displaying a PBF response would still be valid, but were beyond the scope of this project.

Both PBF-HA and untagged-PBF reduced iodide uptake in human primary thyroid cultures, further validating the work previously performed in our group (Smith et al. 2009). Interestingly, SRC also had a negative effect on uptake, independent of *PBF* transfection. However, no cumulative increase was observed when *SRC* and *PBF* were co-transfected. One

explanation for this is that SRC, in isolation, increases phosphorylation of endogenous PBF and this represses NIS to similar levels as seen when PBF is over-expressed, i.e. the total amount of pY174 is similar in the 2 settings. When they are co-transfected, pY174 repression of NIS is already at a maximum and therefore increasing the amount of SRC/PBF is unable to drive the response further.

Following on from this, primary thyrocytes were therefore co-transfected with *PBF* or *SRC* for the purpose of assessing the effect of TKIs on ^{125}I uptake. Initially, the panel of inhibitors was used at the dose (2 μM) and timepoint (30 minutes) shown to have significant effect on pY174 at the protein level as determined by Western blotting. However, none of the inhibitors, including PP1, had any effect on uptake following treatment. pY174 was appropriately repressed as measured by Western blotting (data not shown) but this did not translate into a measurable effect on uptake. A hypothesis to explain this finding was that the 30 minute treatment was not sufficient to allow the relocation of NIS to the cell membrane. Indeed other studies examining iodide uptake in response to various treatments have used 24 hours as a timepoint (Kogai et al. 2006). Therefore the further experiments were carried out with a treatment time of 24 hours.

Initially, the response of untransfected cells to PP1 for 24 hours was assessed. There was a significant 65% increase in ^{125}I uptake in the treated cells compared to those treated with DMSO, indicating that this was a more suitable time-point for this assay. To measure the ability of PP1 to reverse the PBF response, endogenous as opposed to over-expressed SRC was used. This had the added advantage of allowing for a more realistic disease model; we have demonstrated that PBF expression is increased in thyroid cancer (Stratford et al. 2005), but there is no evidence that SRC is regularly over-expressed or aberrantly activated alongside PBF in differentiated thyroid cancers. As a cell line that had previously shown high levels of

iodide uptake, the rat follicular cell-derived line FRTL5 was also employed at this point. PP1 again led to a significant increase in iodide uptake but unfortunately the cells were not amenable to transfection and there was therefore no difference in uptake between blank vector and *PBF* transfected cells.

The most important model, therefore, was one consisting of multiple cultures of human thyrocytes, transfected with either blank vector or *PBF* and treated for 24 hours with PP1. Compared to the untransfected cells, there was no significant increase in uptake in the vector only transfected cells with PP1 treatment. Most important was the finding that treating *PBF-HA* transfected cells with PP1 led to a complete reversal in the repression of iodide uptake, returning levels back to those apparent with vector only transfection.

Concluding remarks

This chapter has demonstrated that SRC over-expression leads to an increase in PBF phosphorylation at Y174, an effect which could be reversed by the SRC family kinase inhibitor PP1, the latter with both endogenous and over-expressed levels of SRC. This effect was also observed in human primary thyrocytes at the protein level. These data suggested that SRC is the likely kinase responsible for phosphorylating PBF.

Functionally, PBF and SRC both (although not cumulatively) reduced iodide uptake in human primary thyrocytes. Treatment of thyrocytes over-expressing PBF, as found in human thyroid cancer, with PP1 significantly increased their avidity for iodide, thus providing a potential new adjuvant treatment modality for radioiodine-refractory thyroid cancer.

Chapter 9 Final conclusions and future directions

The work presented in this thesis described investigations into the binding partners of the product of the proto-oncogene *PBF*, in particular in relationship to thyroid disease. This was based on previous work detailing the important role PBF has in thyroid cancer; increased expression is observed in cancers compared to normal tissues, and high levels of PBF are independently associated with distant metastases, tumour multicentricity, advanced TNM stage, loco-regional recurrence and disease-specific mortality (Stratford et al. 2005; Hsueh et al. 2013). PBF is known to interact with a number of cellular proteins. It was first described as interacting with PTTG (Chien and Pei 2000), a process which was essential for the transactivation of FGF2. Subsequently PBF has been identified as a binding partner for NIS (Smith et al. 2009) and MCT8 (Smith et al. 2012); both of these interactions result in the internalisation of the transporter into the cell, from its usual location at the cell membrane. In the case of NIS, this leads to a reduction in iodide uptake into the thyroid cell. The effects of the internalisation of MCT8 are less well characterised, but it does appear to lead to an increase in intra-thyroidal thyroid hormone levels (Smith et al. 2012), and PBF-transgenic mice exhibit large, macro-follicular goitres (Read et al. 2011). Additional work carried out involving the PBF-Tg mouse model demonstrated that by knocking-down PBF in mouse primary thyroid cultures, iodide uptake could be restored to wild-type levels (Read et al. 2011).

Mapping the PBF interactome

The above research highlighted PBF as a novel and important protein in the thyroid cancer pathway, and also as a potential therapeutic target in the treatment of thyroid cancer as an adjunct to surgery. Although the peptide structure of the protein is known, and several

putative functional domains have been identified, the exact mechanism by which PBF exerts the above effects is not yet known. Tandem mass spectrometry has emerged in the past decade as a powerful and efficient tool with which to determine the range of a protein's interactions within a cell (Downard 2006), and this information may facilitate the identification of methods to alter that protein's function (Sharma et al. 2012). The technique has drawbacks, however, in relation to its sensitivity and the subsequently large datasets generated. Therefore, initial experiments focussed on optimising the protocol for MS/MS, using K1 papillary thyroid cancer cells transfected with *PBF-HA* as a model to reduce contamination and non-specific binding, and then spreadsheet algorithms to determine the most relevant proteins from the software output.

Following optimisation, PBF from K1 and TPC1 cells was immunoprecipitated, using either over-expressed (HA-tagged / untagged), or endogenous PBF. After HPLC and MS/MS, the results from the different runs were combined and analysed according to the parameters set out in Chapter 3. This generated a list of proteins with which PBF may interact and was, as expected, extensive. This list inevitably contained false positives, and by the nature of MS/MS would also have omitted some true binding partners, but would contain a substantial number of binding partners for consideration in future research. This list is presented in Appendix 1.

For the purposes of this work, however, the list was further scrutinised to produce a shortlist of 9 proteins which were thought most likely to interact with PBF, based upon on their score across several runs as well as the number of peptides identified. The proteins included were cortactin, HSP90, thyroglobulin, Src family kinases, LRRK1/2, FAK1, UACA, adenomatous polyposis coli protein, and citron kinase. All of these potential binding proteins

merit further investigation, although only three could be taken forward for further research; these were thyroglobulin, cortactin and the Src family kinases.

Investigating the interaction between PBF and thyroglobulin

The first protein to be assessed was thyroglobulin. This large protein is the precursor to the thyroid hormones T3 and T4; given the phenotype of the PBF transgenic mouse thyroid, an interaction with PBF may alter the metabolic pathway of thyroid hormones within the gland. Attempts at validation using GST pull-down assays were unsuccessful, likely due to the large protein size and multi-step process in the cell which results in its finished form. Co-immunoprecipitation was also technically challenging in the thyroid cell lines, complicated by the multiple subunits identified on Western blotting. When the experiments were repeated in primary cultures and in homogenised thyroid tissue, the MS/MS findings of an interaction were supported. Preliminary studies then highlighted areas of potential co-localisation in intra-cellular vesicles, although these were inconclusive. Future work exploring this interaction and its functional consequences will need to address the problems of protein translation and cell line phenotype; the use of primary thyroid cultures and / or tissue will be key to studying any translational and physiological effects.

Cortactin may be responsible for PBF membrane trafficking and secretion

Cortactin was the highest scoring of the short-listed proteins and has been the focus of increasing research with regards its role in cell invasion and metastases in cancer (Kirkbride et al. 2011). It interacts with the actin cytoskeleton and has an important role in membrane

trafficking, regulating both clathrin-dependent and -independent endocytosis (Weaver et al. 2001; Cao et al. 2003; Kirkbride et al. 2011). It is a commonly used marker to characterise invadopodia - cytoplasmic projections from the cell membrane from which ECM-degrading proteins are secreted (Clark and Weaver 2008).

As for thyroglobulin, independent experiments were first undertaken to validate the findings of MS/MS. Unfortunately, pull-down assays again failed to demonstrate an interaction, and therefore co-immunoprecipitation was performed. Initially, these studies were unsuccessful, due to heavy immunoglobulin / non-specific binding on Western blotting. However, when Myc-tagged cortactin was over-expressed, an interaction was supported. Western blotting did not demonstrate any change in expression of PBF with increased levels of cortactin, and in the reverse experiment cortactin levels remained constant with over-expressed PBF-HA. To begin to determine the functional significance of the interaction between cortactin and PBF, immunofluorescence was performed and demonstrated potential co-localisation within intra-cellular vesicles. This would support a hypothesis that cortactin is responsible for the membrane shuttling of PBF; whether this is an endocytic or exocytic process could not be determined from these experiments. Immunofluorescence studies with a more sensitive anti-HA antibody did indicate what appeared to be membrane protrusions from cells transfected with *PBF-HA*; however this assay was not specific enough to determine if these were invadopodia, or in fact if they represented a step in the secretory mechanism of PBF. Secretion assays were therefore undertaken to investigate if cortactin played a part in PBF export, a process previously explored by our group (Watkins 2010). Initial attempts at this were unsuccessful, and failed to detect any evidence of secreted PBF on Western blotting. However, this study involved endogenous as opposed to over-expressed PBF (as previous work had done), and it is probable, therefore, that the quantity of PBF was below the

detection limit for Western blotting. To overcome this problem, the experiment was repeated but with ELISA as the detection technique. This proved more successful, and identified secreted PBF in the media, but failed to demonstrate any change with either cortactin over-expression or knock-down. This may be due to the fact that cortactin is not involved in PBF secretion, or that it does have a role but the time frame required to demonstrate an effect was not met in these experiments. These data do, however, further increase our understanding of how PBF may be transported around the cell, and work is now on-going to further explore the role of PBF in invadopodia formation, and whether cortactin expression affects PBF secretion.

SRC phosphorylates PBF and reduces iodide uptake

The final protein to be examined was SRC. The Src-family kinases are a group of non-receptor tyrosine kinases which share a significant homology (Aleshin and Finn 2010). LYN and SRC were both identified by MS/MS, and closer inspection of the peptides identified them within a homologous part of the sequence. As phosphorylation is a modification often necessary for a protein to carry out a particular function, and as SRC had been identified by phosphorylation prediction software as a likely kinase for PBF Y174, this was pursued.

In this case, GST pull-down assay as well as forward and reverse co-immunoprecipitation supported an interaction between PBF and SRC, although SRC was over-expressed in the cells due to endogenous levels being poorly detected by Western blotting. Using fluorescence immunocytochemistry, co-localisation was observed at the cell membrane and within intra-cellular vesicles. SRC is active at the cell membrane and it is therefore at this site that phosphorylation of PBF would be most likely to occur. There did

not appear to be any alteration in the sub-cellular localisation of PBF when SRC was over-expressed compared to endogenous levels of the kinase, although further quantitative studies would be needed to formally determine this.

Having confirmed an interaction, experiments were then undertaken to assess the effect of SRC on PBF phosphorylation. An antibody specific to PBF phosphorylated at Y174 (pY174) was already in use within our group and validated for Western blotting. After confirming its suitability also for immunocytochemistry, Western blot studies demonstrated a significant increase in pY174 expression when SRC was over-expressed; supporting the hypothesis that SRC phosphorylates PBF. In HeLa cells, the effect of a panel of TKIs on this finding was tested, with SU11274 and gefitinib significantly reducing this phosphorylation. SU11274 was then shown to have a dose- and time-dependent effect on PBF phosphorylation, as demonstrated by both Western blotting and immunofluorescence. An explanation for the reduction in pY174 observed with both gefitinib and SU11274 (and to a non-significant degree with the other TKIs), was the cross over in signalling pathways that exists within cells and which may be aberrantly activated in transformed cell lines. To further investigate the specificity of SRC as the kinase responsible for phosphorylating PBF, cells were treated with a specific SRC inhibitor, PP1, and its inactive counterpart, PP3. PP1 treatment resulted in a significant reduction in pY174 in cells over-expressing SRC and PBF-HA, an effect replicated in untransfected cells across all 3 cell lines used. Finally, human primary cell cultures were assessed for a response to the TKI panel; a significant reduction in pY174 was observed with PP1 treatment. Taken together, these data provide strong evidence that PBF is phosphorylated by SRC, and that this process can be inhibited by treatment with a specific SRC inhibitor.

To measure the effect of this functionally, iodide uptake assays were then performed. The efficacy of the various cell lines, including with transfection of NIS, was examined, and found to be too low to allow reproducible, reliable data. Experiments were therefore carried out on human primary thyrocytes; these also exhibited significant variation in both uptake and response to TSH, and therefore each prep underwent viability testing prior to uptake studies. PBF and SRC both reduced iodide uptake in primary thyrocytes, although this effect was not cumulative for co-transfection, perhaps an indication that NIS repression is already maximal with either of the genes over-expressed, and therefore no addition reduction can be obtained. To determine if these findings had a clinical relevance to a potential therapeutic strategy, primary thyrocytes were transfected as above and treated with the TKIs. The only inhibitor that caused a significant increase in iodide uptake was PP1. In those cells that underwent *PBF-HA* transfection and subsequent treatment with PP1, iodide uptake was identical to those that were transfected with blank vector. The potential translational implications of this are important: by inhibiting SRC in thyroid tissue over-expressing PBF, NIS repression may be overcome and iodide uptake restored, potentially increasing the tissue sensitivity to radioiodine.

A novel therapeutic strategy for thyroid cancer: Final remarks and future directions

This thesis has generated data that improve the current level of understanding regarding the role of PBF in normal thyroid physiology and in thyroid cancer. The interaction with thyroglobulin (although as yet poorly characterised), and how this may relate to the transgenic mouse phenotype, is the focus of further study within our group. Perhaps the most exciting aspects of this research are the potential roles of cortactin in PBF transport and secretion, and

the ability of SRC inhibition to increase iodide uptake in thyroid tissue over-expressing PBF. Although further studies are required, a working hypothesis can be generated against which to test future experiments (Figure 9.1). These will seek to further define the data described above, using *in vitro* techniques such as cell surface biotinylation, invadopodia assays and PBF mutant analysis to further probe the PBF / cortactin relationship, as well as detailed inhibitor studies to determine the efficacy of SRC inhibitors as therapeutic modalities and potentially progressing to clinical trials. SRC inhibitors are the subject of intensive clinical research, and recent studies have highlighted the potential for SRC inhibitors in subsets of thyroid cancer treatment (Chan et al. 2012). This would be the final translational step and one which has personalised medicine at its base – by studying a patient's thyroid tumour following surgery, if PBF is found to be over-expressed then adjuvant SRC inhibitor treatment could be delivered with radioiodine remnant ablation, thus increasing the efficacy of the therapy and reducing tumour recurrence and subsequent survival.

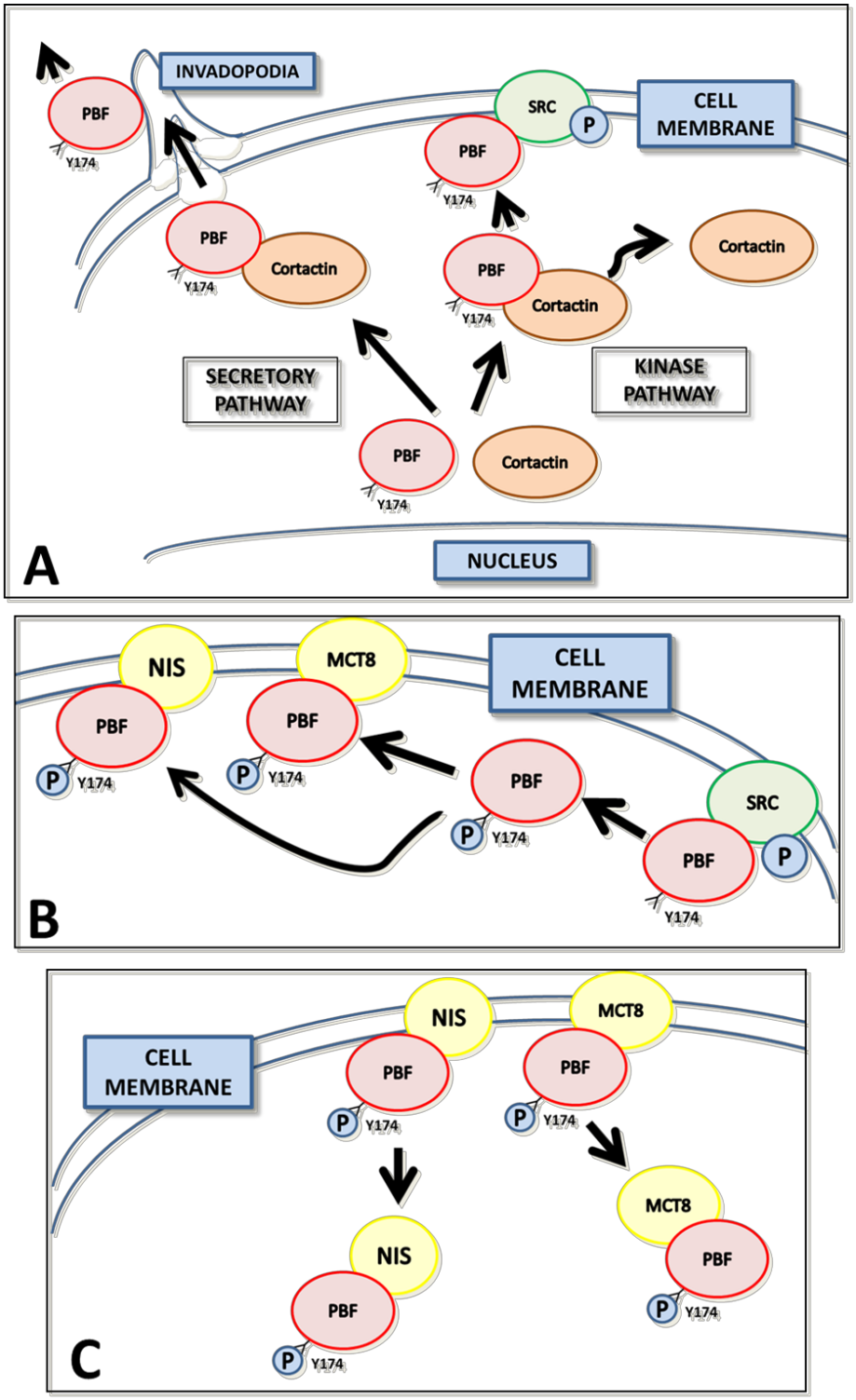

Figure 9.1 Hypothesis regarding the secretion and phosphorylation of PBF. A – PBF interacts with cortactin and is transported to cell membrane invadopodia, where it is secreted into the ECM (Secretory pathway). Alternatively, PBF is transported to the cell membrane where it interacts with Src (Kinase pathway). B – PBF is phosphorylated by Src at Y174 and, now activated, binds NIS or MCT8 at the cell membrane. C – PBF now internalises NIS and MCT8, thereby repressing their function.

Chapter 10 References

.
Aiello, A., G. Pandini, et al. (2006). "Peroxisomal proliferator-activated receptor-gamma agonists induce partial reversion of epithelial-mesenchymal transition in anaplastic thyroid cancer cells." Endocrinology **147**(9): 4463-4475.

Ain, K. B. (1998). "Anaplastic thyroid carcinoma: behavior, biology, and therapeutic approaches." Thyroid : official journal of the American Thyroid Association **8**(8): 715-726.

Aleshin, A. and R. S. Finn (2010). "SRC: a century of science brought to the clinic." Neoplasia **12**(8): 599-607.

Alexander, E. K. (2008). "Approach to the patient with a cytologically indeterminate thyroid nodule." The Journal of clinical endocrinology and metabolism **93**(11): 4175-4182.

Alvarez, R. H., H. M. Kantarjian, et al. (2006). "The role of Src in solid and hematologic malignancies: development of new-generation Src inhibitors." Cancer **107**(8): 1918-1929.

Ambesi-Impiombato, F. S. (1986). Living, fast-growing thyroid cell strain, FRTL-5. U. S. P. Office. USA, Interthyr Research Foundation, Inc.**:** 25.

Anbalagan, M., K. Moroz, et al. (2012). "Subcellular localization of total and activated Src kinase in African American and Caucasian breast cancer." PLoS One **7**(3): e33017.

Antico-Arciuch, V. G., M. Dima, et al. (2010). "Cross-talk between PI3K and estrogen in the mouse thyroid predisposes to the development of follicular carcinomas with a higher incidence in females." Oncogene **29**(42): 5678-5686.

Artym, V. V., Y. Zhang, et al. (2006). "Dynamic interactions of cortactin and membrane type 1 matrix metalloproteinase at invadopodia: defining the stages of invadopodia formation and function." Cancer research **66**(6): 3034-3043.

Barrott, J. J. and T. A. Haystead (2013). "Hsp90, an unlikely ally in the war on cancer." The FEBS journal **280**(6): 1381-1396.

Beimfohr, C., S. Klugbauer, et al. (1999). "NTRK1 re-arrangement in papillary thyroid carcinomas of children after the Chernobyl reactor accident." International journal of cancer. Journal international du cancer **80**(6): 842-847.

Bhaijee, F. and Y. E. Nikiforov (2011). "Molecular analysis of thyroid tumors." Endocrine pathology **22**(3): 126-133.

Bisson, N., D. A. James, et al. (2011). "Selected reaction monitoring mass spectrometry reveals the dynamics of signaling through the GRB2 adaptor." Nature biotechnology **29**(7): 653-658.

Bjorge, J. D., A. Jakymiw, et al. (2000). "Selected glimpses into the activation and function of Src kinase." Oncogene **19**(49): 5620-5635.

Blagosklonny, M. V., P. Giannakakou, et al. (1998). "Effects of p53-expressing adenovirus on the chemosensitivity and differentiation of anaplastic thyroid cancer cells." The Journal of clinical endocrinology and metabolism **83**(7): 2516-2522.

Boelaert, K., C. J. McCabe, et al. (2003). "Pituitary tumor transforming gene and fibroblast growth factor-2 expression: potential prognostic indicators in differentiated thyroid cancer." J Clin Endocrinol Metab **88**(5): 2341-2347.

Boelaert, K., V. E. Smith, et al. (2007). "PTTG and PBF repress the human sodium iodide symporter." Oncogene **26**(30): 4344-4356.

Bork, P., T. Doerks, et al. (1999). "Domains in plexins: links to integrins and transcription factors." Trends in biochemical sciences **24**(7): 261-263.

Bos, J. L. (1989). "ras oncogenes in human cancer: a review." Cancer research **49**(17): 4682-4689.

Bounacer, A., M. Schlumberger, et al. (2000). "Search for NTRK1 proto-oncogene rearrangements in human thyroid tumours originated after therapeutic radiation." British journal of cancer **82**(2): 308-314.

British Association of Endocrine and Thyroid Surgeons (2009). "Third National Audit Report."

British Thyroid Association and Royal College of Physicians (2007). Guidelines for the management of thyroid cancer (Perros P, ed). Report of the Thyroid Cancer Guidelines Update Group. London.

Bryce, N. S., E. S. Clark, et al. (2005). "Cortactin promotes cell motility by enhancing lamellipodial persistence." Current biology : CB **15**(14): 1276-1285.

Brzezianska, E., M. Karbownik, et al. (2006). "Molecular analysis of the RET and NTRK1 gene rearrangements in papillary thyroid carcinoma in the Polish population." Mutation research **599**(1-2): 26-35.

Buchdunger, E., J. Zimmermann, et al. (1996). "Inhibition of the Abl protein-tyrosine kinase in vitro and in vivo by a 2-phenylaminopyrimidine derivative." Cancer research **56**(1): 100-104.

Buday, L. and J. Downward (2007). "Roles of cortactin in tumor pathogenesis." Biochimica et biophysica acta **1775**(2): 263-273.

Burikhanov, R., T. Shrestha-Bhattarai, et al. (2013). "Novel mechanism of apoptosis resistance in cancer mediated by extracellular PAR-4." Cancer research **73**(2): 1011-1019.

Cancer Research UK. (2013). "UK Cancer Incidence (2010) by Country Summary." 2013, from http://info.cancerresearchuk.org/cancerstats/types/thyroid/incidence/index.htm.

Cantara, S., M. Capezzone, et al. (2010). "Impact of proto-oncogene mutation detection in cytological specimens from thyroid nodules improves the diagnostic accuracy of cytology." The Journal of clinical endocrinology and metabolism **95**(3): 1365-1369.

Cao, H., J. D. Orth, et al. (2003). "Cortactin is a component of clathrin-coated pits and participates in receptor-mediated endocytosis." Molecular and cellular biology **23**(6): 2162-2170.

Carta, C., S. Moretti, et al. (2006). "Genotyping of an Italian papillary thyroid carcinoma cohort revealed high prevalence of BRAF mutations, absence of RAS mutations and allowed the detection of a new mutation of BRAF oncoprotein (BRAF(V599lns))." Clinical Endocrinology **64**(1): 105-109.

Ceolin, L., D. R. Siqueira, et al. (2012). "Molecular Basis of Medullary Thyroid Carcinoma: The Role of RET Polymorphisms." International journal of molecular sciences **13**(1): 221-239.

Chan, C. M., X. Jing, et al. (2012). "Targeted inhibition of Src kinase with dasatinib blocks thyroid cancer growth and metastasis." Clinical cancer research : an official journal of the American Association for Cancer Research **18**(13): 3580-3591.

Chen, A. Y., A. Jemal, et al. (2009). "Increasing incidence of differentiated thyroid cancer in the United States, 1988-2005." Cancer **115**(16): 3801-3807.

Chien, W. and L. Pei (2000). "A novel binding factor facilitates nuclear translocation and transcriptional activation function of the pituitary tumor-transforming gene product." J Biol Chem **275**(25): 19422-19427.

Cho, K. R. and M. Shih Ie (2009). "Ovarian cancer." Annual review of pathology **4**: 287-313.

Cho, N. L., C. I. Lin, et al. (2012). "Global tyrosine kinome profiling of human thyroid tumors identifies Src as a promising target for invasive cancers." Biochemical and biophysical research communications **421**(3): 508-513.

Chu, E. C. and A. S. Tarnawski (2004). "PTEN regulatory functions in tumor suppression and cell biology." Medical science monitor : international medical journal of experimental and clinical research **10**(10): RA235-241.

Chung, C., J. Liu, et al. (2011). "Computational Refinement of Post-translational Modifications Predicted from Tandem Mass Spectrometry." Bioinformatics.

Ciampi, R. and Y. E. Nikiforov (2007). "RET/PTC rearrangements and BRAF mutations in thyroid tumorigenesis." Endocrinology **148**(3): 936-941.

Ciardiello, F. (2000). "Epidermal growth factor receptor tyrosine kinase inhibitors as anticancer agents." Drugs **60 Suppl 1**: 25-32; discussion 41-22.

Civiero, L. and L. Bubacco (2012). "Human leucine-rich repeat kinase 1 and 2: intersecting or unrelated functions?" Biochemical Society transactions **40**(5): 1095-1101.

Clark, E. S. and A. M. Weaver (2008). "A new role for cortactin in invadopodia: regulation of protease secretion." European journal of cell biology **87**(8-9): 581-590.

Clark, E. S., A. S. Whigham, et al. (2007). "Cortactin is an essential regulator of matrix metalloproteinase secretion and extracellular matrix degradation in invadopodia." Cancer research **67**(9): 4227-4235.

Cocks, H. C., S. Thompson, et al. (2003). "Role and regulation of the fibroblast growth factor axis in human thyroid follicular cells." American journal of physiology. Endocrinology and metabolism **285**(3): E460-469.

Cooper, D. S., G. M. Doherty, et al. (2009). "Revised American Thyroid Association management guidelines for patients with thyroid nodules and differentiated thyroid cancer." Thyroid **19**(11): 1167-1214.

Davies, H., G. R. Bignell, et al. (2002). "Mutations of the BRAF gene in human cancer." Nature **417**(6892): 949-954.

de Groot, J. W., T. P. Links, et al. (2006). "RET as a diagnostic and therapeutic target in sporadic and hereditary endocrine tumors." Endocr Rev **27**(5): 535-560.

den Hartog, M. T., C. C. Sijmons, et al. (1995). "Importance of the content and localization of tyrosine residues for thyroxine formation within the N-terminal part of human thyroglobulin." European journal of endocrinology / European Federation of Endocrine Societies **132**(5): 611-617.

Di Cosmo, C., X. H. Liao, et al. (2010). "Mice deficient in MCT8 reveal a mechanism regulating thyroid hormone secretion." The Journal of clinical investigation **120**(9): 3377-3388.

Di Cunto, F., S. Imarisio, et al. (2000). "Defective neurogenesis in citron kinase knockout mice by altered cytokinesis and massive apoptosis." Neuron **28**(1): 115-127.

Di Marco, E., M. Mathor, et al. (1993). "Nerve growth factor binds to normal human keratinocytes through high and low affinity receptors and stimulates their growth by a novel autocrine loop." The Journal of biological chemistry **268**(30): 22838-22846.

Di Michele, M., A. Della Corte, et al. (2009). "A proteomic approach to paclitaxel chemoresistance in ovarian cancer cell lines." Biochim Biophys Acta **1794**(2): 225-236.

Dobson, M. E., E. Diallo-Krou, et al. (2011). "Pioglitazone induces a proadipogenic antitumor response in mice with PAX8-PPARgamma fusion protein thyroid carcinoma." Endocrinology **152**(11): 4455-4465.

Dohan, O., A. De la Vieja, et al. (2003). "The sodium/iodide Symporter (NIS): characterization, regulation, and medical significance." Endocrine reviews **24**(1): 48-77.

Donghi, R., A. Longoni, et al. (1993). "Gene p53 mutations are restricted to poorly differentiated and undifferentiated carcinomas of the thyroid gland." The Journal of clinical investigation **91**(4): 1753-1760.

Downard, K. M. (2006). "Ions of the interactome: the role of MS in the study of protein interactions in proteomics and structural biology." Proteomics **6**(20): 5374-5384.

Duffy, B. J., Jr. and P. J. Fitzgerald (1950). "Thyroid cancer in childhood and adolescence; a report on 28 cases." Cancer **3**(6): 1018-1032.

Dunn, J. T. and A. D. Dunn (1999). "The importance of thyroglobulin structure for thyroid hormone biosynthesis." Biochimie **81**(5): 505-509.

Dwight, T., S. R. Thoppe, et al. (2003). "Involvement of the PAX8/peroxisome proliferator-activated receptor gamma rearrangement in follicular thyroid tumors." The Journal of clinical endocrinology and metabolism **88**(9): 4440-4445.

Eggo, M. C., W. J. King, et al. (1996). "Functional human thyroid cells and their insulin-like growth factor-binding proteins: regulation by thyrotropin, cyclic 3',5' adenosine monophosphate, and growth factors." The Journal of clinical endocrinology and metabolism **81**(8): 3056-3062.

Elliott, M. H., D. S. Smith, et al. (2009). "Current trends in quantitative proteomics." Journal of mass spectrometry : JMS **44**(12): 1637-1660.

Fagin, J. A., K. Matsuo, et al. (1993). "High prevalence of mutations of the p53 gene in poorly differentiated human thyroid carcinomas." The Journal of clinical investigation **91**(1): 179-184.

Fallah, M., E. Pukkala, et al. (2013). "Risk of thyroid cancer in first-degree relatives of patients with non-medullary thyroid cancer by histology type and age at diagnosis: a joint study from five Nordic countries." Journal of medical genetics.

Fan, Y., L. Shi, et al. (2009). "Discovery and identification of potential biomarkers of papillary thyroid carcinoma." Molecular cancer **8**: 79.

Fayadat, L., P. Niccoli-Sire, et al. (1998). "Human thyroperoxidase is largely retained and rapidly degraded in the endoplasmic reticulum. Its N-glycans are required for folding and intracellular trafficking." Endocrinology **139**(10): 4277-4285.

Fedele, M., D. Palmieri, et al. (2009). "Impairment of the p27kip1 function enhances thyroid carcinogenesis in TRK-T1 transgenic mice." Endocrine-related cancer **16**(2): 483-490.

Fero, M. L., M. Rivkin, et al. (1996). "A syndrome of multiorgan hyperplasia with features of gigantism, tumorigenesis, and female sterility in p27(Kip1)-deficient mice." Cell **85**(5): 733-744.

Ferraz, C., C. Rehfeld, et al. (2012). "Detection of PAX8/PPARG and RET/PTC rearrangements is feasible in routine air-dried fine needle aspiration smears." Thyroid : official journal of the American Thyroid Association **22**(10): 1025-1030.

Franco, A. T., R. Malaguarnera, et al. (2011). "Thyrotrophin receptor signaling dependence of Braf-induced thyroid tumor initiation in mice." Proceedings of the National Academy of Sciences of the United States of America **108**(4): 1615-1620.

Frasca, F., V. Vella, et al. (2013). "Thyroid Cancer Cell Resistance to Gefitinib Depends on the Constitutive Oncogenic Activation of the Erk Pathway." The Journal of clinical endocrinology and metabolism.

French, C. A., E. K. Alexander, et al. (2003). "Genetic and biological subgroups of low-stage follicular thyroid cancer." The American journal of pathology **162**(4): 1053-1060.

Furukawa, K., D. Preston, et al. (2013). "Long-term trend of thyroid cancer risk among Japanese atomic-bomb survivors: 60 years after exposure." International journal of cancer. Journal international du cancer **132**(5): 1222-1226.

Ganong, W. (1997). The thyroid gland. Review of medical physiology
Stamford, Appleton & Lange**:** 296-311.
Geiger, T., J. Cox, et al. (2010). "Super-SILAC mix for quantitative proteomics of human tumor tissue." Nature methods **7**(5): 383-385.
Gerber, S. A., J. Rush, et al. (2003). "Absolute quantification of proteins and phosphoproteins from cell lysates by tandem MS." Proceedings of the National Academy of Sciences of the United States of America **100**(12): 6940-6945.
Giardiello, F. M., G. J. Offerhaus, et al. (1993). "Increased risk of thyroid and pancreatic carcinoma in familial adenomatous polyposis." Gut **34**(10): 1394-1396.
Gorla, L., P. Mondellini, et al. (2009). "Proteomics study of medullary thyroid carcinomas expressing RET germ-line mutations: identification of new signaling elements." Molecular carcinogenesis **48**(3): 220-231.
Greco, A., C. Miranda, et al. (2010). "Rearrangements of NTRK1 gene in papillary thyroid carcinoma." Molecular and cellular endocrinology **321**(1): 44-49.
Gustafsson, J. O., M. K. Oehler, et al. (2010). "Citric acid antigen retrieval (CAAR) for tryptic peptide imaging directly on archived formalin-fixed paraffin-embedded tissue." J Proteome Res **9**(9): 4315-4328.
Half, E., D. Bercovich, et al. (2009). "Familial adenomatous polyposis." Orphanet J Rare Dis **4**: 22.
Hanke, J. H., J. P. Gardner, et al. (1996). "Discovery of a novel, potent, and Src family-selective tyrosine kinase inhibitor. Study of Lck- and FynT-dependent T cell activation." The Journal of biological chemistry **271**(2): 695-701.
Hibi, Y., T. Nagaya, et al. (2004). "Is thyroid follicular cancer in Japanese caused by a specific t(2; 3)(q13; p25) translocation generating Pax8-PPAR gamma fusion mRNA?" Endocrine journal **51**(3): 361-366.
Holm, L. E., H. Blomgren, et al. (1985). "Cancer risks in patients with chronic lymphocytic thyroiditis." The New England journal of medicine **312**(10): 601-604.
Hou, P., M. Ji, et al. (2008). "Association of PTEN gene methylation with genetic alterations in the phosphatidylinositol 3-kinase/AKT signaling pathway in thyroid tumors." Cancer **113**(9): 2440-2447.
Howlader N, N. A., Krapcho M, Neyman N, Aminou R, Altekruse SF, Kosary CL, Ruhl J, Tatalovich Z, Cho H, Mariotto A, Eisner MP, Lewis DR, Chen HS, Feuer EJ, Cronin KA (2012). SEER Cancer Statistics Review, 1975-2009 (Vintage 2009 Populations). Bethesda, MD, National Cancer Institute.
Hsueh, C., J. D. Lin, et al. (2013). "Prognostic significance of pituitary tumour-transforming gene-binding factor (PBF) expression in papillary thyroid carcinoma." Clinical Endocrinology **78**(2): 303-309.
Irby, R. B., W. Mao, et al. (1999). "Activating SRC mutation in a subset of advanced human colon cancers." Nature genetics **21**(2): 187-190.
Irby, R. B. and T. J. Yeatman (2000). "Role of Src expression and activation in human cancer." Oncogene **19**(49): 5636-5642.
Jin, J., R. Phitayakorn, et al. (2013). "Advances in management of thyroid cancer." Current problems in surgery **50**(6): 241-289.
Jinawath, N., C. Vasoontara, et al. (2010). "Oncoproteomic analysis reveals co-upregulation of RELA and STAT5 in carboplatin resistant ovarian carcinoma." PLoS One **5**(6): e11198.
Kaplan, D. R., B. L. Hempstead, et al. (1991). "The trk proto-oncogene product: a signal transducing receptor for nerve growth factor." Science **252**(5005): 554-558.

Kaplan, E. L., D. Mhoon, et al. (2009). "Radiation-induced thyroid cancer: the Chicago experience." Surgery **146**(6): 979-985.
Kashat, L., A. K. So, et al. (2010). "Secretome-based identification and characterization of potential biomarkers in thyroid cancer." J Proteome Res **9**(11): 5757-5769.
Kim, D., H. Pemberton, et al. (2005). "Pituitary tumour transforming gene (PTTG) induces genetic instability in thyroid cells." Oncogene **24**(30): 4861-4866.
Kim, T. Y., W. B. Kim, et al. (2006). "The BRAF mutation is useful for prediction of clinical recurrence in low-risk patients with conventional papillary thyroid carcinoma." Clinical Endocrinology **65**(3): 364-368.
Kirkbride, K. C., B. H. Sung, et al. (2011). "Cortactin: a multifunctional regulator of cellular invasiveness." Cell adhesion & migration **5**(2): 187-198.
Knauf, J. A., X. Ma, et al. (2005). "Targeted expression of BRAFV600E in thyroid cells of transgenic mice results in papillary thyroid cancers that undergo dedifferentiation." Cancer research **65**(10): 4238-4245.
Kogai, T., K. Taki, et al. (2006). "Enhancement of sodium/iodide symporter expression in thyroid and breast cancer." Endocr Relat Cancer **13**(3): 797-826.
Korr, D., L. Toschi, et al. (2006). "LRRK1 protein kinase activity is stimulated upon binding of GTP to its Roc domain." Cellular signalling **18**(6): 910-920.
Kozlov, G., A. Perreault, et al. (2004). "Insights into function of PSI domains from structure of the Met receptor PSI domain." Biochemical and biophysical research communications **321**(1): 234-240.
Krol, J., I. Loedige, et al. (2010). "The widespread regulation of microRNA biogenesis, function and decay." Nature reviews. Genetics **11**(9): 597-610.
Kroll, T. G., P. Sarraf, et al. (2000). "PAX8-PPARgamma1 fusion oncogene in human thyroid carcinoma [corrected]." Science **289**(5483): 1357-1360.
la Cour, T., L. Kiemer, et al. (2004). "Analysis and prediction of leucine-rich nuclear export signals." Protein engineering, design & selection : PEDS **17**(6): 527-536.
Lee, K. J., Y. J. Cho, et al. (2013). "How many contralateral papillary thyroid carcinomas can be missed?" World journal of surgery **37**(4): 780-785.
Leeman-Neill, R. J., A. V. Brenner, et al. (2013). "RET/PTC and PAX8/PPARgamma chromosomal rearrangements in post-Chernobyl thyroid cancer and their association with iodine-131 radiation dose and other characteristics." Cancer.
Leenhardt, L., M. O. Bernier, et al. (2004). "Advances in diagnostic practices affect thyroid cancer incidence in France." European journal of endocrinology / European Federation of Endocrine Societies **150**(2): 133-139.
Li, C., Y. Wang, et al. (2013). "Hepatitis B virus mRNA-mediated miR-122 inhibition upregulates PTTG1-binding protein, which promotes hepatocellular carcinoma tumor growth and cell invasion." Journal of virology **87**(4): 2193-2205.
Lim, II, T. Hochman, et al. (2012). "Disparities in the initial presentation of differentiated thyroid cancer in a large public hospital and adjoining university teaching hospital." Thyroid : official journal of the American Thyroid Association **22**(3): 269-274.
Liu, Y., A. Bishop, et al. (1999). "Structural basis for selective inhibition of Src family kinases by PP1." Chemistry & biology **6**(9): 671-678.
Liu, Z., J. Falola, et al. (2004). "Antiproliferative effects of Src inhibition on medullary thyroid cancer." The Journal of clinical endocrinology and metabolism **89**(7): 3503-3509.
Lu, Y. W. and E. K. Tan (2008). "Molecular biology changes associated with LRRK2 mutations in Parkinson's disease." Journal of neuroscience research **86**(9): 1895-1901.

Madaule, P., T. Furuyashiki, et al. (2000). "Citron, a Rho target that affects contractility during cytokinesis." Microscopy research and technique **49**(2): 123-126.

Malthiery, Y. and S. Lissitzky (1987). "Primary structure of human thyroglobulin deduced from the sequence of its 8448-base complementary DNA." European journal of biochemistry / FEBS **165**(3): 491-498.

Manne, U., R. G. Srivastava, et al. (2005). "Recent advances in biomarkers for cancer diagnosis and treatment." Drug discovery today **10**(14): 965-976.

Martucciello, G., M. Lerone, et al. (2012). "Multiple endocrine neoplasias type 2B and RET proto-oncogene." Italian journal of pediatrics **38**: 9.

Mazzaferri, E. L. and S. M. Jhiang (1994). "Long-term impact of initial surgical and medical therapy on papillary and follicular thyroid cancer." Am J Med **97**(5): 418-428.

McCabe, C. J., K. Boelaert, et al. (2002). "Vascular endothelial growth factor, its receptor KDR/Flk-1, and pituitary tumor transforming gene in pituitary tumors." J Clin Endocrinol Metab **87**(9): 4238-4244.

McCabe, C. J., J. S. Khaira, et al. (2003). "Expression of pituitary tumour transforming gene (PTTG) and fibroblast growth factor-2 (FGF-2) in human pituitary adenomas: relationships to clinical tumour behaviour." Clinical Endocrinology **58**(2): 141-150.

McGlashan, J. (2008). The thyroid gland: anatomy and physiology. Scott-Brown's Otolaryngology, Head and Neck Surgery. M. Gleeson. London, Hodder Eduction. **1:** 314-326.

McLeod, D. S., A. M. Sawka, et al. (2013). "Controversies in primary treatment of low-risk papillary thyroid cancer." Lancet **381**(9871): 1046-1057.

Meireles, A. M., A. Preto, et al. (2007). "Molecular and genotypic characterization of human thyroid follicular cell carcinoma-derived cell lines." Thyroid : official journal of the American Thyroid Association **17**(8): 707-715.

Mihai, R., A. J. Parker, et al. (2009). "One in four patients with follicular thyroid cytology (THY3) has a thyroid carcinoma." Thyroid : official journal of the American Thyroid Association **19**(1): 33-37.

Miller, E. H. and M. H. Soley (1948). "Treatment of Graves' disease with radioiodine." The American journal of medicine **4**(4): 623.

Miot, F., C. Dupuy, et al. (2012). Thyroid hormone synthesis and secretion. Thyroid Disease Manager. L. E. De groot.

Mohammadi, M., S. Froum, et al. (1998). "Crystal structure of an angiogenesis inhibitor bound to the FGF receptor tyrosine kinase domain." The EMBO journal **17**(20): 5896-5904.

Moretti, F., A. Farsetti, et al. (1997). "p53 re-expression inhibits proliferation and restores differentiation of human thyroid anaplastic carcinoma cells." Oncogene **14**(6): 729-740.

Moulick, K., J. H. Ahn, et al. (2011). "Affinity-based proteomics reveal cancer-specific networks coordinated by Hsp90." Nature chemical biology **7**(11): 818-826.

Mu, D., R. Huang, et al. (2012). "Radioiodine therapy of thyroid carcinoma following Pax-8 gene transfer." Gene therapy **19**(4): 435-442.

Mueller, K. L., L. A. Hunter, et al. (2008). "Met and c-Src cooperate to compensate for loss of epidermal growth factor receptor kinase activity in breast cancer cells." Cancer research **68**(9): 3314-3322.

Namba, H., M. Nakashima, et al. (2003). "Clinical implication of hot spot BRAF mutation, V599E, in papillary thyroid cancers." The Journal of clinical endocrinology and metabolism **88**(9): 4393-4397.

Neu, M., D. Fischer, et al. (2005). "Recent advances in rational gene transfer vector design based on poly(ethylene imine) and its derivatives." J Gene Med **7**(8): 992-1009.

Ngeow, J., J. Mester, et al. (2011). "Incidence and clinical characteristics of thyroid cancer in prospective series of individuals with Cowden and Cowden-like syndrome characterized by germline PTEN, SDH, or KLLN alterations." The Journal of clinical endocrinology and metabolism **96**(12): E2063-2071.

Nikiforov, Y. E. (2002). "RET/PTC rearrangement in thyroid tumors." Endocrine pathology **13**(1): 3-16.

Nikiforov, Y. E. (2004). "Genetic alterations involved in the transition from well-differentiated to poorly differentiated and anaplastic thyroid carcinomas." Endocrine pathology **15**(4): 319-327.

Nikiforova, M. N., P. W. Biddinger, et al. (2002). "PAX8-PPARgamma rearrangement in thyroid tumors: RT-PCR and immunohistochemical analyses." The American journal of surgical pathology **26**(8): 1016-1023.

Nikiforova, M. N., R. A. Lynch, et al. (2003). "RAS point mutations and PAX8-PPAR gamma rearrangement in thyroid tumors: evidence for distinct molecular pathways in thyroid follicular carcinoma." The Journal of clinical endocrinology and metabolism **88**(5): 2318-2326.

Ohkura, T., S. Taniguchi, et al. (2004). "Detection of the novel autoantibody (anti-UACA antibody) in patients with Graves' disease." Biochem Biophys Res Commun **321**(2): 432-440.

Ong, S. E., B. Blagoev, et al. (2002). "Stable isotope labeling by amino acids in cell culture, SILAC, as a simple and accurate approach to expression proteomics." Molecular & cellular proteomics : MCP **1**(5): 376-386.

Paulo, J. A., L. S. Lee, et al. (2011). "Proteomic Analysis of Formalin-Fixed Paraffin-Embedded Pancreatic Tissue Using Liquid Chromatography Tandem Mass Spectrometry." Pancreas.

Pauzar, B., I. Karner, et al. (2012). "PAX8-PPARgamma oncogene in follicular thyroid tumors: RT-PCR and immunohistochemical analyses." Collegium antropologicum **36 Suppl 2**: 79-82.

Pearl, L. H. and C. Prodromou (2006). "Structure and mechanism of the Hsp90 molecular chaperone machinery." Annual review of biochemistry **75**: 271-294.

Petrich, T., H. J. Helmeke, et al. (2002). "Establishment of radioactive astatine and iodine uptake in cancer cell lines expressing the human sodium/iodide symporter." European journal of nuclear medicine and molecular imaging **29**(7): 842-854.

Phizicky, E. M. and S. Fields (1995). "Protein-protein interactions: methods for detection and analysis." Microbiological reviews **59**(1): 94-123.

Pirmohamed, M. (2010). "Acceptance of biomarker-based tests for application in clinical practice: criteria and obstacles." Clinical pharmacology and therapeutics **88**(6): 862-866.

Powell, D. J., Jr., J. Russell, et al. (1998). "The RET/PTC3 oncogene: metastatic solid-type papillary carcinomas in murine thyroids." Cancer research **58**(23): 5523-5528.

Pratt, M. A., M. C. Eggo, et al. (1989). "Regulation of thyroperoxidase, thyroglobulin and iodide levels in sheep thyroid cells by TSH, tumor promoters and epidermal growth factor." Biochimie **71**(2): 227-235.

Preston-Martin, S., L. Bernstein, et al. (1987). "Thyroid cancer among young women related to prior thyroid disease and pregnancy history." British journal of cancer **55**(2): 191-195.

Quiros, R. M., H. G. Ding, et al. (2005). "Evidence that one subset of anaplastic thyroid carcinomas are derived from papillary carcinomas due to BRAF and p53 mutations." Cancer **103**(11): 2261-2268.

Rakheja, D., R. L. Boriack, et al. (2011). "Papillary thyroid carcinoma shows elevated levels of 2-hydroxyglutarate." Tumour biology : the journal of the International Society for Oncodevelopmental Biology and Medicine **32**(2): 325-333.

Rao, R. S. and W. Bernd (2010). "Do N-glycoproteins have preference for specific sequons?" Bioinformation **5**(5): 208-212.

Raymond, E., L. Dahan, et al. (2011). "Sunitinib malate for the treatment of pancreatic neuroendocrine tumors." The New England journal of medicine **364**(6): 501-513.

RCPath (2009). Guidance on the reporting of thyroid cytology specimens. R. C. o. Pathologists.

Read, M. L., G. D. Lewy, et al. (2011). "Proto-oncogene PBF/PTTG1IP regulates thyroid cell growth and represses radioiodide treatment." Cancer research **71**(19): 6153-6164.

Ren, J., X. Gao, et al. (2009). "Systematic study of protein sumoylation: Development of a site-specific predictor of SUMOsp 2.0." Proteomics **9**(12): 3409-3412.

Rexer, B. N., A. J. Ham, et al. (2011). "Phosphoproteomic mass spectrometry profiling links Src family kinases to escape from HER2 tyrosine kinase inhibition." Oncogene.

Ribeiro, F. R., A. M. Meireles, et al. (2008). "Conventional and molecular cytogenetics of human non-medullary thyroid carcinoma: characterization of eight cell line models and review of the literature on clinical samples." BMC Cancer **8**: 371.

Ricci, J. A. and A. E. Alfonso (2012). "Multifocal micropapillary thyroid cancer: a new indication for total thyroidectomy?" The American surgeon **78**(11): 1211-1214.

Rigaut, G., A. Shevchenko, et al. (1999). "A generic protein purification method for protein complex characterization and proteome exploration." Nature biotechnology **17**(10): 1030-1032.

Russell, J. P., D. J. Powell, et al. (2000). "The TRK-T1 fusion protein induces neoplastic transformation of thyroid epithelium." Oncogene **19**(50): 5729-5735.

Salvatore, G., V. De Falco, et al. (2006). "BRAF is a therapeutic target in aggressive thyroid carcinoma." Clinical cancer research : an official journal of the American Association for Cancer Research **12**(5): 1623-1629.

Sanchez, C., C. Lachaize, et al. (1999). "Grasping at molecular interactions and genetic networks in Drosophila melanogaster using FlyNets, an Internet database." Nucleic Acids Res **27**(1): 89-94.

Santoro, M., G. Chiappetta, et al. (1996). "Development of thyroid papillary carcinomas secondary to tissue-specific expression of the RET/PTC1 oncogene in transgenic mice." Oncogene **12**(8): 1821-1826.

Sapio, M. R., D. Posca, et al. (2007). "Detection of RET/PTC, TRK and BRAF mutations in preoperative diagnosis of thyroid nodules with indeterminate cytological findings." Clinical Endocrinology **66**(5): 678-683.

Sattler, M., Y. B. Pride, et al. (2003). "A novel small molecule met inhibitor induces apoptosis in cells transformed by the oncogenic TPR-MET tyrosine kinase." Cancer research **63**(17): 5462-5469.

Sauvonnet, N., A. Dujeancourt, et al. (2005). "Cortactin and dynamin are required for the clathrin-independent endocytosis of gammac cytokine receptor." The Journal of cell biology **168**(1): 155-163.

Schaller, M. D. (2010). "Cellular functions of FAK kinases: insight into molecular mechanisms and novel functions." Journal of cell science **123**(Pt 7): 1007-1013.

Scherer, W. F., J. T. Syverton, et al. (1953). "Studies on the propagation in vitro of poliomyelitis viruses. IV. Viral multiplication in a stable strain of human malignant epithelial cells (strain HeLa) derived from an epidermoid carcinoma of the cervix." The Journal of experimental medicine **97**(5): 695-710.

Schuuring, E., E. Verhoeven, et al. (1993). "The product of the EMS1 gene, amplified and overexpressed in human carcinomas, is homologous to a v-src substrate and is located in cell-substratum contact sites." Molecular and cellular biology **13**(5): 2891-2898.

Schweppe, R. E., A. A. Kerege, et al. (2009). "Inhibition of Src with AZD0530 reveals the Src-Focal Adhesion kinase complex as a novel therapeutic target in papillary and anaplastic thyroid cancer." The Journal of clinical endocrinology and metabolism **94**(6): 2199-2203.

Shaha, A. R. (2012). "Recurrent differentiated thyroid cancer." Endocrine practice : official journal of the American College of Endocrinology and the American Association of Clinical Endocrinologists **18**(4): 600-603.

Shalloway, D., P. M. Coussens, et al. (1984). "Overexpression of the c-src protein does not induce transformation of NIH 3T3 cells." Proceedings of the National Academy of Sciences of the United States of America **81**(22): 7071-7075.

Sharma, N., A. Martin, et al. (2012). "Mining the proteome: the application of tandem mass spectrometry to endocrine cancer research." Endocrine-related cancer **19**(4): R149-161.

Shimwell, N. J., A. Martin, et al. (2009). "Adenovirus 5 E1A is responsible for increased expression of insulin receptor substrate 4 in established adenovirus 5-transformed cell lines and interacts with IRS components activating the PI3 kinase/Akt signalling pathway." Oncogene **28**(5): 686-697.

Sipos, J. A. and E. L. Mazzaferri (2010). "Thyroid cancer epidemiology and prognostic variables." Clinical oncology **22**(6): 395-404.

Slack-Davis, J. K., K. H. Martin, et al. (2007). "Cellular characterization of a novel focal adhesion kinase inhibitor." The Journal of biological chemistry **282**(20): 14845-14852.

Smith, V. E., M. L. Read, et al. (2012). "PTTG-binding factor (PBF) is a novel regulator of the thyroid hormone transporter MCT8." Endocrinology **153**(7): 3526-3536.

Smith, V. E., M. L. Read, et al. (2009). "A novel mechanism of sodium iodide symporter repression in differentiated thyroid cancer." J Cell Sci **122**(Pt 18): 3393-3402.

Sofiadis, A., A. Dinets, et al. (2010). "Proteomic study of thyroid tumors reveals frequent up-regulation of the Ca2+ -binding protein S100A6 in papillary thyroid carcinoma." Thyroid **20**(10): 1067-1076.

Spiro, M. J. (1973). "Subunit heterogeneity of thyroglobulin." The Journal of biological chemistry **248**(12): 4446-4460.

Srisomsap, C., P. Subhasitanont, et al. (2002). "Detection of cathepsin B up-regulation in neoplastic thyroid tissues by proteomic analysis." Proteomics **2**(6): 706-712.

Stanojevic, B., R. Dzodic, et al. (2011). "Mutational and clinico-pathological analysis of papillary thyroid carcinoma in Serbia." Endocrine journal.

Steen, H. and M. Mann (2004). "The ABC's (and XYZ's) of peptide sequencing." Nat Rev Mol Cell Biol **5**(9): 699-711.

Steinhagen, E., J. G. Guillem, et al. (2012). "The prevalence of thyroid cancer and benign thyroid disease in patients with familial adenomatous polyposis may be higher than previously recognized." Clinical colorectal cancer **11**(4): 304-308.

Stock, M., H. Schafer, et al. (2004). "Identification of novel genes of the bone-specific transcription factor Runx2." Journal of bone and mineral research : the official journal of the American Society for Bone and Mineral Research **19**(6): 959-972.

Stratford, A. L., K. Boelaert, et al. (2005). "Pituitary tumor transforming gene binding factor: a novel transforming gene in thyroid tumorigenesis." J Clin Endocrinol Metab **90**(7): 4341-4349.

Stsjazhko, V. A., A. F. Tsyb, et al. (1995). "Childhood thyroid cancer since accident at Chernobyl." BMJ **310**(6982): 801.

Todaro, G. J. and H. Green (1963). "Quantitative studies of the growth of mouse embryo cells in culture and their development into established lines." The Journal of cell biology **17**: 299-313.

Trajkovic-Arsic, M., J. Muller, et al. (2010). "Impact of monocarboxylate transporter-8 deficiency on the hypothalamus-pituitary-thyroid axis in mice." Endocrinology **151**(10): 5053-5062.

Turnell, A. S., R. J. Grand, et al. (2000). "Regulation of the 26S proteasome by adenovirus E1A." The EMBO journal **19**(17): 4759-4773.

Turtoi, A., E. De Pauw, et al. (2011). "Innovative proteomics for the discovery of systemically accessible cancer biomarkers suitable for imaging and targeted therapies." The American journal of pathology **178**(1): 12-18.

Verbeek, H. H., M. M. Alves, et al. (2011). "The Effects of Four Different Tyrosine Kinase Inhibitors on Medullary and Papillary Thyroid Cancer Cells." The Journal of clinical endocrinology and metabolism.

Visser, W. E., A. A. van Mullem, et al. (2011). "The thyroid hormone transporters MCT8 and MCT10 transport the affinity-label N-bromoacetyl-[(125)I]T3 but are not modified by it." Molecular and cellular endocrinology **337**(1-2): 96-100.

Vlotides, G., M. Cruz-Soto, et al. (2006). "Mechanisms for growth factor-induced pituitary tumor transforming gene-1 expression in pituitary folliculostellate TtT/GF cells." Molecular endocrinology **20**(12): 3321-3335.

Volante, M., I. Rapa, et al. (2009). "RAS mutations are the predominant molecular alteration in poorly differentiated thyroid carcinomas and bear prognostic impact." The Journal of clinical endocrinology and metabolism **94**(12): 4735-4741.

Volkel, P., P. Le Faou, et al. (2010). "Interaction proteomics: characterization of protein complexes using tandem affinity purification-mass spectrometry." Biochem Soc Trans **38**(4): 883-887.

Wang, Q., R. Chaerkady, et al. (2011). "Mutant proteins as cancer-specific biomarkers." Proceedings of the National Academy of Sciences of the United States of America **108**(6): 2444-2449.

Wang, X., P. Le, et al. (2003). "Potent and selective inhibitors of the Met [hepatocyte growth factor/scatter factor (HGF/SF) receptor] tyrosine kinase block HGF/SF-induced tumor cell growth and invasion." Molecular cancer therapeutics **2**(11): 1085-1092.

Ward, D. G., S. Nyangoma, et al. (2008). "Proteomic profiling of urine for the detection of colon cancer." Proteome Sci **6**: 19.

Watkins, R. J. (2010). A new pathway in the induction of breast cancer. School of Clinical and Experimental Medicine. Birmingham, University of Birmingham. **PhD**.

Watkins, R. J., M. L. Read, et al. (2010). "Pituitary Tumor Transforming Gene Binding Factor: a New Gene in Breast Cancer." Cancer Res.

Weaver, A. M. (2008). "Cortactin in tumor invasiveness." Cancer letters **265**(2): 157-166.

Weaver, A. M., A. V. Karginov, et al. (2001). "Cortactin promotes and stabilizes Arp2/3-induced actin filament network formation." Current biology : CB **11**(5): 370-374.

WHO (2013). Health risk assessment from the nuclear accident after the 2011 Great East Japan earthquake and tsunami, based on a preliminary dose estimation.

Wilkin, F., V. Savonet, et al. (1996). "Identification and characterization of novel genes modulated in the thyroid of dogs treated with methimazole and propylthiouracil." The Journal of biological chemistry **271**(45): 28451-28457.

Wisniewski, J. R., A. Zougman, et al. (2009). "Universal sample preparation method for proteome analysis." Nature methods **6**(5): 359-362.

Wu, H. and J. T. Parsons (1993). "Cortactin, an 80/85-kilodalton pp60src substrate, is a filamentous actin-binding protein enriched in the cell cortex." The Journal of cell biology **120**(6): 1417-1426.

Xing, M. (2005). "BRAF mutation in thyroid cancer." Endocrine-related cancer **12**(2): 245-262.

Xing, M. (2007). "BRAF mutation in papillary thyroid cancer: pathogenic role, molecular bases, and clinical implications." Endocr Rev **28**(7): 742-762.

Xing, M., R. P. Tufano, et al. (2004). "Detection of BRAF mutation on fine needle aspiration biopsy specimens: a new diagnostic tool for papillary thyroid cancer." The Journal of clinical endocrinology and metabolism **89**(6): 2867-2872.

Xing, M., W. H. Westra, et al. (2005). "BRAF mutation predicts a poorer clinical prognosis for papillary thyroid cancer." The Journal of clinical endocrinology and metabolism **90**(12): 6373-6379.

Yamashiro, S., G. Totsukawa, et al. (2003). "Citron kinase, a Rho-dependent kinase, induces di-phosphorylation of regulatory light chain of myosin II." Molecular biology of the cell **14**(5): 1745-1756.

Yao, Z., P. Yin, et al. (2011). "Serum metabolic profiling and features of papillary thyroid carcinoma and nodular goiter." Molecular bioSystems **7**(9): 2608-2614.

Yaspo, M. L., J. Aaltonen, et al. (1998). "Cloning of a novel human putative type Ia integral membrane protein mapping to 21q22.3." Genomics **49**(1): 133-136.

Yeager, N., A. Klein-Szanto, et al. (2007). "Pten loss in the mouse thyroid causes goiter and follicular adenomas: insights into thyroid function and Cowden disease pathogenesis." Cancer research **67**(3): 959-966.

Yip, L., M. N. Nikiforova, et al. (2009). "Optimizing surgical treatment of papillary thyroid carcinoma associated with BRAF mutation." Surgery **146**(6): 1215-1223.

Yokoyama, A., R. Nomura, et al. (2011). "The C-terminal domain of the adenomatous polyposis coli (Apc) protein is involved in thyroid morphogenesis and function." Medical molecular morphology **44**(4): 207-212.

Zhang, G., B. Fang, et al. (2011). "Mass spectrometry mapping of epidermal growth factor receptor phosphorylation related to oncogenic mutations and tyrosine kinase inhibitor sensitivity." Journal of proteome research **10**(1): 305-319.

Zhang, L. H., B. Tian, et al. (2006). "Dominant expression of 85-kDa form of cortactin in colorectal cancer." Journal of cancer research and clinical oncology **132**(2): 113-120.

Zhao, Z. S. and E. Manser (2005). "PAK and other Rho-associated kinases--effectors with surprisingly diverse mechanisms of regulation." The Biochemical journal **386**(Pt 2): 201-214.

Chapter 11 Appendix 1

11.1 List of potential interacting partners identified by MS/MS

The following is a list of proteins identified as potential binding partners during the MS/MS analysis in Chapter 4. All proteins with an Average Score per Peptide (ASP) less than 20 and a total number of peptides less than 4 were discarded.

Protein	ASP
ELAV-like protein 1	64.3
Protein LYRIC	61.0
Splicing factor, arginine/serine-rich 1	60.5
Eukaryotic translation initiation factor 4 gamma 1	56.5
Complement C1q subcomponent subunit B	55.5
Lamin-B1	55.0
TATA-binding protein-associated factor 2N	54.9
Pituitary tumor-transforming gene 1 protein-interacting protein	53.9
EF-hand domain-containing protein KIAA0494	53.2
Intraflagellar transport protein 140 homolog	53.1
Thioredoxin	50.5
G-protein coupled receptor 39	49.9
Heat shock 70 kDa protein 1	49.6
Nuclease-sensitive element-binding protein 1	49.5
Desmocollin-1	48.5
Cell division control protein 2 homolog	48.3
PH and SEC7 domain-containing protein 4	48.1
Importin-7	47.8
Tolloid-like protein 1	47.7
Heat shock 70 kDa protein 1A	46.9
Adenomatous polyposis coli protein 2	46.3
Actin-related protein 2/3 complex subunit 3	45.3
NHP2-like protein 1	45.2
Lysozyme C	45.0
Neurofilament heavy polypeptide	45.0
Actin-related protein 2/3 complex subunit 5	44.7
Histone H2A type 2-C	44.2
Tubulin-specific chaperone E	44.2
Cystatin-A	43.9

Protein	ASP
Macrophage migration inhibitory factor	43.7
Supervillin	43.6
Histone H2B type 1-K	43.3
Protein-glutamine gamma-glutamyltransferase 2	43.0
PHD and RING finger domain-containing protein 1	42.9
Targeting protein for Xklp2	42.9
Actin-related protein 3	42.7
ADP-ribosylation factor 5	42.1
Calnexin	41.6
Intracellular hyaluronan-binding protein 4	41.0
Endonuclease VIII-like 3	41.0
Trinucleotide repeat-containing gene 18 protein	40.6
Bullous pemphigoid antigen 1, isoform 7 (Fragment)	40.5
Choline transporter-like protein 4	40.4
Uncharacterized protein C1orf125 homolog	40.2
Src substrate cortactin	40.0
Lysosomal-trafficking regulator	39.9
Stress-70 protein, mitochondrial	39.7
SLIT and NTRK-like protein 4	39.7
G patch domain-containing protein 8	39.5
Histone H2B type 3-A	39.5
Peptidyl-prolyl cis-trans isomerase-like 1	39.3
Prohibitin-2	39.0
Apolipoprotein A-I	38.8
Filamin-C	38.8
Ribosome-binding protein 1	38.8
Heat shock protein HSP 90-beta	38.6
Peroxisome proliferator-activated receptor gamma coactivator	38.6
Poly [ADP-ribose] polymerase 1	38.3

Protein	ASP
Survival motor neuron protein	38.1
Peptidoglycan recognition protein 1	37.7
Hemoglobin subunit alpha-A	37.6
High mobility group protein HMG-I/HMG-Y	37.4
Ras GTPase-activating protein-binding protein 2	37.3
Zinc finger protein 407	36.8
Plexin-A1	36.5
Cysteine-rich protein 2	36.4
Syntaxin-binding protein 5	36.3
Replicase polyprotein 1ab	36.3
Transformation/transcription domain-associated protein	36.0
Kinectin	35.6
T-cell surface glycoprotein CD1b-2	35.5
Fibrillin-1	35.4
Ankyrin repeat and KH domain-containing protein 1	35.2
Heterogeneous nuclear ribonucleoprotein G	35.2
Synaptopodin-2	35.2
Ubiquitin carboxyl-terminal hydrolase 25	35.2
Beta-type platelet-derived growth factor receptor precursor	35.1
Protein SFI1 homolog	35.1
Myelin transcription factor 1-like protein	35.0
Pericentrin	35.0
Coatomer subunit gamma	34.7
HHIP-like protein 2	34.7
Pyrroline-5-carboxylate reductase 1, mitochondrial	34.7
Inactive ubiquitin carboxyl-terminal hydrolase 54	34.7
Uncharacterized protein C2orf71 homolog	34.5
Phosphatidylinositol-4-phosphate 3-kinase C2 domain-containing beta polypeptide	34.4

Protein	ASP
StAR-related lipid transfer protein 9	34.3
Basic helix-loop-helix domain-containing protein KIAA2018	34.3
Nucleolysin TIAR	34.2
Peroxisomal biogenesis factor 19	34.2
Coagulation factor X	34.1
Transcription factor 20	34.1
Probable D-lactate dehydrogenase, mitochondrial	33.8
EH domain-containing protein 4	33.7
Actin-related protein 2/3 complex subunit 4	33.6
Vacuolar protein sorting-associated protein 13A	33.5
Thyroglobulin	33.5
Transient receptor potential cation channel subfamily M member 6	33.4
Tyrosine-protein kinase SgK223	33.4
BEN domain-containing protein 3	33.3
Dehydrogenase/reductase SDR family member 4	33.3
Granulins	33.3
Rho guanine nucleotide exchange factor 1	33.2
Actin-related protein 2/3 complex subunit 2	33.2
Hydrocephalus-inducing protein homolog	33.2
Pleckstrin homology domain-containing family H member 1	33.2
Coiled-coil domain-containing protein 46	32.9
Protein TFG	32.9
Elongation factor G 1, mitochondrial	32.9
IQ motif and SEC7 domain-containing protein 3	32.9
Polyadenylate-binding protein 4	32.8
Zinc finger protein GLI1	32.8
FH1/FH2 domain-containing protein 1	32.7
Polypeptide N-acetylgalactosaminyltransferase 5	32.6

Protein	ASP
Tetratricopeptide repeat protein 30B	32.5
Fatty acid-binding protein, epidermal	32.4
Protein MICAL-2	32.4
Coiled-coil domain-containing protein 36	32.3
Transketolase-like protein 2	32.2
Glutathione S-transferase P	32.2
Cytochrome P450 20A1	32.2
Centromere protein F	32.1
FK506-binding protein 15	32.0
Multidrug resistance-associated protein 1	31.9
Proline-rich protein 11	31.9
ATP-citrate synthase	31.9
E3 ubiquitin-protein ligase HUWE1	31.9
Murinoglobulin-1 precursor	31.8
CLIP-associating protein 1	31.6
Histone H2A.V	31.6
A disintegrin and metalloproteinase with thrombospondin motifs 4	31.6
Tudor domain-containing protein 6	31.6
Schlafen family member 5	31.5
Aryl hydrocarbon receptor nuclear translocator	31.5
ADP-ribosylation factor-like protein 2-binding protein-like protein	31.4
Prolactin-inducible protein homolog	31.3
Heparin cofactor 2	31.3
ESF1 homolog	31.2
Cullin-9	31.1
Caspase-7	31.1
Latent-transforming growth factor beta-binding protein 2	31.0

Protein	ASP
Antigen WC1.1	31.0
Methionine aminopeptidase 1D, mitochondrial	30.9
Hemoglobin subunit alpha-2	30.9
Integrin beta-2	30.8
TRAF-interacting protein	30.8
Zinc finger protein 766	30.8
Neurogenic differentiation factor 6	30.8
Testis-specific gene 13 protein	30.8
Multisynthetase complex auxiliary component p43	30.7
Fidgetin-like protein 1	30.7
Heterogeneous nuclear ribonucleoprotein A1	30.6
Inositol 1,4,5-trisphosphate receptor type 2	30.6
Pleckstrin homology-like domain family B member 1	30.5
Lactotransferrin precursor	30.5
Zinc finger protein 608	30.5
Histone H1.2	30.5
ATP-binding cassette sub-family A member 2	30.4
Protein KIAA0284	30.4
Transcription initiation factor TFIID subunit 3	30.3
Metastasis-associated protein MTA1	30.2
Twist-related protein 2	30.2
Interleukin-3	30.0
Thrombospondin-4	30.0
Metabotropic glutamate receptor 5	30.0
Peroxidasin homolog	30.0
Putative uncharacterized protein C12orf63	29.9
Olfactory receptor 52E2	29.9
TNFAIP3-interacting protein 3	29.8
CCAAT/enhancer-binding protein zeta	29.7

Protein	ASP
Huntingtin-interacting protein 1	29.7
Plexin-B1	29.7
ATP synthase subunit beta, mitochondrial	29.6
Renalase	29.6
TRIO and F-actin-binding protein	29.6
Protein virilizer homolog	29.5
Glycerol-3-phosphate acyltransferase 3	29.5
Receptor-type tyrosine-protein phosphatase S	29.5
LON peptidase N-terminal domain and RING finger protein 3	29.4
Vasodilator-stimulated phosphoprotein	29.4
ADP/ATP translocase 2	29.4
Nucleosome-remodeling factor subunit BPTF	29.4
Voltage-dependent T-type calcium channel subunit alpha-1G	29.4
Peptidyl-prolyl cis-trans isomerase B	29.4
Lamin-B2	29.3
Uncharacterized protein C1orf62	29.2
Src Family kinase	29.1
HEAT repeat-containing protein 5B	29.1
Protein TANC1	29.1
Complement C4-B	29.1
Histone H2A type 1-H	29.0
JmjC domain-containing histone demethylation protein 1D	29.0
KN motif and ankyrin repeat domain-containing protein 2	29.0
Ras GTPase-activating-like protein IQGAP3	29.0
WD repeat-containing protein 51B	29.0
Cytospin-A	28.9
BAT2 domain-containing protein 1	28.9
Myb-binding protein 1A	28.9
Tubby-related protein 1	28.9

Protein	ASP
Interleukin-18 receptor 1 precursor	28.9
Multimerin-1	28.9
Calcineurin-binding protein cabin-1	28.8
Calpain-1 catalytic subunit	28.8
Utrophin	28.8
Signal recognition particle receptor subunit alpha	28.8
Uncharacterized coiled-coil domain-containing protein KIAA1984	28.7
Putative tubulin-like protein alpha-4B	28.7
Serine/threonine-protein kinase Nek4	28.7
Peroxisomal membrane protein 11B	28.7
Mutated melanoma-associated antigen 1	28.7
Trans-acting transcriptional protein ICP0	28.7
Lipid phosphate phosphatase-related protein type 3	28.7
VPS10 domain-containing receptor SorCS1	28.7
AF4/FMR2 family member 2	28.6
Bromodomain and WD repeat-containing protein 3	28.6
Glucosamine--fructose-6-phosphate aminotransferase [isomerizing] 2	28.6
HAUS augmin-like complex subunit 6	28.5
Meiosis-specific nuclear structural protein 1	28.5
Centrosomal protein of 120 kDa	28.5
Ninein-like protein	28.5
Deformed epidermal autoregulatory factor 1 homolog	28.5
Transferrin receptor protein 1	28.5
Transcriptional regulator ATRX	28.4
Cadherin-like protein 26	28.4
Putative adenosylhomocysteinase 3	28.4
Thioredoxin domain-containing protein 2	28.4
Protein orai-2	28.4

Protein	ASP
Cubilin precursor	28.3
Voltage-dependent R-type calcium channel subunit alpha-1E	28.3
Pecanex-like protein C14orf135	28.2
Dachshund homolog 2	28.2
Protein cramped-like	28.2
Hyaluronan synthase 3	28.2
Protein Dok-7	28.2
FRAS1-related extracellular matrix protein 1 precursor	28.2
MAP7 domain-containing protein 3	28.2
Myeloid/lymphoid or mixed-lineage leukemia protein 2	28.1
Fructose-bisphosphate aldolase B	28.1
Emerin	28.1
Fanconi anemia group M protein	28.1
CD225 family protein FLJ76511	28.1
Armadillo repeat-containing protein 5	28.1
Arf-GAP with SH3 domain, ANK repeat and PH domain-containing protein 2	28.1
Fibrous sheath-interacting protein 2	28.1
CLIP-associating protein 2	28.0
Complement C1q subcomponent subunit C	28.0
Syncoilin	28.0
Brefeldin A-inhibited guanine nucleotide-exchange protein 2	28.0
Contactin-2	28.0
Nucleoside-triphosphatase C1orf57	27.9
Polymerase delta-interacting protein 3	27.9
Protein LOC339766	27.9
Ankyrin repeat domain-containing protein 7	27.9
Protocadherin Fat 3	27.9
G protein-coupled receptor kinase 5	27.9

Protein	ASP
RIB43A-like with coiled-coils protein 1	27.9
Uncharacterized protein C6orf174	27.8
Syntaxin-4	27.8
T-cell surface protein tactile	27.8
Cell cycle checkpoint control protein RAD9B homolog	27.8
Sodium bicarbonate cotransporter 3	27.8
Sciellin	27.8
Cell growth-regulating nucleolar protein	27.8
Forkhead-associated domain-containing protein 1	27.7
E3 ubiquitin-protein ligase RNF149	27.7
Breast cancer type 1 susceptibility protein homolog	27.7
ADP-ribosylation factor-like protein 8A	27.7
P2X purinoceptor 5	27.7
Uncharacterized protein KIAA0552	27.7
Cell division cycle protein 123 homolog	27.7
Cancer-associated gene 1 protein homolog	27.6
Membrane primary amine oxidase	27.6
Proto-oncogene tyrosine-protein kinase ROS precursor	27.6
Transcription cofactor vestigial-like protein 3	27.6
SH3 and multiple ankyrin repeat domains protein 1	27.6
Leucine-rich repeat flightless-interacting protein	27.5
Kappa-casein	27.5
Macrophage receptor MARCO	27.5
Retinoic acid-induced protein 1	27.5
Transient receptor potential cation channel subfamily M member 1	27.4
Uncharacterized protein C19orf21 homolog	27.4
E3 ubiquitin-protein ligase Praja1	27.4
Spermatid nuclear transition protein 3	27.4

Protein	ASP
SPATS2-like protein	27.3
Sodium channel protein type 11 subunit alpha	27.3
Gephyrin	27.3
Probable carboxypeptidase PM20D1	27.3
Poly [ADP-ribose] polymerase 4	27.3
Plasminogen activator inhibitor 2, macrophage	27.2
Angiopoietin-2	27.2
Plasmalemma vesicle-associated protein	27.2
Serine/threonine-protein kinase VRK2	27.2
Sodium channel protein type 10 subunit alpha	27.2
Vesicle transport through interaction with t-SNAREs homolog 1B	27.2
Probable 10-formyltetrahydrofolate dehydrogenase ALDH1L2	27.1
Protein FAM83G	27.1
Rho GTPase-activating protein 18	27.1
Sperm motility kinase 4a	27.1
Stanniocalcin-2	27.1
Phosphatidylinositol 4-kinase alpha	27.1
Toll-like receptor 5	27.1
Protein-glutamine gamma-glutamyltransferase E	27.0
Disks large homolog 4	27.0
Integrin alpha-11	27.0
Corneodesmosin	27.0
T-box transcription factor TBX22	26.9
Importin subunit alpha-6	26.9
Oxygen-regulated protein 1	26.9
Nucleoporin NUP85	26.9
Putative methyltransferase METT10D	26.8
Leiomodin-2	26.8
Uncharacterized protein C9orf102 homolog	26.8

Protein	ASP
Receptor-type tyrosine-protein phosphatase delta	26.7
Katanin p60 ATPase-containing subunit A-like 1	26.7
Uncharacterized protein C1orf26 homolog	26.7
Centrosome-associated protein 350	26.7
Uncharacterized protein C6orf170	26.7
Zinc finger protein with KRAB and SCAN domains 2	26.7
Regulator of G-protein signaling 3	26.7
ATPase WRNIP1	26.7
Coiled-coil domain-containing protein 40	26.7
1-phosphatidylinositol-4,5-bisphosphate phosphodiesterase eta-2	26.7
Xylosyltransferase 1	26.6
Low-density lipoprotein receptor-related protein 2	26.6
Eosinophil peroxidase	26.6
Ubiquitin carboxyl-terminal hydrolase 29	26.6
Zinc finger protein 322A	26.6
Cholinephosphotransferase 1	26.6
Heterogeneous nuclear ribonucleoprotein A3	26.6
Angiopoietin-4	26.6
B-cell receptor CD22	26.6
EH domain-binding protein 1	26.6
Lactation elevated protein 1	26.6
Ubiquitin carboxyl-terminal hydrolase 49	26.6
Ferritin heavy chain	26.5
Phosphoglycerate mutase family member 5	26.5
FCH and double SH3 domains protein 2	26.5
Transcription factor HIVEP3	26.4
Alanine--glyoxylate aminotransferase 2-like 1	26.4
SCL-interrupting locus protein homolog	26.4

Protein	ASP
IQ and ubiquitin-like domain-containing protein	26.4
Dynamin-2	26.4
Tubulin beta-1 chain	26.4
Uncharacterized protein C3orf63 homolog	26.4
Heat shock-related 70 kDa protein 2	26.4
Bifunctional UDP-N-acetylglucosamine 2-epimerase/N-acetylmannosamine kinase	26.3
Tenascin-X	26.3
Peroxisomal acyl-coenzyme A oxidase 2	26.3
Zinc finger homeobox protein 4	26.3
Protein kinase C theta type	26.3
Histone H1t	26.3
Eukaryotic translation initiation factor 2-alpha kinase 4	26.2
Rho GTPase-activating protein 20	26.2
Protocadherin gamma-B6	26.2
Ubiquitin carboxyl-terminal hydrolase 34	26.2
B-cell receptor-associated protein 29	26.2
C4b-binding protein alpha chain	26.2
RING finger protein 31	26.2
Stonin-2	26.2
Structural maintenance of chromosomes protein 1B	26.2
Zinc finger protein 638	26.2
Prostacyclin synthase	26.2
Arginine-glutamic acid dipeptide repeats protein	26.2
Protein sidekick-2	26.2
cAMP-specific 3',5'-cyclic phosphodiesterase 4B	26.1
Dehydrogenase/reductase SDR family member on chromosome X	26.1
Peripheral-type benzodiazepine receptor-associated protein 1	26.1

Protein	ASP
5'-nucleotidase domain-containing protein 3	26.1
Antigen peptide transporter 1	26.1
Proliferating cell nuclear antigen	26.0
Fibrocystin	26.0
Protein RMD5 homolog A	26.0
Desmin	26.0
Mitochondrial intermediate peptidase	26.0
Serine/threonine-protein kinase MRCK alpha	26.0
Intersectin-2	25.9
Peptidylprolyl isomerase domain and WD repeat-containing protein 1	25.9
Ankyrin repeat domain-containing protein 56	25.9
Actin filament-associated protein 1-like 1	25.9
Bestrophin-1	25.9
Coiled-coil domain-containing protein 146	25.9
Eukaryotic translation initiation factor 3 subunit E	25.9
Heterogeneous nuclear ribonucleoprotein A0	25.9
TRAF family member-associated NF-kappa-B activator	25.9
RING finger protein 113A	25.8
Probable helicase with zinc finger domain	25.8
Ankyrin-2	25.8
Multiple epidermal growth factor-like domains 8	25.7
Transmembrane protein C15orf27	25.7
Dedicator of cytokinesis protein 1	25.7
Fanconi anemia group A protein	25.7
Proto-oncogene serine/threonine-protein kinase mos	25.6
Neuron navigator 2	25.6
Pulmonary surfactant-associated protein D precursor	25.6
2',3'-cyclic-nucleotide 3'-phosphodiesterase	25.6

Protein	ASP
Phosphatase and actin regulator 4	25.6
Signal recognition particle 68 kDa protein	25.6
Rab3 GTPase-activating protein non-catalytic subunit	25.6
Cyclin-J	25.6
B-cell lymphoma 6 protein	25.5
Fatty acid-binding protein, adipocyte	25.5
Pleckstrin homology-like domain family B member 2	25.5
Alpha-enolase	25.5
Uncharacterized protein KIAA1671	25.5
Splicing factor 3B subunit 3	25.5
Pecanex-like protein 1	25.5
AT-rich interactive domain-containing protein 5A	25.4
Huntingtin	25.4
Protein QN1 homolog	25.4
ATP-binding cassette sub-family A member 3	25.4
Coiled-coil domain-containing protein 45	25.4
Ras GTPase-activating protein 3	25.4
Seminal vesicle major clotting proteins	25.4
Probable Coiled-coil domain-containing protein 8	25.4
Ubiquitin carboxyl-terminal hydrolase 4	25.4
Antigen KI-67	25.3
Protein AHNAK2	25.3
Ankyrin repeat domain-containing protein 43	25.3
Coiled-coil domain-containing protein 18	25.3
Uncharacterized protein C14orf80 homolog	25.3
Protocadherin gamma-C3	25.3
DALR anticodon-binding domain-containing protein 3	25.3
Lamina-associated polypeptide 2, isoforms alpha/zeta	25.2
Uncharacterized protein KIAA0947	25.2

Protein	ASP
RUN and FYVE domain-containing protein 1	25.2
Tetratricopeptide repeat protein 3	25.2
Protein BAT2-like	25.2
Calpain-7	25.2
G2/mitotic-specific cyclin-B1	25.2
Voltage-gated potassium channel subunit beta-1	25.2
Bile acid receptor	25.1
Nuclear pore complex protein Nup205	25.1
SH3 and multiple ankyrin repeat domains protein 3	25.1
Uncharacterized protein ENSP00000382514 homolog	25.1
Probable E3 ubiquitin-protein ligase HERC1	25.1
Macrophage scavenger receptor types I and II	25.1
Proto-oncogene tyrosine-protein kinase Fes/Fps	25.1
HIRA-interacting protein 3	25.1
Nesprin-2	25.0
Transcription factor HIVEP2	25.0
Cell cycle progression protein 1	25.0
Replication initiator 1	25.0
Proto-oncogene vav	25.0
WD repeat-containing protein 64	25.0
Disintegrin and metalloproteinase domain-containing protein 28	25.0
Uncharacterized protein C15orf42	25.0
Integrator complex subunit 4	25.0
Proprotein convertase subtilisin/kexin type 7	25.0
Uncharacterized protein C14orf166B homolog	24.9
Protein argonaut	24.9
GTP-binding protein GUF1 homolog	24.9
Prominin-2	24.9
Suprabasin	24.9

Protein	ASP
Serine--pyruvate aminotransferase, mitochondrial	24.9
Uncharacterized protein C12orf55	24.9
ATPase family AAA domain-containing protein 3	24.9
Uncharacterized protein C20orf79 homolog	24.9
Low-density lipoprotein receptor-related protein 1B precursor	24.9
Complement C1q subcomponent subunit A	24.8
Probable global transcription activator SNF2L2	24.8
Cytochrome P450 3A17	24.8
Lethal(3)malignant brain tumor-like 3 protein	24.8
Mitogen-activated protein kinase 12	24.8
Monocarboxylate transporter 10	24.8
Multidrug resistance-associated protein 7	24.8
Long-chain-fatty-acid--CoA ligase ACSBG2	24.7
Catalase	24.7
Coiled-coil domain-containing protein 55	24.7
CD59 glycoprotein	24.7
Uncharacterized protein C18orf34	24.7
Protein dispatched homolog 1	24.7
GAS2-like protein 2	24.7
Putative glycerophosphodiester phosphodiesterase 5	24.7
Raftlin	24.7
Synaptotagmin-15	24.7
SET and MYND domain-containing protein 3	24.7
UHRF1-binding protein 1-like	24.7
Metabotropic glutamate receptor 3	24.7
Heterogeneous nuclear ribonucleoprotein M	24.6
Ubiquitin carboxyl-terminal hydrolase 40	24.6
Microtubule-associated protein tau	24.6
Spermatogenesis-associated serine-rich protein 2	24.6

Protein	ASP
Spindle and kinetochore-associated protein 3	24.6
UPF0606 protein C11orf41	24.6
Protein MON2 homolog	24.6
Tyrosine-protein kinase RYK	24.6
Inverted formin-2	24.5
Liprin-alpha-2	24.5
Kinetochore protein Nuf2	24.5
B-cell CLL/lymphoma 9 protein	24.5
Uncharacterized protein C12orf41 homolog	24.5
Protein Hook homolog 2	24.5
Phosphotidylinositol phosphatase PTPRQ	24.5
Carbohydrate kinase domain-containing protein	24.5
Beta-klotho	24.5
Lysine-specific demethylase 3A	24.4
SH2 domain-containing protein 4A	24.4
GRB2-associated-binding protein 3	24.4
Lipid phosphate phosphatase-related protein type 4	24.4
Tetratricopeptide repeat protein 30A2	24.4
Taste receptor type 1 member 1	24.4
Vascular endothelial growth factor receptor 2	24.4
Putative uncharacterized protein FLJ32790	24.4
Zinc finger protein 350	24.4
Echinoderm microtubule-associated protein-like 4	24.4
Zinc finger protein 22	24.4
Zinc finger SWIM domain-containing protein 1	24.4
Ryanodine receptor 1	24.3
Endoplasmic reticulum aminopeptidase 1	24.3
Protein FAM81B	24.3
Hemicentin-1	24.3

Protein	ASP
Zinc finger protein basonuclin-1	24.3
Cyclin-A1	24.3
Ran-binding protein 10	24.3
Protein asteroid homolog 1	24.3
Focal adhesion kinase 1	24.3
Caspase recruitment domain-containing protein 10	24.3
Probable serine protease HTRA3	24.3
Cytoplasmic protein NCK2	24.3
Protein C16orf88	24.2
UPF0723 protein C11orf83 homolog	24.2
Band 4.1-like protein 1	24.2
Signal transducer and activator of transcription 2	24.2
T-cell surface antigen CD2	24.2
Uncharacterized protein C14orf145	24.2
Fer-1-like protein 4	24.2
Inositol 1,4,5-trisphosphate receptor type 3	24.1
Polycystic kidney disease and receptor for egg jelly-related protein	24.1
PDZ domain-containing protein 2	24.1
Cullin-4B	24.1
Glycine cleavage system H protein, mitochondrial	24.1
Glycine receptor subunit alpha-4	24.1
Mitochondrial inner membrane protein	24.1
Potassium voltage-gated channel subfamily H member 5	24.1
Leucine-rich repeat-containing protein 7	24.1
Ligand-dependent nuclear receptor corepressor-like protein	24.1
Uncharacterized protein C12orf35	24.0
Sickle tail protein	24.0
Calpain-13	24.0

Protein	ASP
Uncharacterized protein C6orf203 homolog	24.0
Septin-9	24.0
Serine palmitoyltransferase 1	24.0
Ubiquitin-conjugating enzyme E2 E2	24.0
Inner centromere protein	24.0
Sentrin-specific protease 6	24.0
Regulating synaptic membrane exocytosis protein 2	23.9
Protocadherin Fat 1 precursor	23.9
U4/U6 small nuclear ribonucleoprotein Prp3	23.9
Telomere length regulation protein TEL2 homolog	23.9
NFX1-type zinc finger-containing protein 1	23.9
Ninein	23.9
Cytokine-inducible SH2-containing protein	23.9
Tyrosine-protein phosphatase non-receptor type 20	23.9
Somatoliberin	23.9
Arf-GAP, Rho-GAP domain, ANK repeat and PH domain-containing protein 2	23.8
Rho guanine nucleotide exchange factor 10-like protein	23.8
Dihydrodipicolinate synthase-like, mitochondrial	23.8
Uncharacterized protein C15orf33 homolog	23.8
Tripartite motif-containing protein 9	23.8
Lung squamous cell carcinoma-related protein 1	23.8
A disintegrin and metalloproteinase with thrombospondin motifs 15	23.8
Protein FAM135A	23.8
Glutamate [NMDA] receptor subunit epsilon-4	23.8
RANBP2-like and GRIP domain-containing protein 4	23.8
PH and SEC7 domain-containing protein 3	23.7
Endonuclease/exonuclease/phosphatase family domain-	23.7

Protein	ASP
containing protein 1	
Haptoglobin	23.7
Ribonucleoside-diphosphate reductase subunit M2	23.7
Semaphorin-7A	23.7
Syntaxin-binding protein 2	23.7
Probable E3 ubiquitin-protein ligase TRIP12	23.7
Heat shock protein 75 kDa, mitochondrial	23.7
ATP-binding cassette sub-family B member 6, mitochondrial	23.6
ATP synthase subunit g, mitochondrial	23.6
C2 domain-containing protein 3	23.6
Nuclear pore complex protein Nup214	23.6
Heat shock protein beta-1	23.6
E3 ubiquitin-protein ligase TRIM33	23.6
Cullin-7	23.5
Semaphorin-3B	23.5
Lipopolysaccharide-binding protein	23.5
Transmembrane protein 131	23.5
Nance-Horan syndrome protein	23.5
Serine-protein kinase ATM	23.5
Uncharacterized protein C22orf30	23.5
Cohesin subunit SA-2	23.5
Inositol hexakisphosphate and diphosphoinositol-pentakisphosphate kinase 2	23.4
Melanoma inhibitory activity protein 3	23.4
Mucin-16	23.4
Peroxiredoxin-5, mitochondrial precursor	23.4
Transcription initiation factor TFIID subunit 1	23.4
Tetratricopeptide repeat protein 18	23.4
Toll-like receptor 9	23.4

Protein	ASP
Rab GDP dissociation inhibitor alpha	23.4
Tumor suppressor p53-binding protein 1	23.4
Signal recognition particle 54 kDa protein	23.3
Thrombospondin type-1 domain-containing protein 7A	23.3
Cathepsin D	23.3
Cytochrome c oxidase subunit 6A2	23.3
Plasminogen activator inhibitor 1	23.3
Receptor-type tyrosine-protein phosphatase U	23.3
Transforming acidic coiled-coil-containing protein 2	23.3
Zinc finger C3H1 domain-containing protein	23.3
Uncharacterized protein C3orf17	23.3
Acyl-coenzyme A oxidase-like protein	23.3
BCL-6 corepressor	23.3
Integrator complex subunit 3	23.3
Leucine-rich repeat-containing protein 33	23.3
TNF receptor-associated factor 6	23.3
LIM domain only protein 7	23.2
Large proline-rich protein BAT2	23.2
Uncharacterized protein KIAA1797	23.2
Ankyrin repeat and LEM domain-containing protein 2	23.2
Circadian locomoter output cycles protein kaput	23.2
Basic fibroblast growth factor receptor 1	23.2
Mitogen-activated protein kinase kinase kinase 4	23.2
Testis-expressed sequence 10 protein	23.2
Voltage-dependent L-type calcium channel subunit alpha-1F	23.2
HERV-K_8p23.1 provirus ancestral Gag polyprotein	23.2
Glutamate [NMDA] receptor subunit epsilon-3	23.2
Fibrocystin-L	23.2
Tubulin alpha chain-like 3	23.2

Protein	ASP
Transcription intermediary factor 1-beta	23.1
Alpha-protein kinase 2	23.1
Bromodomain testis-specific protein	23.1
cAMP-specific 3',5'-cyclic phosphodiesterase 4A	23.1
Interferon beta	23.1
Uncharacterized protein KIAA0467	23.1
Arachidonate 12-lipoxygenase, 12S-type	23.1
Nipped-B-like protei	23.1
Phosphoribosylformylglycinamidine synthase	23.1
Protein ALEX	23.1
Zinc finger protein 24	23.1
Tetratricopeptide repeat protein 21A	23.1
Histone H1oo	23.1
Gamma-interferon-inducible protein Ifi-16	23.1
Type I iodothyronine deiodinase	23.1
Lebercilin	23.1
ADP/ATP translocase 4	23.1
Ribosome biogenesis protein BMS1 homolog	23.1
Induced myeloid leukemia cell differentiation protein Mcl-1 homolog	23.1
Midasin	23.0
Tight junction protein ZO-2	23.0
C-myc promoter-binding protein	23.0
Trinucleotide repeat-containing gene 6B protein	23.0
Bromodomain adjacent to zinc finger domain protein 1A	23.0
Protein DERPC	23.0
Latent-transforming growth factor beta-binding protein 1	23.0
Mitogen-activated protein kinase-binding protein 1	23.0
Papilin	23.0

Protein	ASP
Serine/threonine-protein kinase 36	23.0
WD repeat and FYVE domain-containing protein 3	23.0
Apolipoprotein A-IV	23.0
Histone acetyltransferase MYST4	23.0
LAS1-like protein	23.0
Proline dehydrogenase, mitochondrial	23.0
Coiled-coil domain-containing protein 60	23.0
Canalicular multispecific organic anion transporter 2	22.9
Thymidine phosphorylase	22.9
Protein CASC5	22.9
Lutropin-choriogonadotropic hormone receptor	22.9
E3 ubiquitin-protein ligase UBR4	22.9
Caspase recruitment domain-containing protein 9	22.9
Interleukin-1 receptor-associated kinase-like 2	22.9
Leukocyte cell-derived chemotaxin-2	22.9
Mucin-2	22.9
Pantothenate kinase 1	22.9
Superoxide dismutase [Cu-Zn]	22.9
LINE-1 reverse transcriptase homolog	22.9
Nucleolar protein 11	22.9
Acyl-CoA dehydrogenase family member 10	22.9
Death domain-containing protein CRADD	22.9
ERV-FRD provirus ancestral Env polyprotein	22.9
Platelet receptor Gi24	22.9
Ras-interacting protein 1	22.9
Leucine-rich repeat protein SHOC-2	22.9
Tetratricopeptide repeat protein 23-like	22.9
Small subunit processome component 20 homolog	22.9
Interferon gamma	22.9

Protein	ASP
Thioredoxin reductase 3	22.8
Galectin-1	22.8
Uncharacterized protein C1orf103	22.8
Transmembrane protein 175	22.8
Protein CREG2	22.8
Lactase-phlorizin hydrolase	22.8
Msx2-interacting protein	22.8
SNF-related serine/threonine-protein kinase	22.8
Zinc finger MYM-type protein 3	22.8
Transcription factor GATA-5	22.8
Myopalladin	22.8
Rho guanine nucleotide exchange factor 15	22.7
Myocardin	22.7
A disintegrin and metalloproteinase with thrombospondin motifs 13	22.7
Ankycorbin	22.7
Sarcoplasmic/endoplasmic reticulum calcium ATPase 3	22.7
Rho-related GTP-binding protein RhoG	22.7
Uncharacterized protein C14orf38	22.7
Low-density lipoprotein receptor-related protein 5	22.7
Transmembrane protein 41B	22.7
Zinc finger protein 280D	22.7
Arachidonate 5-lipoxygenase	22.7
E3 ubiquitin-protein ligase UBR3	22.7
Uncharacterized protein C10orf95	22.7
UPF0518 protein FAM160A2	22.7
Protein FAM44A	22.7
Kin of IRRE-like protein 1	22.7
Ly6/PLAUR domain-containing protein 3	22.7

Protein	ASP
PEST proteolytic signal-containing nuclear protein	22.7
Protein SMG7	22.7
Zinc finger protein 18	22.7
Bactericidal/permeability-increasing protein-like 1	22.7
Zinc finger protein DZIP1	22.6
Protein KRBA1	22.6
Otogelin	22.6
V-type proton ATPase subunit C 2	22.6
Centrosomal protein of 170 kDa	22.6
Protein SHQ1 homolog	22.6
Dystroglycan	22.6
Glucocorticoid receptor	22.6
Protein NDRG1	22.6
2',5'-phosphodiesterase 12	22.6
Polymerase delta-interacting protein 2	22.6
Ankyrin repeat domain-containing protein 34C	22.6
Autophagy-related protein 2 homolog B	22.6
Hemoglobin subunit gamma	22.6
ADP-ribosylation factor GTPase-activating protein 3	22.6
Core histone macro-H2A.1	22.6
Phosphorylase b kinase regulatory subunit beta	22.6
SCO-spondin	22.6
Dual specificity protein kinase TTK	22.6
Structural maintenance of chromosomes protein 3	22.5
Apolipoprotein O-like	22.5
Steroid 21-hydroxylase	22.5
Zinc finger protein 227	22.5
ATP-binding cassette sub-family G member 2	22.5
Cytosolic carboxypeptidase 2	22.5

Protein	ASP
DENN domain-containing protein 4C	22.5
Leucine-rich repeat serine/threonine-protein kinase 2	22.5
NADH dehydrogenase [ubiquinone] 1 beta	22.5
Uncharacterized protein FLJ44066	22.5
Centromere protein H	22.5
Calcium-activated chloride channel regulator 4	22.5
Receptor-type tyrosine-protein phosphatase eta	22.5
WSC domain-containing protein 1	22.5
Epiplakin	22.4
GAS2-like protein 1	22.4
Protein ALO17	22.4
2,4-dienoyl-CoA reductase, mitochondrial	22.4
Protein SLC7A6OS	22.4
Troponin I, cardiac muscle	22.4
Tripartite motif-containing protein 72	22.4
GDP-L-fucose synthetase	22.4
Eukaryotic translation initiation factor 3 subunit K	22.4
Sphingosine-1-phosphate lyase 1	22.4
E3 ubiquitin-protein ligase LRSAM1	22.4
Netrin-3	22.4
Splicing factor, arginine/serine-rich 7	22.4
Zinc finger protein 106	22.4
Sucrase-isomaltase, intestinal	22.4
Arf-GAP with SH3 domain, ANK repeat and PH domain-containing protein 1	22.4
Leucine-rich repeat-containing protein 17	22.4
Suppressor of G2 allele of SKP1 homolog	22.4
Tribbles homolog 3	22.4
Alpha-1-antiproteinase	22.4

Protein	ASP
Alstrom syndrome protein 1	22.3
Bromodomain adjacent to zinc finger domain protein 2A	22.3
Disintegrin and metalloproteinase domain-containing protein 5	22.3
Growth hormone receptor	22.3
Protein phosphatase inhibitor 2	22.3
Protein Shroom4	22.3
Alcohol dehydrogenase class-3	22.3
Fer-1-like protein 6	22.3
M-phase phosphoprotein 9	22.3
Pentatricopeptide repeat-containing protein 2	22.3
Solute carrier family 26 member 9	22.3
Tudor domain-containing protein 5	22.3
Glutathione S-transferase Yb-3	22.3
Nitric oxide synthase, endothelial	22.3
Beta-actin-like protein 3	22.2
Synaptonemal complex protein 1	22.2
Toll-like receptor 1	22.2
Protein FAM118B	22.2
Potassium voltage-gated channel subfamily B member 1	22.2
Zinc finger CCCH domain-containing protein 3	22.2
Synembryn-A	22.2
Tenascin-N	22.2
Contactin-6	22.2
Deoxyribonuclease gamma	22.2
Sodium/glucose cotransporter 1	22.2
Ubiquitin-conjugating enzyme E2 O	22.2
Elongation factor Ts, mitochondrial	22.2
Probable G-protein coupled receptor 156	22.2
Septin-7	22.2

Protein	ASP
WD repeat-containing protein 35	22.2
Alkyldihydroxyacetonephosphate synthase, peroxisomal	22.2
UPF0580 protein C15orf58 homolog	22.1
Transmembrane protease, serine 13	22.1
Rho-associated protein kinase 2	22.1
Armadillo repeat-containing protein 3	22.1
Uncharacterized protein C4orf37 homolog	22.1
Centrosomal protein of 68 kDa	22.1
Cytochrome P450 4B1	22.1
Symplekin	22.1
Mitochondrial brown fat uncoupling protein 1	22.1
Death-inducer obliterator 1	22.1
FLYWCH-type zinc finger-containing protein 1	22.1
NADH-ubiquinone oxidoreductase chain 5	22.1
Brefeldin A-inhibited guanine nucleotide-exchange protein 3	22.1
Cathepsin L1	22.1
Hyccin	22.1
S100P-binding protein	22.1
Janus kinase and microtubule-interacting protein 2	22.0
Protein bassoon	22.0
Putative uncharacterized protein ENSP00000382790	22.0
Ankyrin repeat domain-containing protein 6	22.0
Transcription elongation factor B polypeptide 3	22.0
Ribonucleases P/MRP protein subunit POP1	22.0
RIMS-binding protein 2	22.0
Carnitine O-palmitoyltransferase 1, liver isoform	22.0
Alpha-catulin	22.0
Retrotransposon gag domain-containing protein 1	22.0
N-acetyltransferase ESCO1	22.0

Protein	ASP
Amine oxidase [flavin-containing] B	22.0
Brefeldin A-inhibited guanine nucleotide-exchange protein 1	22.0
Protein DGCR14	22.0
Complement component C9	21.9
Protein dopey-1	21.9
Oxoeicosanoid receptor 1	21.9
Zinc finger protein 40	21.9
Trichohyalin	21.9
B-lymphocyte antigen CD20	21.9
Dynamin-3	21.9
Ecotropic viral integration site 5 protein	21.9
Exophilin-5	21.9
Transcription factor Dp-1	21.9
Sorbin and SH3 domain-containing protein 1	21.9
Leucine-rich repeat and IQ domain-containing protein 1	21.9
Intestinal alkaline phosphatase 1	21.9
Perforin-1	21.9
StAR-related lipid transfer protein 13	21.9
Cholinesterase	21.9
RING finger protein 180	21.9
10-formyltetrahydrofolate dehydrogenase	21.8
Golgin subfamily A member 2	21.8
Limbin	21.8
U2-associated protein SR140	21.8
Uncharacterized protein C19orf47	21.8
Leucine-rich repeat and WD repeat-containing protein	21.8
Roundabout homolog 4	21.8
Plexin-B3	21.8
Protein RRP5 homolog	21.8

Protein	ASP
Fanconi anemia group I protein homolog	21.8
Partitioning defective 3 homolog	21.8
PMS1 protein homolog 1	21.8
Small G protein signaling modulator 1	21.8
Protein unc-45 homolog A	21.7
Rootletin	21.7
Tight junction-associated protein 1	21.7
E3 ubiquitin-protein ligase MARCH6	21.7
Trinucleotide repeat-containing gene 6A protein	21.7
Protein Daple	21.7
Neuronal PAS domain-containing protein 1	21.7
Brain-specific angiogenesis inhibitor 1-associated protein 2	21.7
Protein FAM161B	21.7
Huntingtin-interacting protein 1-related protein	21.7
Origin recognition complex subunit 6	21.7
Peptidyl-glycine alpha-amidating monooxygenase	21.7
AF4/FMR2 family member 4	21.7
Beta-galactosidase-1-like protein 3	21.7
Centrosomal protein of 78 kDa	21.6
Dual oxidase 1	21.6
Deubiquitinating protein VCIP135	21.6
Armadillo repeat-containing protein 6	21.6
L-amino-acid oxidase	21.6
Rho GTPase-activating protein 27	21.6
RING finger protein 213	21.6
Calpain-12	21.6
Zinc finger protein 167	21.6
Nuclear fragile X mental retardation-interacting protein 1	21.6
Teashirt homolog 2	21.6

Protein	ASP
Magnesium transporter MRS2 homolog, mitochondrial	21.5
Splicing factor, arginine/serine-rich 5	21.5
UPF0704 protein C6orf165 homolog	21.5
SWI/SNF-related matrix-associated actin-dependent regulator of chromatin subfamily A-like protein 1	21.5
Interleukin-21	21.5
Uncharacterized protein C15orf52	21.5
Eukaryotic translation initiation factor 2-alpha kinase 1	21.5
SEL1-like repeat-containing protein KIAA0746	21.5
Uncharacterized protein LOC340228 homolog	21.5
p130Cas-associated protein	21.5
YLP motif-containing protein 1	21.5
Amyloid beta A4 precursor protein-binding family B member 3	21.5
Bromodomain-containing protein 4	21.5
Nuclear receptor coactivator 2	21.4
Uncharacterized protein C12orf40	21.4
Disintegrin and metalloproteinase domain-containing protein 7	21.4
Plastin-2	21.4
Reticulon-4	21.4
Pulmonary surfactant-associated protein A	21.4
Stonin-1	21.4
T-box transcription factor TBX19	21.4
Tetratricopeptide repeat protein 24	21.4
Pancreatic triacylglycerol lipase	21.4
Sodium channel protein type 9 subunit alpha	21.4
Fanconi anemia group D2 protein	21.4
Nuclear pore complex protein Nup98-Nup96	21.4
C-type lectin domain family 4 member F	21.4
Ankyrin repeat and zinc finger domain-containing protein 1	21.4

Protein	ASP
Uncharacterized protein C1orf77	21.4
Cathepsin S	21.4
Chitotriosidase-1	21.4
Cytochrome P450 2C19	21.4
Lactadherin	21.4
Nuclear pore membrane glycoprotein 210	21.4
Protein FAM63A	21.4
Ankyrin repeat domain-containing protein 24	21.3
Armadillo repeat-containing X-linked protein 1	21.3
D-beta-hydroxybutyrate dehydrogenase, mitochondrial	21.3
RING finger protein 112	21.3
Protein furry homolog-like	21.3
Amyloid protein-binding protein 2	21.3
Dual specificity tyrosine-phosphorylation-regulated kinase 4	21.3
Otoancorin precursor	21.3
Zinc finger protein 187	21.3
ATP-dependent Clp protease ATP-binding subunit clpX-like, mitochondrial	21.3
Disco-interacting protein 2 homolog B	21.3
Far upstream element-binding protein 2	21.3
Versican core protein	21.3
A disintegrin and metalloproteinase with thrombospondin motifs 12	21.3
Cell division cycle-associated protein 2	21.3
Disco-interacting protein 2 homolog A	21.3
Extracellular matrix protein FRAS1	21.3
RAB6-interacting golgin	21.3
Leiomodin-1	21.3
Solute carrier family 43 member 3	21.3

Protein	ASP
Structural maintenance of chromosomes protein 1A	21.3
COP9 signalosome complex subunit 7a	21.3
Centrosomal protein of 135 kDa	21.2
Solute carrier family 22 member 6	21.2
Ankyrin-3	21.2
Uveal autoantigen with coiled-coil domains and ankyrin repeats	21.2
GTPase IMAP family member 8	21.2
Potassium voltage-gated channel subfamily H member 2	21.2
Na(+)/H(+) exchange regulatory cofactor NHE-RF3	21.2
Uncharacterized protein C3orf32 homolog	21.2
Protein Shroom2	21.2
Voltage-dependent T-type calcium channel subunit alpha-1I	21.2
Cadherin-23	21.2
Protein phosphatase 1 regulatory subunit 14A	21.2
Leucine-rich repeat and WD repeat-containing protein 1	21.1
Ankyrin repeat domain-containing protein 17	21.1
Rho-guanine nucleotide exchange factor	21.1
Tctex1 domain-containing protein 3	21.1
Tetratricopeptide repeat protein 16	21.1
Alpha-L-iduronidase	21.1
Adenomatous polyposis coli protein	21.1
Histone H2B type 1-C/E/F/G/I	21.1
Protein phosphatase 1 regulatory subunit 3A	21.1
Autophagy-related protein 2 homolog A	21.1
Advillin	21.1
Fibrinogen-like protein 1	21.1
Methylthioribose-1-phosphate isomerase	21.1
Lysyl oxidase homolog 4	21.1
Cerebellar degeneration-related protein 2	21.1

Protein	ASP
Ephrin type-A receptor 8	21.1
Serine/threonine-protein phosphatase 1 regulatory subunit 10	21.1
Tyrosine-protein kinase-protein kinase SgK269	21.1
Carboxypeptidase A5	21.1
Serine protease inhibitor Kazal-type 2	21.1
Ewing's tumor-associated antigen 1 homolog	21.0
Uncharacterized protein C6orf222 homolog	21.0
Coagulation factor VII	21.0
Calmodulin-regulated spectrin-associated protein 1-like protein 1	21.0
Centrosomal protein of 57 kDa	21.0
Tyrosine-protein phosphatase non-receptor type 2	21.0
Teneurin-1	21.0
Nicotinamide phosphoribosyltransferase	21.0
Zinc finger protein 512	21.0
Coiled-coil domain-containing protein 61	21.0
E1A-binding protein p400	21.0
Matrix-remodeling-associated protein 5	21.0
Protein SDA1 homolog	21.0
Sodium/potassium-transporting ATPase subunit alpha-2	21.0
Cytochrome c oxidase subunit 4 isoform 1	21.0
Mesoderm posterior protein 1	21.0
Mucosal pentraxin	21.0
Inhibin beta B chain	21.0
Major facilitator superfamily domain-containing protein 2	21.0
Tudor domain-containing protein 7	21.0
Calpain-3	20.9
Long palate, lung and nasal epithelium carcinoma-associated protein 3	20.9

Protein	ASP
Phosphoinositide 3-kinase regulatory subunit 4	20.9
Protein phosphatase Slingshot homolog 1	20.9
Phosphatidylinositol 3,4,5-trisphosphate-dependent Rac exchanger 1 protein	20.9
Cytochrome c oxidase subunit 5A, mitochondrial	20.9
UPF0501 protein KIAA1430 homolog	20.9
Netrin-4 precursor	20.9
Vomeronasal type-1 receptor 2	20.9
Thyroid adenoma-associated protein homolog	20.9
Uncharacterized protein C12orf24 homolog	20.9
Neurobeachin-like protein 2	20.9
Rho GTPase-activating protein 23	20.9
Secernin-3	20.9
Rab3 GTPase-activating protein catalytic subunit	20.9
Glutaminase kidney isoform, mitochondrial	20.9
Proteasome subunit beta type-10	20.9
Translocation protein SEC63 homolog	20.9
Methylcrotonoyl-CoA carboxylase subunit alpha, mitochondrial	20.8
Semenogelin-2	20.8
THO complex subunit 2	20.8
Leucine-rich repeat and death domain-containing protein	20.8
Mitochondrial Rho GTPase 1	20.8
Tubulin beta-6 chain	20.8
Toll-like receptor 2	20.8
Secretory phospholipase A2 receptor	20.8
Alanine aminotransferase 1	20.8
Coiled-coil domain-containing protein 125	20.8
Hepatocyte growth factor receptor	20.8
Sterol regulatory element-binding protein 2	20.8

Protein	ASP
Polycomb group RING finger protein 6	20.8
Scavenger receptor class A member 3	20.8
Ankyrin repeat domain-containing protein 13A	20.7
Protein Shroom1	20.7
Uncharacterized protein C9orf79	20.7
Coiled-coil domain-containing protein 154	20.7
Semaphorin-6D	20.7
Cysteine and histidine-rich domain-containing protein 1	20.7
Ubiquinone biosynthesis methyltransferase COQ5, mitochondrial	20.7
Glutathione S-transferase A2	20.7
IQ domain-containing protein H	20.7
WD repeat-containing protein 78	20.7
Protein capicua homolog	20.7
Fetal and adult testis-expressed transcript protein homolog	20.7
AP-3 complex subunit beta-1	20.7
Probable G-protein coupled receptor 150	20.7
Orexigenic neuropeptide QRFP	20.7
PAXIP1-associated protein 1	20.7
Serpin B7	20.6
Rho GTPase-activating protein 24	20.6
Clusterin	20.6
Glutathione synthetase	20.6
F-box only protein 30	20.6
Dynamin-1	20.6
Mucin-5B	20.6
Proteasome-associated protein ECM29	20.6
Coiled-coil domain-containing protein 64A	20.6
Coiled-coil and C2 domain-containing protein 2A	20.6

Protein	ASP
Golgi integral membrane protein 4	20.6
NACHT, LRR and PYD domains-containing protein 1	20.6
Tetratricopeptide repeat protein 21B	20.5
Microtubule-associated serine/threonine-protein kinase-like	20.5
Niemann-Pick C1 protein	20.5
Transmembrane protein 131-like	20.5
Cell division cycle-associated protein 3	20.5
Importin subunit alpha-4	20.5
Laminin subunit beta-2	20.5
Serine/threonine-protein kinase Nek9	20.5
High affinity cAMP-specific and IBMX-insensitive 3',5'-cyclic phosphodiesterase 8A	20.5
Tubulin beta-5 chain	20.5
Usherin	20.5
Coiled-coil and C2 domain-containing protein 1B	20.5
NADH-ubiquinone oxidoreductase chain 4L	20.5
Proprotein convertase subtilisin/kexin type 6	20.5
Phospholipase B1, membrane-associated	20.5
Signal-induced proliferation-associated 1-like protein 1	20.4
Probable E3 ubiquitin-protein ligase HERC2	20.4
Neurolysin, mitochondrial	20.4
Leucine-rich repeats and immunoglobulin-like domains protein	20.4
TIR domain-containing adapter molecule 1	20.4
General transcription factor IIH subunit 2	20.4
Liprin-alpha-4	20.4
Pyruvate kinase isozyme R	20.4
Fibrillin-2	20.4
Eukaryotic translation initiation factor 3 subunit H	20.4
Fibronectin type 3 and ankyrin repeat domains 1 protein	20.4

Protein	ASP
Vasculin	20.4
Serum amyloid A protein	20.4
CD160 antigen	20.4
Serine/threonine-protein kinase N1	20.4
Protein EMSY	20.3
Cadherin EGF LAG seven-pass G-type receptor 3	20.3
Putative Polycomb group protein ASXL3	20.3
Protein FAM81A	20.3
Gamma-aminobutyric acid receptor subunit theta precursor	20.3
Glycine receptor subunit alpha-3	20.3
Leucine-rich repeat and coiled-coil domain-containing protein 1	20.3
TBC1 domain family member 4	20.3
Cytoskeleton-associated protein 2-like	20.3
Nuclear receptor corepressor 1	20.3
Centrobin	20.3
Oligophrenin-1	20.3
Putative CDC37-like protein ENSP00000350273	20.3
Werner syndrome ATP-dependent helicase homolog	20.2
Zinc finger protein DZIP1L	20.2
5-aminolevulinate synthase, erythroid-specific, mitochondrial	20.2
Agrin	20.2
MACRO domain-containing protein 1	20.2
Lupus brain antigen 1 homolog	20.2
InaD-like protein	20.2
Retinol-binding protein 3	20.2
Sterol regulatory element-binding protein 1	20.2
Telomeric repeat-binding factor 2	20.2
Disintegrin and metalloproteinase domain-containing protein 20	20.2
Prostate stem cell antigen	20.2

Protein	ASP
Reticulon-3	20.2
Formin-1	20.2
Protein Niban	20.2
1-phosphatidylinositol-4,5-bisphosphate phosphodiesterase delta-4	20.2
Aminopeptidase N	20.2
Cyclin-dependent kinase inhibitor 2A, isoform 1	20.2
Fc receptor-like B	20.2
Formimidoyltransferase-cyclodeaminase	20.2
Nucleolar complex protein 3 homolog	20.2
Pancreatic lipase-related protein 1	20.1
Argininosuccinate lyase	20.1
Enoyl-CoA hydratase domain-containing protein 1	20.1
Rab GDP dissociation inhibitor beta	20.1
Guanine nucleotide-binding protein-like 3	20.1
Putative E3 ubiquitin-protein ligase SH3RF1	20.1
Apoptosis regulatory protein Siva	20.1
Spermatogenesis-associated protein 7 homolog	20.1
Myomesin-1	20.1
Microtubule-associated serine/threonine-protein kinase 4	20.1
Polyamine-modulated factor 1-binding protein 1	20.1
Beta-crystallin A1	20.1
ATP-binding cassette sub-family A member 5	20.1
Disintegrin and metalloproteinase domain-containing protein	20.1
Ras-related protein Rab-3C	20.1
ATP-binding cassette transporter sub-family C member 8	20.0
Protein MAK10 homolog	20.0
Probable urocanate hydratase	20.0
Protein MICAL-3	20.0

Protein	ASP
Uncharacterized protein C10orf88 homolog	20.0
Dimethylaniline monooxygenase [N-oxide-forming] 4	20.0
Follitropin subunit beta	20.0
Solute carrier organic anion transporter family member 1B2	20.0
Paired amphipathic helix protein Sin3b	20.0
Vinculin	20.0
Eukaryotic translation initiation factor 4B	20.0
Sex-determining region Y protein	20.0
Interferon-induced very large GTPase 1	19.9
Nuclear mitotic apparatus protein 1	19.9
Coagulation factor V	19.9
Protocadherin Fat 2	19.9
Junction-mediating and -regulatory protein	19.9
Uncharacterized protein KIAA1680	19.9
Microtubule-associated protein 4	19.8
Zinc finger ZZ-type and EF-hand domain-containing protein 1	19.8
Uncharacterized protein C19orf44 homolog	19.8
Synaptonemal complex central element protein 1	19.7
Poly(ADP-ribose) glycohydrolase	19.6
Coiled-coil domain-containing protein 57	19.6
Threonine synthase-like 1	19.6
Centromere-associated protein E	19.6
E3 ubiquitin-protein ligase MARCH7	19.5
Telomere-associated protein RIF1	19.5
Stress-induced-phosphoprotein 1	19.5
Sodium/potassium-transporting ATPase subunit beta-2	19.4
Voltage-dependent L-type calcium channel subunit alpha-1C	19.4
Sulfide:quinone oxidoreductase, mitochondrial	19.4
Leukocyte receptor cluster member 1 homolog	19.3

Protein	ASP
Citron Rho-interacting kinase	19.2
Afadin	19.2
Dimethylaniline monooxygenase [N-oxide-forming] 5	19.2
Nuclear autoantigenic sperm protein	19.1
Toll-like receptor 4	19.1
Cystic fibrosis transmembrane conductance regulator	19.1
EF-hand calcium-binding domain-containing protein 5	19.1
Neurogenic locus notch homolog protein 3	19.1
Fibrinogen alpha chain	19.1
Uncharacterized protein KIAA1310 homolog	19.0
Sperm flagellar protein 2	19.0
Leucine-rich repeat-containing protein 18	19.0
Methionine synthase	19.0
Uncharacterized protein C18orf19 homolog	19.0
UPF0681 protein KIAA1033	18.9
Coiled-coil domain-containing protein 54	18.9
Cytochrome b	18.8
Disco-interacting protein 2 homolog C	18.8
Disintegrin and metalloproteinase domain-containing protein 2	18.7
Amyloid beta A4 precursor protein-binding family A member 3	18.7
Nestin	18.7
Kinetochore protein NDC80 homolog	18.7
Putative COBW domain-containing protein 7	18.6
RE1-silencing transcription factor	18.6
Protein FAM65C	18.6
Hornerin	18.6
A-kinase anchor protein 9	18.5
Chromobox protein homolog 2	18.5
Talin-2	18.5

Protein	ASP
14-3-3 protein zeta/delta	18.5
Peroxiredoxin-2	18.4
Microtubule-actin cross-linking factor 1	18.4
Proteoglycan 4	18.4
Spermatogenesis-associated protein 17	18.3
Ryanodine receptor 2	18.3
Taste receptor type 1 member 2	18.3
Vacuolar protein sorting-associated protein 13B	18.3
Fatty acid synthase	18.2
Serine/threonine-protein kinase 10	18.2
Serine/threonine-protein kinase MRCK beta	18.2
Guanylate-binding protein 6	18.1
Neurogenic locus notch homolog protein 4	18.0
Serotransferrin precursor	18.0
Mucin-5AC	18.0
Mitogen-activated protein kinase kinase kinase 12	18.0
Probable methylcytosine dioxygenase TET2	17.9
Enhancer of polycomb homolog 1	17.9
Receptor-type tyrosine-protein phosphatase N2	17.9
Dedicator of cytokinesis protein 9	17.9
Uncharacterized protein FLJ44048 homolog	17.9
Uncharacterized protein KIAA1109	17.8
Gag-Pro-Pol polyprotein	17.8
NADH-ubiquinone oxidoreductase chain 2	17.8
Ankyrin repeat domain-containing protein 30A	17.8
UDP-glucose:glycoprotein glucosyltransferase 1	17.8
Capsid polyprotein	17.7
EH domain-binding protein 1-like protein 1	17.7
Cell division cycle-associated 7-like protein	17.7

Protein	ASP
Acetyl-CoA carboxylase 2	17.7
Tetratricopeptide repeat protein 28	17.7
Voltage-dependent N-type calcium channel subunit alpha-1B	17.7
Tudor and KH domain-containing protein	17.7
Thrombospondin type-1 domain-containing protein 7B	17.7
Coiled-coil domain-containing protein 138	17.6
Protein disulfide-isomerase A4	17.6
UPF0474 protein C5orf41	17.6
Ankyrin repeat domain-containing protein 31	17.5
Talin-1	17.4
Protein tyrosine kinase 2 beta	17.4
Protein KIAA1881	17.4
Fibulin-7	17.4
Meiotic recombination protein REC8 homolog	17.3
Sulfotransferase 1C2	17.3
Coiled-coil alpha-helical rod protein 1	17.2
Histone deacetylase 9	17.1
Interleukin-10	17.0
Carnitine O-palmitoyltransferase 1, muscle isoform	17.0
Stabilin-1	16.9
Lebercilin-like protein	16.9
Nuclear receptor coactivator 6	16.9
Strumpellin	16.8
Intraflagellar transport protein 172 homolog	16.8
Centrosomal protein of 164 kDa	16.8
Uncharacterized protein KIAA0556	16.7
Macoilin	16.7
Cytosolic carboxypeptidase 3	16.6
Dapper homolog 2	16.6

Protein	ASP
von Willebrand factor A domain-containing protein 3A	16.6
Phosphoserine phosphatase	16.5
Apolipoprotein B-100	16.4
Synaptonemal complex protein 2	16.4
Intersectin-1	16.3
Tumor necrosis factor receptor superfamily member 8	16.1
Rho GTPase-activating protein 22	16.1
LYR motif-containing protein 1	16.0
Follicle-stimulating hormone receptor	15.9
Guanine nucleotide exchange factor VAV3	15.9
WD repeat-containing protein 62	15.9
Lipopolysaccharide-responsive and beige-like anchor protein	15.8
Retinitis pigmentosa 1-like 1 protein	15.8
Putative glycerol kinase 5	15.7
Coiled-coil domain-containing protein 74A	15.7
Transcription elongation factor SPT6	15.6
Zinc finger protein 536	15.5
USP6 N-terminal-like protein	15.5
WD repeat-containing protein 48	15.4
Vasopressin V1a receptor	14.3
Transcription factor TFIIIB component B'' homolog	14.0
WD repeat-containing protein 19	13.6
Protein unc-45 homolog B	13.6
Uncharacterized protein FLJ40521	13.0
Vascular endothelial growth factor receptor 1	12.9
Ufm1-specific protease 2	12.7
Coiled-coil domain-containing protein 52	12.3
Zinc finger CCCH domain-containing protein 13	12.2

Chapter 12 Bibliography

PTTG-Binding Factor (PBF) Is a Novel Regulator of the Thyroid Hormone Transporter MCT8

V. E. Smith, M. L. Read, A. S. Turnell, N. Sharma, G. D. Lewy, J. C. W. Fong, R. I. Seed, P. Kwan, G. Ryan, H. Mehanna, S. Y. Chan, V. M. Darras, K. Boelaert, J. A. Franklyn, and C. J. McCabe

School of Clinical and Experimental Medicine (V.E.S., M.L.R., N.S., G.D.L., J.C.W.F., R.I.S., P.K., G.R., S.Y.C., K.B., J.A.F., C.J.M.), Institute of Biomedical Research, and School of Cancer Sciences (A.S.T.), University of Birmingham, B15 2TT, United Kingdom; Institute of Head and Neck Studies and Education (H.M.), University Hospitals Coventry and Warwickshire National Health Service Trust, Coventry, CV2 2DX, United Kingdom; and Laboratory of Comparative Endocrinology, Animal Physiology, and Neurobiology (V.M.D.), Katholieke Universiteit Leuven, Naamsestraat 61, B-3000 Leuven, Belgium

Within the basolateral membrane of thyroid follicular epithelial cells, two transporter proteins are central to thyroid hormone (TH) biosynthesis and secretion. The sodium iodide symporter (NIS) delivers iodide from the bloodstream into the thyroid, and after TH biosynthesis, monocarboxylate transporter 8 (MCT8) mediates TH secretion from the thyroid gland. Pituitary tumor-transforming gene-binding factor (PBF; PTTG1IP) is a protooncogene that is up-regulated in thyroid cancer and that binds NIS and modulates its subcellular localization and function. We now show that PBF binds MCT8 *in vitro*, eliciting a marked shift in MCT8 subcellular localization and resulting in a significant reduction in the amount of MCT8 at the plasma membrane as determined by cell surface biotinylation assays. Colocalization and interaction between PBF and Mct8 was also observed *in vivo* in a mouse model of thyroid-specific PBF overexpression driven by a bovine thyroglobulin (Tg) promoter (PBF-Tg). Thyroidal Mct8 mRNA and protein expression levels were similar to wild-type mice. Critically, however, PBF-Tg mice demonstrated significantly enhanced thyroidal TH accumulation and reduced TH secretion upon TSH stimulation. Importantly, Mct8-knockout mice share this phenotype. These data show that PBF binds and alters the subcellular localization of MCT8 *in vitro*, with PBF overexpression leading to an accumulation of TH within the thyroid *in vivo*. Overall, these studies identify PBF as the first protein to interact with the critical TH transporter MCT8 and modulate its function *in vivo*. Furthermore, alongside NIS repression, PBF may thus represent a new regulator of TH biosynthesis and secretion. **(*Endocrinology* 153: 3526–3536, 2012)**

Pituitary tumor-transforming gene (PTTG)-binding factor (PBF; PTTG1IP) (1) is a protooncogene implicated in endocrine cancer. Widely expressed in normal tissue (1, 2), PBF is overexpressed in a number of tumors including thyroid (3), pituitary (4), and breast (5). In thyroid cancer, higher PBF expression is independently associated with early tumor recurrence (3).

The primary function of PBF remains unknown. However, some functional information has been obtained through its interactions with other proteins. PBF was first identified through its interaction with the human securin PTTG and is thought to promote the nuclear translocation of PTTG in a manner dependent upon the nuclear localization signal at the C-terminal end of PBF (2).

More recently, we have demonstrated an interaction with the sodium iodide symporter (NIS), an integral membrane glycoprotein located in the basolateral plasma membrane of thyroid follicular epithelial cells (6). NIS is responsible for mediating iodide uptake and is consequently essential for thyroid hormone (TH) synthesis. Although

ISSN Print 0013-7227 ISSN Online 1945-7170
Printed in U.S.A.

doi: 10.1210/en.2011-2030 Received November 25, 2011. Accepted April 11, 2012.
First Published Online April 25, 2012

Abbreviations: GST, Glutathione-S-transferase; HA, hemagglutinin; KO, knockout; MCT8, monocarboxylate transporter 8; NIS, sodium iodide symporter; PBF, PTTG-binding factor; PTTG, pituitary tumor-transforming gene; Tg, thyroglobulin; TH, thyroid hormone; VO, vector only; WT, wild type.

radioiodine has long been used to successfully image and treat tumors of the thyroid and their metastases, many of these cancers demonstrate reduced iodide uptake and those with reduced NIS activity are generally associated with a poor prognosis (7).

Through investigating the mechanisms underlying the repression of NIS activity, we found that PBF inhibited iodide uptake and NIS expression *in vitro* (8). Furthermore, we elucidated a posttranslational mechanism of NIS repression by which PBF binds NIS and alters its subcellular localization, thereby regulating its ability to uptake iodide (6). These data were recently recapitulated *in vivo* in a mouse model of thyroid-specific PBF overexpression driven by a bovine thyroglobulin (Tg) promoter (PBF-Tg), where Nis mRNA expression was significantly reduced by approximately 50% and iodide uptake in primary thyroid cell cultures was down-regulated by approximately 70% (9).

These studies led us to question whether other membrane transporters could be similarly regulated by PBF. Monocarboxylate transporter 8 (MCT8) is a highly specific TH transporter (10, 11). Patients with inactivating mutations in the gene encoding MCT8 present with neurological abnormalities including severe psychomotor impairment, strongly suggesting that TH uptake via MCT8, particularly in the brain, is of critical importance. These patients typically have abnormal tests of thyroid function, with high serum free and total T_3, low free and total T_4, low rT_3, and normal-high TSH concentrations (12, 13).

MCT8 is highly expressed in the human thyroid gland (14) and is the most abundant TH transporter in both the human and mouse thyroid (15, 16). Like NIS, MCT8 is expressed in the basolateral membrane of thyroid follicular epithelial cells (15–17). Recent evidence suggests that MCT8 is involved in the secretion of TH from the thyroid after biosynthesis (15, 17). However, there is still little known about the regulation of MCT8 expression and activity (18).

Due to the similarity between MCT8 and NIS in terms of thyroidal subcellular localization and a role in TH biosynthesis and secretion, we investigated a potential relationship between MCT8 and PBF. A physical interaction between MCT8 and PBF was observed *in vitro*. PBF overexpression *in vitro* resulted in a shift in MCT8 subcellular localization from the plasma membrane into intracellular vesicles where the two proteins colocalized both with each other and the late endosome marker CD63. Colocalization between Mct8 and PBF was also observed *in vivo* in the significantly enlarged thyroid gland of the PBF-Tg mouse, and coimmunoprecipitation assays in these thyroid glands revealed an interaction between PBF and Mct8 *in vivo*. The PBF-Tg mouse bears a phenotypic resemblance to the Mct8-knockout (KO) mouse that, as a result of the loss of Mct8-mediated TH secretion, displays enlarged thyroid follicles due to TH accumulation (15, 17). In keeping with this, thyroidal T_3 and T_4 content were significantly elevated and TSH-stimulated T_4 secretion was significantly reduced in our mouse model of thyroidal PBF expression. These studies thus suggest that PBF is a novel interacting partner of MCT8 that may regulate its localization and therefore its function.

Materials and Methods

Cell lines and plasmids

The COS-7 African green monkey kidney epithelial cell line was maintained in DMEM (Life Technologies, Inc., Paisley, Scotland, UK) supplemented with 10% fetal bovine serum, penicillin (10^5 U/liter), and streptomycin (100 mg/liter).

Plasmids containing the full-length PBF cDNA with and without a hemagglutinin (HA) tag have previously been described (3).

The expression vector for human MCT8 with a C-terminal HA tag (MCT8-HA) has been described previously (19). MCT8 cDNA was also subcloned into the *Eco*RI and *Xho*I restriction sites of the pcDNA3.1+ vector (Invitrogen, Carlsbad, CA) with the addition of the Myc epitope at the 3′ end using the forward primer GCC GAA TTC ATG GCG CTG CAA AGC and reverse primer CGG CTC GAG TCA GGA TCC CAG GTC CTC CTC GGA AAT CAG CTT CTG CTC GAT TGG TTC CTC AGG GTT GG (MCT8-MYC).

Cells were transfected using Fugene 6 reagent (Roche, Indianapolis, IN) following the manufacturer's instructions at a 3:1 reagent to DNA ratio. For cell surface biotinylation assays, immunofluorescence staining and coimmunoprecipitation assays, cells were seeded in six-well plates, six-well plates with sterile coverslips, and T25 flasks, respectively, and transfected with 2 μg (six-well) or 5 μg (T25) DNA after 24 h.

In vitro transcription: translation and glutathione-S-transferase (GST) pull-down assays

The TNT coupled reticulocyte lysate system (Promega, Madison, WI) was used to express protein from the MCT8-HA plasmid, and PBF was expressed as a fusion protein with GST from a pGEX plasmid (Amersham Biosciences, Little Chalfont, Buckinghamshire, UK) as described previously (6). Along with a GST protein-only control, 20 μg GST-tagged PBF protein was combined with 10 μl of the L-α-[^{35}S]methionine-labeled MCT8 protein and incubated for 1 h on ice. After the addition of 400 μl of a low-salt buffer [50 mM Tris (pH 7.4), 150 mM NaCl, 1% Nonidet P-40], 40 μl packed glutathione agarose beads was added to each reaction, which was subsequently incubated with end-over-end mixing using a rotator for 90 min at 4 C. After washing with the low-salt buffer, bound GST-PBF protein was eluted with 40 μl 25 mM glutathione in 50 mM Tris (pH 8) on ice for 1 h. The protein samples were then analyzed by SDS-PAGE, using a 12% acrylamide gel, along with 1 μl L-α-[^{35}S]methionine-labeled MCT8 protein in 20 μl Laemmli sample buffer (Bio-Rad Laboratories, Hercules, CA) with 5% (vol/vol) β-mercaptoethanol, used as a control demonstrating 10% input. After electrophoresis, the gel was fixed and stained. The gel was then immersed

in Amplify fluorographic reagent (Amersham) to increase the sensitivity of signal detection, dried at 65 C for 2 h, and finally, exposed to autoradiographic film at −20 C.

Coimmunoprecipitation assays

COS-7 cells in T25 flasks were transiently transfected with MCT8-MYC and pCI-neo vector only (VO), PBF-HA and pcDNA3.1+ (VO), or MCT8-MYC and PBF-HA. Cells were harvested in 500 μl RIPA buffer [50 mM Tris-HCl (pH 7.4), 150 mM NaCl, 1% vol/vol Igepal CA-630, 6 mM sodium deoxycholate, 1 mM EDTA] containing protease inhibitor cocktail (Sigma, Poole, Dorset, UK). After a brief sonication step, cell lysates were centrifuged at 13,000 rpm for 20 min and transferred to a clean microcentrifuge tube. Each lysate was incubated with 10 μl mouse monoclonal anti-Myc-Tag (9B11) antibody (Cell Signaling Technology, Inc., Danvers, MA) at 4 C overnight with end-over-end rotating. After the addition of 25 μl packed beads prepared from protein G Sepharose 4 Fast Flow (Amersham), the samples were incubated for another 2 h at 4 C with end-over-end rotating. Protein G Sepharose beads were centrifuged and, after the removal of any unbound protein, washed four times with 500 μl RIPA buffer. Bound protein was eluted in 50 μl Laemmli sample buffer containing 5% (vol/vol) β-mercaptoethanol and 1% (wt/vol) sodium dodecyl sulfate at 37 C for 30 min.

Proteins were separated by SDS-PAGE using a 12% acrylamide gel and transferred to polyvinylidene difluoride membrane. The membrane was blocked with 5% milk in Tris-buffered saline containing 0.025% Tween 80, and PBF-HA protein was probed with mouse monoclonal anti-HA.11 antibody (Covance Research Products, Emeryville, CA) at a concentration of 1:1000 in blocking buffer. After incubation with 650 ng/ml horseradish peroxidase-conjugated polyclonal rabbit antimouse Ig (Dako, Glostrup, Denmark) as secondary antibody, the antigen-antibody complexes were detected using the ECL-Plus chemiluminescence detection system (Amersham). Total protein cell lysate (20 μg) taken before the coimmunoprecipitation steps was also separated by SDS-PAGE using 12% acrylamide gels to confirm MCT8-MYC and PBF-HA expression. PBF-HA was probed in the same way as the coimmunoprecipitation samples, and MCT8-MYC was detected with mouse anti-Myc antibody at a concentration of 1:1000. β-Actin expression was assessed as a loading control for each protein.

The reciprocal experiment was performed in the same way by precipitating PBF-HA with 10 μl rabbit polyclonal anti-HA (Y-11) antibody (Santa Cruz Biotechnology, Santa Cruz, CA) and probing for coimmunoprecipitated MCT8-MYC with mouse anti-Myc antibody.

Mouse thyroid glands were homogenized in 350 μl RIPA buffer and centrifuged at 13,000 rpm for 10 min. Lysate was pooled from eight wild-type (WT) and six PBF-Tg thyroid glands, and protein concentration was measured using the bicinchoninic acid assay (Pierce, Rockford, IL). Using the method described above with an additional preclearing step consisting of a 2-h incubation at 4 C with 100 μl protein G Sepharose 4 Fast Flow/ml lysate, endogenous Mct8 was immunoprecipitated with 5 μl rabbit anti-MCT8 antibody (Atlas, Stockholm, Sweden) from 0, 0.3, 0.5, and 1 mg WT and PBF-Tg protein lysate. Coimmunoprecipitation of PBF-HA was detected through Western blotting using the mouse monoclonal anti-HA.11 antibody (Covance Research Products).

Immunofluorescence staining

Immunofluorescence staining using COS-7 cells was as carried out as described previously (6). The following antibodies were used: mouse monoclonal anti-HA.11 antibody (Covance Research Products), rabbit polyclonal anti-HA (Y-11) antibody (Santa Cruz Biotechnology), rabbit polyclonal anti-PBF antibody [made by Eurogentec (Seraing, Belgium) for our laboratory using the full-length PBF protein as an epitope], and mouse monoclonal anti-CD63 antibody (kindly provided by Fedor Berditchevski, School of Cancer Sciences, University of Birmingham, Birmingham, UK).

For the preparation of frozen tissue sections, thyroid glands were excised from WT and PBF-Tg mice and fixed in 4% formaldehyde. After cryoprotection of the tissue using an increasing sucrose gradient (10–30%), the tissues were embedded in OCT (Thermo Fisher Scientific, Waltham, MA) and frozen on dry ice. Sections of 6 μm were prepared on a cryostat.

Before staining, the OCT was dissolved in PBS for 10 min, and tissue was permeabilized with 0.1% Triton X-100 (Sigma) for 5 min. After blocking in 10% normal calf serum (NCS) for 1 h, tissues were incubated overnight at 4 C with rabbit anti-MCT8 antibody (Atlas) at 1:500 in 1% BSA. Incubation with secondary antibody Alexa Fluor 594-conjugated goat antirabbit IgG (Invitrogen) was performed at room temperature for 1 h at 1:500 in 1% BSA, with 2% NCS and Hoechst stain for nuclei (1:1000). PBF-HA was stained using mouse monoclonal anti-HA.11 antibody (Covance Research Products) at 1:500 and the Mouse on Mouse (M.O.M.) fluorescein immunodetection kit (Vector Laboratories Inc., Burlingame, CA) following the manufacturer's instructions.

Epifluorescent microscopy was performed using a ×40 objective on a Zeiss Axioplan fluorescent microscope (Zeiss, Oberkochen, Germany). A Zeiss confocal LSM 510 microscope with a ×63 objective was used to perform confocal microscopy.

Cell surface biotinylation

MCT8-MYC and either pCI-neo (VO) or PBF plasmids were transiently transfected into COS-7 cells. Forty-eight hours after transfection, the cell surface protein isolation kit (Pierce) was used to biotinylate and isolate membrane-associated proteins as described previously (6) with some minor modifications. Briefly, cells were exposed to 2× 1 ml EZ-Link Sulfo-NHS-SS-Biotin for 25 min at 4 C followed by 2× 2 ml 100 mM glycine for 20 min at 4 C. Cells from each of two wells of a six-well plate were combined in 700 μl lysis buffer (1% Triton X-100 in PBS) containing protease inhibitor cocktail (Sigma) and vortexed every 15 min for an hour on ice. The lysate was centrifuged at 13,000 × *g* for 15 min at 4 C, and 40 μl of the supernatant was retained as whole-cell lysate. The remaining cell lysate was incubated with immobilized NeutrAvidin gel overnight at 4 C with end-over-end mixing using a rotator, and after washing away unbound protein, membrane proteins were eluted in 100 μl SDS-PAGE sample buffer [62.5 mM Tris-HCl (pH 6.8), 3% sodium dodecyl sulfate, 10% glycerol] containing 70 mM dithiothreitol for 1 h at room temperature with end-over-end rotating.

MCT8-MYC was detected in the membrane protein and whole-cell lysate fractions through immunoblotting. Proteins were separated by SDS-PAGE using a 10% acrylamide gel, and MCT8 protein was probed with mouse monoclonal anti-Myc-Tag (9B11) antibody at a concentration of 1:1000, followed by

secondary antibody, 650 ng/ml horseradish peroxidase-conjugated polyclonal rabbit antimouse Ig (Dako). Membranes were subsequently reprobed with mouse monoclonal anti-flotillin-1 antibody (BD Biosciences, Franklin Lakes, NJ) at 1:1000 to determine equal protein loading (6). Experiments were carried out on three separate occasions, and scanning densitometry used to quantitate mean changes in expression *vs.* flotillin controls.

Mct8 mRNA and protein expression measurement

Total RNA was extracted from mouse thyroids using the RNeasy Micro Kit (QIAGEN, Hilden, Germany) and reverse transcribed using the reverse transcription system (Promega), as previously described (9). Expression of Mct8 mRNA was determined by quantitative PCR (8) using the TaqMan gene expression assay Mm00486202_m1 with analysis on the 7500 real-time PCR system (Applied Biosystems, Foster City, CA). Mct8 mRNA expression was normalized to the expression of the housekeeping gene 18s by subtracting the 18s cycle threshold (Ct) values from the Mct8 Ct values for each sample (ΔCt). Protein extracted from homogenized thyroid glands in RIPA buffer was analyzed by Western blotting using the rabbit anti-MCT8 antibody (Atlas) at 1:500.

Thyroidal TH content analysis

WT and transgenic PBF-Tg (thyroid-targeted expression of PBF-HA) mice were bred at the University of Birmingham and all experiments performed in accordance with United Kingdom Home Office regulations. The generation of the transgenic PBF-Tg line has been described previously (9).

Thyroid glands were harvested from 8-wk-old WT and PBF-Tg mice. After weighing, glands were frozen and stored at −80 C until analysis of non-Tg-bound and total hormone content as described before (17). Thyroid glands were homogenized in 500 μl ice-cold barbital buffer (0.05 M, pH 8.6) using a glass/Teflon Potter tissue grinder system. This first step was followed by additional ultrasonic homogenization (twice for 25 sec). Homogenates were then centrifuged and supernatants were transferred to new tubes. Part of the supernatant was directly frozen and stored at −20 C, and 150 μl of the supernatant was used for enzymatic degradation of Tg by addition of 150 μl protease [Sigma P-5147, 6.25 mg protease, and 3.13 mg 2-thiouracil in 10 ml Tris-HCl buffer 0.75 M (pH 8.8)] and 15 μl toluol. Tubes were stoppered and incubated for 2 d in a shaking water bath at 37 C. Finally, tubes were placed in boiling water for 2 min to inactivate the Pronase enzyme, frozen, and stored at −20 C. T_4 and T_3 concentrations were measured by RIA (20) in dilutions of untreated homogenates (non-Tg hormone levels) and enzymatically digested homogenates (total hormone levels) and non-Tg and total hormone content were calculated per thyroid gland.

T_4 and T_3 concentrations were also measured in serum obtained from the same mice using 25 and 100 μl serum, respectively, by RIA (MP Biomedicals, Santa Ana, CA).

TSH stimulation test

WT (n = 10) and PBF-Tg (n = 14) mice were treated with daily ip injections of 5 μg L-T_3 (Sigma) for 4 d to suppress endogenous TSH and basal T_4 concentration. Blood was obtained from the tail vein to provide a basal level of T_4 before administration of 50 mU bovine TSH (Sigma) via ip injection. Both L-T_3 and TSH were administered in PBS with 0.02% BSA. After 3 h, blood was obtained via cardiac puncture, and all animals were euthanized humanely. T_4 concentrations were measured using 25 μl serum using RIA (MP Biomedicals).

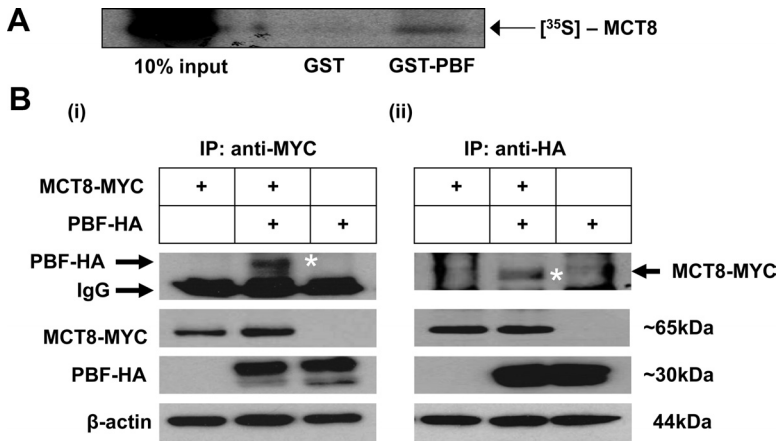

FIG. 1. PBF binds MCT8 in vitro. A, Pull-down assay showing *in vitro*-translated L-α-[^{35}S]methionine-labeled MCT8 binding GST-tagged PBF *vs.* a GST-only control. B, Coimmunoprecipitation assays in COS-7 cells transfected with MCT8-MYC and VO, MCT8-MYC and PBF-HA, or PBF-HA and VO. i, After immunoprecipitation (IP) with the anti-MYC antibody, a band corresponding to PBF (*arrows* and *asterisk*) was observed at approximately 30 kDa in lysates transfected with both MCT8-MYC and PBF-HA but was not present when either MCT8-MYC or PBF-HA was transfected with VO. Analysis of total protein cell lysate shown below demonstrates the presence of MCT8-MYC or PBF-HA in each sample along with a β-actin loading control. IgG is light-chain Ig. (ii) Reciprocal assay whereby MCT8-MYC was coprecipitated along with PBF-HA and detected as a band at approximately 65 kDa (*arrows* and *asterisk*).

Results

PBF binds MCT8 *in vitro*

To investigate PBF and MCT8 binding *in vitro*, pull-down assays were performed with *in vitro*-translated L-α-[^{35}S]methionine-labeled MCT8 and GST-tagged PBF. Binding reactions consistently demonstrated an interaction between labeled MCT8 and GST-PBF but not with a GST protein-only control (Fig. 1A).

Coimmunoprecipitation assays were subsequently used to assess this interaction in a more physiological, cellular environment, given that *in vitro*-translated MCT8 may not be processed correctly. After the transient transfection of HA-tagged PBF (PBF-HA) and MYC-tagged MCT8 (MCT8-MYC) into COS-7 cells, MCT8-MYC was precipitated from the cell lysate with an anti-MYC antibody. Probing with an

anti-HA antibody after Western blotting established that PBF-HA had coprecipitated along with MCT8-MYC (Fig. 1Bi). In contrast, PBF remained undetected in controls in which MCT8-MYC and VO or PBF-HA and VO were transfected (Fig. 1Bi). The reciprocal coimmunoprecipitation assay, in which PBF-HA was precipitated using the anti-HA antibody, confirmed coimmunoprecipitation of MCT8-MYC after immunoblotting with the anti-MYC antibody (Fig. 1Bii). Finally, a mass spectrometry screen to detect binding partners of PBF in K1 thyroid carcinoma cells also detected coimmunoprecipitation of MCT8 (data not shown). Thus, GST pull-down assays, coimmunoprecipitation assays, and mass spectrometry experiments all demonstrated that PBF and MCT8 bind *in vitro*.

MCT8 colocalizes with PBF *in vitro*

We have demonstrated previously that HA-tagged MCT8 (MCT8-HA) showed intense cell surface expression after transient transfection into the pluripotent human central nervous system precursor NT2 cell line and colocalized with the plasma membrane marker CD8 (19). In the present studies, the subcellular localization of exogenous MCT8-HA and PBF was analyzed using immunofluorescent staining in COS-7 cells, which are highly amenable to immunofluorescent studies. As seen in NT2 cells, MCT8-HA was observed predominantly at the plasma membrane (Fig. 2A). As shown previously (6), endogenous PBF was expressed at relatively low levels in the nucleus, whereas the majority of PBF protein was concentrated within intracellular vesicles in the cytoplasm (Fig. 2A). When PBF was cotransfected along with MCT8-HA, there was an apparent increase in MCT8 staining within intracellular vesicles and a concomitant reduction in membrane staining (Fig. 2B). Merged images demonstrated strong colocalization between PBF and MCT8-HA, particularly within vesicles (Fig. 2B).

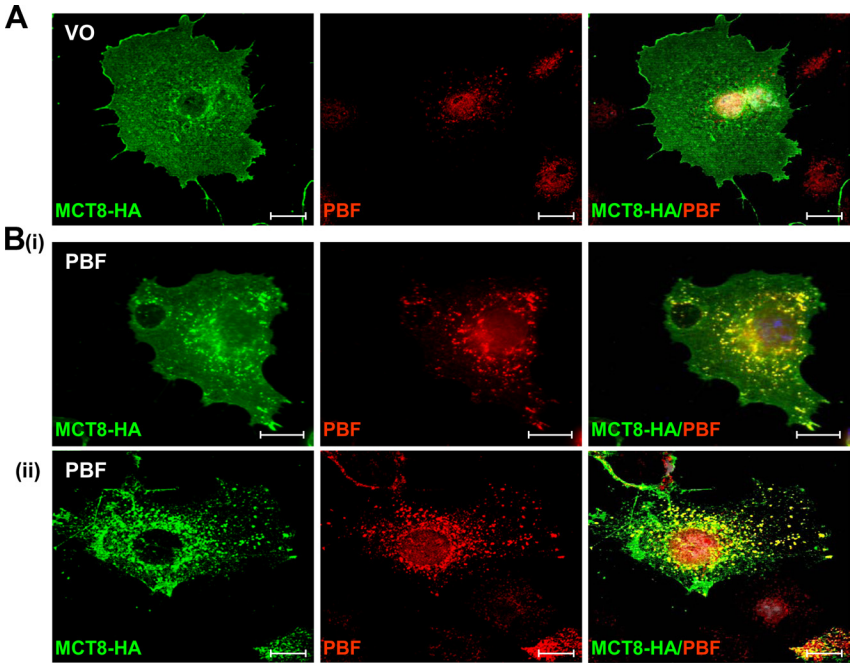

FIG. 2. MCT8 and PBF localization in COS-7 cells. A, Confocal images of MCT8-HA after cotransfection with a VO control into COS-7 cells, and endogenous PBF, both detected by immunofluorescent analysis. MCT8-HA (*green*) was located predominantly within the plasma membrane, whereas endogenous PBF (*red*) was found in the nucleus and within intracellular vesicles. B, Representative fluorescent immunocytochemistry experiments examining staining of PBF (*red*) and MCT8-HA (*green*) after transient cotransfection into COS-7 cells using both epifluorescent (i) and confocal (ii) microscopy. PBF was predominantly expressed within cytoplasmic vesicles. MCT8-HA demonstrated increased staining within intracellular vesicles where it strongly colocalized with PBF, as seen in *yellow* in the merged images. *Scale bars*, 20 μm.

PBF alters the subcellular localization of MCT8

Given the apparent alteration in MCT8 localization, we next investigated by quantitative means whether PBF overexpression was associated with diminished MCT8 localization at the cell membrane, where it serves as a functional transporter. COS-7 cells were transfected with MCT8-MYC and either VO control or PBF, and cell surface biotinylation assays were performed. Compared with VO treatment, there was a significant reduction in MCT8 expression at the plasma membrane after PBF transfection ($56 \pm 7\%$ reduction, $P = 0.005$, $n = 3$) (Fig. 3A). Total MCT8-MYC expression was not significantly altered by PBF overexpression compared with VO ($10 \pm 7\%$ reduction, $P = 0.245$, $n = 3$) (Fig. 3B), confirming an alteration in localization rather than an overall reduction in MCT8 expression. Hence, plasma membrane expression of MCT8 was significantly reduced with PBF overexpression in COS-7 cells.

MCT8 colocalization with CD63

We have previously demonstrated colocalization of both PBF and NIS with endogenous expression of the late endosome marker CD63, a member of the tetraspanin family that is commonly associated with clathrin-dependent trafficking (6). Upon transfection of PBF-HA into COS-7 cells, we again showed a high degree of colocalization between PBF and CD63 (Fig. 4A). When MCT8-HA was transfected into COS-7 cells, there was no apparent association between MCT8 and CD63 staining (Fig. 4Bi). However, after cotransfection of PBF, the vesicles in which MCT8 was now detected showed strong colocalization with endogenous CD63 (Fig. 4Bii). This sug-

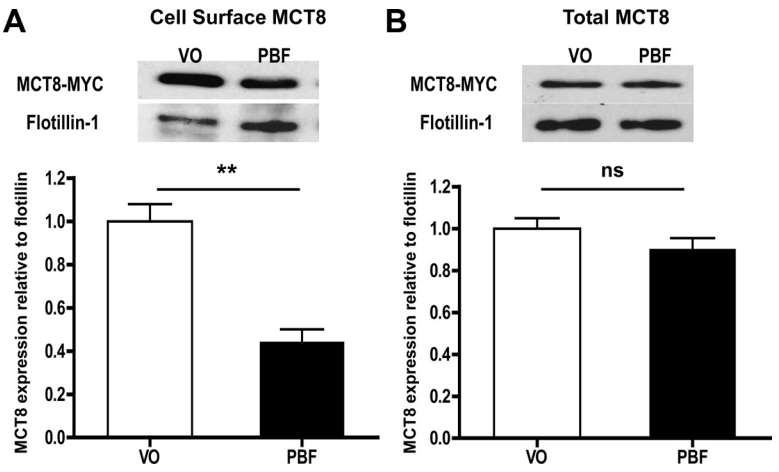

FIG. 3. PBF alters the subcellular localization of NIS. Cell surface biotinylation assays in COS-7 cells transfected with a VO control or with human PBF. A, Representative immunoblot analysis of surface-biotinylated proteins precipitated with streptavidin-agarose beads and probed with anti-MYC antibody, which revealed MYC-tagged human MCT8 detection at around 60 kDa. Flotillin-1 was used as a marker of membrane protein expression to determine loading between samples. *Bottom panel*, Three separate experiments were performed, with scanning densitometry used to quantify mean differences in cell surface expression of MCT8, relative to alterations in flotillin-1 expression. B, Representative immunoblot analysis of total MCT8-MYC protein expression with results of densitometry shown *below*, demonstrating no significant alteration in expression after PBF overexpression. Data are presented as mean ± SEM. **, $P < 0.01$; ns, not significant.

gests that the vesicles in which MCT8 was observed are late endosomes and that the mechanism by which PBF alters the subcellular localization of MCT8 may involve clathrin-dependent endocytosis.

Mct8 expression in an *in vivo* model of thyroidal PBF overexpression

Given that PBF binds MCT8 and alters its subcellular localization, we next investigated Mct8 expression and function *in vivo* in a mouse model in which HA-tagged PBF overexpression is targeted specifically to the thyroid gland (PBF-Tg) (9). Compared with WT mice, thyroidal Mct8 mRNA expression was unaltered in PBF-Tg mice (mean ΔCt: PBF-Tg = 10.49 ± 0.13; *cf.* WT = 10.35 ± 0.13, $P = 0.482$, n = 6) (Fig. 5Ai). Thyroidal Mct8 protein expression, as determined by Western blot analysis, was also similar in WT and PBF-Tg mice (0.98 ± 0.07-fold, $P = 0.878$, n = 8) (Fig. 5Aii). Thus, in keeping with the *in vitro* data above, high expression of PBF *in vivo* did not alter Mct8 expression in the thyroid.

PBF and Mct8 colocalization and interaction *in vivo*

To further investigate an association between PBF and Mct8 *in vivo*, frozen sections of thyroid glands taken from PBF-Tg mice were immunofluorescently labeled using HA and MCT8 antibodies. PBF-HA and Mct8 showed intense areas of colocalization, predominantly within the cytoplasm of the thyroid follicular epithelial cells of the PBF-Tg mice (Fig. 5B). To determine whether these proteins interact within these regions of colocalization, coimmunoprecipitation assays were performed on protein lysate extracted from mice thyroid glands. After the immunoprecipitation of endogenous Mct8, a band of rising intensity corresponding to PBF-HA was detected in increasing amounts of protein lysate from PBF-Tg thyroid glands but not in equivalent amounts of lysate taken from WT thyroids (Fig. 5C). In addition, examination of Mct8 localization in the thyroid follicular epithelial cells of WT mice revealed strong basolateral membrane expression (Fig. 5Di) that is in agreement with published data (15–17) and that appeared markedly reduced in the PBF-Tg thyroid cells (Fig. 5Dii). Hence, PBF and Mct8 colocalize and interact within the thyroid *in vivo* and, in keeping with our *in vitro* data, there appears to be a shift in the subcellular localization of Mct8 in the presence of PBF overexpression.

Increased TH levels in the PBF-Tg thyroid glands

Given the reduction in cell surface MCT8 expression after PBF overexpression *in vitro*, we hypothesized that increased levels of PBF might result in diminished TH secretion from the thyroid. To test this, thyroidal TH content was analyzed in 8-wk-old WT (n = 8) and PBF-Tg (n = 10) mice. Mean thyroid weight for these WT and PBF-Tg mice were 2.25 ± 0.12 and 5.54 ± 0.26 mg, respectively. Thyroidal non-Tg-bound TH content in the PBF-Tg mice was significantly higher compared with WT mice. Non-Tg-T_3 content in the PBF-Tg thyroid glands was 1.9-fold higher than in WT thyroids (11.5 ± 1.2 *vs.* 6.2 ± 0.7 ρmol/thyroid, $P = 0.004$) (Fig. 6Ai), and non-Tg-T_4 content was increased 2.4-fold (339.5 ± 41.8 *vs.* 144.3 ± 25.8 ρmol/thyroid, $P = 0.002$) (Fig. 6Aii). Tg-bound T_3 content was increased 1.9-fold in PBF-Tg thyroid glands, although this was not significantly higher than in their WT counterparts (567.8 ± 113.9 *vs.* 293.2 ± 62.7 ρmol/thyroid, $P = 0.100$) (Fig. 6Bi). Thyroidal Tg-T_4 content was 4.2-fold higher in PBF-Tg mice than in WT mice (8349.5 ± 1966.2 *vs.* 1968.2 ± 412.2 ρmol/thyroid, $P = 0.019$) (Fig. 6Bii). In addition, TH concentrations were also measured in the sera of these mice. Mean serum T_3 concentrations for the WT and PBF-Tg mice were 165.3 ± 8.6 and 150.1 ± 10.4 ng/dl, respectively, and serum T_4 levels were 2.9 ± 0.1 and 3.6 ± 0.2 μg/dl, respectively. Subsequently, when the ratio of total thyroid

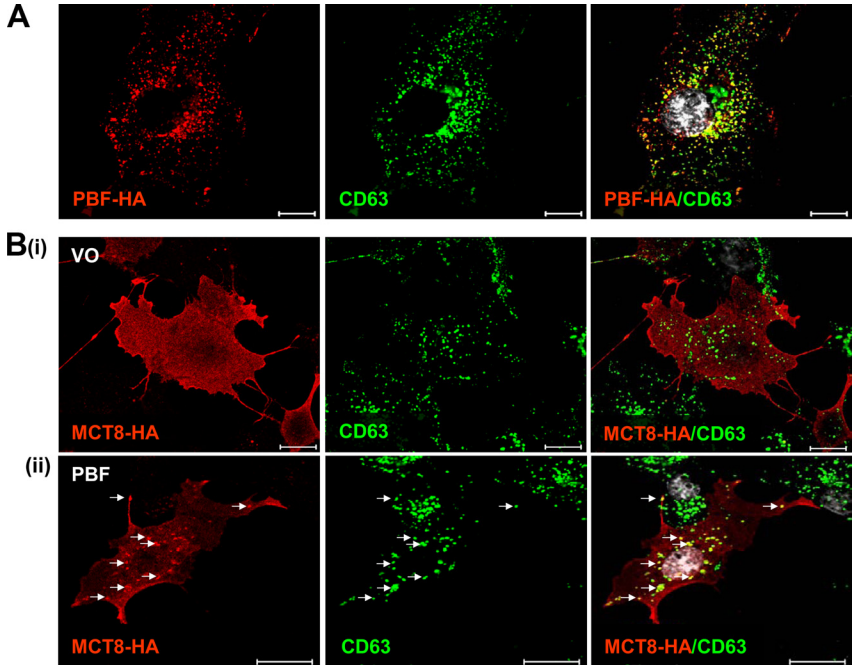

FIG. 4. Colocalization of PBF and MCT8 with CD63 *in vitro*. A, Confocal images of PBF-HA, after transfection into COS-7 cells, and endogenous CD63. PBF-HA (*red*) and endogenous CD63 (*green*) colocalized within late endosomes. B, Representative confocal images examining staining of MCT8-HA (*red*) after transient transfection into COS-7 cells and endogenous CD63 (*green*). i, With cotransfection of VO control, MCT8-HA was predominantly expressed in the plasma membrane and showed no colocalization with CD63. ii, In contrast, cotransfection of PBF resulted in the appearance of MCT8-HA within intracellular vesicles (*arrows*) where it strongly colocalized with CD63, as seen in *yellow* in the merged images. *Scale bars*, 20 μm.

TH content (picomoles per thyroid) to circulating TH concentration (nanograms per deciliter) was assessed in each mouse, a significantly higher ratio was observed in PBF-Tg mice compared with WT mice both for T_3 (2.2-fold increase; $P = 0.046$) and T_4 (3.2-fold increase; $P = 0.029$) (Supplemental Fig. 1, published on The Endocrine Society's Journals Online web site at http://endo.endojournals.org).

Decreased TSH-stimulated T_4 secretion from the PBF-Tg thyroid gland

To further investigate whether a reduction in Mct8 function, and hence TH secretion, was at least partly responsible for the accumulation in TH within the thyroid glands of PBF-Tg mice, we measured the release of T_4 after TSH stimulation. To suppress the basal serum T_4 and TSH concentrations, WT (n = 10) and PBF-Tg (n = 14) mice were treated daily with 5 μg L-T_3 for 4 d before administration of 50 mU bovine TSH. After TSH stimulation, a significant increase in serum T_4 was observed in WT mice (1.59 ± 0.17 *vs.* 1.37 ± 0.03 μg/dl, $P = 0.007$) (Fig. 6Ci). In contrast, no increase in serum T_4 was detected in PBF-Tg mice (1.35 ± 0.10 *vs.* 1.36 ± 0.05 μg/dl, $P = 0.629$). Basal serum T_4 levels were not significantly different between WT and PBF-Tg mice (1.37 ± 0.03 *vs.* 1.36 ± 0.05 μg/dl, $P = 0.884$), whereas after TSH administration, significantly less serum T_4 was present in PBF-Tg compared with WT mice (1.35 ± 0.10 *vs.* 1.59 ± 0.17 μg/dl, $P = 0.013$) (Fig. 6Ci). Furthermore, when differences in serum T_4 levels before and after TSH stimulation (ΔT_4) were calculated for each individual animal, there was a significant decrease in ΔT_4 in PBF-Tg compared with WT mice (0.00 ± 0.06 *vs.* 0.22 ± 0.05 μg/dl, $P = 0.021$) (Fig. 6Cii).

Taken together, these data implicate PBF as a novel interacting partner of MCT8, which regulates MCT8 localization, hence altering TH secretion from the thyroid.

Discussion

Little is known about the regulation of the critical TH transporter MCT8 (18). Studies of the mouse *Mct8* gene have demonstrated cell-specific induction of *Mct8* expression by retinoic acid (21), although the effect on *Mct8* expression in the thyroid remains unknown. Given its recently discovered role in mediating TH secretion from the thyroid gland (15, 17), we investigated a role for PBF in MCT8 regulation.

We have previously described a posttranslational mechanism of NIS regulation by which PBF binds NIS and modulates its subcellular localization, thereby down-regulating NIS activity (6). In the present study, we have addressed the hypothesis that PBF can regulate other membrane transporters in addition to NIS and, through investigation of a possible relationship between PBF and MCT8, we have identified a novel mode of posttranslational regulation for MCT8.

MCT8 was confirmed as a novel binding partner for PBF through *in vitro* pull-down and coimmunoprecipitation assays in COS-7 cells and mass spectrometry experiments in K1 thyroid carcinoma cells. As observed with NIS in previous experiments (6), PBF overexpression *in vitro* resulted in an increase in MCT8 expression within intracellular vesicles where it colocalized with PBF. Importantly, increased expression of PBF was accompanied by a significant reduction in MCT8 expression at the plasma membrane, as determined through cell surface biotinylation assays. Thus, MCT8 and PBF colocalize and

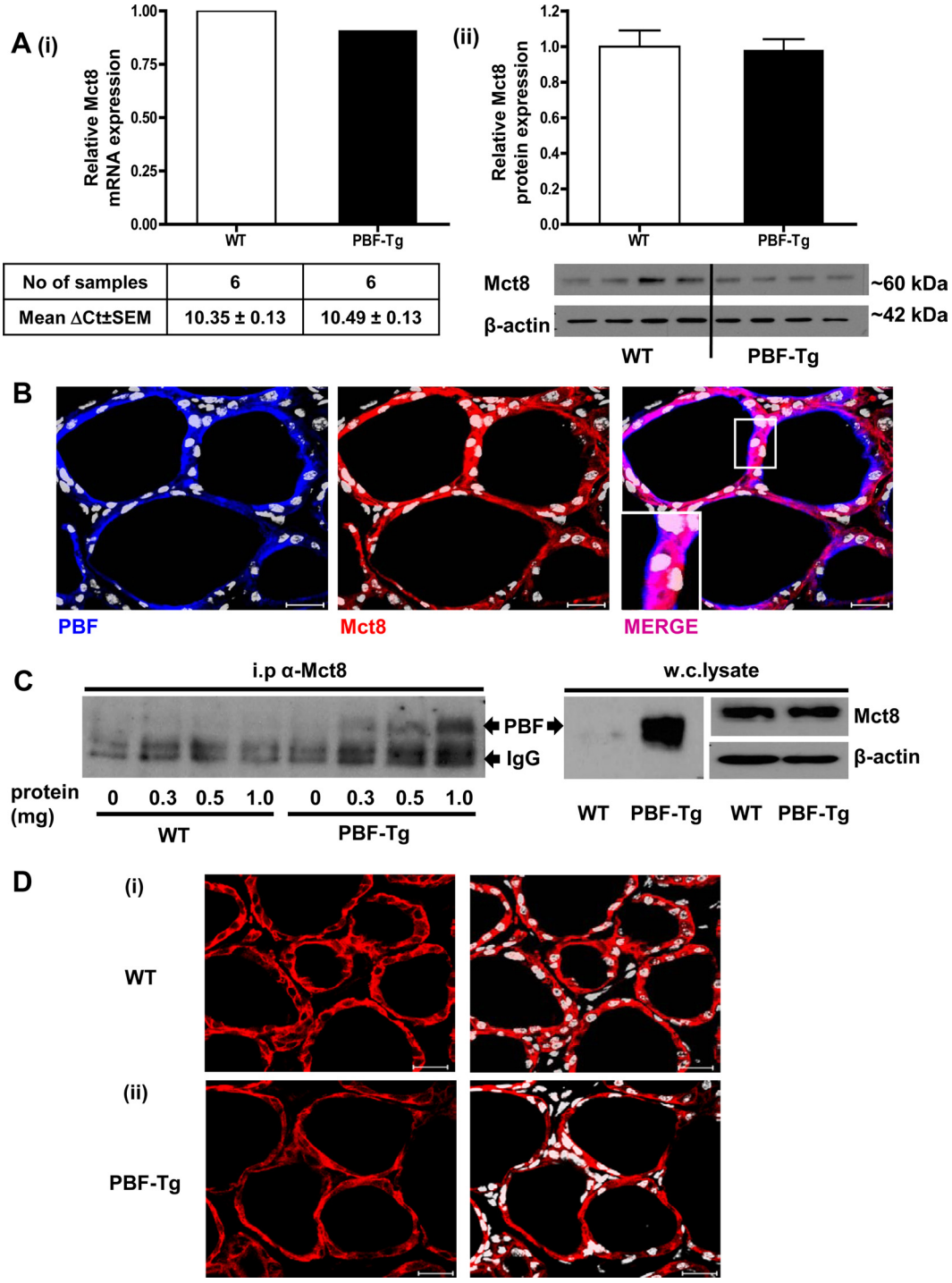

FIG. 5. Mct8 expression and localization in the PBF-Tg mouse. Ai, Relative Mct8 mRNA expression in thyroid glands of PBF-Tg mice compared with WT mice (n = 6); ii, representative immunoblot demonstrating similar thyroidal Mct8 protein levels in PBF-Tg mice compared with WT mice, using β-actin as a loading control (n = 8). Results of densitometry are presented as mean ± SEM. B, Immunostaining of frozen sections of PBF-Tg thyroid. PBF-HA (*blue*) and Mct8 (*red*) were labeled using HA and MCT8 antibodies, respectively, and demonstrated intense areas of colocalization (*magenta*) detected using confocal microscopy. *Scale bars*, 20 μm. C, Western blot analysis showing the detection of PBF-HA coimmunoprecipitation after the immunoprecipitation (i.p) of endogenous Mct8 in increasing amounts of protein lysate taken from PBF-Tg mice. Whole-cell (w.c.) lysate (30 μg) controls on the *right* show the relative expression levels of PBF-HA and Mct8 in WT (n = 8) and PBF-Tg (n = 6) mice, and β-actin was used as a loading control. IgG is light-chain Ig. D, Confocal images of endogenous Mct8 expression in frozen sections of mouse thyroid gland. Mct8 (*red*) demonstrated intense basolateral membrane expression in WT thyroid cells (i), which was diminished in the PBF-Tg thyroid (ii). *Scale bars*, 20 μm.

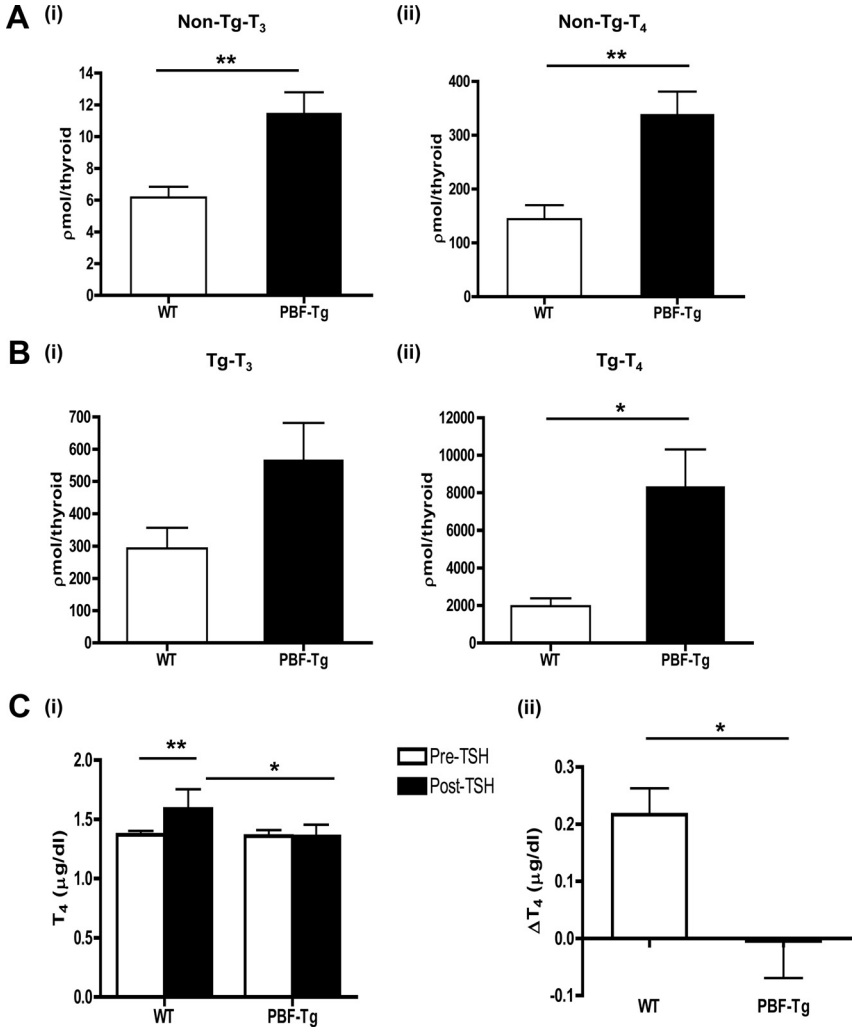

FIG. 6. Thyroidal TH content and TSH-stimulated TH secretion in the PBF-Tg mouse. Comparison of non-Tg-bound (A) and Tg-bound (B) TH content within the thyroid glands of WT (n = 8) and PBF-Tg (n = 10) mice. Levels of non-Tg-T_3 and Tg-T_3 (i) and non-Tg-T_4 and Tg-T_4 (ii) are presented as mean ± SEM. Ci Serum T_4 levels before and 3 h after the administration of 50 mU TSH in WT (n = 10) and PBF-Tg (n = 14) mice; ii, for each individual animal, the difference in T_4 concentration before and after TSH stimulation was calculated and expressed as ΔT_4. Presentation of the mean ± SEM ΔT_4 illustrates a significant reduction in T_4 secretion in the PBF-Tg mice compared with WT. **, $P < 0.01$; *, $P < 0.05$.

bind each other, and PBF is able to alter the subcellular localization of MCT8 *in vitro*. In addition, having previously demonstrated that PBF and NIS are associated with endogenous expression of the late endosome marker CD63 (6), we have now shown that MCT8 is also found in late endosomes after PBF overexpression. Thus, the mechanism by which PBF internalizes both MCT8 and NIS is likely to involve clathrin-dependent endocytosis resulting in the enrichment of these transporters within late endosomes.

To investigate the physiological relevance of these observations, we used our recently constructed PBF-Tg transgenic mouse model in which PBF is specifically overexpressed in the thyroid gland (9). Although Nis mRNA and protein expression was significantly repressed in the PBF-Tg thyroid, both Mct8 mRNA and protein expression were similar to WT mice. Although PBF does not appear to regulate Mct8 transcription, the presence of a posttranslational mechanism of regulation *in vivo* was supported through immunofluorescent studies of PBF-Tg thyroid sections where PBF colocalized with Mct8, particularly within the cytoplasm of the follicular epithelial cells. Furthermore, an *in vivo* interaction between PBF and Mct8 was demonstrated within thyroid glands taken from PBF-Tg mice, and comparison of Mct8 localization in thyroid follicular cells in PBF-Tg mice indicated a decrease in the clearly defined basolateral membrane expression that is seen in WT mice.

In addition to the reduced thyroidal Nis expression and iodide uptake, the PBF-Tg mouse has a notable phenotype. PBF-Tg mice have significantly enlarged thyroid glands (with 100% penetrance) that are associated with hyperplastic lesions (9). Interestingly, these characteristics are shared with the Mct8-KO mouse (15, 16). At 14 wk of age, the thyroid glands of Mct8-KO mice weigh around 4.1 mg compared with a mean thyroid weight of 2.6 mg for WT mice (15). This 1.6-fold increase is comparable to the increase in PBF-Tg mean thyroid weight compared with WT mice of a similar age (9). The thyroidal enlargement in the PBF-Tg and Mct8-KO mice was largely due to a significant (1.5-fold) increase in mean follicle size accompanied by the development of macrofollicles (9, 15–17).

The reduction in TH secretion in the Mct8-KO mice resulted in an accumulation of TH within the thyroid gland, which was both Tg and non-Tg bound (15, 17). To assess the effect of PBF overexpression on Mct8-mediated secretion, TH content was measured in the PBF-Tg mice. Both Tg and non-Tg-bound TH were significantly increased in the PBF-Tg thyroid compared with WT mice. Furthermore, T_4 secretion after TSH stimulation was significantly impaired in PBF-Tg mice compared with WT mice. Lack of TH secretion from the Mct8-KO mouse thyroid gland partially contributes to the abnormal serum TH profile that reproduces the high T_3 and low T_4 levels seen in human subjects with mutations in the *MCT8* gene

(15, 17). In contrast, despite the strikingly enlarged thyroid, PBF-Tg mice have normal serum TSH and circulating TH concentrations (9). There are a number of differences between the PBF-Tg and Mct8-KO mice that could explain the variation in serum TH profile. In the Mct8 total KO mouse, there would be no TH secretion via Mct8 whatsoever, whereas PBF overexpression is likely to only partially prevent Mct8-mediated secretion. Furthermore, the loss of Mct8 in the peripheral tissues and the subsequent alteration of deiodinase activity are known to significantly contribute to the abnormal TH profile of the Mct8-KO mouse (22–24), but Mct8 would still be fully functional within these tissues in the PBF-Tg mouse. PBF may also regulate the activity of other transporters such as Mct10, another TH transporter expressed in both mouse and human thyroid glands (14, 17).

In addition, although iodide uptake is normal in the Mct8-KO mouse (17), the reduction in Nis expression and iodide uptake in the PBF-Tg mouse adds further complexity (9). It might be expected that the reduction in Nis activity would result in diminished TH synthesis. However, although serum TSH concentrations are normal, the thyroid glands are significantly enlarged and appear to fully compensate for this lack of iodide uptake, with maintenance of normal serum TH concentrations. One potential mechanism for this may be the reported increase in TSH receptor expression (9), which may result in increased sensitivity to TSH. Importantly, the ratio of total thyroidal TH to total circulating TH is significantly increased in the PBF-Tg mouse, further suggesting that TH secretion is perturbed. Future studies will endeavor to elucidate the contribution of reduced TH secretion via Mct8 to the overall thyroid phenotype of the PBF-Tg mouse.

Overall, the present studies have identified a mechanism of posttranslational regulation of MCT8 by which PBF binds and alters its subcellular localization *in vitro*, with PBF overexpression resulting in a reduction in TH secretion and an accumulation of TH within the thyroid gland *in vivo*. These data add to the recent increase in our understanding of the final stages of TH synthesis and secretion and highlight PBF as an important regulator of this process.

Acknowledgments

We thank Dr. Josh Rappoport (School of Biosciences, University of Birmingham, Birmingham, UK) and Dr. Sally James (University of York, York, UK) for their technical expertise and advice and Dr. Fedor Berditchevski (School of Cancer Sciences, University of Birmingham, UK) for the kind provision of antibodies.

Address all correspondence and requests for reprints to: Prof. C. J. McCabe, School of Clinical and Experimental Medicine, Institute for Biomedical Research, University of Birmingham, Birmingham, B15 2TT, United Kingdom. E-mail: mccabcjz@bham.ac.uk.

This work was supported by the Medical Research Council and the Get-A-Head Charity.

Disclosure Summary: The authors have nothing to disclose.

References

1. **Yaspo ML, Aaltonen J, Horelli-Kuitunen N, Peltonen L, Lehrach H** 1998 Cloning of a novel human putative type Ia integral membrane protein mapping to 21q22.3. Genomics 49:133–136
2. **Chien W, Pei L** 2000 A novel binding factor facilitates nuclear translocation and transcriptional activation function of the pituitary tumor-transforming gene product. J Biol Chem 275:19422–19427
3. **Stratford AL, Boelaert K, Tannahill LA, Kim DS, Warfield A, Eggo MC, Gittoes NJ, Young LS, Franklyn JA, McCabe CJ** 2005 Pituitary tumor transforming gene binding factor: a novel transforming gene in thyroid tumorigenesis. J Clin Endocrinol Metab 90:4341–4349
4. **McCabe CJ, Khaira JS, Boelaert K, Heaney AP, Tannahill LA, Hussain S, Mitchell R, Olliff J, Sheppard MC, Franklyn JA, Gittoes NJ** 2003 Expression of pituitary tumour transforming gene (PTTG) and fibroblast growth factor-2 (FGF-2) in human pituitary adenomas: relationships to clinical tumour behaviour. Clin Endocrinol (Oxf) 58:141–150
5. **Watkins RJ, Read ML, Smith VE, Sharma N, Reynolds GM, Buckley L, Doig C, Campbell MJ, Lewy G, Eggo MC, Loubiere LS, Franklyn JA, Boelaert K, McCabe CJ** 2010 Pituitary tumor transforming gene binding factor: a new gene in breast cancer. Cancer Res 70:3739–3749
6. **Smith VE, Read ML, Turnell AS, Watkins RJ, Watkinson JC, Lewy GD, Fong JC, James SR, Eggo MC, Boelaert K, Franklyn JA, McCabe CJ** 2009 A novel mechanism of sodium iodide symporter repression in differentiated thyroid cancer. J Cell Sci 122:3393–3402
7. **Smith VE, Franklyn JA, McCabe CJ** 2011 Expression and function of the novel proto-oncogene PBF in thyroid cancer: a new target for augmenting radioiodine uptake. J Endocrinol 210:157–163
8. **Boelaert K, Smith VE, Stratford AL, Kogai T, Tannahill LA, Watkinson JC, Eggo MC, Franklyn JA, McCabe CJ** 2007 PTTG and PBF repress the human sodium iodide symporter. Oncogene 26:4344–4356
9. **Read ML, Lewy GD, Fong JC, Sharma N, Seed RI, Smith VE, Gentilin E, Warfield A, Eggo MC, Knauf JA, Leadbeater WE, Watkinson JC, Franklyn JA, Boelaert K, McCabe CJ** 2011 Proto-oncogene PBF/PTTG1IP regulates thyroid cell growth and represses radioiodide treatment. Cancer Res 71:6153–6164
10. **Friesema EC, Ganguly S, Abdalla A, Manning Fox JE, Halestrap AP, Visser TJ** 2003 Identification of monocarboxylate transporter 8 as a specific thyroid hormone transporter. J Biol Chem 278:40128–40135
11. **Friesema EC, Kuiper GG, Jansen J, Visser TJ, Kester MH** 2006 Thyroid hormone transport by the human monocarboxylate transporter 8 and its rate-limiting role in intracellular metabolism. Mol Endocrinol 20:2761–2772
12. **Friesema EC, Grueters A, Biebermann H, Krude H, von Moers A, Reeser M, Barrett TG, Mancilla EE, Svensson J, Kester MH, Kuiper GG, Balkassmi S, Uitterlinden AG, Koehrle J, Rodien P, Halestrap AP, Visser TJ** 2004 Association between mutations in a thyroid hormone transporter and severe X-linked psychomotor retardation. Lancet 364:1435–1437
13. **Dumitrescu AM, Liao XH, Best TB, Brockmann K, Refetoff S** 2004

A novel syndrome combining thyroid and neurological abnormalities is associated with mutations in a monocarboxylate transporter gene. Am J Hum Genet 74:168–175
14. **Nishimura M, Naito S** 2008 Tissue-specific mRNA expression profiles of human solute carrier transporter superfamilies. Drug Metab Pharmacokinet 23:22–44
15. **Di Cosmo C, Liao XH, Dumitrescu AM, Philp NJ, Weiss RE, Refetoff S** 2010 Mice deficient in MCT8 reveal a mechanism regulating thyroid hormone secretion. J Clin Invest 120:3377–3388
16. **Wirth EK, Sheu SY, Chiu-Ugalde J, Sapin R, Klein MO, Mossbrugger I, Quintanilla-Martinez L, de Angelis MH, Krude H, Riebel T, Rothe K, Köhrle J, Schmid KW, Schweizer U, Grüters A** 2011 Monocarboxylate transporter 8 deficiency: altered thyroid morphology and persistent high triiodothyronine/thyroxine ratio after thyroidectomy. Eur J Endocrinol 165:555–561
17. **Trajkovic-Arsic M, Müller J, Darras VM, Groba C, Lee S, Weih D, Bauer K, Visser TJ, Heuer H** 2010 Impact of monocarboxylate transporter-8 deficiency on the hypothalamus-pituitary-thyroid axis in mice. Endocrinology 151:5053–5062
18. **Visser WE, Friesema EC, Visser TJ** 2011 Thyroid hormone transporters: the knowns and the unknowns. Mol Endocrinol 25:1–14
19. **James SR, Franklyn JA, Reaves BJ, Smith VE, Chan SY, Barrett TG, Kilby MD, McCabe CJ** 2009 Monocarboxylate transporter 8 in neuronal cell growth. Endocrinology 150:1961–1969
20. **Darras VM, Huybrechts LM, Berghman L, Kühn ER, Decuypere E** 1990 Ontogeny of the effect of purified chicken growth hormone on the liver 5′ monodeiodination activity in the chicken: reversal of the activity after hatching. Gen Comp Endocrinol 77:212–220
21. **Kogai T, Liu YY, Richter LL, Mody K, Kagechika H, Brent GA** 2010 Retinoic acid induces expression of the thyroid hormone transporter, monocarboxylate transporter 8 (Mct8). J Biol Chem 285: 27279–27288
22. **Dumitrescu AM, Liao XH, Weiss RE, Millen K, Refetoff S** 2006 Tissue-specific thyroid hormone deprivation and excess in monocarboxylate transporter (mct) 8-deficient mice. Endocrinology 147: 4036–4043
23. **Trajkovic M, Visser TJ, Mittag J, Horn S, Lukas J, Darras VM, Raivich G, Bauer K, Heuer H** 2007 Abnormal thyroid hormone metabolism in mice lacking the monocarboxylate transporter 8. J Clin Invest 117:627–635
24. **Trajkovic-Arsic M, Visser TJ, Darras VM, Friesema EC, Schlott B, Mittag J, Bauer K, Heuer H** 2010 Consequences of monocarboxylate transporter 8 deficiency for renal transport and metabolism of thyroid hormones in mice. Endocrinology 151:802–809